Snowmass White Paper Contribution: Physics with the Phase-2 ATLAS and CMS Detectors

The ATLAS and CMS Collaborations

The ATLAS and CMS Collaborations actively work on developing the physics program for the High-Luminosity LHC. This document contains short summaries of physics contributions to the Energy Frontier and to the Rare Processes and Precision Measurements groups of Snowmass 2021. The summary is based on the physics potential estimates that were included in the CERN Yellow Report "Physics at the HL-LHC, and Perspectives for the HE-LHC", and also contains a number of recent results.

Contents

1 Introduction

Research in high energy physics is in an exciting phase. Despite its great success, the Standard Model (SM), the theory that describes with astonishing precision the matter and the forces that act upon it, leaves many questions unanswered. For example, it does not describe dark matter (DM), which dominates the matter composition in the Universe; it does not explain why there are three generations of particles; it does not provide any reason behind the matter-antimatter asymmetry in the Universe. New theories, generally denoted as new physics (NP), attempt to answer these and other open questions by introducing new particles or new microscopic forces. The Large Hadron Collider (LHC) is a unique infrastructure located at CERN that provides the opportunity to study the particles that constitute our world and give answers to the many pressing questions. The two large general-purpose experiments of the LHC, ATLAS [1] and CMS [2], currently probe the SM with unprecedented precision. While so far they see no evidence for deviations from the SM, they have only been exposed to hardly 5% of the total dataset envisaged to be delivered in the lifetime of the LHC: its high-luminosity upgrade will provide the experiments with 20 times the dataset they currently have available. These unprecedented datasets will allow particle physicists to observe and study SM phenomena that remain elusive so far due to their small rates, as well as to extend of the reach of searches for new processes beyond the Standard Model (BSM). At the same time, these new data will boost the potential of the experiments to direct discoveries that can revolutionize the human understanding of nature.

The ATLAS and CMS Collaborations are continuously developing the physics program for the High-Luminosity LHC (HL-LHC). The HL-LHC will extend the LHC program to the first half of the 2040's, with pp collisions at $\sqrt{s}$ =14 TeV with an expected integrated luminosity of 3000 fb^{-1}for each of the ATLAS and CMS experiments, and PbPb and pPb collisions with integrated luminosities of 13 nb^{-1} and 50 nb^{-1}, respectively. The ATLAS and CMS Collaborations recognize the importance of the Snowmass process to the high-energy physics community in the US and beyond. Continued strong US participation is in particular critical to the success of the HL-LHC physics program, as the Phase-2 detector upgrades, the HL-LHC data-taking operations and the physics analyses based on the HL-LHC dataset will not be able to proceed without the support of the US community. The physics contributions to the Energy Frontier (EF) and to the Frontier for Rare Processes and Precision Measurements (RF) groups of Snowmass 2021 are based on the studies that are summarized in the CERN Yellow Report on the Physics at the HL-LHC, and Perspectives for the HE-LHC (YR18) [3]; some of these contributions are updated based on the most recent Run 2 results, and a few new studies are presented. Detailed theory references can be found in Ref. [3] and in the ATLAS and CMS documents presenting the new studies in full details.

For the HL-LHC both experiments are planning significant modification of the detectors (Phase-2 upgrade) which should allow for effective data taking and event reconstruction at increased luminosity and pileup (PU), with up to 200 additional interactions per bunch crossing and up to an order of magnitude larger radiation dose. For both detectors, in order to maintain or even lower the trigger thresholds with respect to the current ones, the triggering systems will be replaced. New tracker systems will be installed, extending the tracking coverage up to pseudorapidities of about $|\eta| = 4$. The addition of new timing detectors, covering up to $|\eta| = 3$ for CMS and $2.4 < |\eta| < 4$ for ATLAS, will introduce new PU rejection capabilities in the challenging HL-LHC environment, as well as new handles for the detection of long-lived particles. The existing ATLAS liquid argon and tile calorimeters as well as the CMS barrel electromagnetic and hadron calorimeters will be upgraded with new electronics. The CMS endcap electromagnetic and hadron calorimeters will be replaced with a new high-granularity combined sampling calorimeter. Finally, the muon systems will be upgraded with new electronics and additional muon chambers both for ATLAS and

CMS. A more detailed overview of the detector upgrade program is presented for ATLAS in Refs. [4–10] and for CMS in Refs. [11–17]. Strategies to develop software and computing capable of processing the HL-LHC data have been outlined in Refs. [18–20]. Expected performance of the reconstruction algorithms and PU mitigation both with upgraded CMS and ATLAS detectors have been studied and summarized in Refs. [21–24]. The technical design reports referenced above also present concrete examples highlighting how the Phase-2 improvements in detectors, triggers and reconstruction will extend sensitivity in precision measurements and new physics searches. Further examples will be shown in the next chapters.

The results related to precision Higgs properties measurements and the study of its self-coupling contribute to the work of the first subgroup of the Energy Frontier group (**EF01**). Constraints from searches for BSM decays of the Higgs boson or from searches for new particles connected to the Higgs sector are presented in **EF02**. Precision measurements of top quark properties represent an important test of the SM, considering the top quark, as the heaviest particle in the SM, is a particularly sensitive probe to NP. The flavor physics program at the HL-LHC also comprises many probes to NP with significant discovery potential, extending the reach of direct searches. Those topics are discussed in **EF03** and in **RF01**, respectively. Other studies of SM processes based on electroweak measurements are presented in **EF04**, while precision QCD measurements and analyses probing photon-photon interactions are discussed in **EF05** and **EF06**, respectively. Heavy-ion-related analyses, covering in particular studies of the quark-gluon plasma, contribute to **EF07**. Prospective results assessing the ATLAS and CMS sensitivity in BSM searches at the HL-LHC are reported in **EF08** for model-specific explorations, **EF09** for more general explorations and **EF10** for DM searches.

There are two strategies employed for ATLAS projections: (1) extrapolations based on Run 2 results scaled to the HL-LHC luminosity taking the change in center-of-mass energy, triggers, and expected object-level performance into account, and (2) parametric simulations based on detailed simulations of the upgraded detectors under HL-LHC conditions to provide the expected performance for reconstructed objects. In CMS some analyses use full simulation of the Phase-2 detector response, some use DELPHES [25], based on parameterized detector response, and in some cases projections of existing Run 2 results are performed. The treatment of theoretical and experimental uncertainties, as well as the upgraded detector performance, are described in Refs. [21, 22]. For the extrapolation from Run 2 measurements, a baseline scenario (YR18 systematic uncertainties) was devised to estimate the uncertainties. This scenario assumes that the ultimate future performance of the two experiments in terms of detector and trigger performance will be comparable to the performance achieved during the LHC Run 2, most of the experimental uncertainties are scaled down with the square root of the integrated luminosity, and that improvements will be done to theoretical predictions so that their uncertainties can be halved with respect to current values. A 1% luminosity uncertainty is used for this scenario. The YR18 systematic uncertainties are used in the results presented in this document, unless specified otherwise. Full Phase-2 or parametric simulations offer the possibility to investigate the evolution in object reconstruction performance as well as the impact of increased detector acceptance, possible thanks to the upgrade of the tracking systems, while Run 2 extrapolations directly benefit from the well-studied systematics models developed for the Run 2 analyses.

2 EF01: EW Physics: Higgs boson properties and couplings

The discovery of the Higgs boson by the ATLAS and CMS Collaborations in 2012 [26–28] marks a milestone in the history of particle physics. The Electroweak Symmetry Breaking (EWSB) mechanism is central to the functioning of the SM, and connects with many of the outstanding questions in physics today. Studying the properties of the Higgs boson is a key mission of the LHC program. Small deviations from its expected behavior can have large implications on the structure of nature, as predicted in many BSM scenarios.

The EWSB mechanism maintains the structure of gauge interactions while generating the masses of electroweak gauge bosons (W/Z). This is achieved through the introduction of a self-interacting complex EW doublet scalar field Φ described by a kinetic scalar term and a potential of the form $V(\Phi) = \mu^2 \Phi^\dagger \Phi + \lambda \left(\Phi^\dagger \Phi \right)^2$. The spontaneous symmetry breaking is induced by the neutral component of Φ acquiring a vacuum expectation value (VEV) $v \approx 246$ GeV. In this process, three massless Goldstone bosons are absorbed to generate masses of the W and the Z gauge bosons. The remaining component of the complex doublet becomes a massive Higgs boson scalar field, for which the mass was measured to be 125 GeV with an uncertainty already at the per-mil level [29, 30]. The masses of all fermions are also a consequence of EWSB since the Higgs doublet is assumed to couple to fermions through Yukawa interactions.

While EWSB establishes the type and strength of the Higgs boson interactions with other SM particles, the careful study of its properties represents an essential task to test the self-consistency of the SM and to collect new possible hints of BSM effects. Beyond the discovery of the Higgs boson, the data collected by the ATLAS and CMS experiments during the first two Runs of the LHC has yielded a large number of measurements of its properties, addressing in detail its production and decay mechanisms. The dominant production modes at the LHC have been measured, and the decay channels in pairs of photons, vector-bosons, b-quarks and τ leptons have been firmly observed. The Run 2 data also presented the first evidence for the Higgs boson coupling to second generation fermions through the measurement of $H \rightarrow \mu^+ \mu^-$ [31, 32]. Other rare decays, such as $H \rightarrow Z\gamma$ [33, 34], have been studied. Further measurements targeted its mass, total width, spin, tensor structure, the total and differential cross-sections for several production modes, and the study of its couplings to bosons and fermions. Constraints on the Higgs self-coupling and on the shape of the Higgs potential have been derived, driven by the search for Higgs boson pair production. While the Higgs measurement results obtained so far are in agreement with the SM prediction, the precision achievable at the moment is not enough to significantly challenge many BSM models.

2.1 Precision Higgs Measurements at the HL-LHC. Yellow Report Summary

The reach in Higgs boson measurements with the HL-LHC dataset was estimated as a cross-collaboration effort and reported in Ref. [3]. Whenever possible, results were presented as the joint LHC sensitivity, combining the ATLAS+CMS prospects. Future sensitivities at 3000 fb^{-1} are extrapolated from the corresponding Run 2 measurements (with 36 or 80 fb^{-1}). However, the potential of the HL-LHC cannot be completely assessed through Run 2 extrapolations because of the difficulty in quantifying the improved acceptance and performance of the detectors and to account for yet-unexplored analysis techniques. Therefore dedicated Monte Carlo studies with HL-LHC conditions are used in particular cases.

2.1.1 Higgs boson production cross-sections and decay branching ratios: measurements and interpretations

An extrapolation to the HL-LHC luminosity of the measurements in the main SM Higgs boson decay channels (ATLAS and CMS: $\gamma\gamma$, ZZ, W^+W^-, $\tau^+\tau^-$, $b\bar{b}$, and $\mu^+\mu^-$; ATLAS only: $Z\gamma$) was performed per experiment [35, 36] and then combined using a simplified treatment. The four dominant production mechanisms of the Higgs boson at the LHC are the gluon fusion process (ggF), the vector-boson fusion process (VBF), the production associated with a vector boson (VH) and the production associated with a pair of top quarks ($t\bar{t}H$). The expected precision on their measurement is shown in Figure 1(a). The projected precision ranges from 1.6% (ggF) to 5.7% (WH). Theoretical uncertainties in the prediction of the Higgs boson production in the phase space of the analyses will play a very important role. In terms of per-decay-mode branching ratios (normalized to the SM expectations), the combined ATLAS+CMS precision also reaches the few percent level, dominated by the theoretical uncertainty, for the main decay modes $\gamma\gamma$ (2.6%), ZZ (2.9%), W^+W^- (2.8%), $\tau^+\tau^-$ (2.9%), $b\bar{b}$ (4.4%). For the rarer decay modes, $\mu^+\mu^-$ and $Z\gamma$, the measurement will remain statistically limited, and will reach a precision of 8.2% and 19.1% respectively.

The combined analysis can be extended to include an interpretation in terms of coupling modifiers, κ, which parameterize potential deviations from the SM predictions that would introduce a linear change of the Higgs boson couplings to SM bosons and fermions. This framework is described in detail in Ref [37]. In this implementation, six coupling modifiers corresponding to the tree-level Higgs boson couplings are defined: κ_W, κ_Z, κ_t, κ_b, κ_τ, and κ_μ and three effective coupling modifiers, κ_g, κ_γ, and $\kappa_{Z\gamma}$, are introduced to describe the loop-induced processes $gg \rightarrow H$, $H \rightarrow gg$, $gg \rightarrow ZH$, $H \rightarrow \gamma\gamma$ and $H \rightarrow Z\gamma$. The expected uncertainties for the ATLAS+CMS HL-LHC sensitivity to κ parameters are summarized in Figure 1(b). The total expected uncertainty is at the few percent level, ranging from 1.5% for κ_Z to 4.3% for κ_μ, and only approaching 10% for $Z\gamma$. Theoretical uncertainties play an important role, and are particularly remarkable in the case of κ_t, κ_b, and κ_g. The expected precisions on the coupling modifiers assume that only decays to SM particles are allowed. An expected uncertainty on the branching ratio of BSM decays $B_{BSM} = 2.5\%$ is derived by extending the parameterization and introducing an additional constraint on $|\kappa_V| \leq 1$, which avoids a complete degeneracy in the total width where all of the coupling modifiers can be scaled equally to account for a non-zero B_{BSM}.

The absence of conclusive BSM signals at the LHC suggests an important separation of scales between the SM and BSM effects. The Standard Model Effective Field Theory (SMEFT) provides a powerful framework to interpret the Higgs boson measurements along with precision observables coming from SM measurements in a search for evidence of higher order interactions between the SM particles. Such a study was included in Ref [3] using as inputs the production and decay mode sensitivities discussed above.

Rarer Higgs boson decays are also a target for the HL-LHC. Limits on the coupling to first and second generation quarks can be placed both through searches for exclusive decays (like $H \rightarrow \rho Z/\gamma$ for the first generation, $H \rightarrow \phi Z/\gamma$ for the s-quark and $H \rightarrow J/Psi Z/\gamma$ for the c-quark), following the analysis strategies already explored in Refs. [38–40], and through indirect constraints coming from differential cross-sections fits, the total width, or a global interpretations of the couplings. A special case is the coupling to the charm quark, probed directly through $H \rightarrow c\bar{c}$ searches where future development in charm tagging techniques could result in a significant increase of the sensitivity. A combination of ATLAS, CMS and LHCb results could potentially set constraints of the order of $\kappa_c \approx 1$ [3].
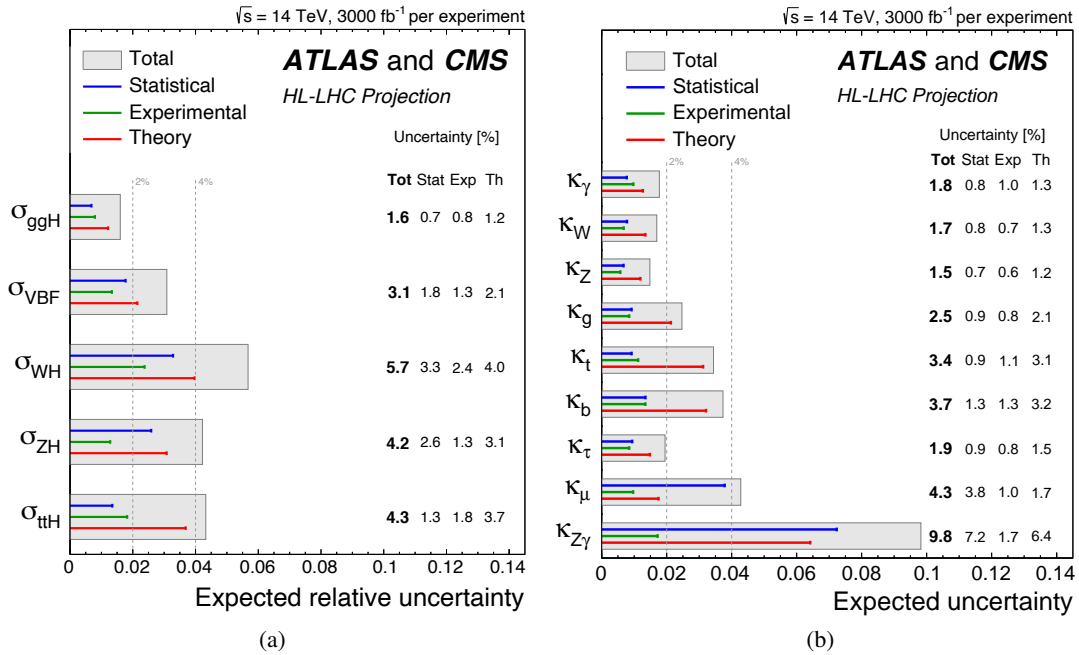
Figure 1: Summary plots showing the total expected uncertainties on (a) the per-production-mode cross-sections normalised to the SM predictions and (b) the coupling modifier parameters (κ), for the combination of ATLAS and CMS extrapolations. For each measurement, the total uncertainty is indicated by a grey box while the statistical, experimental and theory uncertainties are indicated by a blue, green and red line respectively. In addition, the numerical values are also reported. [3]

2.1.2 Differential measurements

Differential measurements can significantly extend the sensitivity of the LHC data to the Higgs boson mechanism beyond the reach of inclusive measurements of the product of production modes and branching ratios. Extrapolations of the differential distributions of gluon-gluon fusion production cross-sections in the ZZ, $\gamma\gamma$ and $b\bar{b}$ final states as a function of the Higgs boson transverse momentum p_T^H, angular distributions of decay products, and number of jets can be found in Refs. [36, 41]. In the higher p_T^H region, the precision will improve as the dataset grows but will remain limited by statistical uncertainties at the HL-LHC. Improved analysis techniques exploiting jet substructure tools to reconstruct the decay products of the Higgs boson produced with large p_T^H can significantly enhance the sensitivity of these analyses.

With the larger samples available, rarer production modes will become accessible for in-depth studies. A key example is $t\bar{t}H$ where the measurements will be limited by theoretical uncertainties in signal and background modeling, particularly in the $H \rightarrow b\bar{b}$ mode. The large dataset will enable precise measurements of the differential cross-sections in p_T^H bins, at the level of 20–40% with the $H \rightarrow \gamma\gamma$ channel as shown by CMS in Ref. [42]. In channels where the Higgs boson 4-momentum can be reconstructed ($t\bar{t}H, H \rightarrow \gamma\gamma$ and $t\bar{t}H, H \rightarrow b\bar{b}$), a measurement of the p_T^H spectrum can further improve the constraint on the top quark Yukawa coupling. Projections also show that a sensitivity close to the SM cross-section could be reached for the top-Higgs (tH) associated production [36].

9

2.1.3 Higgs boson width and CP measurements

Direct measurements of the Higgs boson width are challenging at hadron colliders, and limited by detector resolution [43]. A constraint on $\Gamma_H/\Gamma_H^{\mathrm{SM}}$ can be derived from a modification of the couplings fit described above, with the assumption that $|\kappa_V| \leq 1$. This results in an uncertainty of 4% for CMS for a collected luminosity of 3000 fb^{-1} [36]. Constraints on the Higgs boson width can also by obtained through the comparison of the on-shell and off-shell $H \rightarrow ZZ$ production, performed under the assumption that the Higgs couplings to gluons and Z bosons evolve off-shell as in the SM [44, 45]. At the HL-LHC, this approach is projected to yield a precision of $4.1^{+0.7}_{-0.8}$ MeV for a combination of ATLAS and CMS, dominated by theory uncertainties [36, 46].

Measurements of the CP properties of the Higgs boson show that it is consistent with a CP-even scalar particle ($J^P = 0^+$) as expected in the SM. However, studies of the Higgs boson couplings to SM particles could reveal a more complex tensor structure. In the bosonic sector, CP measurements can be performed in the $H \rightarrow ZZ$ and the $H \rightarrow W^+W^-$ decay channels as well as in the VBF production mode. On-shell/off-shell Higgs boson production can also be used to probe the tensor structure of the Higgs boson, searching for anomalous contributions in $H \rightarrow VV$ interactions, characterized by the coefficients a_2, a_3, Λ_1, and Λ_Q. The bounds are set on the product $f_{ai}\cos(\phi_{ai})$ where f_{ai} represents the relative contribution to the cross-section obtained by setting all coefficients to 0 except a_i and ϕ_{ai} is the phase as described in Refs. [47, 48]. The HL-LHC reach for $f_{a3}\cos(\phi_{a3})$ is found to be $[-1.6, 1.6] \times 10^{-4}$ at 95% confidence level (CL) in Ref. [36], with the assumptions that $\phi_{ai} = 0$ or π, $a_i^{ZZ} = a_i^{WW}$, and $\Gamma_H = \Gamma_H^{SM}$. In the fermionic sector, measurements in the $t\bar{t}H$ production and $H \rightarrow \tau^+\tau^-$ decay mode exploit the decay products of the top quark and the τ-leptons to build variables sensitive to the CP structure of the $H \rightarrow f\bar{f}$ vertex [49].

2.2 New results

2.2.1 Projection of the Higgs boson mass and on-shell width measurements in the $H \rightarrow ZZ \rightarrow 4\ell$ decay channel with CMS at the HL-LHC [50]

The mass of the Higgs boson, m_H, has been measured with a precision of around 0.11% ($m_H = 125.38 \pm 0.14$ GeV) by the CMS collaboration with a combination of measurements performed in the $\gamma\gamma$ and the ZZ decay channels using the Run 1 and 2016 dataset [29]. The natural width of a particle is yet another important characteristic. In the SM, the natural Higgs boson width is not a free parameter; it is predicted to be about 4 MeV. Experimentally, a particle's natural width can be assessed from the observed invariant mass of its decay products or, in the case of the Higgs boson, with better precision through a combined measurement of on-shell and off-shell production. The width measurement from the on-shell Higgs boson production is constrained to be < 1.10 GeV at 95% confidence level [51]. We can further improve on the precision of the measurements of the Higgs boson properties by taking advantage of the increase in luminosity and the upgraded detectors at the HL-LHC.

In this section, we present projections for the precision Higgs boson mass and on-shell width measurements expected to be achieved by CMS at the HL-LHC. The measurement methodologies mostly follow those described in Ref. [52] with a few improvements. The projection is based on Run 2 Monte Carlo samples, where expected signal and background event yields are scaled up by taking into account changes in their production cross sections at $\sqrt{s} = 14$ TeV and assuming the nominal expected HL-LHC integrated luminosity of 3000 fb^{-1}. The performance of trigger and object reconstruction is assumed to be the same as for Run 2, but for significantly increased PU. Depending on the flavor of leptons forming the two pairs of Z bosons,

we form four event categories: 4μ, $4e$, $2e2\mu$, $2\mu2e$, where $2e2\mu$ and $2\mu2e$ consider $2e$ or 2μ to be the closest to the nominal Z mass, respectively. Beam spot information is used in measuring muon transverse momenta, which improves the measurement precision by 5%. In decays $H \rightarrow ZZ \rightarrow 4\ell$, one Z boson (Z_1) is often on-shell and its invariant mass distribution is expected to have a characteristic Breit-Wigner peak at $m_{2\ell} \sim m_Z$ with a width $\sim \Gamma_Z$, and a low-mass off-shell tail. We use this well-predicted m_Z line shape for the SM Higgs boson decays as a constraint in the reconstruction of the momenta of the two leptons forming the Z_1 pair. This helps to improve the four-lepton mass resolution by 9%. Categorization based on the assessed per-event four-lepton mass resolution is introduced. Treating events with different four-lepton mass resolutions separately in the statistical framework of the Higgs boson mass measurement helps to improve the measurement precision by 10%. Finally, we use a matrix element based kinematic discriminant that helps to discriminate $gg \rightarrow H \rightarrow ZZ \rightarrow 4\ell$ events from background $q\bar{q}/gg \rightarrow ZZ \rightarrow 4\ell$. The usage of such kinematic discriminant brings an additional 4% improvement in the Higgs boson mass measurement. The dominant systematic uncertainties in the Higgs boson mass measurement are associated with how well we know the muon/electron energy scales and four-lepton mass resolutions. In Run 2 we achieve 0.01% (0.15%) uncertainties on the muon(electron) energy scale and 10% uncertainty on the four-lepton mass resolution regardless of the flavors of the four leptons. We use these values in the presented projections.

Table 1 summarizes the projected Higgs boson mass and on-shell width measurements. For the purposes of the mass measurement, the natural width of the Higgs boson is assumed to be much smaller than the instrumental four-lepton mass resolution. In the width measurement, the Higgs boson mass is treated as a nuisance parameter. The projected measurement uncertainty for the Higgs boson mass is $\pm22(\text{stat}) \pm 20(\text{syst}) = \pm30$ MeV. From the by-channel breakdown of the results, it can be seen that the overall Higgs boson mass precision would be nearly completely driven by the 4μ final state, which would be still statistically limited. The projected upper limits at 95% CL on the Higgs boson width are 177 MeV with all statistical and systematic uncertainties, and 94 MeV for statistical uncertainties only. While this upper limit on the width cannot reach the precision of the on-shell/off-shell measurement discussed in Section 2.1.3, it provides a complementary constraint limited only by detector resolution.

Table 1: Expected uncertainty on the Higgs boson mass measurement and 95 %CL upper limit on the Higgs boson total width estimated in the $H \rightarrow ZZ \rightarrow 4\ell$ channel for an integrated luminosity of 3000 fb^{-1}.

	Mass uncertainty (MeV)				Width upper limit at 95 % CL (MeV)
	Combined	4μ	4e	$2e2\mu$	$2\mu2e$	Combined
Stat. uncertainty	22	28	83	51	59	94
Syst. uncertainty	20	15	189	94	95	150
Total	30	32	206	107	112	177

In comparison to the Run 2, the CMS Detector will undergo substantial upgrades for the HL-LHC. Since muon performance is the main contributor to the Higgs boson mass measurement, we highlight the expected measurement implications for the 4μ final state. Trigger and muon reconstruction efficiencies for the 4μ events with all muons in the Run 2 acceptance phase space are not expected to change. With the new Tracker, the four-muon invariant mass resolution at $m_{4\ell} \sim m_H$ is expected to improve by 25%. The new muon station ME0 will extend the CMS muon acceptance from $|\eta| <2.4$ to 2.8 [15] with a net effect on the accuracy of measuring the rate of $H \rightarrow ZZ \rightarrow 4\mu$ events of about 7%. A similar improvement in the statistical uncertainty of the mass measurement can be reasonably expected. With these changes, the statistical uncertainty on the Higgs boson mass measurement in the 4μ channel can be expected to improve

from 28 to ~20 MeV, leading to a total, statistical plus systematic, uncertainty of ~25 MeV.

2.2.2 A projection of the precision of the Higgs boson mass measurement in the diphoton decay channel with CMS at the HL-LHC [53]

Although the $\gamma\gamma$ decay channel has a small ($\approx$0.23%) branching ratio, it provides a clean final state topology with a mass peak that can be reconstructed with high precision. We have carried out a projection of the Higgs boson mass measurement in the diphoton decay channel for an integrated luminosity of 3000 fb^{-1}, incorporating a few key improvements arising out of a more accurate calibration of the CMS detector in Run 2 and an improved method to measure and correct the non-linear discrepancies in the photon energy scale and resolution in data and simulation. The projections use Run 2 simulation samples and data, to model the signal and estimate the background respectively, with the same center of mass energy and theoretical uncertainties but an increased integrated luminosity. The key assumptions for this projection are that the performance of the trigger and object reconstruction will be the same as in Run 2, but for significantly increased pile-up conditions and radiation dose, which is justifiable from the new reconstruction algorithms under development and the projected performance of the upgraded CMS detector for the HL-LHC. The expected precision of m_H is projected to be m_H = 125.38 $\pm$ 0.02 (stat) $\pm$ 0.07 (syst) GeV. The result of the likelihood scan is presented in Figure 2. The projected precision of 0.07 GeV on the m_H measurement in the diphoton decay channel is better by nearly a factor of 3 compared to the current measurement [29] with the 2016 dataset. In addition to the factor of $\approx$10 increase in luminosity, the new tracker with less material, the precision and stability of the HGCAL, the improvements to the barrel calorimeters and the pileup suppression provided by the new MTD, new algorithms being developed for improved electromagnetic objects reconstruction and calibration have all led to this improvement. The limiting factor in this measurement arises out of the precision with which we can calibrate the photon energy scale, which is at the level of $\approx$0.05%. Any further improvements in the calibration strategy of the photon object can further enhance the precision of the m_H measurement in this channel.

2.2.3 Study of sensitivity to the *CP* structure of the Yukawa coupling between the Higgs boson and τ leptons with CMS at the HL-LHC [54]

Projections for the measurement of the *CP* properties of the Higgs boson coupling to τ leptons at HL-LHC have been derived, based on the Run 2 CMS analysis [54]. Relatively small modification to the CP-structure of the coupling to τ leptons could account for the observed baryon asymmetry of the universe in certain baryogenesis models, while the indirect bounds from electric dipole moment measurements are significantly weaker compared to other couplings (e.g. the top Yukawa coupling). The *CP* nature of the interaction is described in terms of an effective mixing angle $\alpha^{H\tau\tau}$, defined in Ref. [54]. A mixing angle of $\alpha^{H\tau\tau}$ = 0 (90)$^\circ$ corresponds to a pure scalar (pseudoscalar) coupling. For any other value of $\alpha^{H\tau\tau}$, the Higgs boson has a mixed coupling with both *CP*-even and *CP* odd components, implying *CP* violation.

This extrapolation is carried at $\sqrt{s}$=13 TeV, as the differences in cross-section going to $\sqrt{s}$=14 TeV are not expected to significantly impact the conclusions of this study. The extrapolations have been made using various assumptions about the systematic uncertainties: no systematic uncertainties, assuming the same systematic uncertainties as for the Run 2 analysis, YR18 systematic uncertainties, and with "bin-by-bin" systematic uncertainties related to the finite statistics in the signal and background histograms scaled by $1/\sqrt{\mathcal{L}}$ while all other systematic uncertainties are scaled following the YR18 scheme.
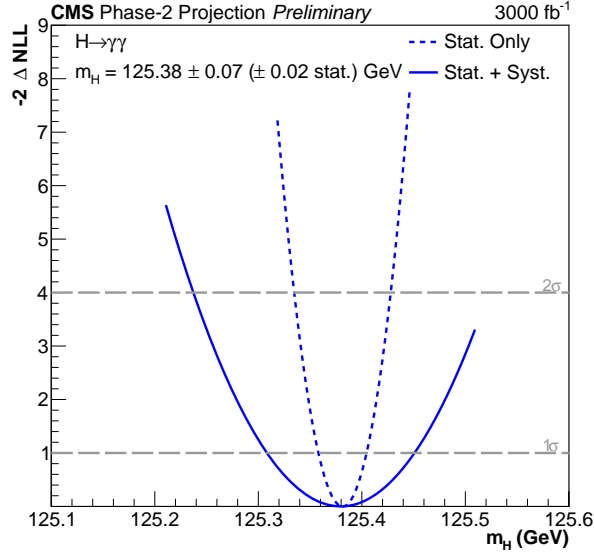
Figure 2: The likelihood scan of the projected Higgs boson mass in the diphoton decay channel corresponding to an integrated luminosity of 3000 fb^{-1} foreseen at the HL-LHC . The solid lines are for the full likelihood scan including all systematic uncertainties, while the dashed lines denote the same with the statistical uncertainty only. [53]

The projected negative log-likelihood scans are shown in Figure 3. For all systematic uncertainty schemes, the total expected uncertainty on $\alpha^{H\tau\tau}$ is 5°, but the sensitivities to the larger $\alpha^{H\tau\tau}$ values are different depending on the assumption made about the systematic uncertainties.

2.2.4 Prospects for the precise measurement of the Higgs boson properties in the $H \rightarrow \mu^+\mu^-$ decay channel with CMS at the HL-LHC [55]

After analyzing the full Run 2 dataset (138 fb^{-1}), the CMS Collaboration reported the first evidence for the Higgs boson decay to two muons [31] with observed (expected) signal significance 3.0σ (2.5σ), and uncertainty on the signal cross-section of 42%, dominated by the statistical component. This result is extrapolated to the HL-LHC assuming a dataset corresponding to an integrated luminosity of 3000 fb^{-1} at a center-of-mass energy $\sqrt{s} = 14$ TeV. A detailed description of the extrapolation technique and the results can be found in Ref. [55]. The Run 2 search featured multiple event categories targeting different production modes of the Higgs boson, whereas only the two most sensitive categories – Higgs boson production via gluon-gluon fusion (ggF) and via vector boson fusion (VBF) – are considered for this projection.

A major improvement to the $H \rightarrow \mu^+\mu^-$ analysis sensitivity at the HL-LHC is expected given the improved muon momentum resolution after the Phase-2 upgrade of the CMS tracking system [12], which translates into an improvement of about 30% in the dimuon mass resolution with respect to Run 2 in the phase space of the $H \rightarrow \mu^+\mu^-$ search. This effect is evaluated by comparing the width of the signal mass spectrum after the full $H \rightarrow \mu^+\mu^-$ event selection for Run 2 datasets with results of the Phase-2 DELPHES simulation. The impact of the improved mass resolution is taken into account in both the ggH category, where it directly affects the width of the parametric signal model, and in the VBF category, where the effect is estimated
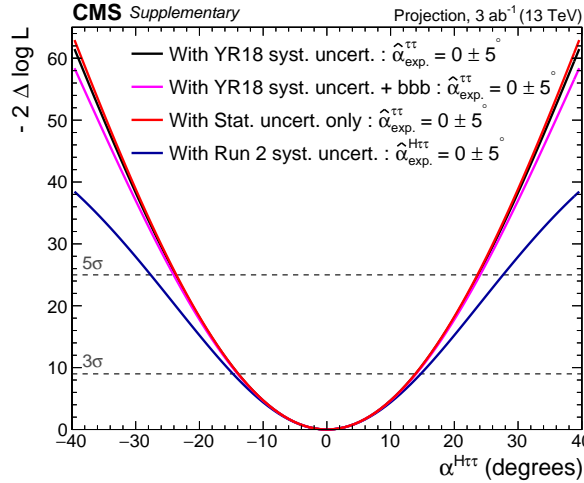
Figure 3: Projections of the expected negative log-likelihood scans as a function of the CP mixing angle, described in the text, based on an integrated luminosity of 3000 fb^{-1}. The extrapolations have been made using different assumptions about the systematic uncertainties: no systematic uncertainties (red), assuming the same systematic uncertainties as for the Run 2 analysis (blue), the YR18 systematic uncertainty scheme [3] (black), and with bin-by-bin uncertainties scaled by $1/\sqrt{\mathcal{L}}$ while all other systematic uncertainties are scaled following the YR18 scheme (magenta). [54]

by reweighting the signal DNN template according to the ratio of the dimuon mass spectra in DELPHES simulation and Run 2 datasets. The Phase-2 detector will also feature an extended pseudorapidity coverage of the muon system (up to $|\eta| < 2.8$), resulting in 10% increase in signal acceptance and 15–18% increase in background acceptance, as compared to Run 2.

The effect of the increase of center-of-mass energy from $\sqrt{s}$ =13 to 14 TeV is taken into account by rescaling the cross-sections of leading signal and background processes. The cross-sections of the two main signal processes (ggF and VBF) are both increased by approximately 12%, while the cross-section of the dominating source of background, the Drell–Yan (DY) process, is increased by 8%. The cross-section increase for other important backgrounds, top-quark pair production ($t\bar{t}$) and electroweak production of Z boson (Zjj-EW), are 21% and 10%, respectively, but their relative contribution to the total background yield is small.

The evolution of the uncertainty on the $H \rightarrow \mu^+\mu^-$ signal strength for an integrated luminosity up to 3000 fb^{-1} is shown in Figure 4(a), while the uncertainty on the coupling strength modifier κ_μ is shown in Figure 4(b). The extrapolation is performed for two uncertainty scenarios: in the first scenario (S1), all systematic uncertainties are kept at the same level as in Run 2, while in the second systematic uncertainty scenario (S2), the YR18 systematic uncertainties are used. The breakdown of the uncertainties into statistical, theoretical, and experimental components is shown in Tables 2 and 3, along with their comparison to the results reported in Refs. [56] and [3].

2.2.5 Projection of the search for $VH(H \rightarrow c\bar{c})$ with CMS at the HL-LHC [57]

Due to the challenging c quark identification in hadronic environment, the smallness of the branching fraction, and the very large QCD multijet background, a direct measurement of $H \rightarrow c\bar{c}$ at the LHC is extremely challenging. Recently, the CMS collaboration reported [57] the results of a direct search using
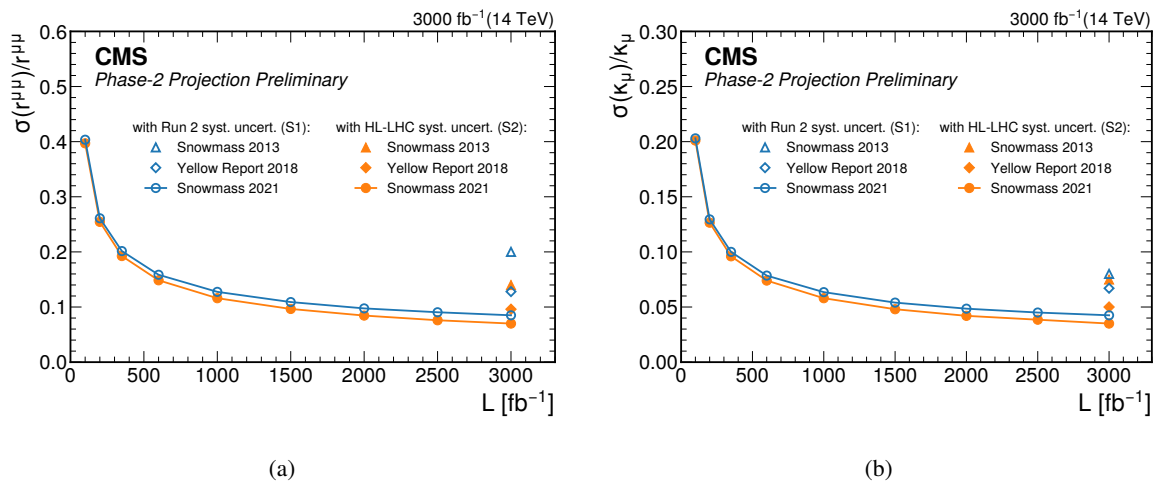
Figure 4: Evolution of the uncertainty on (a) the signal strength modifier $r^{\mu\mu}$ and (b) κ_μ as a function of the integrated luminosity. The new projection is represented by circles. For comparison, triangles show the results of the extrapolation performed for Snowmass 2013 [56] and diamonds the projections included in Ref. [3]. The two uncertainty scenarios described in the text, S1 and S2, are shown in blue and orange respectively. [55]

Table 2: Uncertainty on the signal strength modifier $r^{\mu\mu}$ at 3000 fb^{-1}.

		Statistical	Experimental	Theoretical	Total
	Snowmass 2013	-	-	-	20.0%
S1	YR 2018	9.1%	7.6%	4.8%	12.8%
	Snowmass 2021	6.4%	3.7%	4.2%	8.5%
	Snowmass 2013	-	-	-	14.0%
S2	YR 2018	9.1%	1.7%	2.7%	9.6%
	Snowmass 2021	6.4%	2.0%	2.0%	7.0%

the full Run 2 data for the Higgs boson produced in association with a W or Z boson, where the Higgs boson decays to a pair of c quarks, the Z decays to two neutrinos or two leptons, and the W decays to a lepton and a neutrino final state. Novel tools for jet reconstruction and identification as well as improved analysis techniques were developed for the search.

This section presents the extrapolation of the analysis to the HL-LHC scenario. The projection is based on the merged-jet topology of the Run 2 analysis. The large radius jet p_T threshold is lowered to 200 GeV, which allows the measurement using only the merged-jet topology to reach a sensitivity comparable to the full combination of the resolved-jet and merged-jet topologies in the Run 2 analysis. The Run 2 analysis contains three $c\bar{c}$-enriched categories, defined based on three working points of the ParticleNet [58, 59] $c\bar{c}$-discriminant, with approximately 58, 40, and 16% efficiencies for identifying a $c\bar{c}$ pair, and misidentification rates of 2(9), 0.7(5), and 0.08(1)% for light quark and gluons jets (bottom jets). Furthermore, three $b\bar{b}$-enriched categories are added, enabling the analysis to simultaneously measure the $VH(H \rightarrow b\bar{b})$ and $VH(H \rightarrow c\bar{c})$ processes. These categories are defined based on three working points of the ParticleNet $b\bar{b}$-discriminant, with approximately 80, 62, and 26% efficiencies for identifying a $b\bar{b}$ pair, and misidentification rates of 1(9), 0.6(4), and 0.08(1)% for light quark and gluons jets (charm jets). For the few percent overlap between the new $b\bar{b}$ categories and the original $c\bar{c}$ categories, events are

Table 3: Uncertainty on the coupling modifier κ_μ at 3000 fb^{-1}.

		Statistical	Experimental	Theoretical	Total
	Snowmass 2013	-	-	-	8.0%
S1	YR 2018	4.7%	2.7%	3.9%	6.7%
	Snowmass 2021	3.2%	1.9%	2.2%	4.3%
	Snowmass 2013	-	-	-	7.5%
S2	YR 2018	4.7%	1.5%	1.1%	5.0%
	Snowmass 2021	3.2%	1.1%	0.8%	3.5%

assigned to the $c\bar{c}$ categories and removed from the $b\bar{b}$ categories if the $c\bar{c}$ discriminant is higher than the $b\bar{b}$-discriminant, and vice versa.

For the projection, the yields of the signal and background processes are scaled to an integrated luminosity of 3000 fb^{-1}. Differences in the production cross sections at $\sqrt{s}$ = 14 TeV and $\sqrt{s}$ = 13 TeV are also taken into account with an inclusive scaling factor for each process. The YR18 systematic uncertainties are used except for the uncertainties on the $b\bar{b}$ and $c\bar{c}$ tagging efficiencies, which are directly constrained in the analysis by the $VZ(Z \rightarrow b\bar{b})$ and $VZ(Z \rightarrow c\bar{c})$ events, to approximately 3% and 5%, respectively. Misidentification of a $b\bar{b}$ pair as a $c\bar{c}$ pair has a significant impact on the determination of the $VH(H \rightarrow c\bar{c})$ signal strength, and the uncertainty of the misidentification rate is assumed to be 20% at the HL-LHC. Uncertainty due to the limited size of Run 2 simulated samples are neglected in the projection.

A combined fit of the $b\bar{b}$- and $c\bar{c}$-enriched categories is performed to simultaneously measure the $VH(H \rightarrow b\bar{b})$ and $VH(H \rightarrow c\bar{c})$ processes. The expected best fit values of the signal strength modifiers are:

$$\mu_{VH(H \rightarrow b\bar{b})} = 1.00 \pm 0.03(\text{stat}) \pm 0.04(\text{syst}),$$
$$\mu_{VH(H \rightarrow c\bar{c})} = 1.0 \pm 0.6(\text{stat}) \pm 0.5(\text{syst}).$$

The 2D profile likelihood scan as a function of $\mu_{VH(H \rightarrow b\bar{b})}$ and $\mu_{VH(H \rightarrow c\bar{c})}$ is displayed in Figure 5(a). The result is interpreted in the κ-framework and a 2D profile likelihood scan as a function of κ_b and κ_c is shown in Figure 5(b), where all the other Higgs couplings are fixed at the SM values.

2.2.6 Search for rare Higgs boson decays with mesons with CMS at the HL-LHC [60]

Rare decays of the Higgs boson into final states with quarkonium mesons Q have very low branching fractions in the SM, but they are promising laboratories to search for BSM physics. Such BSM physics might alter Yukawa couplings to quarks, possibly resulting in higher decay rates than predicted by the SM. In the SM, the Higgs decay vertices in the contributing amplitudes at leading order for the decay channels γQ, ZQ, and QQ are the same. First measurements at LHC find 95% CL upper limits on the branching fractions about 2 to 3 orders of magnitude larger than predicted by the SM [40]. Two decays of the 125 GeV Higgs boson are considered to benchmark the 95% CL upper limit reach with the CMS detector at the HL-LHC: into ZJ/ψ with sizable background, and into Υ pairs with negligible background. Both are representative for the different decay channels including mesons. The Z boson and the J/ψ and Υ mesons are reconstructed from their decay into $\mu^+\mu^-$. The channel with $Z \rightarrow e^+e^-$ is also included. The signal is searched for as resonant peak in the distribution of the four-lepton invariant mass. The results are obtained with MC simulated signal events and pseudodata simulated based on
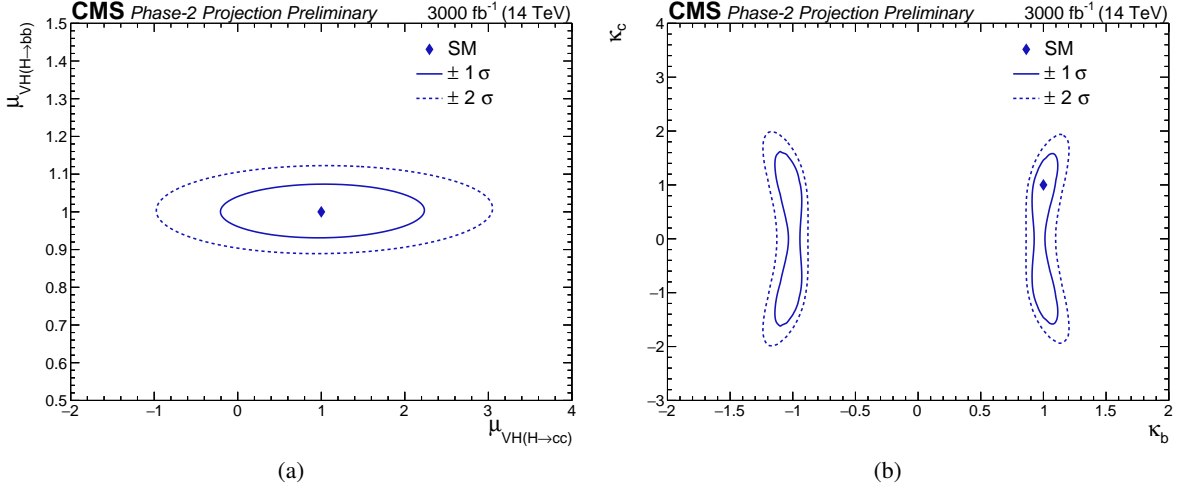
Figure 5: Profile likelihood scans as a function of (a) $\mu_{VH(H\to c\bar{c})}$ and $\mu_{VH(H\to b\bar{b})}$, and (b) κ_b and κ_c. The black marker shows the SM expected best fit point. The solid and dashed lines show the expected one and two standard deviation contours. [57]

parameterizations of the four-lepton invariant mass distributions obtained in Run 2. The samples are scaled to the HL-LHC integrated luminosity of 3000 fb^{-1}, and 4500 fb^{-1} to include the case of extended HL-LHC, and center-of-mass energy, $\sqrt{s} = 14$ TeV. The event selection is also reoptimized for the higher luminosity. Upper limits at 95% CL are determined with the modified frequentist CLs criterion, in which the profile likelihood ratio modified for upper limits is used as the test statistic.

The expected gain in the upper limit with respect to Run 2 values is found to be a factor 6 (7) for the ZJ/ψ final state and 27 (41) for the Υ pair final state at an integrated luminosity of 3000 fb^{-1} (4500 fb^{-1}). Similar factors are expected to apply to the related final states ZQ, γQ, or QQ. Particularly, the Υ pair decay of the Higgs boson is expected to be observed according to earlier SM predictions of decay rates of about 10^{-5}. At an integrated luminosity of 3000 fb^{-1}, observation of this channel requires the detection of more than 3 signal events, and evidence corresponds to more than one signal event. The upper limits are listed in Table 4 together with the factors with respect to SM predictions. Representative four-muon invariant mass distributions for the two channels under investigation are shown in Figure 6.

Table 4: Estimated upper limit branching fractions for rare Higgs decays into mesons at 95% CL, for integrated luminosities of 3000 and 4500 fb^{-1}. The factors with respect to SM predictions are listed in brackets. The $\Upsilon(nS)$ refers to the $n = 1, 2, 3$ states that are combined.

Channel	3000 fb^{-1}	($\times$SM)	4500 fb^{-1}	($\times$SM)
$H \to ZJ/\psi$	2.9×10^{-4}	(126)	2.7×10^{-4}	(117)
$H \to \Upsilon(mS)\Upsilon(nS)$	1.3×10^{-5}	(0.2)	8.5×10^{-6}	(0.14)
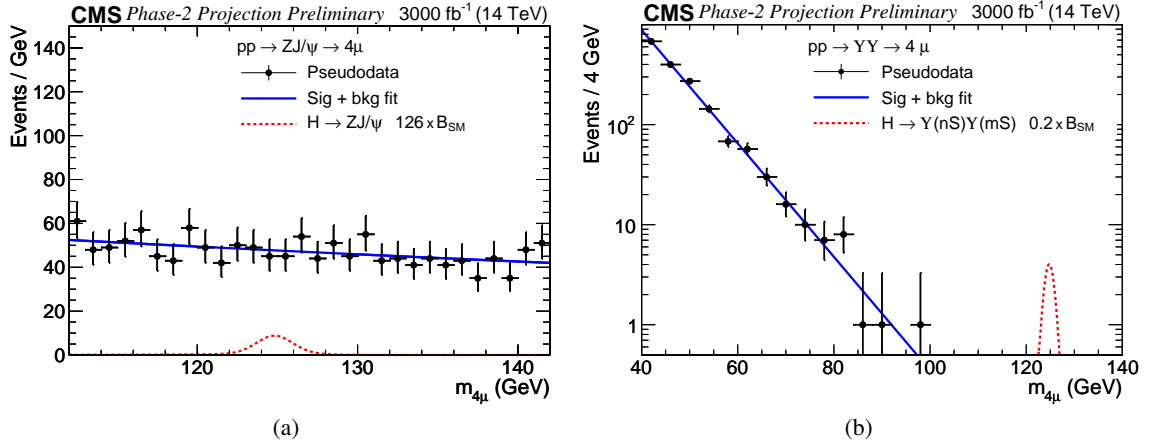
Figure 6: Four-muon invariant mass distributions for (a) a representative simulated ZJ/ψ and (b) $\Upsilon(mS)\Upsilon(nS)$ event sample with the fit to the background superimposed (blue line). The plots show simulated signals (dashed red line) normalized to the upper limit branching fractions in Tab. 4. [60]

2.2.7 Prospects for the measurement of $t\bar{t}H, H \rightarrow b\bar{b}$ production in the opposite-sign di-leptonic channel with CMS at the HL-LHC [61]

Measuring the coupling of the Higgs boson to the top quark, the heaviest known particle, is of major importance since it is a crucial parameter of the SM and may be sensitive to physics beyond it. Top quark-antiquark associated Higgs boson production ($t\bar{t}H$) is the best direct probe of the top-Higgs Yukawa coupling (y_t).

In this analysis, the expected sensitivity of the measurement of $t\bar{t}H$ production in the di-leptonic final state is investigated, with the Higgs boson decaying hadronically to a $b\bar{b}$ pair ($t\bar{t}H, H \rightarrow b\bar{b}$), produced in proton-proton (pp) collisions at $\sqrt{s} = 14$ TeV at the HL-LHC. The analysis approach uses a novel method for reconstructing the Higgs boson invariant mass by solving analytically the kinematic equations of the system, and a data driven approach to estimate the main background that stems from $t\bar{t}$ production.

Projections of the measurement significance are made for the integrated luminosity anticipated after Run 3 and the HL-LHC. Different scenarios for the size of the systematic uncertainties are employed. These include a scenario that assumes statistical uncertainties only, a scenario that assumes Run 2 uncertainties, a conservative scenario where uncertainties with statistical origin are scaled with the increase in luminosity, and a realistic scenario corresponding to the YR18 systematic uncertainties. The expected significance as a function of the integrated luminosity is shown in Figure 7(a), while in Figure 7(b) the signal strength modifiers, μ, are shown for different values of integrated luminosity and different uncertainty scenarios. With this analysis approach, one should be able to achieve observation of $t\bar{t}H$ production with the dilepton channel alone at 1000 fb^{-1} already. A measurement with 12% total uncertainty on the signal cross-section, which translates to a similar level of precision in measuring y_t, will allow us to probe possible deviations from the SM expectation.
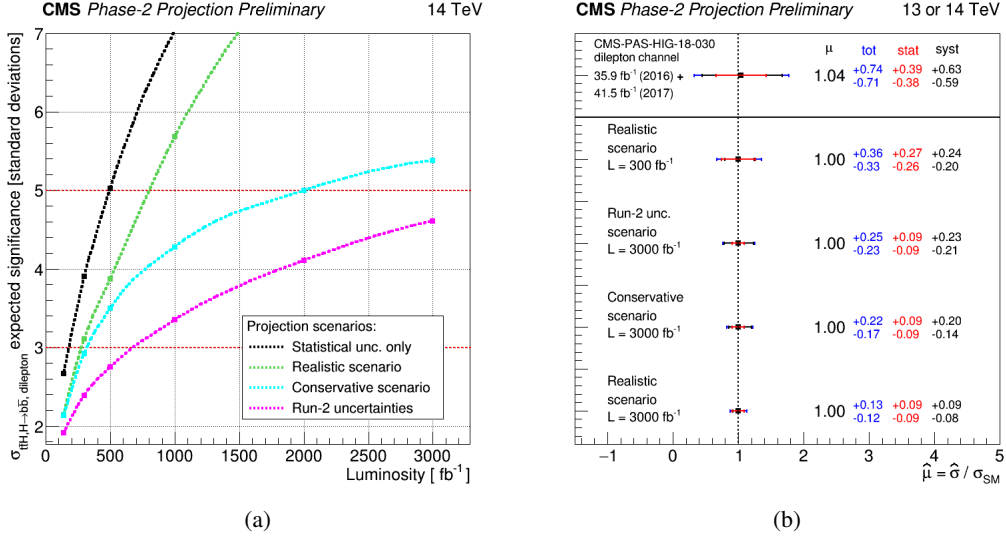
Figure 7: (a) Projected estimated significance shown as a function of the integrated luminosity for different uncertainty scenarios. (b) Best fit value of the signal strength modifier μ measured in the dileptonic channel in the latest CMS published result [62] (top) and for the fit of the Asimov dataset (background-only pre-fit) constructed for 300 fb^{-1} and 3000 fb^{-1} for different uncertainty scenarios. Also shown are the 68% expected confidence intervals (blue error bar) which are additionally split into their statistical (red error bar) and systematic (black error bar) components. [61]

2.2.8 Sensitivity to $H \to b\bar{b}$ and $H \to c\bar{c}$ decays in VH production with ATLAS at the HL-LHC [63]

Extrapolation setup The extrapolation from the Run 2 $VH, H \to b\bar{b}$ and $VH, H \to c\bar{c}$ analyses to the expectation for the HL-LHC is performed by scaling the signal and background expectations to an increased integrated luminosity of 3000 fb^{-1} and a center-of-mass energy of $\sqrt{s} =$ 14 TeV. Uncertainties related to limited simulation sample size are neglected.

$VH, H \to b\bar{b}$ extrapolation results The extrapolation is performed based on the analysis strategy outlined in Ref. [64]. The measurement of $H \to b\bar{b}$ decays is targeted, produced in association with a vector boson. Jets are identified as b-jets (b-tagged) using a multivariate discriminant. Analysis regions are split by vector boson momentum, jet multiplicity and signal/control regions, and a Boosted Decision Tree (BDT) output is used as the discriminating variable. At the HL-LHC, measurements in the WH and ZH production mode are expected to have a precision of 8% and 7% respectively. Cross-section measurements are performed in bins of p_T^V and jet multiplicity defined at truth level according to the reduced VH, V $\to$ leptons stage-1.2 Simplified Template Cross Sections (STXS) scheme [65]. The expected uncertainties vary between 8% in the highest p_T^V region and 17% in the lowest p_T^V region. The measurements is expected to be limited by systematic uncertainties, with the signal modeling uncertainties having the largest impact.

$VH, H \to c\bar{c}$ extrapolation results The $VH, H \to c\bar{c}$ analysis is described in Ref. [66]. A search is conducted for $H \to c\bar{c}$ decays produced in association with a vector boson. Jets are c-tagged using a multivariate discriminant and analysis regions are split by number of c-tags, vector boson momentum,

jet multiplicity and signal/control regions. The invariant mass of the two leading jets m_{cc} is used as the discriminant. At the HL-LHC an upper limit of 6.4 times the Standard Model prediction of the $VH, H \rightarrow c\bar{c}$ signal strength is expected at the 95% CL. The statistical and systematic uncertainties are expected to have a similar impact, and the largest single contribution to systematic uncertainties comes from the modeling of the $Z + \text{jets}$ background. The signal strength can be parameterized in terms of the Higgs boson coupling modifier κ_c, where a constraint of $|\kappa_c| < 3.0$ is expected at 95% CL at HL-LHC. The expected limit on the $VH, H \rightarrow c\bar{c}$, using the full Run-2 dataset, is a factor 4 lower in the analysis from the CMS Collaboration (see Sec. 2.2.5) than the expected limit from the ATLAS Collaboration [66]. Two main reasons for this difference are: the usage of advanced multivariate techniques in the analysis categories targeting two resolved jets, and the inclusion of boosted analysis categories using substructure methods.

$VH, H \rightarrow b\bar{b}/c\bar{c}$ extrapolation results   The two analyses can be combined by performing a fit to the $VH, H \rightarrow b\bar{b}$ and $VH, H \rightarrow c\bar{c}$ signal regions simultaneously and allowing both signal strengths to float. Uncertainties are left largely uncorrelated between the two analyses. The resulting expected best fit signal strengths at HL-LHC are $\mu_{VH}^{b\bar{b}} = 1.00 \pm 0.06$ and $\mu_{VH}^{c\bar{c}} = 1.00 \pm 3.20$. It is possible to perform a fit to the κ coupling modifiers, which results in an expected constraint of $|\kappa_c/\kappa_b| < 2.7$ at 95% CL (compared to 5.1 for the full Run-2 result). The resulting likelihood scans for the fit to the signal strengths and coupling modifiers are shown in Figure 8.
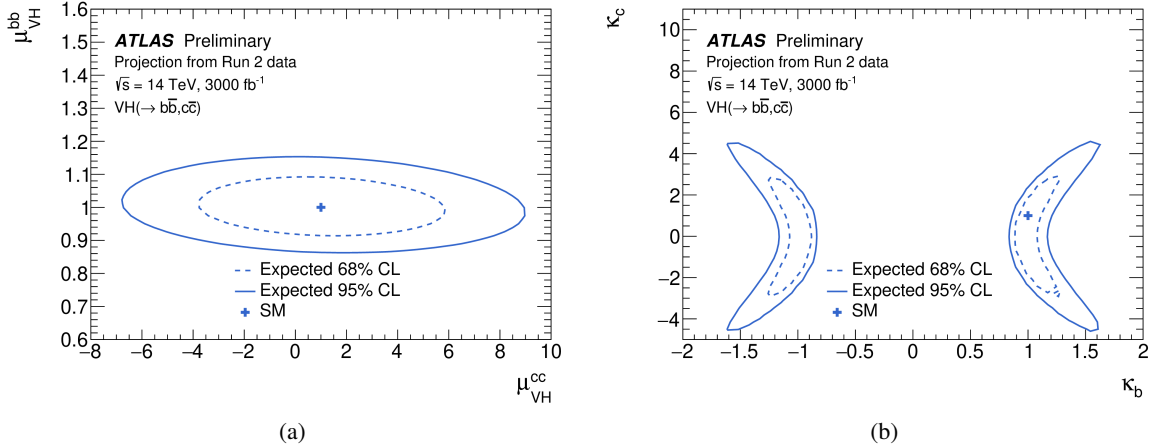
Figure 8: Expected profile likelihood scans for the $VH, H \rightarrow b\bar{b}/c\bar{c}$ combination extrapolated to a dataset of 3000 fb^{-1} at $\sqrt{s} = 14$ TeV. A two-dimensional scan is shown for (a) a simultaneous fit to $\mu_{VH}^{c\bar{c}}$ and $\mu_{VH}^{b\bar{b}}$ and (b) a simultaneous fit to κ_b and κ_c [63].

2.2.9 $H \rightarrow \tau\tau$ cross-section measurement results with ATLAS at the HL-LHC [67]

An extrapolation aiming to assess the expected sensitivity of $pp \rightarrow H \rightarrow \tau^+\tau^-$ cross-section measurements at the HL-LHC is performed using the results obtained with 139 fb^{-1} of pp collisions at $\sqrt{s} = 13$ TeV [68]. A HL-LHC scenario corresponding to a dataset of 3000 fb^{-1} of pp collisions at $\sqrt{s} = 14$ TeV is considered. The results consist of the measurement of the total $pp \rightarrow H \rightarrow \tau^+\tau^-$ cross-section as well as that of the four main Higgs boson production cross-sections. A study of their kinematic dependence is also presented within the Simplified Template Cross-Section (STXS) framework. The uncertainty related to the finite size

of Monte Carlo background samples is reduced under the assumption that the size of these samples will increase proportionately to the integrated luminosity.

At the HL-LHC, the inclusive $pp \to H \to \tau^+\tau^-$ cross-section measurement is projected to have a precision of 5%, corresponding to a value of $\sigma(pp \to H \to \tau^+\tau^-)_{\text{exp}}/\sigma(pp \to H \to \tau^+\tau^-)_{\text{SM}} = 1.00 \pm 0.05 = 1.00 \pm 0.01(\text{stat.}) \pm 0.04(\text{sig. th.}) \pm 0.02(\text{syst.})$.

The projected precision of the four dominant production mode measurements are 11%, 7%, 14% and 24% for ggF, VBF, VH and $t\bar{t}H$ respectively, which corresponds to the observation of all production modes except for $t\bar{t}H$, where the significance reaches 4.4σ. Theoretical uncertainties on the signal prediction dominate the uncertainty for the ggF and VBF projections, while in the VH projection there are similar contributions from experimental uncertainties and uncertainties coming from the data sample size. For the $t\bar{t}H$ projection, the largest impact is from the various experimental uncertainties, although closely followed by theoretical uncertainties on the signal prediction and from the data sample size. In all cases systematic uncertainties have a larger contribution than the statistical ones from the data sample size. These results are presented in a comparison to their Run 2 counterparts and to the current and projected theoretical uncertainties in Figure 9.

In the STXS framework, the most sensitive projected measurements are the VBF $+ V(\to qq)H$ cross-section in events with at least two jets and a di-jet invariant mass of at least 350 GeV (VBF topology), with an uncertainty of 7%, and the ggF $+ gg \to Z(\to qq)H$ cross-section in events with Higgs boson transverse momentum between 200 and 300 GeV, with an uncertainty of 10%, and above 300 GeV, with an uncertainty of 11%. The last two are expected to be some of the most sensitive measurements of Higgs boson production in that momentum range possible at the HL-LHC. All other STXS bins are projected to have uncertainties below 25% except for the bin corresponding to ggF $+ gg \to Z(\to qq)H$ events with at least two jets, di-jet invariant mass above 350 GeV and Higgs boson transverse momentum below 200 GeV, which is expected to reach a precision of around 50%. These results are also shown in Figure 10 in a comparison to the Run 2 measurements and to the current and projected theoretical uncertainties.

2.3 Higgs boson pair production and Higgs boson self-coupling. Yellow Report Summary

The study of the Higgs boson self-interaction is one of the primary goals of the HL-LHC due to its role in cosmological theories involving, for example, the vacuum stability and inflation. Among all the Higgs boson self-interaction terms, the trilinear self-interaction is the only one in the reach of the HL-LHC and it is parametrized by the coupling strength $\lambda_{HHH} = m_H^2/2v^2$. A direct measurement of λ_{HHH} would provide constraints on the shape of the Higgs potential and the verification of the EWSB mechanism of the SM. The existence of an extended scalar sector or the presence of new dynamics at higher energy scales could also modify the measured value of λ_{HHH} with respect to the SM prediction $\lambda_{HHH}^{\text{SM}} \cong 0.13$. These effects are generally quantified using the Higgs boson self-coupling modifier $\kappa_\lambda \equiv \lambda_{HHH}/\lambda_{HHH}^{\text{SM}}$.

Higgs boson pair production (HH) generally offers the most sensitive signature to set direct constraints on λ_{HHH}. The production rate of HH events in the SM is approximately 1000 times smaller than that of single Higgs bosons, which makes this process extremely challenging to measure at the HL-LHC. In this context, a statistical combination of the complete datasets collected by the ATLAS and CMS experiments at the HL-LHC will be needed to maximize the sensitivity to HH production and provide maximal constrains on λ_{HHH}.
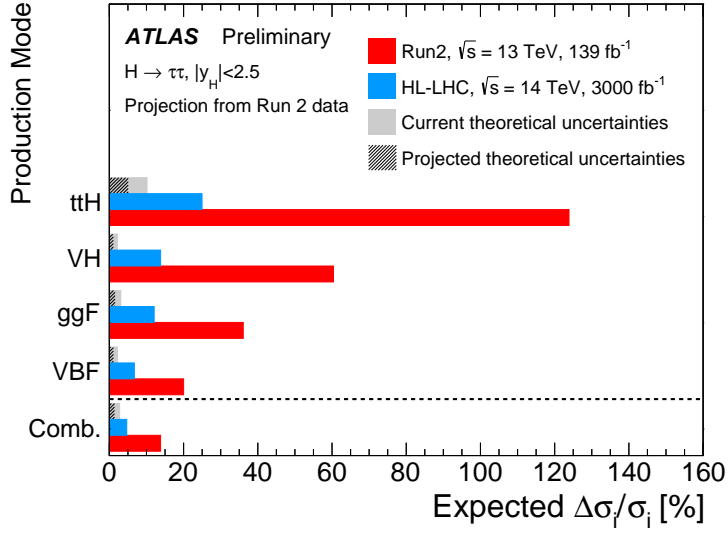
Figure 9: Run 2 (red) and projected HL-LHC (blue) expected precision of the $H \to \tau^+\tau^-$ production mode measurements for ggF, VBF, VH and $t\bar{t}H$, scaled to their cross-section expectation values. The precision of the combined result for the inclusive cross-section, also scaled to its expectation value, is included at the bottom. The uncertainty on the predicted signal cross-section for each production mode, illustrating the current (light grey) and projected HL-LHC (hashed) precision of theory calculations, is also shown. [67]
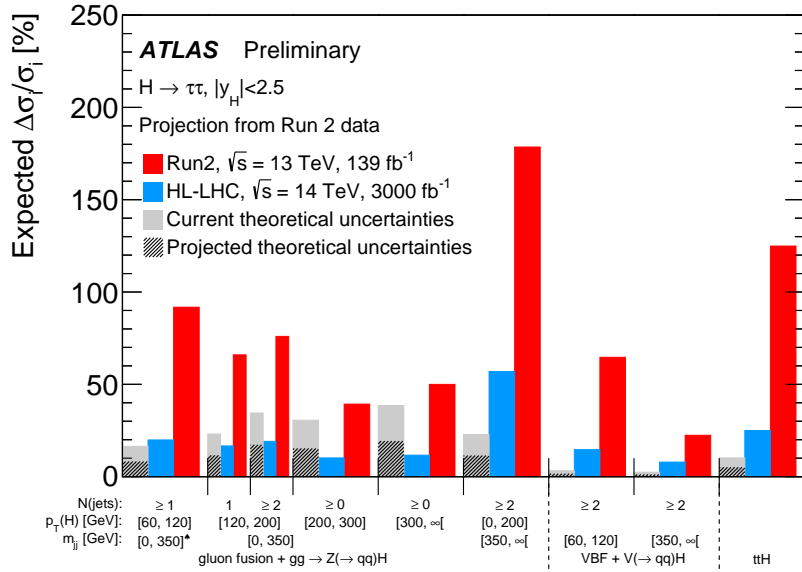
Figure 10: Run 2 (red) and projected HL-LHC (blue) expected precision of the $H \to \tau^+\tau^-$ measurement scaled to the cross-section expectation value ($\Delta\sigma_i/\sigma_i$) in various STXS bins labelled i. The uncertainty on the predicted signal cross-section in each bin is also shown, illustrating the current (light grey) and projected HL-LHC (hashed) precision of theory calculations. [67]

The production of pairs of Higgs bosons is dominated by the gluon-gluon fusion (ggF) process followed by the vector-boson fusion (VBF) one. The small SM cross-sections of these processes implies that the main experimental signatures will be those where at least one of the two Higgs bosons decays into a final state with a large branching ratio, *i.e.* $H \to b\bar{b}$. Among all the possible channels, the most sensitive signatures are $HH \to b\bar{b}b\bar{b}$, $HH \to b\bar{b}\tau^+\tau^-$ and $HH \to b\bar{b}\gamma\gamma$, with branching ratios of 33.9%, 7.3% and 0.26% respectively. Other channels, such as $b\bar{b}ZZ$, $b\bar{b}W^+W^-$, $W^+W^-\gamma\gamma$, $\tau^+\tau^-\gamma\gamma$ are also explored. Due to the different experimental advantages of each decay channel, these analyses are complementary to target BSM physics effects in HH. Even though at the end of the LHC Run 2 some of the systematic effects of these searches are starting to play a role, statistical uncertainties are the dominant source of uncertainty limiting the sensitivity to the search of the SM HH process. At the HL-LHC, the impact of systematic uncertainties will become more important due to the significant reduction of statistical uncertainties.
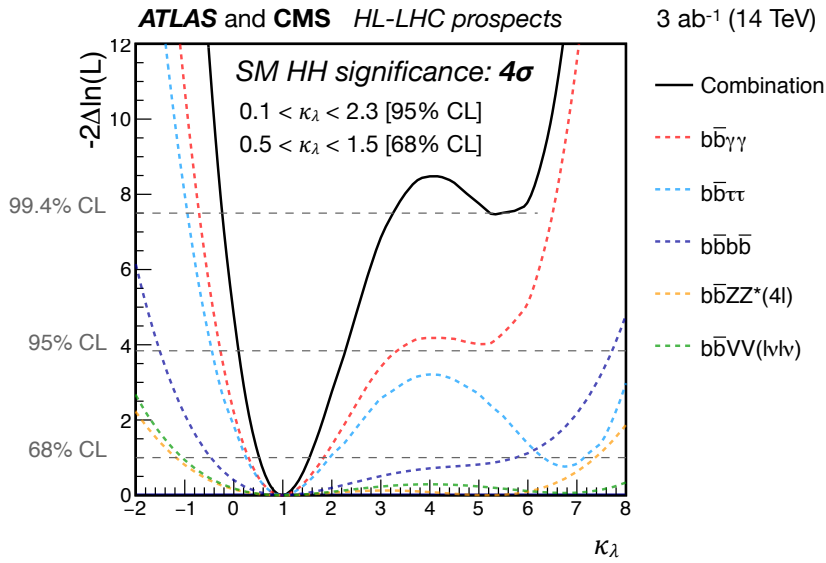
Figure 11: Negative-log-likelihood scan as a function of κ_λ, calculated by performing a conditional signal+background fit to the background and SM signal. The colored dashed lines correspond to the combined ATLAS and CMS results by channel, and the black line their combination. [3]

In the YR, combined projections of the ATLAS and CMS Collaborations [69, 70] showed that a discovery significance of 4.0σ can be achieved with 3000 fb^{-1}. When systematic uncertainties were neglected, statistical significance was shown to increase to 4.5σ. In addition to the significance, the combined ATLAS and CMS sensitivity to κ_λ was also assessed through likelihood scans, as shown in Figure 11. These curves illustrate the analysis likelihoods when the shapes and normalizations of the HH signal distributions, as well as the normalizations of the single Higgs boson background distributions, are modified with κ_λ. Through estimation of 68% CL (1σ) κ_λ intervals, these curves express the separation power of the single and combined HH searches between the hypotheses $\kappa_\lambda = 1$ and $\kappa_\lambda \neq 1$. After combination, the total 68% CL intervals are expected to be

$$0.52 \leq \kappa_\lambda < 1.5 \quad \text{with systematic uncertainties,} \tag{1}$$

$$0.57 \leq \kappa_\lambda < 1.5 \quad \text{without systematic uncertainties,} \tag{2}$$

The second minimum at $\kappa_\lambda \approx 6.0$, caused by the limited signal acceptance of some analyses, was shown to be excluded at 99.4% CL after combination of all the different analyses. The hypothesis corresponding to

the absence of self-coupling ($\kappa_\lambda = 0$) was also excluded at the 95% CL when partial Run 2 systematic uncertainties were included.

Single Higgs boson measurements offer a complementary approach to constrain κ_λ due to the next-to-leading order electro'weak corrections of single Higgs production from κ_λ [71–73]. CMS studied the HL-LHC reach with an interpretation of the $t\bar{t}H+tH$, $H \to \gamma\gamma$ differential cross-section measurements at 3000 fb^{-1} in terms of deviations of the self coupling, setting limits at 95% CL of $-4.1 < \kappa_\lambda < 14.1$ [42]. Incorporating other decay and production modes will increase the sensitivity of this approach.

For the Snowmass 2021 process, some of these projections were updated to the latest Run 2 analysis methodologies and expected HL-LHC detector performance. New results are discussed in the next section.

2.4 New results

2.4.1 Prospects for nonresonant HH production measurement in $bb\gamma\gamma$ final states with CMS at the HL-LHC [74]

In this study, the production of Higgs pair production through gluon-gluon fusion (ggHH) and vector-boson fusion (VBF) is studied in the $b\bar{b}\gamma\gamma$ final state using Delphes simulated samples.

The analysis uses machine learning techniques at various stages to discriminate the signal against the background after preliminary selections. By categorizing the signal sensitivity becomes enhanced. There are two different classes of backgrounds; (i) nonresonant or continuum: $\gamma\gamma/\gamma + $ jets, $t\bar{t} + \gamma\gamma$, $t\bar{t} + \gamma + $ jets, $t\gamma+$jets, inclusive $t\bar{t}$ and (ii) single Higgs boson production with $H \to \gamma\gamma$. Events are required to have two isolated photons and two b jets within pseudorapidity of $|\eta| < 2.5$. The jets are reconstructed with anti-k_t clustering algorithm with a distance parameter R=0.4. The conditions on transverse momenta are $p_T(\gamma_1, \gamma_2) > 30, 20$ GeV and $p_T(\text{b-jet}) > 30$ GeV. Individual Higgs boson candidates are formed using invariant mass constraints: $m_{\gamma\gamma}$: [100, 180] GeV and m_{bb}: [70, 190] GeV where the 2 jets are selected for pair-wise highest sum of b-tagged score. For VBF event selection, additionally, two jets with $|\eta| < 5$ and $p_T > 40$ and 30 GeV are required with the highest available invariant mass (m_{jj}).

Among all the $H \to \gamma\gamma$ processes, the dominant single Higgs boson production mode ($H + X$) in the signal region is $t\bar{t}H$, since it replicates the same final state of two b jets originating from the top quarks. Hence a multivariate discriminant, based on Gradient BDT, has been developed to reject the $t\bar{t}H$ events with 90% signal efficiency and $t\bar{t}H$ background rejection of about 85%(90%) in the ggHH (VBFHH) event class.

After the kinematic selection the rates of the nonresonant $\gamma\gamma + $ jets and $\gamma + $ jets background processes remain overwhelming compared to ggHH+VBFHH signal. Consequently a second discriminant is trained to classify the event sample in terms of purity against $\gamma\gamma/\gamma + $ jets backgrounds, separately for ggHH and VBFHH events. Furthermore, the correlation between the reconstructed invariant masses of the HH system and the individual Higgs boson candidates is also used to separate between signal and background events.

The extraction of the signal significance is performed via a simultaneous fit to the $m_{\gamma\gamma}$ and m_{bb} distributions assuming they are uncorrelated. The shapes of $m_{\gamma\gamma}$ signal and single H backgrounds are modeled by a Crystal Ball function in the range of [115,135] GeV. The m_{bb} is fitted by a combined function consisting of the sum of a Crystal Ball and a Gaussian function. The continuum backgrounds in $m_{\gamma\gamma}$ and m_{bb} distributions are modeled with exponential functions.

The extracted significance for the SM ggHH+VBFHH signal is estimated to be 2.16 σ compared to 1.8 σ reported in the previous projection.

2.4.2 Prospects for HH measurements in the $W^+W^-\gamma\gamma$ and $\tau^+\tau^-\gamma\gamma$ final states with CMS at the HL-LHC [75]

A di-Higgs search in the WW$\gamma\gamma$ and $\tau\tau\gamma\gamma$ channels is performed benefitting from the sensitive $H \to \gamma\gamma$ process which provides a clean and distinguishable signature [75]. This is the first study providing the expected significance numbers in these channels at the HL-LHC. In the WW$\gamma\gamma$ process, three final states are possible, as the W boson can decay both leptonically and hadronically: Semi-Leptonic ($WW \to qql\nu$), Fully-Leptonic ($WW \to l\nu l\nu$) and Fully-Hadronic ($WW \to qqqq$) decay modes, where $l = e, \mu$ or τ. For the Fully-Hadronic decay mode, QCD induced processes are a major background and given the limited size of the Monte Carlo samples, this background is not well described. Hence, this final state is not considered in this study. The other two final states are tagged with separate selections and categorization, and their corresponding signal and background estimates are combined with these from the $\tau\tau\gamma\gamma$ channel to improve the overall analysis sensitivity.

All the signal and background samples are simulated with Phase-2 upgraded CMS detector geometry using DELPHES fast simulation with average pile-up of 200 interactions and at $\sqrt{s} = 14$ TeV. The signal samples are generated separately for the three possible final states in WW$\gamma\gamma$. For $\tau\tau\gamma\gamma$ signal samples, all possible decays for taus are allowed in the same sample. The analysis is affected by backgrounds from single-Higgs-boson production modes and by non-resonant backgrounds mainly coming from $\gamma\gamma$+jets, γ+jets, Z/W+jets and top induced backgrounds.

All the events are required to have invariant mass of photons ($m_{\gamma\gamma}$) in the range $100 < m_{\gamma\gamma} < 180 GeV$, where leading (subleading) photon is required to have transverse momentum (p_T) above 35 GeV (25 GeV). Minimal lepton (e/μ) p_T is required to be 10 GeV, while for taus this requirement is 20 GeV. All the photons, leptons and taus are required to be within $|\eta| < 2.5$. Events are then categorized in four mutually exclusive final states with exactly one lepton, at least two leptons, one tau, and at least 2 taus. A multiclass Deep Neural Network (DNN) is employed in the one lepton final state and in the one τ final state whereas the remaining two final states use a cut-based approach. Based on the DNN score in one lepton (one τ) final state, 4 (2) categories are defined to get the best sensitivity.

The invariant mass distribution of the two photons for the one lepton final state inclusive of all categories are shown in Figure 12. The expected significance is extracted by fitting the $m_{\gamma\gamma}$ distributions in all the categories using a binned maximum likelihood approach with all systematic uncertainties treated as nuisance parameters with log-normal distributions using the Higgs Combine tool. Given high fluctuations in the $m_{\gamma\gamma}$ distribution for the continuum background across different categories, the shape fitted with exponential function has been used for describing the continuum background. The correlations among different sources of uncertainties are taken into account while the different final states are considered as independent channels in the fit.

Combining all final states, the expected significance for signal in WW$\gamma\gamma$ and $\tau\tau\gamma\gamma$ is 0.22σ including systematic uncertainties at integrated luminosity of 3000 fb^{-1} at the HL-LHC.
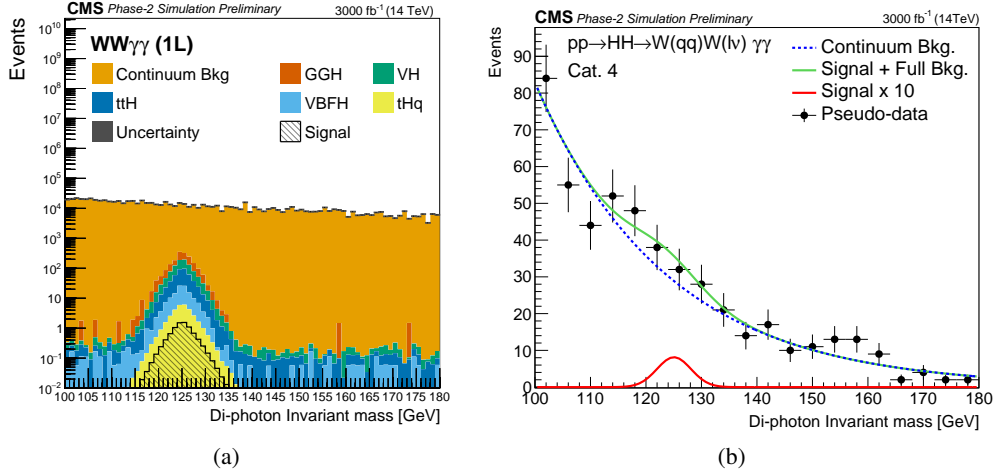
Figure 12: $m_{\gamma\gamma}$ distribution in (a) one leptonic final state and (b) its most sensitive category. In (b), for illustration purposes, signal along with the single Higgs and continuum background is described using a Gaussian and exponential function. The (pseudo-)data are generated using the fit parameters and scaled according to the total contribution from signal, single Higgs and continuum backgrounds, normalized to an integrated luminosity of 3000 fb^{-1}.

2.4.3 Search for the nonresonant $t\bar{t}HH$ production in the semileptonic decay of the top quark pair and the Higgs boson pair decaying into b-quarks with CMS at the HL-LHC [76]

The production of a top quark-antiquark pair associated with a pair of Higgs bosons (t$\bar{t}$HH) has the third largest cross section among the HH production modes, and offers the possibility to explore the interplay between the HH and t$\bar{t}$H measurements. This process is also highly sensitive to BSM contributions. A dedicated analysis is performed to assess the experimental sensitivity to t$\bar{t}$HH with the upgraded Phase-2 CMS detector at the HL-LHC [76]. In addition, the study explores the HL-LHC sensitivity to BSM contributions to t$\bar{t}$HH within the context of the Minimal Composite Higgs Models (MCHM). The analysis considers Higgs boson decays to b-quark pairs and semileptonic decays of the top quark pair, which leads to final states with a single lepton, multiple jets, multiple b-jets and moderate missing transverse momentum.

The study is based on signal and background events generated at a center-of-mass energy of $\sqrt{s}$ =14 TeV. Signal consists of the SM t$\bar{t}$HH process, which has a cross section of 0.948 fb. Additionally, two representative MCHM benchmark scenarios, namely MCHM$_5^{C2}$ (1.47 fb) and MCHM$_{14}^{D7}$ (2.15 fb), are generated. Backgrounds include t$\bar{t}$+jets, t$\bar{t}$ + 4b, t$\bar{t}$H, t$\bar{t}$Z, t$\bar{t}$ZZ and t$\bar{t}$ZH. The samples with Higgs and/or Z boson production are all simulated including only the Higgs or Z boson decay into a pair of b-quarks, except the t$\bar{t}$Z sample which is inclusive in both t$\bar{t}$ and Z. The Phase-2 CMS detector response is simulated using the DELPHES fast detector simulation framework.

The candidate t$\bar{t}$HH events are required to have exactly one lepton, $\geq$ 4 jets, $\geq$ 3 b-jets and $p_T^{miss} > 20$ GeV. A 2-step DNN is implemented to enhance the signal sensitivity, based on input including jet and b-jet multiplicities, jet and b-jet transverse momenta and pseudorapidities, b-jet identification scores, hadronic transverse momenta, mass averages, angular separation variables and event shape variables. Additionally, χ^2 values obtained from reconstructing the HH, ZZ and HZ systems are included along with masses of the reconstructed Higgs and Z bosons. In the first step, a DNN is trained to compute a discriminant separating

tṫHH, tṫZH and tṫZZ events. This discriminant and all other variables are input to the second DNN, which classifies the selected events into several categories with different expected signal and background rates. Dedicated DNNs are trained for the SM and MCHM tṫHH signals. After the DNN categorization, events are divided into three channels based on their b-jet multiplicity, having number of jets $N_{jets} = 3, = 4$ and ≥ 5, respectively.

A statistical analysis is performed by simultaneously fitting the multi-classifier DNN discriminants in all available categories for the three b-jet multiplicity channels using a profile likelihood ratio method, which includes the effect of the systematic uncertainties on signal and backgrounds as nuisance parameters. With 3000 fb^{-1}, and considering the YR18 systematic uncertainties, it is expected that the upper limit at the 95%CL on the combined tṫZZ + ZH + HH production cross section is $0.84^{+0.34}_{-0.54}\times$ SM. If tṫZZ is taken as background, the upper limit on the combined tṫZH + HH production is expected to be $1.31^{+0.53}_{-0.37}\times$ SM. If tṫZZ + ZH are taken as backgrounds, the upper limit on the tṫHH production alone is expected to become $3.14^{+1.27}_{-0.9}\times$ SM. For the MCHM case, the upper limits at the 95% CL on the tṫHH cross sections are obtained as $1.72^{+0.76}_{-0.53} \times$ MCHM$_5^{C2}$ and $1.08^{+0.43}_{-0.30} \times$ MCHM$_{14}^{D7}$, respectively. Figure 13 summarizes the signal strength expectations for the SM and MCHM cases for the three alternative scenarios of systematic uncertainties considered in this analysis.

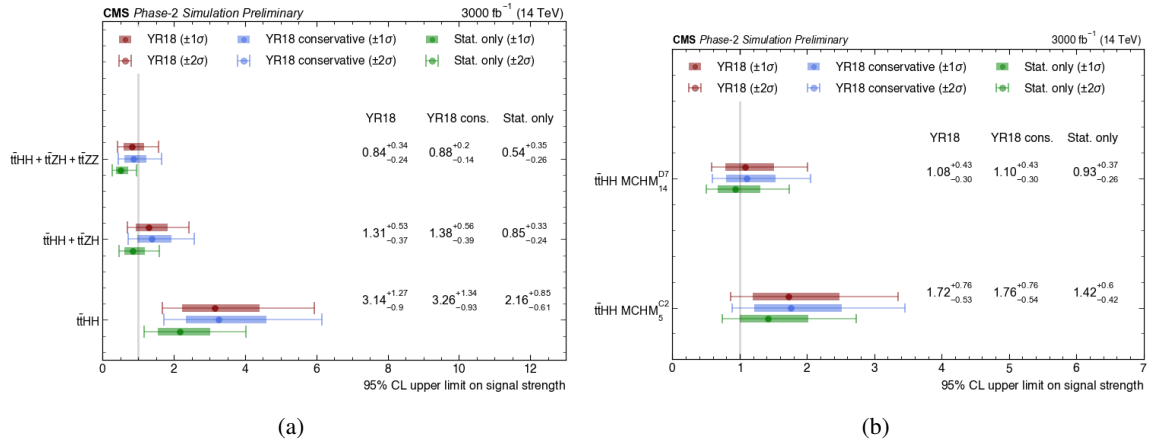Figure 13: The 95% upper limits on the signal strength shown for (a) the SM tṫHH, tṫHH + tṫZH and tṫHH + tṫZH + tṫZZ processes and (b) the BSM tṫHH processes predicted by the MCHM$_5^{C2}$ and MCHM$_{14}^{D7}$ scenarios for different scenarios of systematic uncertainties. [76]

2.4.4 Updated prospects of Higgs boson pair production in the $b\bar{b}\gamma\gamma$ and $b\bar{b}\tau^+\tau^-$ final states with ATLAS at the HL-LHC [77–80]

Following the results presented in Ref. [3], the ATLAS Collaboration updated the projections for non-resonant HH production, based on refined b-tagging performance estimates for HL-LHC [77] and yielding a combined significance for the main channels $HH \to b\bar{b}b\bar{b}$, $b\bar{b}\tau^+\tau^-$ and $b\bar{b}\gamma\gamma$ of 2.9σ (3.3σ) with (without) systematic uncertainties. In response to the Snowmass 2021 process, several updates have been produced regarding the HL-LHC projections for non-resonant HH production in the $b\bar{b}\gamma\gamma$ and $b\bar{b}\tau^+\tau^-$ final states [78, 79]. These results contain substantial improvements with respect to the previous projections, in particular regarding the analysis methodologies which were updated to the latest Run 2 analyses [81, 82]. A statistical combination of these updated projections was also performed starting from the updated $HH \to b\bar{b}\tau^+\tau^-$ and $HH \to b\bar{b}\gamma\gamma$ results [80].

This section presents a short summary of the updated projections, which were obtained by scaling the likelihoods of the most recent Run 2 results at $\sqrt{s}=13$ TeV to a total integrated luminosity of $3000\,\mathrm{fb}^{-1}$ at $\sqrt{s}=14$ TeV. Effects of κ_λ on VBF processes, not considered in the previous iteration of the HL-LHC projections, were introduced in the updated results. Object reconstruction and identification efficiencies at the HL-LHC are assumed to be identical to the full Run 2 analysis. In particular, revised studies of the updated ATLAS Inner Tracker layout at the HL-LHC confirmed a similar performance in b-tagging efficiency relative to the latest Run 2 performance [24]. Improvements to the estimation of systematic uncertainties are considered by testing different uncertainty scenarios:

1. No systematic uncertainties scenario;

2. Baseline scenario: YR18 systematic uncertainties;

3. Theoretical uncertainties halved scenario: theoretical uncertainties reduced by a factor of 2 while experimental uncertainties kept at the same level as in Run 2;

4. MC stat. uncertainties neglected scenario: Monte Carlo statistical uncertainties are removed while all other uncertainties are kept at the same level as in Run 2;

5. Run 2 systematic uncertainties scenario: same theoretical and experimental uncertainties as in Run 2.

$HH \to b\bar{b}\tau^+\tau^-$ projection [78] The Run 2 $HH \to b\bar{b}\tau^+\tau^-$ analysis [81] exploits the large branching ratio of the $b\bar{b}\tau^+\tau^-$ channel (7.3%) to search for Higgs boson pair production in events with two b-tagged jets and two τ-leptons. The leptonic tau selection is used to categorize events in two different regions: the $\tau_{\mathrm{had}}\tau_{\mathrm{had}}$ region, which looks at events with two opposite-sign τ-leptons, and the $\tau_{\mathrm{lep}}\tau_{\mathrm{had}}$ region, which targets semi-leptonic tau decays by selecting events with one lepton (e/μ) and one hadronic tau with opposite charge. After categorization, a set of multivariate (MVA) discriminants is used to separate HH signals from background processes represented by top-quark, Z+jets, W+jets, di-boson, single Higgs boson and multi-jet production. In the full Run 2 search, the $b\bar{b}\tau^+\tau^-$ analysis set 95% CL observed (expected) upper limits on the SM HH signal strength at 4.7 (3.9) and 135 fb (114 fb) on the SM HH cross-section.

The updated $HH \to b\bar{b}\tau^+\tau^-$ projection leads to a 95% CL upper limit on the HH signal strength of 0.71 times the SM prediction. The previous extrapolation, based on the partial Run 2 dataset [70], yielded a limit of 0.99 times the SM prediction. This constitutes an improvement of 28%, which can be attributed to the updated reconstruction algorithms [83–85] and analysis methods used in the Full Run 2 search. Similarly, the significance of the SM HH production is now projected to be 2.8σ at the HL-LHC, while it

Figure 14: (a) Projected significance and (b) likelihood distributions as a function of κ_λ for the $HH \to b\bar{b}\tau^+\tau^-$ channel [78].

reached 2.1σ in the previous extrapolation. The κ_λ dependency of the statistical significance is shown in Figure 14(a). Under the baseline uncertainty scenario, evidence ($> 3\sigma$) for HH production can be found at the HL-LHC if $\kappa_\lambda < 0.8$ or $\kappa_\lambda > 6.3$, while a discovery ($> 5\sigma$) can be made if $\kappa_\lambda < -0.6$ or $\kappa_\lambda > 7.8$. Figure 14(b) shows the κ_λ likelihood scans in the $\tau_{\text{had}}\tau_{\text{had}}$, $\tau_{\text{lep}}\tau_{\text{had}}$ regions and their combination. Aside from the minimum at $\kappa_\lambda = 1$, the likelihood curves show a second minimum at $\kappa_\lambda \approx 6$. This is due to an increase of the HH cross-section and the simultaneous decrease of the signal acceptance leading to a similar signal shape to the $\kappa_\lambda = 1$ signal. Assuming baseline uncertainties, the updated $b\bar{b}\tau^+\tau^-$ projection provides 1σ confidence interval (CI) at $\kappa_\lambda \in [0.3, 1.9] \cup [5.2, 6.7]$ which, compared to the previous projection, results in an improvement of 28%. While the full Run 2 search is dominated by statistical uncertainties, the updated projection clearly shows that systematic uncertainties will become a limiting factor of the $b\bar{b}\tau^+\tau^-$ analysis at the HL-LHC. In particular, the theoretical uncertainties related to the production of ggF HH in association with b and c jets, as well as the uncertainty of single top-quark production related to the interference between the Wt and $t\bar{t}$ processes, are found to be the leading uncertainties in the projection results, aside of the Monte Carlo statistical uncertainties which will be significantly reduced in the next years. This can also be seen on Figure 14(a), where the gap between the baseline and Run 2 systematics scenarios is shown to be mainly due to these systematic uncertainties. In future, the reduction of systematic uncertainties from the theory community will represent an essential ingredient to measure HH production at the HL-LHC.

$HH \to b\bar{b}\gamma\gamma$ projection [79]   The Run 2 $HH \to b\bar{b}\gamma\gamma$ analysis [82] exploits the large $H \to b\bar{b}$ branching ratio in combination with the excellent ATLAS photon resolution, allowing the search for a sharply peaking $H \to \gamma\gamma$ signal in the smoothly falling distribution of the $m_{\gamma\gamma}$ di-photon mass spectrum. The analysis was performed using the complete Run 2 dataset ($139\,\text{fb}^{-1}$) collected with the ATLAS detector during the 2015-2018 period, and it employed events containing two photons and two b-tagged jets. A categorization based on the output of a BDT discriminant and the modified four-body mass $m^*_{b\bar{b}\gamma\gamma} = m_{b\bar{b}\gamma\gamma} - (m_{b\bar{b}} - 125\,\text{GeV}) - (m_{\gamma\gamma} - 125\,\text{GeV})$ allowed to increase significantly the sensitivity of this search with respect to the partial Run 2 results ($36\,\text{fb}^{-1}$) [86]. The variable $m^*_{b\bar{b}\gamma\gamma}$ is sensitive

to κ_λ, and it is used to define a high mass region ($m^*_{b\bar{b}\gamma\gamma} \geq 350\,\text{GeV}$) targeting SM-like signals, as well as a low mass region ($m^*_{b\bar{b}\gamma\gamma} < 350\,\text{GeV}$) targeting BSM-like scenarios. In the full Run 2 search, the statistical results were obtained from a simultaneous fit of the $m_{\gamma\gamma}$ distribution in all the analysis categories, and 95% CL observed (expected) upper limits were set at $130\,\text{fb}$ ($180\,\text{fb}$) on the non-resonant HH production cross-section and 4.2 (5.7) on the SM signal strength. The allowed κ_λ range was found to be $\kappa_\lambda \in [-1.5, 6.7]$ ($\kappa_\lambda \in [-2.4, 7.7]$) at 95% CL.
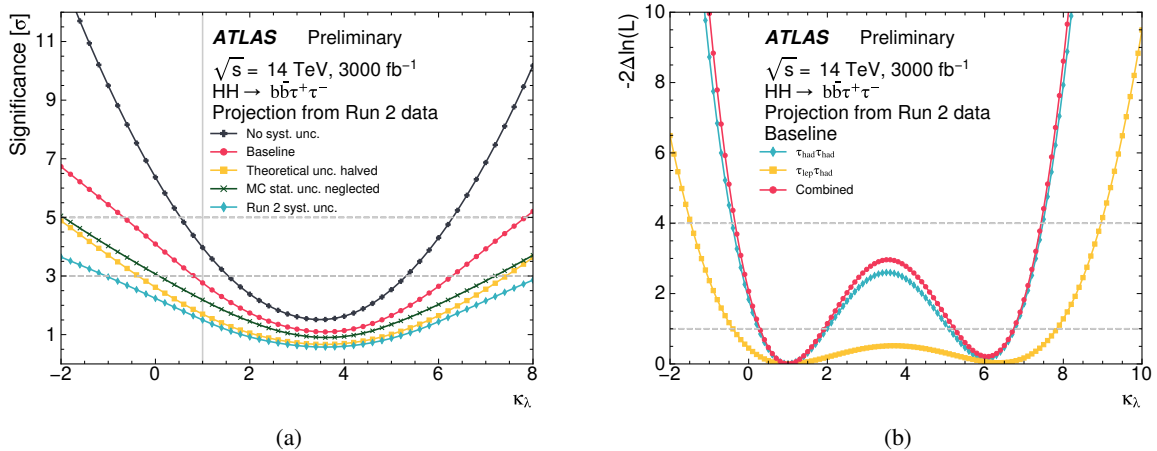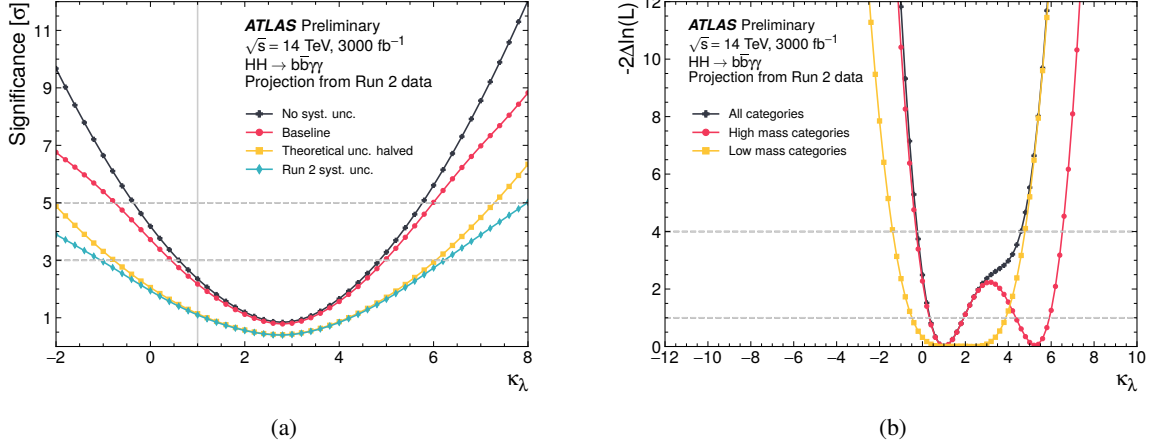

Figure 15: (a) Projected significance and (b) likelihood distributions as a function of κ_λ for the $HH \rightarrow b\bar{b}\gamma\gamma$ channel [79].

In the updated $HH \rightarrow b\bar{b}\gamma\gamma$ projection, the significance of the SM signal ($\kappa_\lambda = 1$) with (without) the baseline HL-LHC systematic scenario is found to be 2.2σ (2.3σ), while the 95% CL upper limits on the SM signal strength are set at 0.93 (0.86) with a precision of 50% (46%). This represents a clear improvement with respect to the previous projection, which placed the expected significance at 2.0σ (2.1σ) with (without) systematic uncertainties [70]. The dependency of the significance on κ_λ in different systematic uncertainty scenarios is shown in Figure 15(a). Figure 15(b) shows the relative dependency of the high mass and low mass categories on the total likelihood curve in the baseline systematic scenario. Here, it can be seen that the high mass categories offer a superior precision near $\kappa_\lambda = 1$, but they are unable to disentangle the minimum at $\kappa_\lambda = 1$ from the secondary likelihood minimum at $\kappa_\lambda \approx 5$ also observed in the $HH \rightarrow b\bar{b}\tau^+\tau^-$ projection. Nevertheless, the low-mass categories are capable to exclude this secondary minimum at 95% CL thanks to the higher signal acceptance of the $b\bar{b}\gamma\gamma$ analysis which allow these categories to be more sensitive to BSM κ_λ scenarios. The combination of all categories results in a 1σ confidence interval (CI) on κ_λ of [0.3, 1.9] ([0.4, 1.8]) with (without) systematic uncertainties. This represents again an improvement with respect to the previous $b\bar{b}\gamma\gamma$ projection, which established the allowed 1σ CI at [−0.2, 2.5] ([−0.1, 2.4]).

Combined $HH \rightarrow b\bar{b}\tau^+\tau^-$ and $HH \rightarrow b\bar{b}\gamma\gamma$ projection [80] The combination of the updated $HH \rightarrow b\bar{b}\tau^+\tau^-$ and $HH \rightarrow b\bar{b}\gamma\gamma$ projections [80] is performed through multiplication of the single analysis likelihoods into a combined likelihood function. The different searches are then fit to the data in order to constrain simultaneously the parameters of interest and the nuisance parameters. The systematic uncertainties of various analyses are correlated following the strategy of Ref. [87].

The expected SM HH signal significance and the measured signal strength in the updated projection is shown in Figure 16(a) for the various systematic uncertainties scenarios also assumed in the $b\bar{b}\tau^+\tau^-$ and $b\bar{b}\gamma\gamma$ projections. In the baseline scenario, a significance of 3.2σ is expected to be reached at the HL-LHC when combining the $b\bar{b}\tau^+\tau^-$ and $b\bar{b}\gamma\gamma$ channels. This result represents an improvement with respect to the previous ATLAS projection [77], which provided a total combined significance of 2.9σ when combining the $b\bar{b}\tau^+\tau^-$, $b\bar{b}\gamma\gamma$ and $b\bar{b}b\bar{b}$ final states. In the updated projection, when systematic uncertainties are not considered, the combined significance increases to 4.6σ. This represents another important improvement with respect to the previous ATLAS projection which reported a significance of 3.3σ without systematic uncertainties. Figure 16(b) also shows the κ_λ likelihood scans of the single and combined searches in the baseline systematic scenario. After combination, the 1σ confidence intervals on κ_λ are found to be $[0.5, 1.6]$ in the baseline scenario and $[0.6, 1.5]$ without systematic uncertainties. These intervals show once more an improvement with respect to the previous projection [70] which established a 1σ CI at $[0.25, 1.9]$ ($[0.4, 1.7]$) with (without) systematic uncertainties. The future addition of the ATLAS $b\bar{b}b\bar{b}$ channel could improve even further the expected ATLAS sensitivity to HH production at the HL-LHC.

Uncertainty scenario	Significance [σ]			Combined signal strength precision [%]
	$b\bar{b}\gamma\gamma$	$b\bar{b}\tau^+\tau^-$	Combination	
No syst. unc.	2.3	4.0	4.6	$-23/+23$
Baseline	2.2	2.8	3.2	$-31/+34$
Theoretical unc. halved	1.1	1.7	2.0	$-49/+51$
Run 2 syst. unc.	1.1	1.5	1.7	$-57/+68$

(a)
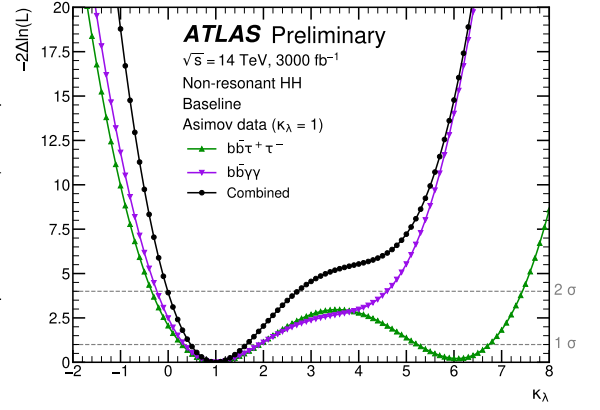
(b)

Figure 16: (a) Projected significance for different systematic scenarios and (b) likelihood distributions as a function of κ_λ for the $HH \to b\bar{b}\tau^+\tau^-$, $HH \to b\bar{b}\gamma\gamma$ and their combination [80].

3 EF02: EW Physics: Higgs boson as a portal to new physics

3.1 Yellow Report summary

The HL-LHC provides us with the opportunity to probe a large parameter space of new physics through dedicated direct searches in extended Higgs sectors, complemented by the in-depth study of the nature of the Higgs boson discussed in Section 2 (EF01).

BSM decays of the Higgs boson, often called 'exotic', cover a large range of scenarios. Higgs portal [88] and dark photon models [89] connect the Higgs boson to dark matter physics. Decays in the Higgs sector to light mass scalars and pseudoscalars, prompt or long-lived, offer a plethora of new signatures to explore. The unprecedented dataset expected at the HL-LHC allows us to study branching ratios as low as 10^{-6}, such as the search for decays of the Higgs boson to pairs of pseudoscalar bosons in the final state of two muons and two τ leptons when the pseudoscalar boson mass is below 25 GeV [90]. Innovations in the detector upgrades (trigger, timing) open up currently inaccessible parameter spaces of BSM models.

The searches for additional Higgs bosons at higher and lower masses will benefit from the increased sample size and detector improvements. The sensitivity of the searches for heavy resonances decaying to Higgs bosons will be similarly enhanced, with the potential to study unexplored production modes and decay processes. The mass reach for new heavy Higgs bosons can be pushed to a few TeV. A hypothetical composite nature of the Higgs boson will be explored as well.

In the following subsections (3.1.1 to 3.1.4) the experimental prospects for BSM Higgs boson searches included in Ref. [3] are briefly summarized. New projections prepared exclusively for the Snowmass process are presented in Section 3.2.

3.1.1 Invisible Higgs boson decays and Higgs portal interpretations

A common feature of BSM models which include a light dark matter particle that couples to the Higgs boson is a decay to invisible particles which manifest themselves in the LHC detectors as missing transverse energy (E_T^{miss}). The SM branching ratio for Higgs boson decays to neutrinos is very small ($B(H \to ZZ \to 4\nu) \approx 0.1\%$), and well below the current experimental limits. Current ATLAS and CMS Run 2 direct searches for invisible Higgs decays reach expected upper limits of 10% on $B(H \to inv)$ at 95% CL [91–95]. All production modes are considered, and the sensitivity is driven by the VBF production mode, which relies on forward jet identification to mitigate the large experimental backgrounds. With the large HL-LHC dataset as well as dedicated primary vertex selection techniques (see Ref. [96]), the sensitivity can be significantly improved.

An experimental challenge is the impact of the high PU conditions of the HL-LHC on the reconstruction of E_T^{miss}. The CMS projection [97] presents a simulation study using a fast parameterization of the upgraded CMS detector, based on DELPHES [25]. The analysis strategy is based on the early 2016 CMS publication [98], reoptimized for HL-LHC conditions. The event selection considers a range of E_T^{miss} thresholds to address the adverse effect from the increase of PU interactions on the transverse missing energy resolution performance, and shows that the upper limit on $B(H \to inv)$ can be maintained even if the transverse missing energy resolution is degraded by a factor of two with respect to the Run 2 levels. The expected 95% CL upper limit on $B(H \to inv)$ at 3000 fb^{-1} is found to be at 3.8% for thresholds values of 190 GeV on E_T^{miss}. Events originating from ZH production, with a larger signal-over-background ratio but

smaller cross-section, have also been studied by the ATLAS Collaboration in Ref. [99], obtaining an 8% upper limit on the branching ratio. The combination of the VBF and ZH channels, assuming comparable results can be obtained by both experiments and neglecting possible correlations of experimental and theoretical uncertainties, sets a HL-LHC limit on $B(H \rightarrow inv) < 2.5\%$ also at 95% CL. These results were interpreted in terms of Higgs Portal scenarios in Ref. [3].

3.1.2 Exotic decays of the 125 GeV Higgs boson

Extensions of the SM predict that the Higgs boson could decay to light new particles that eventually decay back to SM ones. The sensitivity to decays to new scalars, long-lived particles, pseudoscalars, dark photons and axion-like particles was projected from the LHC Run 2 to the HL-LHC conditions. In many scenarios studied, the sensitivity to branching ratios of 10^{-5} or smaller can be accessed. For example, the CMS Collaboration [90] presented a search for the exotic decay of the Higgs boson in a pair of pseudoscalars, denoted as a, which subsequently decay to a pair of muons and a pair of tau leptons, using the entire HL-LHC dataset. Limits on the branching ratio were projected to range from $0.5 \cdot 10^{-5}$ to $1.5 \cdot 10^{-5}$ for the pseudoscalar mass ranging from $m_a = 15$ GeV to 60 GeV. A different CMS study [100] shows the sensitivity for exotic Higgs boson decays into dark photons in a broad ranges of dark photon masses $(1 - 30 \text{ GeV})$ and lifetimes $(c\tau = 0.01 - 10 \text{ m})$ in the context of Dark Supersymmetry models. Innovative experimental reconstruction techniques such as jet reconstruction with the first level trigger or displaced track finding for long-lived particle signatures [16, 101, 102] will play a key role to explore these signatures, as outlined in Section 12.1.6.

3.1.3 Searches for additional Higgs bosons

One of the most important questions in the Higgs sector is to understand whether the Higgs boson discovered is part of an extended scalar sector such as the two-Higgs-doublet model (2HDM) [103], which predicts the existence of additional neutral or charged Higgs bosons. Extending the experimental reach, such as searching additional Higgs bosons at high and low masses, considering decays into a pair of vector bosons or fermions, charged and neutral Higgs bosons, is an important part of the HL-LHC Higgs physics program.

The ATLAS and CMS Collaborations extrapolated to high luminosity the Run 2 searches for heavy Higgs bosons decaying to τ leptons pairs $(H/A \rightarrow \tau\tau)$ [104, 105]. For H/A masses above 1 TeV, the 95% CL upper limit on the cross-section is expected to improve by about one order of magnitude at the HL-LHC [104]. The CMS Collaboration also extrapolated the search for $H/A \rightarrow ZZ \rightarrow llqq$ using 36 fb^{-1} of Run 2 data [106] to the HL-LHC [107]. In the mass range between 550 – 3000 GeV, cross-sections of H/A decaying to a pair of Z bosons above 0.7 – 5 fb and 0.8 – 9 fb are expected to be excluded for the VBF and ggF production modes, respectively. This represents a factor of 10 improvement with respect to the results obtained using 36 fb^{-1} of Run 2 data [106].

The HL-LHC reach in the minimal supersymmetric standard model (MSSM) parameter space is presented in Figure 17, comparing the indirect exclusion from the precision coupling measurements of the 125 GeV Higgs boson discussed in Section 2 and the direct search in the $H/A \rightarrow \tau\tau$ channel. The HL-LHC data is expected to be able to exclude new heavy Higgs boson masses up to 2.5 TeV for $\tan(\beta) = 50$ using the $H/A \rightarrow \tau\tau$ decay channel. Complementarily, the precision measurements of the Higgs boson couplings

discussed in Section 2 are able to exclude the parameter space of $\tan(\beta) < 8$ and the heavy Higgs boson mass smaller than approximately 1 TeV [3].
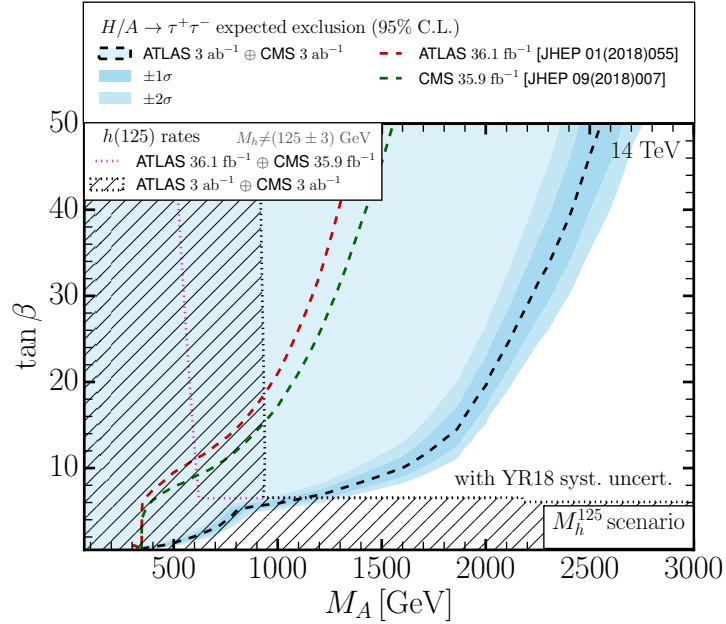
Figure 17: The expected exclusion limit in the $\tan(\beta)$ and M_A parameter space from the direct search for $H/A \to \tau\tau$ is shown in black-dashed line and compared to the limit obtained using 36 fb^{-1} of LHC Run 2 data in red and green-dashed lines for the ATLAS and CMS experiments, respectively. The indirect constraint from single Higgs boson precision coupling measurements is shown as a black shaded area. [3]

3.1.4 Searches for new massive resonances decaying into Higgs boson pairs

Several BSM scenarios predict new resonances decaying to a pair of Higgs bosons. The HL-LHC dataset provides an excellent opportunity to extend the parameter space probed by the di-Higgs decay channel. The projected sensitivity of the searches for the gluon fusion and VBF production modes of the new spin-0 and spin-2 particles by the ATLAS and CMS Collaborations at the HL-LHC was derived using the $HH \to 4b$ channel, where both Higgs bosons decaying to a pair of b-quarks are highly Lorentz-boosted and the hadronisation products of the two bottom quarks are reconstructed as a single large-radius jet [3, 108]. This gives access to the postulated new particles of masses up to a few TeV as shown in Figure 18. The ATLAS Collaboration projected the search for gluon fusion production of the spin-2 graviton G_{KK} in the warped extra dimensional (WED) model with parameter $k/\overline{M_{Pl}} = 0.5$ and 1.0 where k is the warp factor and M_{Pl} is the reduced Planck scale. In this scenario, G_{KK} masses of up to about 3 TeV can be excluded by 95% CL, increasing the mass reach by more than a factor of 2 with respect to the analysis of 36 fb^{-1} of Run 2 data [3]. A corresponding search by the CMS Collaboration focuses on the VBF production mode using Monte Carlo samples fully simulated under the HL-LHC conditions. Assuming a signal production cross-section of 1 fb at HL-LHC, the discovery potential reaches 2.6σ signal significance for a bulk graviton with a mass of 2 TeV [108]. The experimental reach at the HL-LHC is expected to be expanded with improved boosted $H \to b\bar{b}$ tagging capability due to future detector upgrades and improvements of the reconstruction methods [59, 109, 110].
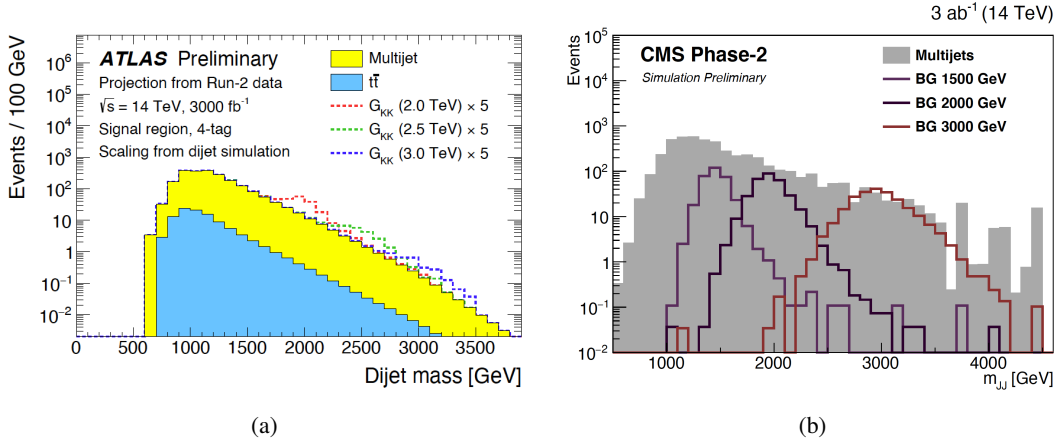
Figure 18: Dijet mass distributions for (a) the 4b subjet 4-tag (signal and background processes are stacked) and (b) 3-tag (signal and background processes are overlaid) events in the signal regions projected for 3000 fb^{-1} at $\sqrt{s}$ =14 TeV at HL-LHC, in the searches for heavy resonances decaying to a pair of Higgs bosons in the 4b final state via the gluon fusion and VBF production modes, by (a) the ATLAS and (b) CMS Collaboration, respectively. The signal processes shown are spin-2 bulk gravitons. [3]

3.2 New results

3.2.1 Search for high mass resonances decaying into W^+W^- in the di-leptonic final state with CMS at the HL-LHC [111]

This analysis is an extrapolation of the Run 2 search for a high mass resonance decaying into a pair of W bosons in the di-leptonic final state [111]. The projection is based on a scaling of the expected signal and background yields from 138 fb^{-1} to 3000 fb^{-1}. This extrapolation is carried with a fixed center-of-mass energy of $\sqrt{s}$ =13 TeV.

The results are given in the form of model independent limits on the product of the cross-section and branching fraction of a new particle with a resonance mass between 115 and 5000 GeV. One such limit is shown in Figure 19(a). Using the expected product of the cross-section and branching fraction of a high mass Higgs boson with SM-like couplings as reference (red line), the projection predicts an exclusion of such a particle up to mass of about 2600 GeV.

Additionally, model dependent exclusion limits are presented for a few MSSM scenarios and a more generic Type-II 2HDM scenario where $\cos(\beta - \alpha) = 0.1$ is assumed [111]. The expected excluded region for the M_h^{125} scenario is shown in Figure 19(b). The region that is expected to be excluded over the m_A-tan β-plane is larger by a few orders of 10 GeV over m_A compared to the results of the Run 2 analysis.
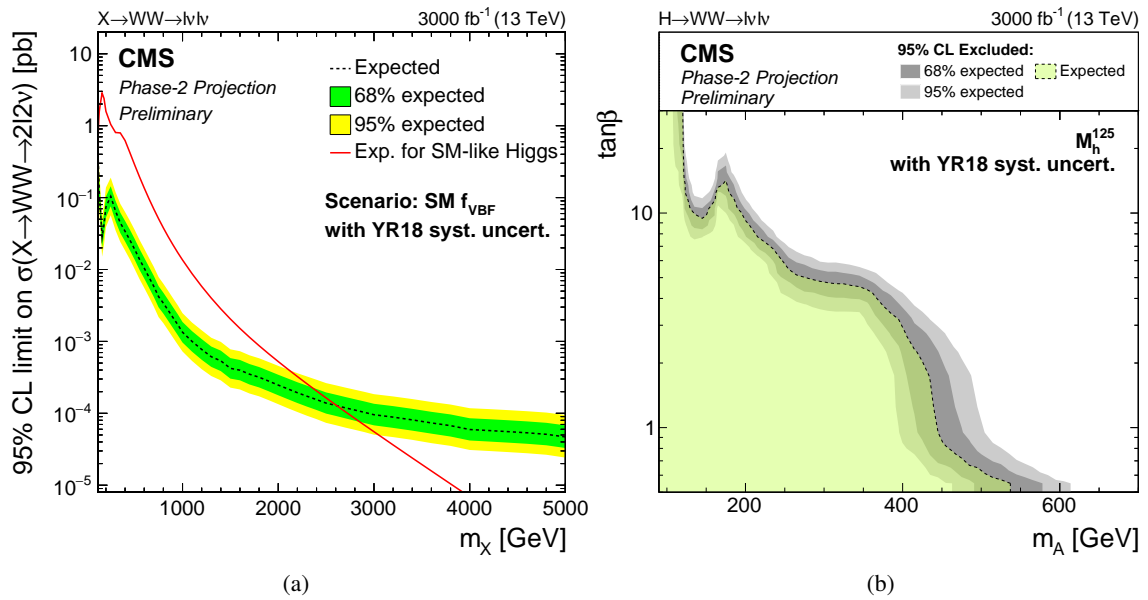
Figure 19: (a) 95% CL limit on the product of the cross-section and branching fraction of a new heavy resonance. This limit assumes the resonance has a ggF and a VBF contribution of the same order as expected from a SM-like Higgs boson at a higher mass. (b) Exclusion limit for the M_h^{125} scenario. [111]

4 EF03: EW Physics: Heavy flavor and top quark physics

4.1 Yellow Report summary

As the heaviest particle in the SM, the top quark plays a crucial role in electroweak symmetry breaking and offers a gateway to searching for signs of new physics beyond the SM. This section highlights several experimental prospects for top quark physics in both the ATLAS and CMS Collaborations within the context of the HL-LHC, as documented in Ref. [3].

4.1.1 Top quark mass measurements

The top quark Yukawa coupling is one of the fundamental parameters of the SM and is expected to be close to unity. The top quark mass, directly connected to the top Yukawa coupling, has been extensively measured using various techniques in different decays channels by both the ATLAS and CMS Collaborations. The most precise methods to date for top quark mass measurements at the LHC exploit kinematic information of the decay products and their combinations. The uncertainties on the latest mass measurements are on the order of 500 to 600 MeV, and at the HL-LHC this is projected to be reduced to 200 MeV [112]. This is expected to be further reduced as new techniques are explored for top quark mass measurements.

In particular, the ATLAS Collaboration presented projections for the top quark mass measurement accuracy using $t\bar{t} \rightarrow$ leptons + jets events with a J/ψ decaying into a muon-antimuon pair [113]. The technique relies on a template method exploiting the top quark mass sensitivity of the invariant mass $m(l\mu^+\mu^-)$ of the system made of the $J/\psi \rightarrow \mu^+\mu^-$ meson candidate and the isolated lepton coming from the associated W boson decay. A statistical uncertainty of 0.14 GeV is expected, with a systematic uncertainty of 0.48 GeV. The dominant sources to the uncertainty on m_{top} using $m(l\mu^+\mu^-)$ templates are coming from the signal modeling uncertainties related to the fragmentation functions and fractions of b-flavored hadrons and the uncertainties related to the jet energy scale and resolution. Also the CMS Collaboration directly measured the top quark mass in the lepton + jets channel with a J/ψ decaying into a muon-antimuon pair [112]. This measurement is expected to yield an ultimate relative precision below 0.1% at the HL-LHC.

4.1.2 Differential $t\bar{t}$ cross-section measurements

A projection of differential $t\bar{t}$ cross-section measurements in the e/μ+jets channels at the HL-LHC with an integrated luminosity of 3000 fb^{-1} at $\sqrt{s}$ = 14 TeV was performed by CMS [114]. The most significant reduction of uncertainty is expected to come from an improved jet energy calibration and a reduced uncertainty in the b-jet identification, which are the dominant components of the systematic uncertainties. The final projected uncertainty is estimated below 5%. The precision in the measurement of the differential cross-sections will profit from the enormous amount of data and the extended η-coverage of the Phase-2 CMS detector, which enables fine-binned measurements at high rapidity that are not possible with the current detector.

In addition, normalized double-differential cross-sections as a function of $M(t\bar{t})$ vs $|y(t\bar{t})|$ can be used to study the constraints on the parton distribution functions (PDF), estimated using a profiling technique. A consistent impact of the $t\bar{t}$ data on the PDFs is observed for all PDF sets considered (ABMP16, CT14, and NNPDF3.1) at high invariant masses of the $t\bar{t}$ system, with scale $\mu_f^2 = 30000$ GeV$^2 \simeq m_t^2$. In particular,

the uncertainties of the gluon distribution are drastically reduced, as shown in Figure 20(a), and depend directly on the uncertainty of the integrated luminosity (assumed to be 1%).

(a) (b)
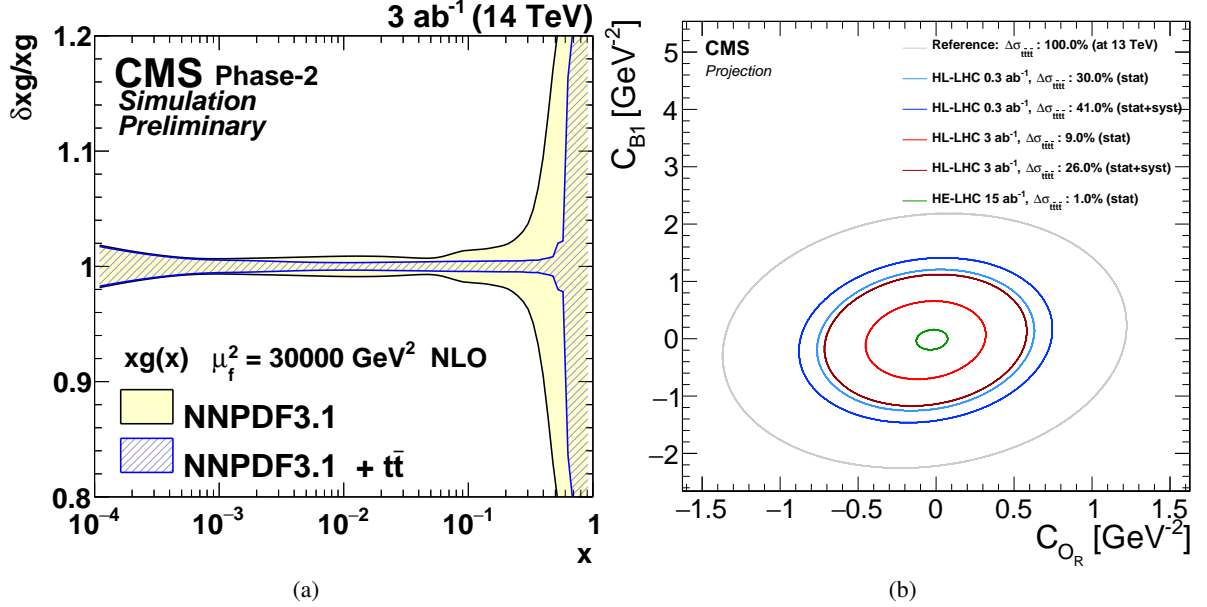
Figure 20: Prospects at HL-LHC of the (a) relative gluon uncertainties of the original and profiled NNPDF3.1 PDF set [114] and the (b) expected limits on EFT contact interaction operators for the $t\bar{t}t\bar{t}$ process [115].

4.1.3 Study of rare processes involving top quarks

The production of four top quarks ($t\bar{t}t\bar{t}$) is a rare process with $\sigma_{t\bar{t}t\bar{t}} \sim 12$ fb, not yet observed at the LHC, It is one of the rare processes in top quark physics that has large sensitivity to new physics effects, while at the same time it is interesting in the SM context as a complex QCD process. Projections of the $t\bar{t}t\bar{t}$ production at the HL-LHC have been performed by CMS using same-sign dilepton and multilepton final states [115]. Several different scenarios for the systematic uncertainties have been considered. For HL-LHC datasets of 3000 fb^{-1}, the cross-section can be constrained down to 9% statistical uncertainty and 18% to 28% total uncertainty, depending on the considered systematic uncertainties, while a 4.5σ significance is expected with the most optimistic systematics scenario. The expected sensitivity on the $t\bar{t}t\bar{t}$ cross-section is also used to provide constraints on effective field theory (EFT) four-top contact interaction operators, setting limits on their Wilson coefficients as shown in Figure 20(b).

Another process of interest at the HL-LHC is the associated production of a top quark pair with a high-p_T photon. Such $t\bar{t}\gamma$ measurements have been studied by the ATLAS Collaboration [116], based on the $\sqrt{s} = 13$ TeV $t\bar{t}\gamma$ analysis [117]. The fiducial cross-section measurement can reach an uncertainty as low as 3%(8%) in the channel with two (one) leptons, while the expected uncertainties of differential cross-section measurements are in general well below 5%. The expected uncertainty of the absolute differential cross-section as a function of the photon p_T is interpreted as 95% CL limits for EFT operators relevant to $t\bar{t}\gamma$ production, as shown in Table 5.

Table 5: Expected 95% CL intervals for the three Wilson coefficients relevant to $t\bar{t}\gamma$ production [116].

Operator	O_{tB}	O_{tG}	O_{tW}
Single lepton	[-0.5,0.3]	[-0.1,0.1]	[-0.3,0.5]
Dilepton	[-0.6,0.4]	[-0.1,0.1]	[-0.4,0.3]

4.1.4 Constraints on flavor-changing neutral currents couplings

In the SM, the flavor-changing neutral currents (FCNC) couplings of the top quark are predicted to be very small ($\sim 10^{-10}$) and are not detectable at current experimental sensitivity. However, they can be significantly enhanced in various SM extensions, so any deviations from heavily suppressed top quark FCNC rates would be a clear sign of new physics. Prospects for a search for gluon-mediated FCNC in the top quark production via tug and tcg vertices were studied using the CMS Phase-2 detector at the HL-LHC [118]. The dominant uncertainty is the normalization uncertainty on the multijet background. The 95% C.L. expected exclusion limits on the coupling strengths of the FCNC interactions in the tug and tcg vertices, shown in Figure 21(a), are $|\kappa_{tug}|/\Lambda < 1.8 \times 10^{-3}$ TeV^{-1} and $|\kappa_{tcg}|/\Lambda < 5.2 \times 10^{-3}$ TeV^{-1}, respectively. The corresponding limits on branching fractions are $B(t \to ug) < 3.8 \cdot 10^{-6}$ and $B(t \to cg) < 32 \cdot 10^{-6}$. The exploitation of the full HL-LHC dataset with the upgraded CMS detector will therefore allow to improve the current limits by an order of magnitude.

FCNC couplings have also been studied by the ATLAS Collaboration, focusing this time on the tqZ vertex, in Ref. [119], following the strategy of the Run-2 analysis detailed in Ref. [120]. The study is performed in the three charged lepton final state, in which the leptons are produced through the decay of top quark pairs $t\bar{t} \to bWqZ \to bl\nu qll$. The dominant sources of uncertainties, in both signal and background estimations, are from the theoretical normalization and the modeling of the background processes in the Monte Carlo simulations. The limits on the branching ratio are at the level of 4 to 5×10^{-5}, depending on the considered scenario assumed for the systematic uncertainties, corresponding to an improvement by a factor four with respect to the $\sqrt{s}$ = 13 TeV analysis results based on 36.1 fb^{-1}, achieved thanks to the larger integrated luminosity and the improved treatment of the systematic uncertainties.

Potential FCNC couplings of the top quark would also impact the electroweak dipole moments of the top quark, as well as the (axial-)vector couplings of the top quark to the Z boson. The expected sensitivity of the CMS detector to anomalous electroweak couplings of the top quark based on differential cross-section measurements of the $t\bar{t}Z$ process in the three lepton final state is provided for a HL-LHC scenario with 3000fb^{-1}of proton-proton collision data at $\sqrt{s}$ = 14 TeV [121]. The results are interpreted in terms of the SM effective field theory. Limits are set on the relevant Wilson coefficients of the Warsaw basis, corresponding to modified neutral-current interactions ($C_{\phi t}$ and $C_{\phi Q}$) and dipole moment interactions (C_{tZ} and $C_{tZ}^{[Im]}$). The dominant systematic uncertainties are related to the b-jet identification and to the theoretical predicted cross section of background samples. With the reduced theoretical and experimental uncertainties, tight constraints are expected on the limits, shown in Figure 21(b) for the dipole moment parameters.
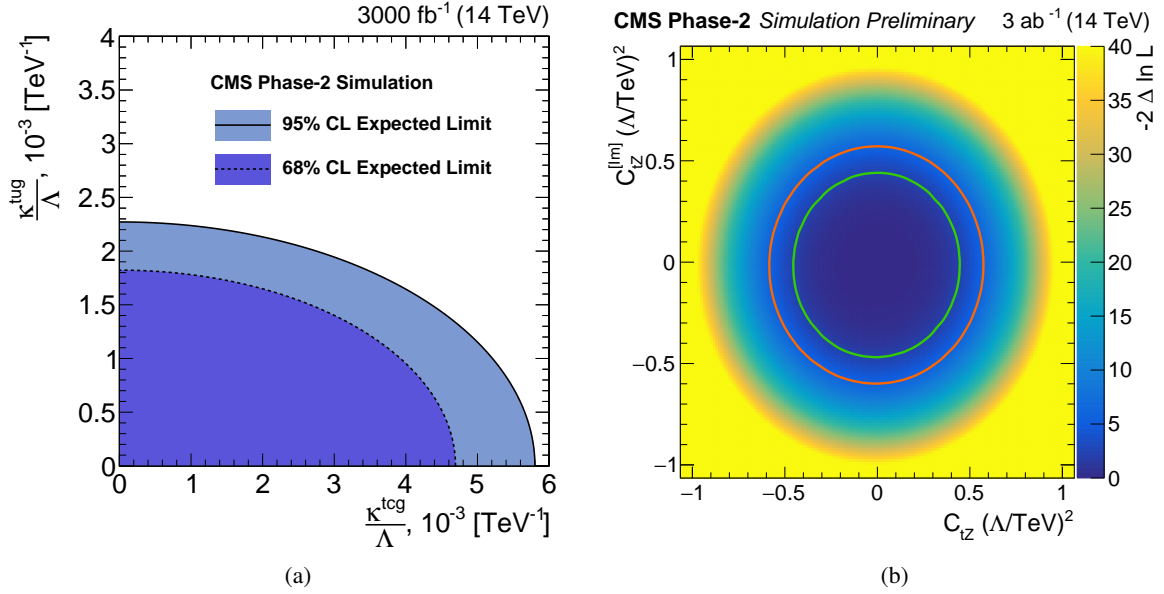
Figure 21: Prospects at HL-LHC of (a) the expected limits on the FCNC top quark couplings [118] and the (b) expected sensitivity to anomalous couplings of the top quark in the $t\bar{t}Z$ process [121].

4.2 New results

4.2.1 Sensitivity to the measurement of the Standard Model four top quark cross section with ATLAS at the HL-LHC [122]

The following summarizes the prospect for measuring the SM $t\bar{t}t\bar{t}$ cross section, detailed in Ref [122], in the context of the HL-LHC with 3000 fb^{-1} of proton-proton collisions at $\sqrt{s}$ = 14 TeV with the ATLAS experiment. The results presented here use events with two same-sign leptons or at least three leptons. They are based on the extrapolation of the 139 fb^{-1} results at $\sqrt{s}$ = 13 TeV [123]. Several SM processes can produce events with topologies similar to those of $t\bar{t}t\bar{t}$ events. The dominant source of these backgrounds is $t\bar{t}$ production associated with jets and other particles, such as a Higgs boson ($t\bar{t}H$+jets), W boson ($t\bar{t}W$+jets), or Z boson ($t\bar{t}Z$+jets). Significant backgrounds also come from events in which one of the leptons is reconstructed with an incorrect charge and from events that contain leptons arising from heavy-flavor decays, photon conversions or misidentified jets, the latter three being collectively referred to as "fake/non-prompt". The heavy-flavor decays are the dominant source for non-prompt muons, while the other sources mostly affect electrons. The charge misassignment and fake/non-prompt background comes mainly from $t\bar{t}$ events.

The extrapolation is performed under two different scenarios of the evolution of detector performance and associated systematic uncertainties. The first one, referred to as "Run 2", corresponds to the model closest to the 139 fb^{-1} analysis, where all the systematic uncertainties are kept equal to their Run 2 values except for the $t\bar{t}W$+jets production with seven jets and with eight jets or more. The uncertainties associated with these events take into account the post-fit values of the corresponding nuisance parameters. The second model, referred to as "Run 2 Improved", still includes the scaling of $t\bar{t}W$+jets production from the previous model but also includes a decrease of the systematic uncertainties compared to the 139 fb^{-1} analysis, based

on the YR18 systematic uncertainties. A summary of the systematic uncertainty treatment in this model is given in Ref [122]. The uncertainty linked to the Monte Carlo simulation sample size is assumed to be negligible. The uncertainties on $t\bar{t}W$+jets production with seven jets and with eight or more jets are scaled down with the constraints on the corresponding nuisance parameters observed in the 139 fb^{-1} analysis.

In the "Run 2" ("Run 2 Improved") scenario, a significance of 4.2σ (6.4σ) is expected with 3000 fb^{-1}, while the uncertainty in the cross section over the full phase space is expected to be around 20% (14%), as shown in Figure 22. In the "Run 2" scenario, the expected experimental uncertainty is reaching the current uncertainty on the SM theory cross section [124], while for the "Run 2 Improved" scenario, the experimental precision is expected to be significantly better than the precision of the current SM computation. The better sensitivity in the "Run 2 Improved" scenario is driven by the smaller theoretical uncertainties assumed in the $t\bar{t}t$ cross section and the modeling of the $t\bar{t}W/Z$ production in association with heavy-flavor jets, as well as the smaller b-tagging experimental uncertainties.
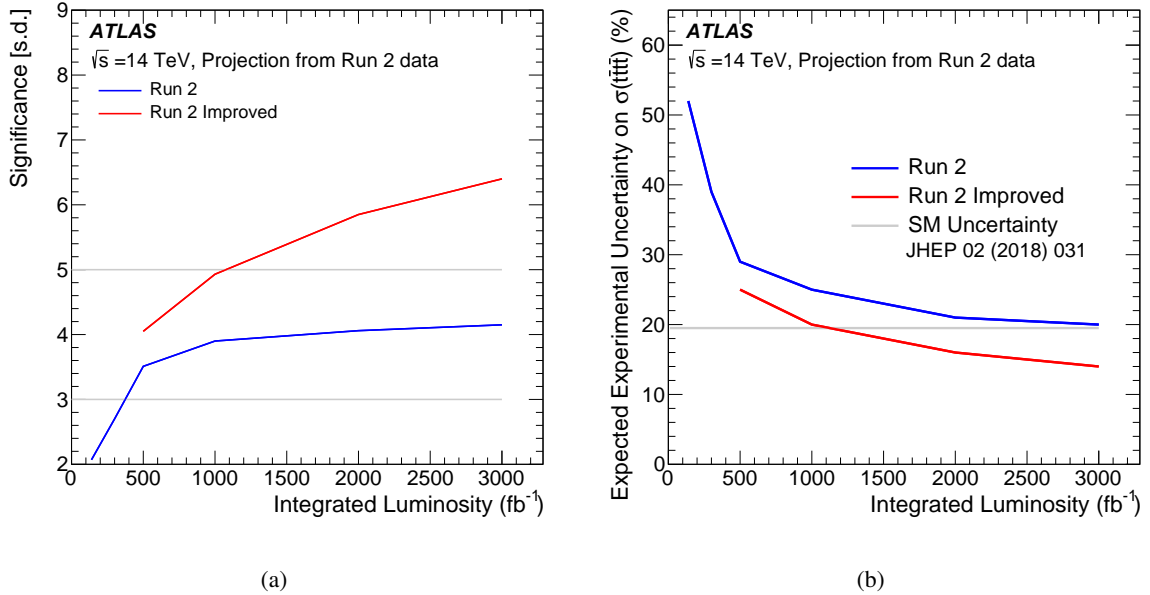

Figure 22: (a) Expected significance for the measured $t\bar{t}t\bar{t}$ cross section and (b) expected experimental uncertainty, assuming two different scaling scenarios for the systematic uncertainties [122]

5 RF01: Weak decays of *b* and *c* quarks

5.1 Yellow Report summary

Beauty hadron decays offer a rich phenomenology to explore and are a fertile ground for indirect searches of NP, namely via virtual processes allowing to probe energies greater than TeV which are not directly accessible in collisions at the current colliders. Precision measurements can unveil new particles modifying the decay rates with respect to the Standard Model predictions, both in FCNC $b \rightarrow s\ell^+\ell^-$ and $b \rightarrow d\ell^+\ell^-$ loop-level decays and in $b \rightarrow c\ell\nu$ tree-level semileptonic transitions. Combining the physics reach of the upgraded ATLAS, CMS and LHCb detectors, the LHC will be a crucial facility given its potential to distinguish between some plausible NP scenarios, while improving the sensitivity to the scale of NP thanks to the increasing precision in probing statistically-limited FCNC processes.

The rare decays $B_s^0 \rightarrow \mu^+\mu^-$ and $B_d^0 \rightarrow \mu^+\mu^-$ are FCNC transitions that can occur at the one-loop level via electroweak penguin and box diagrams in the standard model (SM). In addition, these decays are helicity suppressed. The SM predictions of their branching ratios are at the level of $\sim 10^{-9}$ and $\sim 10^{-10}$ respectively. NP models predict enhancements of the branching ratios for these rare decays and therefore the study of these decays provides an excellent opportunity to search for NP. With the HL-LHC dataset each experiment predicts measurements of the branching ratios with combined statistical and systematic uncertainty of about $7 - 15\%$ for $\mathcal{B}(B_s \rightarrow \mu^+\mu^-)$ and $15 - 30\%$ for $\mathcal{B}(B_d \rightarrow \mu^+\mu^-)$.

Instead, the $B^0 \rightarrow K^{*0}(892)\mu^+\mu^-$ decay is semi-rare (its branching fraction is at the level of $\sim 10^{-7}$) and allows to measure important angular parameters including the so-called P_5' variable introduced in Refs. [125, 126]. The differential decay rate for this decay can be expressed in terms of the dimuon invariant mass squared (q^2) and three angular variables as a combination of spherical harmonics weighted by q^2-dependent angular parameters; the latter in turn depend upon complex decay amplitudes which are described by Wilson coefficients in the Effective Field Theory Hamiltonian. Precise measurements are needed to investigate current tensions existing between some measurements performed so far and the SM predictions, though these tensions depend on the various implementations of long-distance effects. The sensitivity in the P_5' measurement is expected to improve by a factor about 5 to 15 times according to the experiment and the considered trigger scenarios.

The $B_s^0 \rightarrow J/\psi\phi$ decay is considered the golden channel for the study of CP violation in the B_s^0 sector. A measurable phase ϕ_s arises from the interference between the oscillation of the bottom-strange meson and its decay via $b \rightarrow c\bar{c}s$ transition, which allows the final state to be the same for mixed and unmixed mesons. Neglecting sub-leading penguin contributions, the SM CP-violating phase can be derived from CKM matrix elements and thus from SM global fits to experimental heavy flavor data. Thus any significant deviation from this precisely predicted value may be interpreted as an effect of New Physics beyond the SM. In CMS and ATLAS ϕ_s is measured from a fit to the angular distribution of the $B_s^0 \rightarrow J/\psi\phi$ decay products as a function of the B_s^0 decay time. The sensitivity in the ϕ_s measurement is expected to improve by a factor about 9 to 20 times according to the experiment and the investigated flavour tagging and trigger scenarios. Considering that the final state is a superposition of CP-even and CP-odd states, the measurement of ϕ_s requires disentangling these components; in the future, with larger statistics, it will also be feasible for CMS and ATLAS to explore the CP amplitude dependence of ϕ_s, namely by measuring it for the different perpendicular, longitudinal and parallel transversity amplitudes of the $B_s^0 \rightarrow J/\psi\phi$ decay.

5.1.1 Sensitivity studies for rare B_s and B_d decays in two muons

The ATLAS [127] and CMS [128] projections of rare muonic neutral B decays at the HL-LHC era are extrapolated from the corresponding Run 1 analyses [129, 130] , accounting for the mass resolution improvements expected at HL-LHC, and relying on the flexibility of the upgraded trigger systems to maintain the di-muon trigger selection efficient at relatively low transverse momenta. While the uncertainty on $\mathcal{B}(B_d \to \mu^+\mu^-)$ remains statistically limited for HL-LHC projections, the projected uncertainty on $\mathcal{B}(B_s \to \mu^+\mu^-)$ depends on the assumptions made for the systematic uncertainties. With the HL-LHC dataset, precise measurements of additional observables will be possible, namely the effective lifetime, $\tau_{\mu\mu}^{eff}$, and the time-dependent CP asymmetry of $B_s \to \mu^+\mu^-$ decays.

ATLAS projects the $B_s \to \mu^+\mu^-$ branching ratio uncertainty to have a significant contribution from external sources, in particular from the relative b-quark hadronisation probability with an s or d quark f_s/f_d and normalization modes branching fractions uncertainties, assumed to be at the same level of the Run 1 analysis. The ATLAS di-muon invariant mass resolution is expected to improve by 20% to 50% with respect to Run 2, in the $|\eta|$ range $[0, 2.5]$. Further assumptions include the training of a multivariate classifier capable of similar background rejection and signal purities, and an analysis selection with comparable pileup immunity as Run 1. The study takes into account the scaling of B meson production cross-section and integrated luminosity relative to Run 1, and explores different triggering scenarios corresponding to different di-muon transverse momentum thresholds. For each of these scenarios the sensitivity is categorized on the basis of the signal statistics expected relative to the Run 1 analysis (15x, 60x and 75x respectively, in 3000 fb^{-1} of HL-LHC ATLAS data), yielding the projected 68.3%, 95.5% and 99.7% likelihood contours in Figure 23.

The CMS study is being performed in two pseudorapidity regions, $|\eta_f| < 0.7$ and $0.7 < |\eta_f| < 1.4$ (see Figure 24). The inner tracker of the Phase-2 detector provides an order of 40%-50% improvement on the mass resolutions over the Run 2 case that will allow precise measurements of the $B_s^0 \to \mu^+\mu^-$ and $B_d^0 \to \mu^+\mu^-$ rare decays. The semileptonic background contribution into the signal regions will be reduced substantially in Phase-2. With an integrated luminosity of 3000 fb^{-1}, CMS will have the capability to measure the $B_s^0 \to \mu^+\mu^-$ branching fraction with a precision (statistical and systematic) of about 7% and the effective lifetime with an error of 0.05 ps. CMS will be also able to observe the $B_d^0 \to \mu^+\mu^-$ decay with more than 5σ significance and to measure the branching ratio with a precision (statistical and systematic) of about 16% (the quoted precision refers to the SM central value).

5.1.2 P_5' sensitivity in the $B^0 \to K^{*0}\mu^+\mu^-$ decays

CMS [132] adopts a conservative assumption that trigger thresholds and efficiencies will remain the same thus overlooking improvements in the trigger strategy, in the mass resolution and in the selection strategy. The latter has been proven to be not significantly affected by the pileup increase. The mis-tag rate is expected to be the same as in Run 1.

ATLAS [133] estimates the yields assuming three different trigger scenarios, with muon p_T thresholds ranging from 6 to 10 GeV, and considers the same mis-tagging level and fit models of Run 1. The statistical precision of the angular parameters (assumed to follow the predictions from [134]) is inferred through toy simulations. Detector acceptance and background shapes are identical to the Run 1 analysis, but account for a 30% improvement in invariant mass resolution. Systematic uncertainties are all expected to improve: fit model and peaking backgrounds are assumed to reduce as $1/\sqrt{L_{int}}$; detector acceptance and

mis-tagging systematics, are driven by Monte Carlo sample size and are therefore neglected. The existing measurements of S-wave [135] contributions to the signal decay and improved methods of correcting residual misalignments [136] will allow reduction of the corresponding systematic uncertainties by factors of $\sim 5\times$ and $\sim 4\times$. As a result of this estimation of the systematic effects all the angular parameters determinations are expected to be statistically limited.

The Phase-2 precision in the P'_5 parameter is illustrated in Figure 25 where the projected statistical and total uncertainties in each q^2 bin are reported. For ATLAS it is expected to improve by factors of $\sim 9\times$, $\sim 8\times$ and $\sim 5\times$ with respect to Run 1 measurement in the three trigger scenarios considered, whereas for CMS it is expected to be improved up to a factor of $\sim 15\times$ compared to Run 1. For the latter experiment the uncertainties are shown also for a finer q^2 binning allowed by the increased amount of collected data.

(a)   (b)

(c)

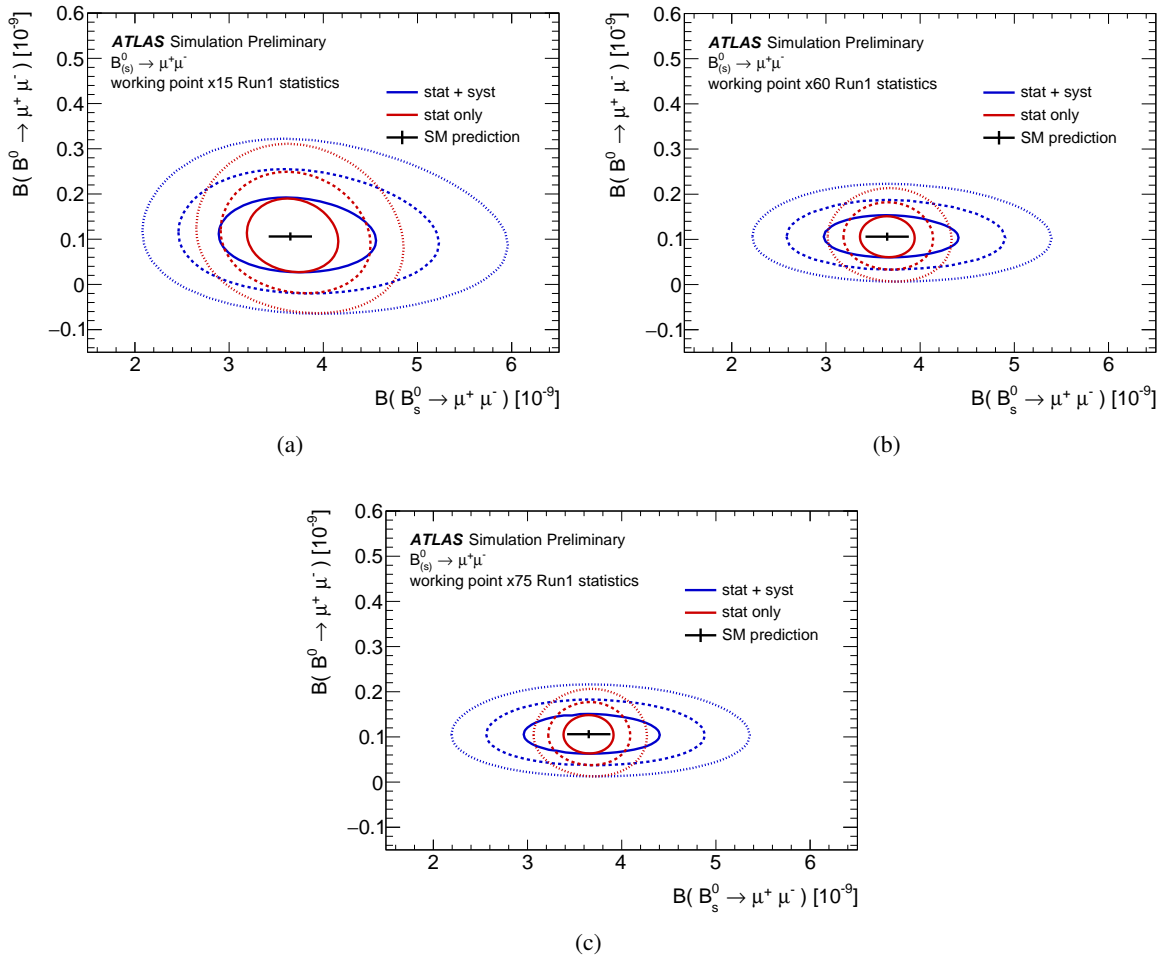Figure 23: ATLAS projected 68.3% (solid), 95.5% (dashed) and 99.7% (dotted) CL profiled likelihood ratio contours for the (a) "conservative", (b) "intermediate" (middle) and (c) "high-yield" HL-LHC extrapolations [127]. Red contours do not include the systematic uncertainties, which are then included in the blue ellipsoids. The black point shows the SM theoretical prediction and its uncertainty [131].
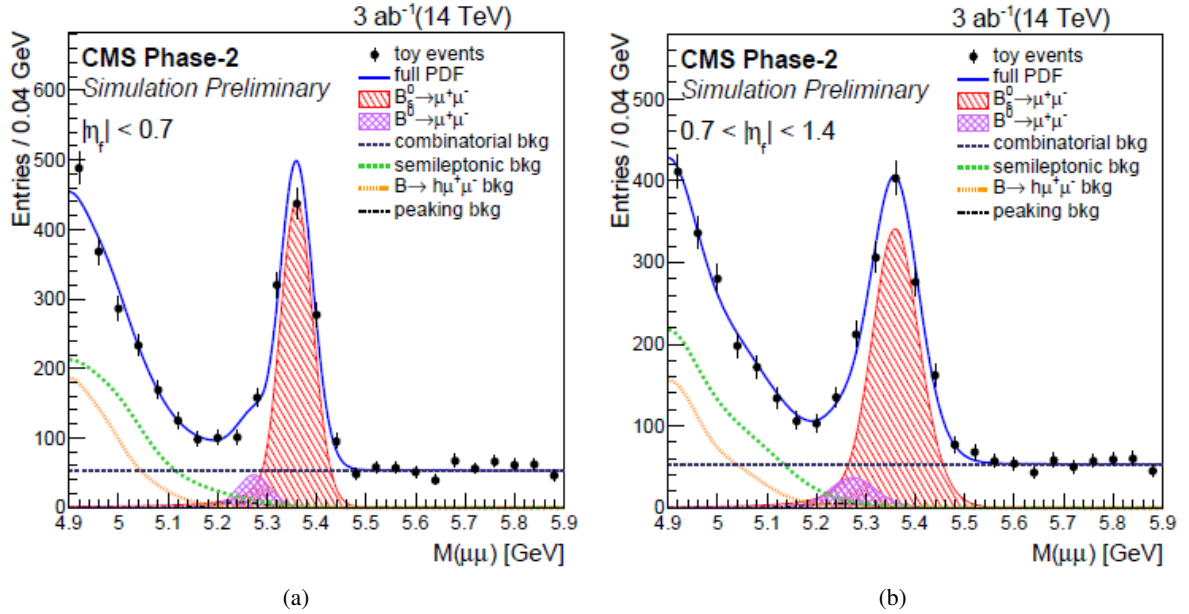
Figure 24: Projected CMS HL-LHC dimuon invariant mass distributions with overlaid fit results for the $B_{d,s}^0 \to \mu^+\mu^-$ analysis, in the pseudorapididty regions of (a) $|\eta_f| < 0.7$ and (b) $0.7 < |\eta_f| < 1.4$ [128].

5.1.3 CP violating phase ϕ_s sensitivity in $B_s^0 \to J/\psi\phi$ decay

The ATLAS [139] and CMS [140] studies present an estimate of the precision in the ϕ_s measurement achievable at the end of Phase-2 by extrapolation from their Run 1 analysis results [141, 142] obtained using full detector simulation data and studying the fit performance with Monte Carlo pseudo-experiments.

The main ingredients in the estimation of the sensitivity at the end of Phase-2 are the signal yield, the tagging performance and the proper decay length uncertainty (namely the B_s^0 proper decay time resolution). For CMS, the latter is expected to be well enhanced (3 times smaller thanks to the Phase-2 Tracker). In Figure 26(a) the CMS proper time uncertainty distribution is shown for Phase-2 Tracker and compared with Run 1 data. The upgraded ATLAS tracking system will improve tracking and vertexing precision, enhancing the proper time resolution by 21% and 39%, relative to Run 2 and Run 1 respectively: Figure 26(b) illustrates this resolution as a function of the B_s^0 transverse momentum, comparing with the Run 1 and Run 2 (including the pixel Insertable B-Layer (IBL) module) simulated detector performances.

Another large improvement for CMS is expected to come from the presence of the tracker timing layer which will mitigate the effect of the increased pileup, thus providing a signal-to-background level similar to the one at 8 TeV. The analysis strategy follows the one used for the $\sqrt{s} = 8$ TeV result whereas three different flavor tagging performance scenarios have been considered, correspondingly based on: 1) muons and jet charge, 2) a muon and electron, 3) leptons, jet-charge and same-side jet-charge and kaon-tagging. Furthermore the systematic uncertainties should be reasonably kept under control so that 1) the total uncertainty on ϕ_s could be still statistically limited at the end of Phase-2, whereas 2) the statistical and systematic uncertainties are assumed to contribute about equally for the decay width difference $\Delta\Gamma_s$ between the light and heavy eigenstates.
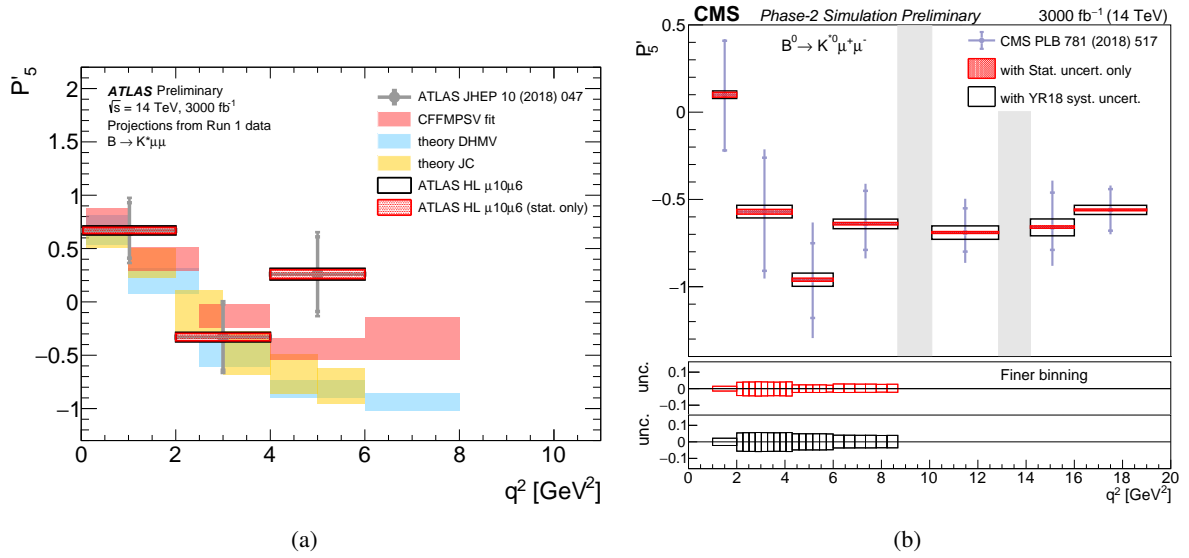
Figure 25: Projected measurement precision of the P'_5 parameter in the HL-LHC scenario by (a) ATLAS [133] and (b) CMS [132], provided in (different) q^2 bins and compared to the Run 1 measurements that are shown by circles with inner vertical bars representing the statistical uncertainties and outer vertical bars representing the total uncertainties. Projections are represented by hatched/colored regions and open boxes when considering statistical-only or total (statistical and systematic) uncertainties. (a) ATLAS projection is given for the intermediate trigger scenario; alongside theory predictions (CFFMPSV [137], DHMV [134], JC [138]) are also shown. (b) The vertical shaded regions correspond to the J/ψ and $\psi(2S)$ resonances. The two bottom pads represent the CMS statistical (upper) and total (lower) uncertainties with the finer q^2 binning.
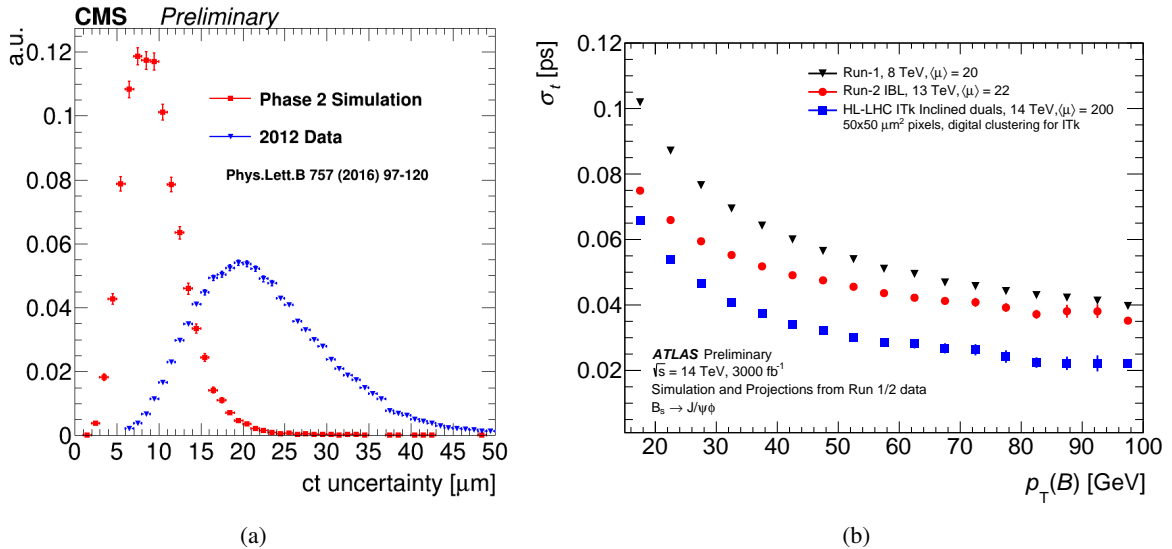
Figure 26: (a) CMS proper time uncertainty distribution in 2012 data (blue) and Phase-2 Monte Carlo (red) samples [140]. (b) ATLAS dependence of the proper time resolution on the B_s^0 transverse momentum for Run 1 (ID), Run 2 (IBL) and upgrade HL-LHC Monte Carlo simulations [139].

Without performing a complete analysis, ATLAS extrapolates the ϕ_s precision mainly on the basis of the same key factors (the number of signal and background events and the B-flavor tagging performance besides the proper time resolution) from Run 1 results. ATLAS considers three trigger scenarios, targeting the $J/\psi \to \mu^+\mu^-$ decay, with three muon transverse momentum thresholds: 6 GeV for both muons or 6 GeV and 10 GeV or 10 GeV for both muons, and a nominal tagging power of 1.5%.

Assuming the best tagging scenario characterized by a tagging power in the range $1.2 - 2.4\%$, CMS can estimate the ϕ_s uncertainty to be in the range $5 - 6$ mrad (namely (17-20) times the Run 1 uncertainty) and the $\Delta\Gamma_s$ full uncertainty of $\approx 2 \cdot 10^{-3}$ ps^{-1}. Figure 27(a) shows the 68% CL contour from the fit of a toy Monte Carlo pseudo-experiment generated in the third tagging scenario. Figure 27(b) shows the expected ATLAS precision on ϕ_s and $\Delta\Gamma$ (with the 68% CL contours combining statistical and systematic uncertainties) for the three trigger scenarios considered; since the correlation between ϕ_s and $\Delta\Gamma$ in Run 1 was found to be smaller than 10%, the extrapolated contours of ATLAS HL-LHC are made with zero correlation. Within the three trigger scenarios the ATLAS statistical precision is expected to fall in the range $4 - 9$ mrad for ϕ_s and $1.1 - 3 \cdot 10^{-3}$ ps^{-1} for $\Delta\Gamma_s$.

(a)   (b)
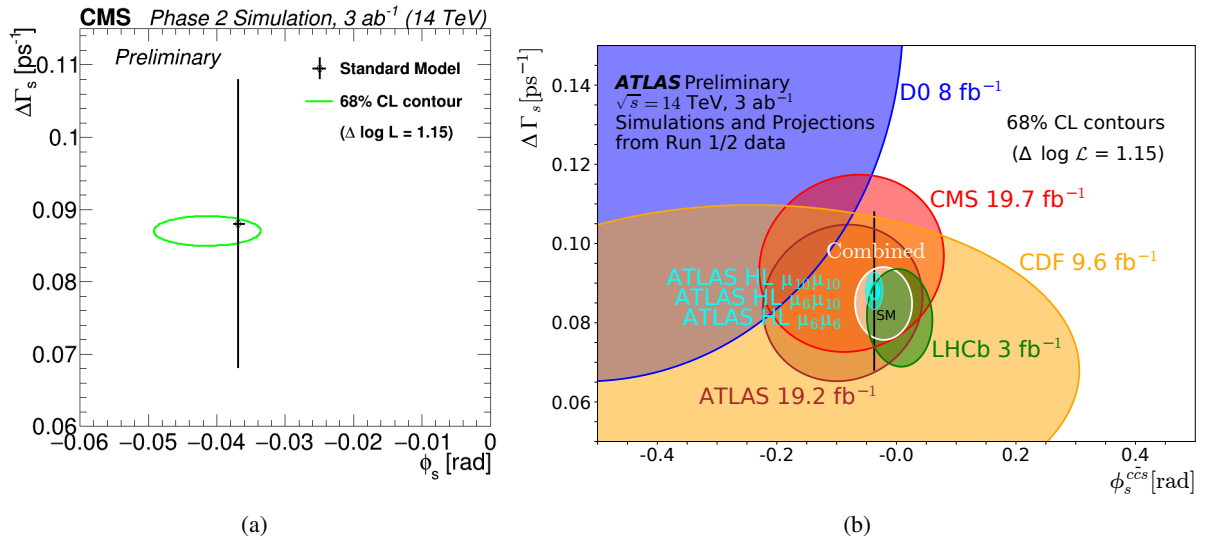
Figure 27: (a) CMS 68% CL contour from the fit of a toy Monte Carlo pseudo-experiment generated in the third tagging scenario [140]. The contour combines statistical and systematic uncertainties and the black cross represents the SM expectation. (b) ATLAS contours (combining statistical and systematic uncertainties) for the three trigger scenarios considered [139]. The result is overlaid with the precisions on ϕ_s and $\Delta\Gamma$ extracted using Run 1 data. The figure the modification of the original one taken from [143, 144] where the presented LHC results are those based on Run 1 data.

6 EF04: EW Physics: EW precision physics and constraining new physics

6.1 Yellow Report summary

This section summarizes various projections of electroweak (EW) measurements for the HL-LHC and expected improvements in measuring SM processes compared to the LHC. Electroweak measurements will be important for constraining PDFs, understanding electroweak symmetry breaking, and measuring fundamental properties of the SM. The large HL-LHC dataset will enable precision measurements of various electroweak processes, many of which are currently limited by statistical uncertainties. In addition, the tracking detector upgrades will allow for better forward jet and lepton reconstruction, both of which are used by many of these analyses.

6.1.1 Weak mixing angle measurements

The most precise measurements of the effective weak mixing angle, $\sin^2\theta_{\text{eff}}$, were performed by the LEP and SLD experiments [145], with a precision of 1.6×10^{-4}. There is, however, a known tension of about 3σ between these two measurements. Measurements of $\sin^2\theta_{\text{eff}}$ were also reported by the LHC and Tevatron experiments [146–151]. The analyses in Refs. [152, 153] present proposals for measuring the weak mixing angle using the forward-backward asymmetry (A_{FB}) of Drell-Yan dilepton events in pp collisions at $\sqrt{s} = 14$ TeV with the CMS and ATLAS detectors at the HL-LHC. In both analyses, $\sin^2\theta_{\text{eff}}$ is measured by fitting the rapidity dependence of the observed A_{FB} in dilepton events and the dilepton mass.

The ATLAS study [152] is performed in dielectron events, and will benefit from improved reconstruction of forward leptons from the extended reach of the ITk upgrade [4, 9]. With the full HL-LHC dataset, this result will be dominated by the PDF uncertainties. To asses them, three different projected PDF sets are considered. As in the $\sqrt{s} = 8$ TeV ATLAS result [154], the PDF uncertainties are simultaneously constrained by the measurement. As seen in Figure 28(a), the HL-LHC measurement will greatly improve the precision for any of the PDF choices, and is expected to achieve a precision similar to that of LEP and SLD. Further improvements to PDFs will be critical for the measurements of $\sin^2\theta_{\text{eff}}$, and can increase the sensitivity.

The CMS study [153] is performed in dimuon events, and will benefit both from the increased luminosity and the upgraded part of the muon system that extends the pseudorapidity coverage of the CMS experiment from $|\eta| < 2.4$ to $|\eta| < 2.8$ for muons. A Monte Carlo data sample of $\sqrt{s} = 14$ TeV pp events corresponding to an integrated luminosity of 3000 fb^{-1} is used and results are compared to the CMS measurements at $\sqrt{s} = 8$ TeV. The analysis is done at the generator level, since the smearing due to detector effects is expected not to be significant. The analysis finds that extending the lepton acceptance decreases the statistical uncertainties by about 30% and PDF uncertainties by about 20%. It was also shown that the PDF uncertainty could be constrained to improve the precision of $\sin^2\theta_{\text{eff}}$ as shown in Figure 28(b).

6.1.2 VBS diboson measurements

ATLAS and CMS were successful in performing the first observations of several EW diboson processes using the $\sqrt{s} = 13$ TeV LHC collisions, including measurements of leptonic decays of VBS $W^\pm W^\pm$ [155, 156], VBS $W^\pm Z$ [157, 158], VBS ZZ [159, 160], and VBS $Z\gamma$ [161]. For both ATLAS and CMS, these

(a)

(b)
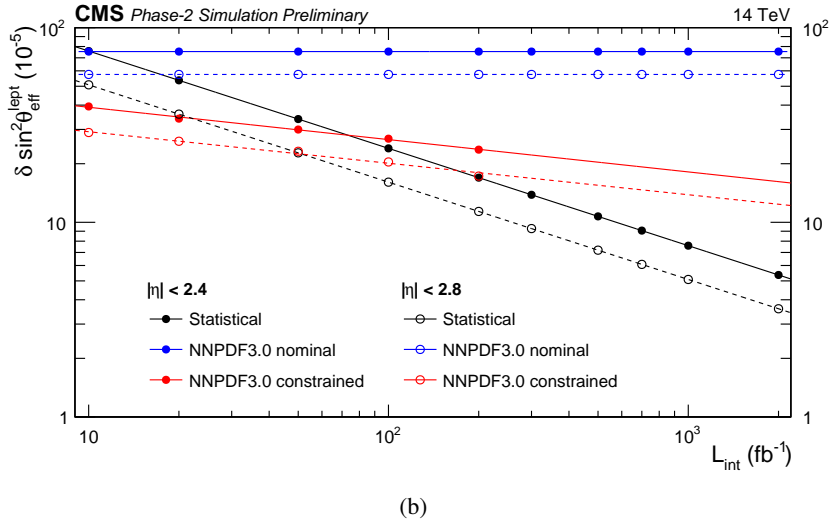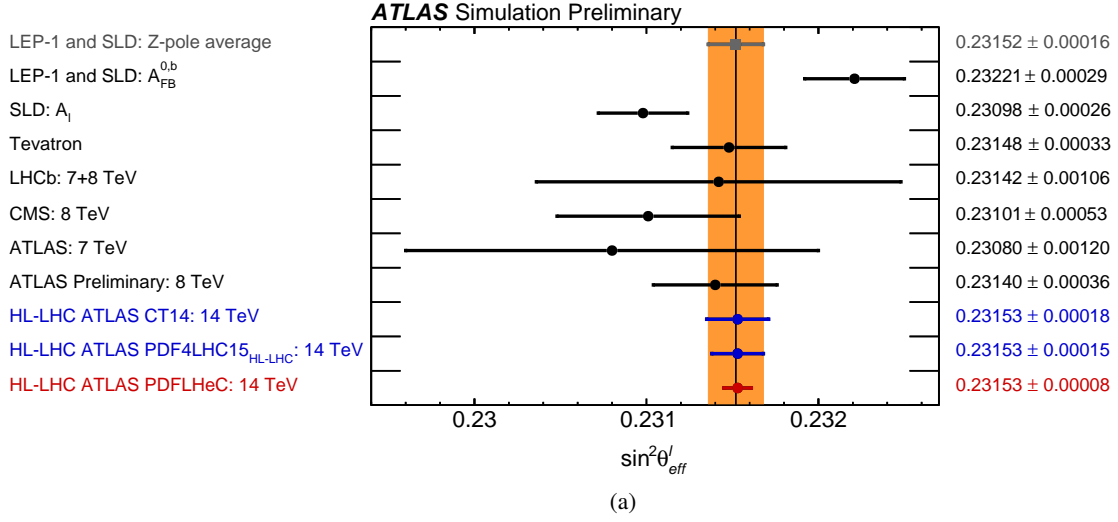
Figure 28: (a) Comparison of the expected precision of the effective leptonic weak mixing angle presented in this note to previous measurements. The ATLAS projections from this analysis are shown with different PDF set scenarios, with 3000 fb^{-1} at $\sqrt{s}$ = 14 TeV [152]. (b) Projected statistical, nominal PDF and constrained PDF uncertainties in $\sin^2\theta_{\text{eff}}$ extracted by fitting $A_{\text{FB}}(m_{\mu\mu}, y_{\mu\mu})$ distributions at $\sqrt{s}$ = 14 TeV with different values of integrated luminosities and for $|\eta| < 2.4$ and $|\eta| < 2.8$ acceptance selections for the muons [153].

analyses will benefit greatly from the large dataset, as well as from detector upgrades enabling forward lepton reconstruction, and improving PU jet rejection for forward jets.

ATLAS and CMS have performed projections of analysis sensitivities for measuring the cross-sections of leptonic decays of electroweak production of several VBS diboson processes, including $W^\pm W^\pm$ [162, 163], $W^\pm Z$ [164, 165], and ZZ [166, 167]. These analyses are based on strategies of existing measurements from ATLAS and CMS, with some optimization for the HL-LHC conditions. ATLAS (CMS) expect to measure the cross-section of EW production of VBS $W^\pm W^\pm$ to 6% (3%) using 3000 fb^{-1}, with some improvements expected from the combination of these results, as shown in Figure 29(a) and Figure 29(c). The ATLAS projected sensitivity for the measurement of EW production of VBS $W^\pm Z$ predict a significance over 5σ, and large improvements are shown through a multivariate analysis strategy, and by reducing the uncertainty on the background through improvements to the control regions enabled by the increase in the number of events. The CMS results for $W^\pm Z$ predict that the EW WZ cross-section measurement can be achieved to an accuracy of 3–5% at an integrated luminosity of 3000 fb^{-1}. The ATLAS projections for the measurement of EW VBS ZZ depend strongly on the size of the theoretical modeling uncertainties for QCD $ZZjj$, and the projected measurement uncertainty ranges from 20–100% when varying the background uncertainty from 5% to 30%. The projected uncertainty from CMS for the same process, and using a background uncertainty of 10%, ranges from 8.5% to 9.8%, depending on the size of the systematic uncertainties and the η coverage for electrons. Overall, the HL-LHC will provide a significant opportunity to study electroweak diboson processes, and will enable measurements of their cross-sections with an increased precision.

While leptonic decays provide a cleaner final state with lower backgrounds, the semi-leptonic decays provide a higher cross-section due to the larger branching fraction of the vector boson decays, and jet substructure techniques enable reconstruction of the vector boson at high transverse momentum. As shown in Ref. [168], semi-leptonic decays are also able to provide sensitivity to EW VBS diboson processes. In particular, prospective measurements of WW/WZ events in the $\ell\nu qq$ final state were performed. The ATLAS results show an observed significance of 2.7σ [169]. The event selection follows the strategy used for resonance searches decaying into a WW or WZ boson pair with the ATLAS detector. The precision of this cross-section measurement is expected to be 6.5% with 3000 fb^{-1}, as shown in Figure 29(b).

In addition to increasing the precision of diboson measurements, of particular interest is the measurement of the case where both bosons are longitudinally polarized ($V_L V_L$). In the SM, this process is unitarized thanks to the presence of Higgs boson contributions, and deviations from this would indicate the presence of BSM physics. The cross-section for the longitudinally polarized state is small (6–7% of the total cross-section), making this a challenging but important part of the HL-LHC physics program. Both ATLAS and CMS have explored the sensitivity to measuring $W_L W_L$ in leptonic final states by using the $\Delta\phi_{jj}$ distribution, where $\Delta\phi_{jj}$ is the difference in ϕ between the two tagging jets [155, 156]. Using 3000 fb^{-1}, ATLAS (CMS) project an expected significance of 1.8σ (2.7σ) as shown in Figure 30. ATLAS projects the sensitivity for $W_L^\pm Z_L$ to be less than 1σ [157], and CMS also concludes that sensitivity to this would require improved analysis techniques such as machine learning, or combinations of results with other decay channels [158]. CMS projects the sensitivity of $Z_L Z_L$ to be 4σ with 3000 fb^{-1} (see 6.2.1). Further optimization and new analysis strategies may strengthen the sensitivity of these results, and these measurements will also benefit from the combination of ATLAS and CMS results.
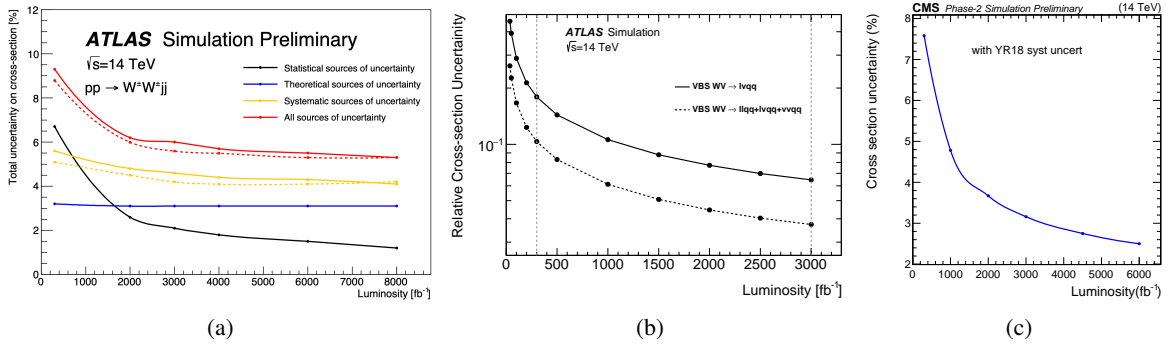
Figure 29: (a) Projection of the statistical, theoretical, systematic and total uncertainties on the cross-section of same-sign WW as a function of integrated luminosity, for the optimized event selection using the baseline scenario for uncertainties (solid lines) and optimistic scenario (dashed lines), where the optimistic scenario assume that the non-data-driven background uncertainties are aggressively reduced, as described in Ref. [162]. (b) The expected cross-section uncertainty for the semileptonic WV analysis as function of integrated luminosity up to 3000 fb^{-1}. The solid black curve is the uncertainty from the $\ell\nu q\bar{q}$ channel, while the dashed curve shows the expected uncertainty from all semi-leptonic channels, assuming equal sensitivity [168]. (c) The expected uncertainty in the CMS EWK $W^{\pm}W^{\pm}$ cross-section measurement as a function of the integrated luminosity [163].
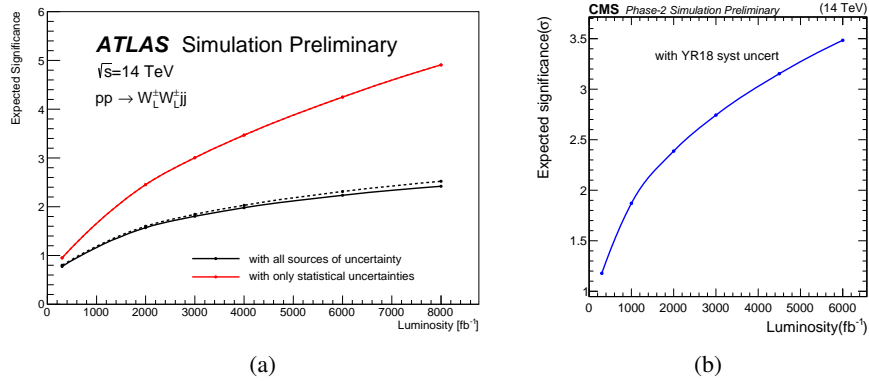
Figure 30: (a) Projection of the expected significance of the observation of the longitudinally-polarized same-sign WW process in the fully leptonic final state as a function of integrated luminosity. The solid lines show the baseline scenario for the uncertainties, while the dashed lines show the optimistic scenario, which assumes that the non-data-driven background uncertainties are aggressively reduced, as described in the [162]. (b) Significance of the observation of the scattering of a pair of longitudinally polarized, and leptonically decaying W bosons as a function of the integrated luminosity [163].

6.1.3 Charged lepton flavor violation

Standard model charged lepton flavor violation effects are too small to be observed at LHC, but limits on the cross-section will provide constraints on several BSM models. The ATLAS experiment has constrained charged lepton flavor violation by searching for $\tau \rightarrow 3\mu$ decays using the $\sqrt{s}$ =8 TeV dataset, using τ leptons originating from W bosons [170]. This study [171] also explores a new channel where the τ leptons originate from heavy flavor meson decays. Three scenarios are considered, based on expected changes to low-p_T muon triggers and improvements in the mass resolution from better tracking and vertexing provided by the detector upgrades. The expected sensitivity is calculated using a a profile likelihood fit of a BDT discriminant and 3-muon mass shape to the expected event yields in the signal region. As seen in Figure 31, analysis improvements will have a significant impact on the sensitivity of these results, and can improve over the existing analysis by up to a factor of 50. Further improvements may be possible using the τ leptons produced from heavy flavor meson decays, primarily from D_s decays, which provide around 40 times more τ leptons than the W-boson channel.
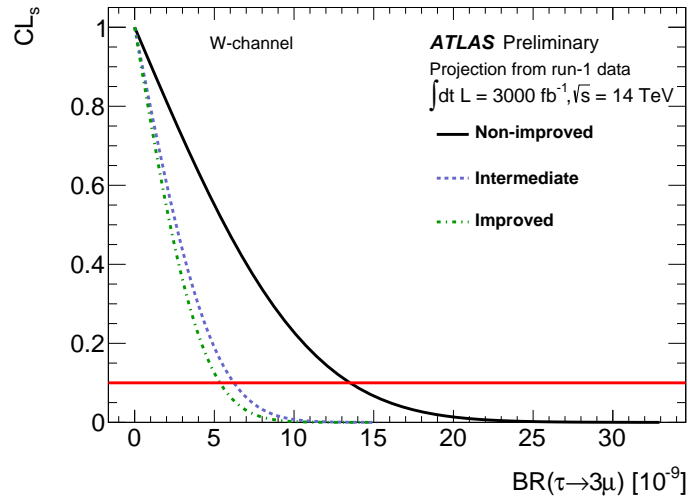
Figure 31: CL$_s$ as a function of the $\tau \rightarrow 3\mu$ branching fraction, BR($\tau \rightarrow 3\mu$), for the scenarios discussed in the text for the W-channel. The horizontal red line denotes the 90% CL [171].

6.1.4 W boson mass

Ref. [172] studies the potential for measuring the W-boson mass with the ATLAS detector at the HL-LHC. Unlike the other analyses here, this measurement would require a dedicated dataset collected at low instantaneous luminosity in order to reconstruct the missing transverse momentum with sufficient precision. Nonetheless, this measurement would benefit from forward lepton reconstruction enabled by the inner tracking detector upgrade, enhancing the current statistical precision of 7 MeV using 4.6 fb^{-1}of data. While the amount of low-μ data has not yet been decided, the statistical precision could reach 10 MeV with 200 pb^{-1}, and 3 MeV with 1 fb^{-1}. As shown in Figure 32, the precision of this measurement depends on improvements to PDFs as well as the amount of data taken at low instantaneous luminosity.

Figure 32: Measurement uncertainty for the W boson mass using different PDF sets, combining $p_{T,\ell}$ and m_T fits for $|\eta_\ell| < 4$, and for 200 pb^{-1} and 1 fb^{-1} collected at $\sqrt{s} = 14$ TeV [172].

6.2 New results

6.2.1 Prospects for the measurement of vector boson scattering production in leptonic WW and WZ diboson events with CMS at the HL-LHC [173]

The CMS prospects for measuring the $W^\pm W^\pm$ and WZ electroweak vector boson scattering processes are studied in Ref. [173]. The measurements are performed in the leptonic decay modes $W^\pm W^\pm \to \ell^\pm \nu \ell'^\pm \nu$ and $WZ \to \ell \nu \ell' \ell'$, where $\ell, \ell' = $ e, μ. The analysis is based on existing measurements at $\sqrt{s} = 13$ TeV, that are extrapolated to the full integrated luminosity at the High-Luminosity LHC at $\sqrt{s} = 14$ TeV.

This analysis presents a prospective study of VBS production in the EW WW and WZ channels with proton-proton collisions at $\sqrt{s} = 14$ TeV, by extrapolating existing measurements [156, 158] using the Run 2 dataset at $\sqrt{s} = 13$ 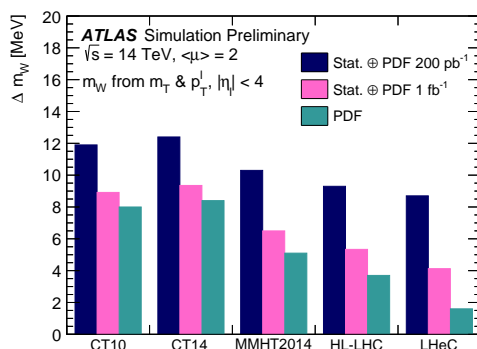TeV. The measurements were performed in the leptonic decay modes $WW \to \ell^\pm \nu \ell'^\pm \nu$ and $WZ \to \ell^\pm \nu \ell'^\pm \ell'^\mp$, where $\ell, \ell' = $ e, μ. Candidate events contain either two identified leptons of the same charge or three identified charged leptons with the total charge of ± 1, moderate missing transverse momentum, and two jets with large dijet invariant mass (m_{jj}) and large rapidity separation ($\Delta\eta_{jj}$). The requirements on m_{jj} and $\Delta\eta_{jj}$ reduce the contribution from the quantum chromodynamics (QCD) induced production of boson pairs in association with two jets and other background processes, allowing to extract the signal.

After a baseline selection is applied, the EW $W^\pm W^\pm$, EW $W^\pm Z$, and QCD $W^\pm Z$ signal production cross-sections are simultaneously measured by performing a binned maximum-likelihood fit of several distributions sensitive to these processes. The QCD $W^\pm W^\pm$ contribution is small and is taken from the SM prediction.

In the $W^\pm W^\pm$ channel, each of the W bosons can be polarized either longitudinally (W_L) or transversely (W_T), leading to three distinct contributions $W_L^\pm W_L^\pm$, $W_L^\pm W_T^\pm$, and $W_T^\pm W_T^\pm$. The prospective precision of the $W_L^\pm W_L^\pm$ cross-section measurement and the significance of the observation of this component are studied. Two sets of results are reported, with the helicity eigenstates defined either in the $W^\pm W^\pm$ center-of-mass reference frame or in the initial-state parton-parton one. A fit is performed for the simultaneous measurements of the $W_L^\pm W_L^\pm$ and $W_T^\pm W_T^\pm$ cross-sections, where the event kinematic properties are used to extract the various contributions.

The projected estimated uncertainty in the inclusive EW $W^{\pm}W^{\pm}$, EW $W^{\pm}Z$, and QCD $W^{\pm}Z$ cross-section measurements as a function of the integrated luminosity is shown in Figure 33(a). The projected estimated significance of the $W_L^{\pm}W_L^{\pm}$ process as a function of integrated luminosity is shown in Figure 33(b). By combining CMS and ATLAS measurements we expect to observe the $W_L^{\pm}W_L^{\pm}$ production at the HL-LHC.

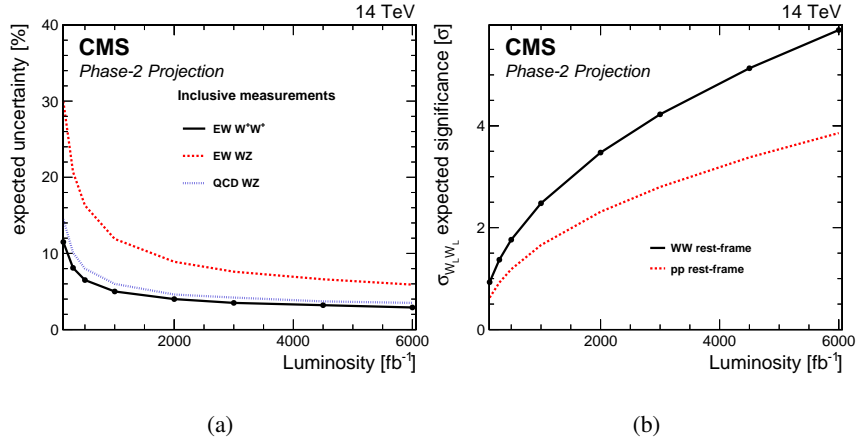

(a) (b)

Figure 33: (a) Projected estimated uncertainty in the EW $W^{\pm}W^{\pm}$, EW $W^{\pm}Z$, and QCD $W^{\pm}Z$ cross-section measurements as a function of the integrated luminosity, and (b) projected estimated significance for the EW $W_L^{\pm}W_L^{\pm}$ process as a function of the integrated luminosity for the $W^{\pm}W^{\pm}$ and parton-parton center-of-mass reference frames. [173]

7 EF05: QCD and strong interactions: Precision QCD

7.1 Yellow Report summary

Precision measurements of perturbative QCD are critical components of the LHC physics program. Measurements of jet and photon cross-sections are able to constrain PDFs and measure the running of the strong coupling α_s. These measurements are also useful for understanding backgrounds for many processes at the LHC. This section provides an overview of the results from Ref [174, 175], which cover the prospects for several different jet and photon cross-section measurements with the ATLAS detector, as well as high-p_T jet measurements with the CMS detector. The HL-LHC will will provide the opportunity to test the behavior of QCD with better precision, particularly at high energies which are currently limited by statistical uncertainties.

7.1.1 Jet cross-section measurements

The prospects for inclusive and dijet cross-section measurements at the HL-LHC with the ATLAS detector are discussed in Ref [174]. For these studies, the inclusive jet cross-section measurement is done differentially in y_j and $p_{T,j}$, while the dijet measurement is done differentially in m_{jj} and $0.5 \times (y_{j_1} - y_{j_2})$, where y is the rapidity of the jet. Figure 34 shows the ratio of several PDF sets as a function of $p_{T,j}$ and m_{jj}, and large differences are seen between different PDF sets for the high-p_T and high-m_{jj} because of their sensitivity to the gluon density in the proton. The large dataset will be beneficial to improve the statistical precision in these regions

Ref. [176] explores the impact of including HL-LHC measurements in PDF fits, using projections of measurements of jet cross section measurements, inclusive gauge boson production, top quark pair production, W-boson production, and a measurement of $p_{T,Z}$. This results in a significant reduction in the PDF uncertainties compared to the CT14 PDF set, as shown in Figure 35. With its sensitivity to the gluon density, jet cross-section measurements will be crucial for these improvements.
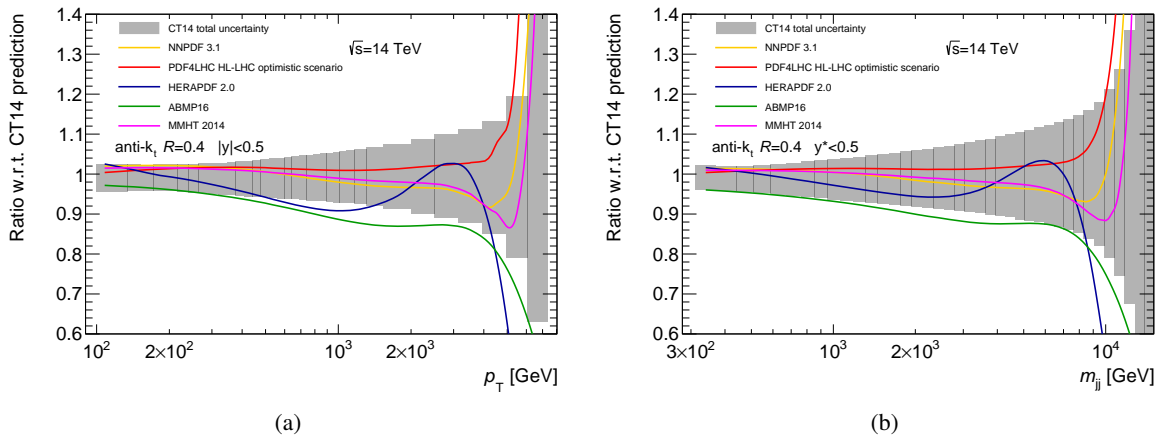
Figure 34: Ratio of cross-sections predictions from several PDF sets to the CT14 PDF prediction in the (a) inclusive jet and (b) dijet cross-sections at $\sqrt{s} = 14$ TeV. The gray band depicts the total NLO pQCD uncertainty in cross-section calculated using CT14 PDF set. [174]
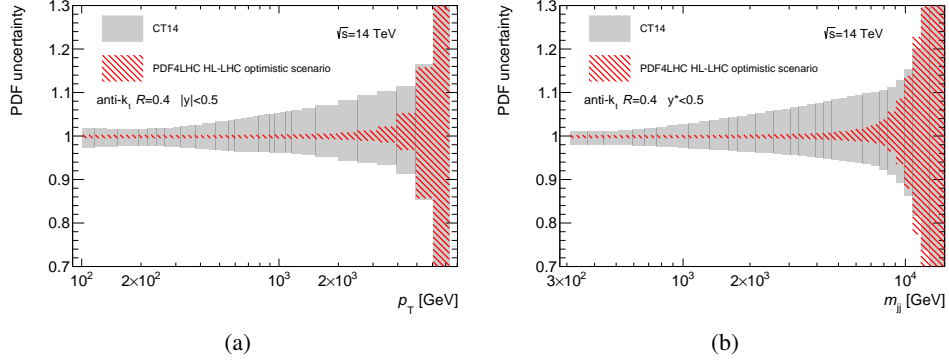
Figure 35: Comparison of the PDF uncertainty in the (a) inclusive jet and (b) dijet cross-sections calculated using the CT14 PDF and PDF4LHC HL-LHC sets at $\sqrt{s} = 14$ TeV with 3000 fb^{-1}. [174]

7.1.2 Photon cross-section measurements

The inclusive photon production has been studied differentially in E_T^γ and η^γ by ATLAS [174]. Figure 36 shows a comparison of the ratios of predictions from several PDF sets to the size of the dominant systematic uncertainties for the inclusive photon measurement. Large differences between PDF sets are seen for high values of E_T^γ, and the full HL-LHC dataset will enable measurements in these regions. Improvements in the photon energy scale and resolution uncertainties will be important to improve the impact of this measurement on PDFs and tests of perturbative QCD. The photon+jets measurement is performed differentially in E_T^γ, p_T^{jet}, $\cos\theta^*$, and $m^{\gamma j}$. With the full 3000 fb^{-1}dataset, the reach of these measurements will increase, from 3 TeV to 7 TeV in $m_{\gamma j}$, and from 2.5 TeV to 3.5 TeV for E_T^γ and p_T^{jet}.
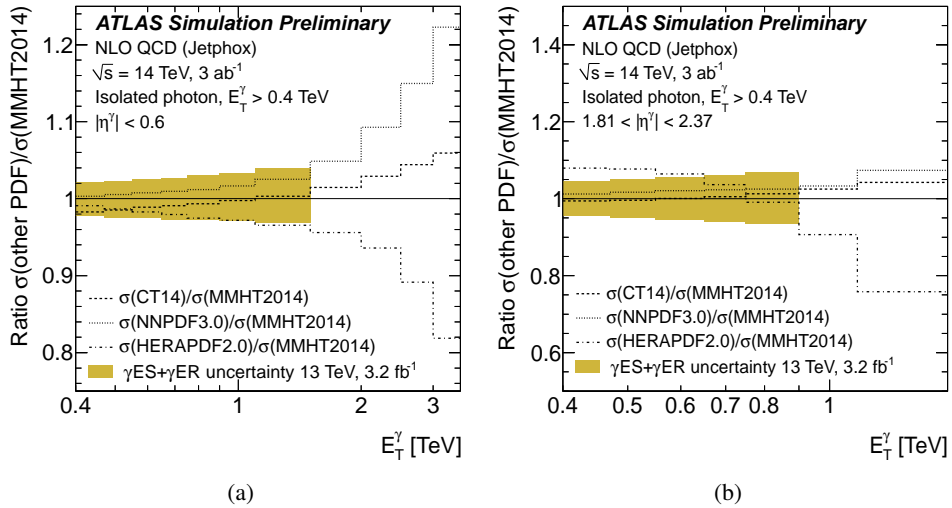
Figure 36: Ratios of the predicted number of inclusive isolated photon events using different PDFs as functions of E_T^γ for (a) $|\eta^\gamma| < 0.6$, and (b) $1.81 < |\eta^\gamma| < 2.37$. The shaded band represents the relative systematic uncertainty due to the photon energy scale (γES) and resolution (γER) estimated with 3.2 fb^{-1}of pp collisions at $\sqrt{s} = 13$ TeV. [174]

The projected impact of these and other precision measurements at the HL-LHC is shown in Figure 37,

which compares the PDF uncertainties from the MMHT2014 PDF set to PDF sets derived using projections of measurements from the HL-LHC [176].
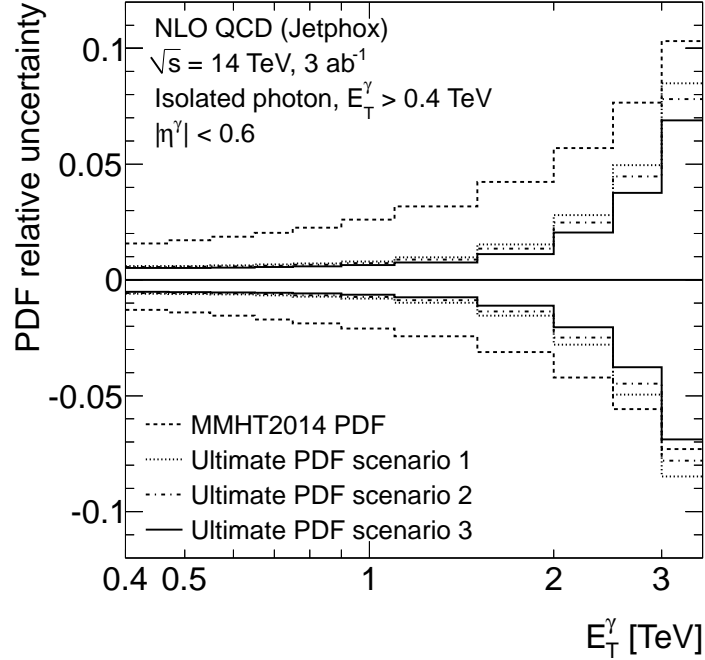
Figure 37: Relative uncertainty in the predicted number of inclusive isolated photon events due to the uncertainties in the PDFs as a function of E_T^γ. [174]

7.1.3 High-p_T jet measurements at the HL-LHC

Perturbative QCD and the structure of the proton at the highest accessible energy scales can be probed through inclusive jet production. In addition, such measurements can be used to test theoretical calculations which are available at next-to-leading order (NLO), or at next-to-next-to-leading order (NNLO) or NLO including resummation of next-to-leading logarithmic soft gluon terms.

In this analysis by the CMS Collaboration [175], kinematic distributions of jets in inclusive jet production, top quark jets and jets arising out of the hadronic decay of W-bosons have been studied, following previous $\sqrt{s}$ =7 TeV analyses [177–180]. Higher order radiative effects in QCD affect angular correlations. When jets are back-to-back, the plane transverse to these jets acquires sensitivity to multiple "soft" gluon contributions. The interference arising from these contributions between initial and final state can be significant. In the production of top quark processes, t jets are defined when the top quark decays hadronically and the decay products are clustered as a single jet. The $t\bar{t}$ cross-section as a function of the leading top quark p_T and as a function of the $\Delta(\phi)$ between the two leading $t\bar{t}$ jets is shown in Figure 38. The azimuthal correlation between the two jets is indicative of the interference effects arising out of the color connection of the jets.
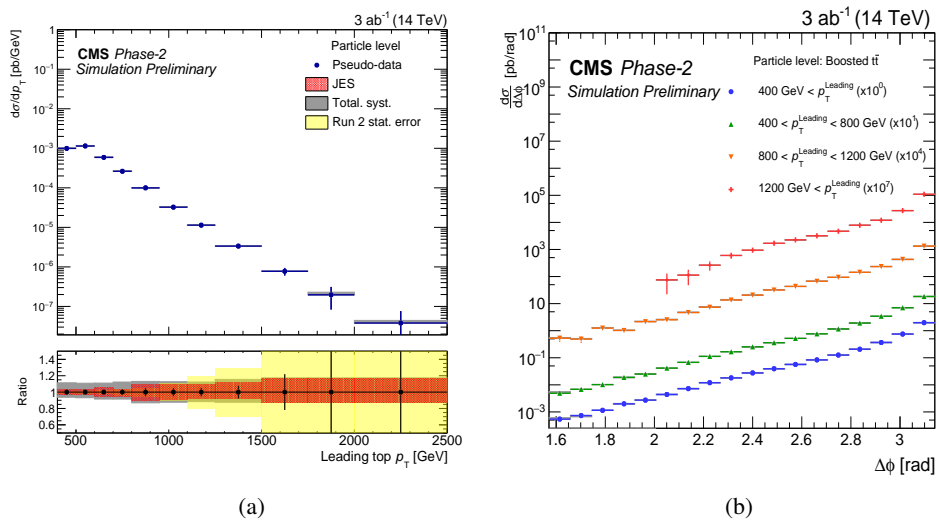
Figure 38: The particle level cross-section of the $t\bar{t}$ process as a function of (a) the leading top quark p_{T} and (b) the $\Delta(\phi)$ between the two leading $t\bar{t}$ jets. [175]

8 EF06: QCD and strong interactions: Hadronic structure and forward QCD

While the LHC is typically used to study proton-proton collisions, it can also be used to study photon-photon interactions through the use of ultra-peripheral collisions. These collisions have been used to observe processes such as light-by-light scattering and exclusive WW production. The yellow report does not include any results from ATLAS or CMS on this topic, but since this time, dedicated studies in this area have begun. One such analysis, studying exclusive WW production in photon scattering, is covered in this section, and more analyses are expected at the HL-LHC. While these analyses will benefit from upgrades to forward detectors, such as the ATLAS Forward Proton (AFP) spectrometer [181], and the CMS TOTEM proton spectrometer [182], further studies are necessary in order to understand their impact.

8.1 New results

8.1.1 Sensitivity to $\gamma\gamma \to W^{\pm}W^{\mp} \to e^{\pm}\nu_e\mu^{\mp}\nu_{\mu}$ with ATLAS at the HL-LHC [183]

The $\gamma\gamma \to WW$ process is unique because it occurs at leading-order only via electroweak gauge boson couplings, and is thus an ideal probe for searching for new physics via anomalous gauge boson couplings. The rare electroweak process $\gamma\gamma \to W^{\pm}W^{\mp} \to e^{\pm}\nu_e\mu^{\mp}\nu_{\mu}$ was first observed (rejecting the background-only hypothesis with a significance of 8.4σ) in proton-proton collisions at the LHC by the ATLAS Collaboration in 2020 using 139 fb^{-1} of data collected in Run 2 [184].

To understand the impact of the HL-LHC environment and planned ATLAS detector upgrade on the $\gamma\gamma \to W^{\pm}W^{\mp}$ measurement and identify which areas could benefit from R&D, we study the expected sensitivity at the HL-LHC when using a similar approach as in the Run 2 analysis [183].

The increased luminosity at the HL-LHC will allow a large improvement in the statistical precision of measurements of rare processes such as $\gamma\gamma \to W^{\pm}W^{\mp}$ and will allow making differential measurements. The drawback of this increase is the increase ($\times$ 5-6) in the average number of interactions per bunch crossing μ, which will adversely affect the exclusivity criterion, whichrequires that the only tracks in the event come from the W boson decay products.

The increase in statistical precision at the HL-LHC will allow studying the high-energy tails of the distributions limited by statistical uncertainties in Run 2. We perform a differential measurement in the dilepton invariant mass, $m_{\ell\ell}$, with the aim to probe the sensitivity in the high-$m_{\ell\ell}$ region for EFT prospects most sensitive to dimension-8 operators [185]. These results were studied with three different tracking scenarios:

- using only central tracks ($|\eta| < 2.5$) with the baseline HL-LHC track p_T cuts of 900 MeV for $|\eta| < 2.0$ and 400 MeV for $|\eta| > 2.0$,

- using central and forward tracks $|\eta| < 4.0$ with the baseline HL-LHC track p_T cuts,

- using only central tracks, with a track p_T cut of 500 MeV.

Figure 39(a) shows the expected signal and background yields at the HL-LHC shown stacked and as a function of $m_{\ell\ell}$, which illustrates the improvements at high dilepton mass compared to the Run 2 analysis. Figure 39(b) compares the main sources of the uncertainty for the HL-LHC and the Run 2 analyses. While the Run 2 analysis is mainly limited by statistical uncertainties, the background systematic uncertainty
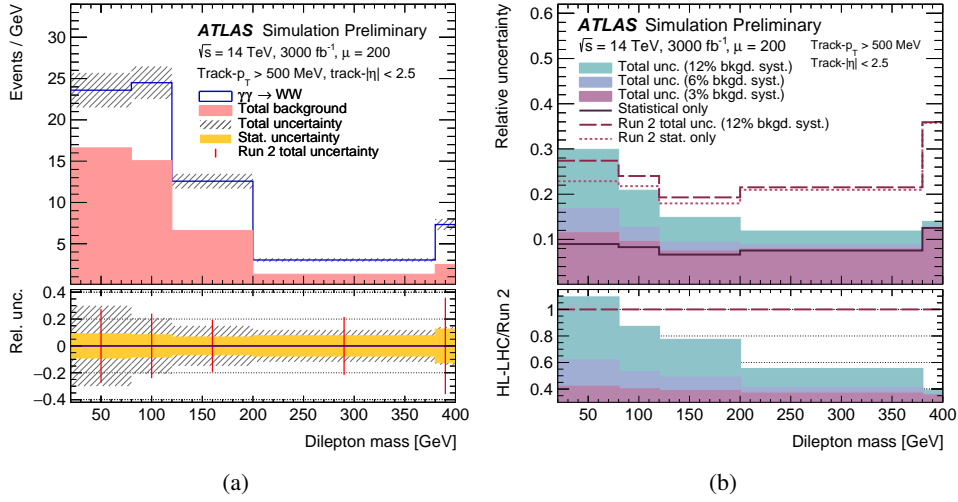
Figure 39: (a) The expected signal and background yields at the HL-LHC shown stacked and as a function of the dilepton mass, with the relative statistical and total uncertainty on the signal shown in the bottom panel assuming the same background systematic as in Run 2 of 12%. (b) A comparison of the total uncertainty when considering a reduction in the nominal background systematic by a factor of 2 and 4 and compared to the Run 2 relative uncertainties, with the ratio of the total relative uncertainty on the signal yield at the HL-LHC as a ratio to the Run 2 uncertainty shown in the bottom panel. The average pileup in Run 2 was $<\mu>=33.7$. [183]

will be dominant for most of the dilepton mass spectrum at the HL-LHC. It demonstrates the impact of the background modeling uncertainty by considering a reduction in this uncertainty by a factor of 2 and 4 compared to the Run 2 relative uncertainties. Improvements to the modeling uncertainty will have a significant impact on the precision of this measurement at the HL-LHC. Both figures are shown using central tracks, with a track p_T cut of 500 MeV, which gives the best performance of the three cuts studied.

In this study [183], we show that the higher pileup environment at the HL-LHC will give rise to important challenges to the accurate identification of exclusive final states. Efforts to reduce the theoretical modeling uncertainty will be necessary to avoid limiting the uncertainty on the extracted cross-section. In addition, the reconstructed track-p_T threshold will be a key experimental consideration in the prospects for $\gamma\gamma \rightarrow W^{\pm}W^{\mp}$ analysis at the HL-LHC. Futher R&D is required to optimize low-p_T methods at the HL-LHC.

9 EF07: QCD and strong interactions: Heavy ions

9.1 Yellow Report summary

The heavy-ion (HI) program at the LHC has proven to be a successful and important part of the LHC physics program in Runs 1 and 2. Its chief aim was the identification and characterization of a Quark Gluon Plasma (QGP) in lead-lead (Pb-Pb) collisions. In addition to QGP studies, the program has included many advances in the understanding of partonic nuclear structure, collectivity in small collision systems, and electromagnetic (EM) interactions. A detailed plan for the goals and expected measurements at the HL-LHC is presented in Ref. [3]. These are summarized below covering results on jet modification and heavy-flavor (HF) hadrons, primarily in Pb-Pb collisions, bulk particle collectivity in both Pb-Pb as well as smaller collision systems, nuclear parton density in proton-lead (p-Pb) and photonuclear collisions, and finally EM interactions from ultra-peripheral Pb-Pb collisions.

The nominal expectations for the LHC Run 3 and Run 4 are for: $13\,\text{nb}^{-1}$ of Pb-Pb collisions at $\sqrt{s_{\text{NN}}} = 5.5\,\text{TeV}$ and $1.2\,\text{pb}^{-1}$ of p-Pb collisions at $\sqrt{s_{\text{NN}}} = 8.8\,\text{TeV}$ (we note that some of the projections were not made at these exact values). In addition to the larger available luminosity, detector upgrades planned for both ATLAS and CMS experiments will benefit the HI program. In particular, the increased charged particle tracking pseudo-rapidity acceptance will be a boon to bulk particle measurements, the upgraded Zero Degree Calorimeters (ZDC) [186, 187] will improve triggering and identification for ultra-peripheral collisions (UPC), and the addition of time-of-flight particle identification capability enabled by the MIP Timing Detector [17] will allow to differentiate among low momentum charged hadrons, such as pions, kaons, or protons, improving the HF measurements.

9.1.1 Jet modification studies

Studies of jet modification in heavy ion collisions, compared to pp collisions, provide information on the interaction between high energy partons and the QGP. The energy of the jets in particular tends to be reduced through interactions with the QGP medium, a phenomenon called jet quenching. The large data samples and the improved jet reconstruction due to the upgrade of the tracking system of the CMS and ATLAS detectors will provide significantly reduced statistical and systematic uncertainties for key measurements of medium modification of light (heavy) quark jets using photon/Z (D^0-meson) tagged samples [188, 189]. By measuring the jets tagged against recoiling isolated photons, one can unambiguously access the energy loss of a parton by using the photon energy as the reference for that of the parton before quenching. In particular, the jet fragmentation functions and the jet shapes will be measured precisely for high-z region where the difference between pp and Pb-Pb collisions is not resolved yet [188, 189], as shown in Figure 40(a), thus providing information on the medium-modified structure of quark-initiated jets. The azimuth and transverse momentum correlations between bosons and jets, measured in γ+jets and Z+jets events presented in Figure 40(b), are valuable observables to study parton energy loss in the QGP [188]. Another significant improvement expected at the HL-LHC is the measurement of radial distribution of D^0 mesons in jets [188]. By studying the modification of this observable in Pb-Pb compared to pp, one can gain insights into the dynamics of heavy quarks in the QGP. In addition, the large low-PU pp data samples at $\sqrt{s}$ =14 TeV can be a great opportunity for precision measurements of the system-size dependence of the jet quenching phenomena. In this regard, high multiplicity pp events provide the reference results in small systems, thus complete the system-size dependence of the jet quenching phenomena.
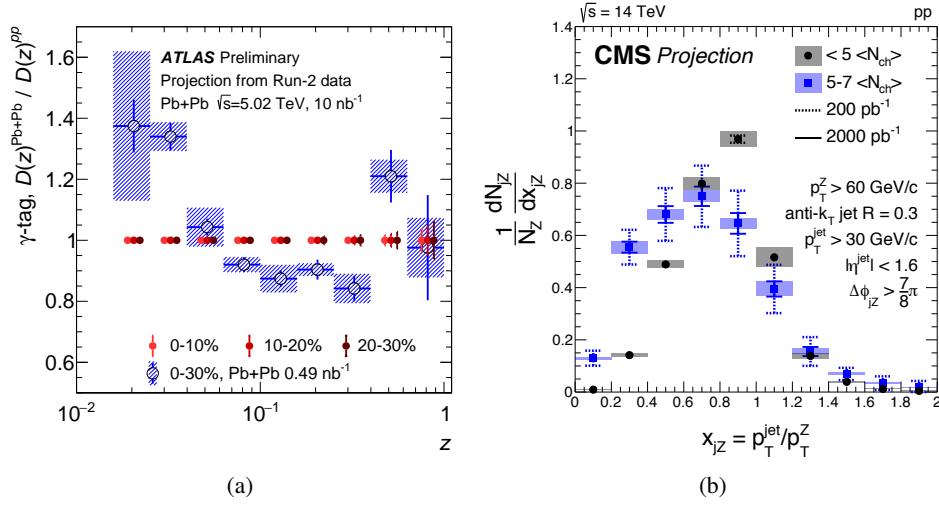
Figure 40: (a) The statistical precision of the ratio of jet fragmentation functions in Pb–Pb and pp collisions at $\sqrt{s_{NN}}$ = 5.02 TeV in ATLAS for jets recoiling from a photon [189]. The error bars at unity for $0-10\%$, $10-20\%$, and $20-30\%$ centrality classes show the expected statistical uncertainties at the HL-LHC. (b) Prospects of Z boson-jet transverse momentum balance distribution in pp collisions at $\sqrt{s}$ =14 TeV in CMS [188].

9.1.2 Heavy-flavor hadrons

HF hadrons are excellent probes of the strongly-interacting medium formed in HI collisions. Charm and beauty quarks, as a consequence of their large masses ($m_{c,b} > \lambda_{QCD}$), are mostly produced during the early stages of the collision in hard scattering processes. As HF quarks propagate through the medium, they lose energy via elastic (collisional) and inelastic (gluon radiation) interactions with the medium constituents. These interactions may lead to the thermalization of low-momentum HF quarks, which would then take part in the expansion and hadronization of the medium. In addition, HF mesons, such as quarkonia, can be dissociated in the medium due to Debye color screening or recombined from individual heavy quarks and anti-quarks diffusing through the medium [190–192]. Therefore, the measurement of HF hadrons can provide crucial information on the full evolution of the system and allows to get information on the quark-mass dependence of the medium-induced processes.

The larger experimental data samples at the HL-LHC, combined with improved detector performance and measurement techniques, will allow the CMS and ATLAS experiments to significantly improve over the current HF measurements. The p_T dependence of the quarkonium nuclear modification factor (R_{AA}) will be measured with high precision up to about 80 GeV for prompt J/ψ and 50 GeV for $\Upsilon(1S)$ [193] (compared to 50 and 30 GeV respectively, with the present data), allowing to discern whether quarkonium formation at high p_T is determined by the Debye screening mechanism, or by energy loss of the heavy quark or the quarkonium in the medium. The elliptic flow measurements of charm mesons in p-Pb collisions [194] and of HF decay muons [195] and $\Upsilon(1S)$ mesons [193] in Pb-Pb collisions will be significantly improved as observed in Figure 41, providing insights on the collective expansion and degree of thermalization of HF quarks in the medium at low p_T, and on the presence of recombination of bottomonia from deconfined beauty quarks in the QGP. The production of strange B mesons and charm baryons in pp and Pb-Pb collisions [193] will also be measured with sufficient precision to further investigate the interplay between the predicted enhancement of strange quark production and the quenching mechanism of beauty quarks, and the contribution of recombination of HF quarks with lighter quarks to the hadronization process in

HI collisions. Finally, the precise measurements of beauty mesons in p-Pb collisions [193] will help to elucidate the relative contribution of hadronization and nuclear-matter effects (e.g. nuclear PDF, gluon saturation and coherent energy loss), as well as serve as a baseline for the understanding of beauty-quark energy loss in Pb-Pb collisions.

(a)

(b)

(c)
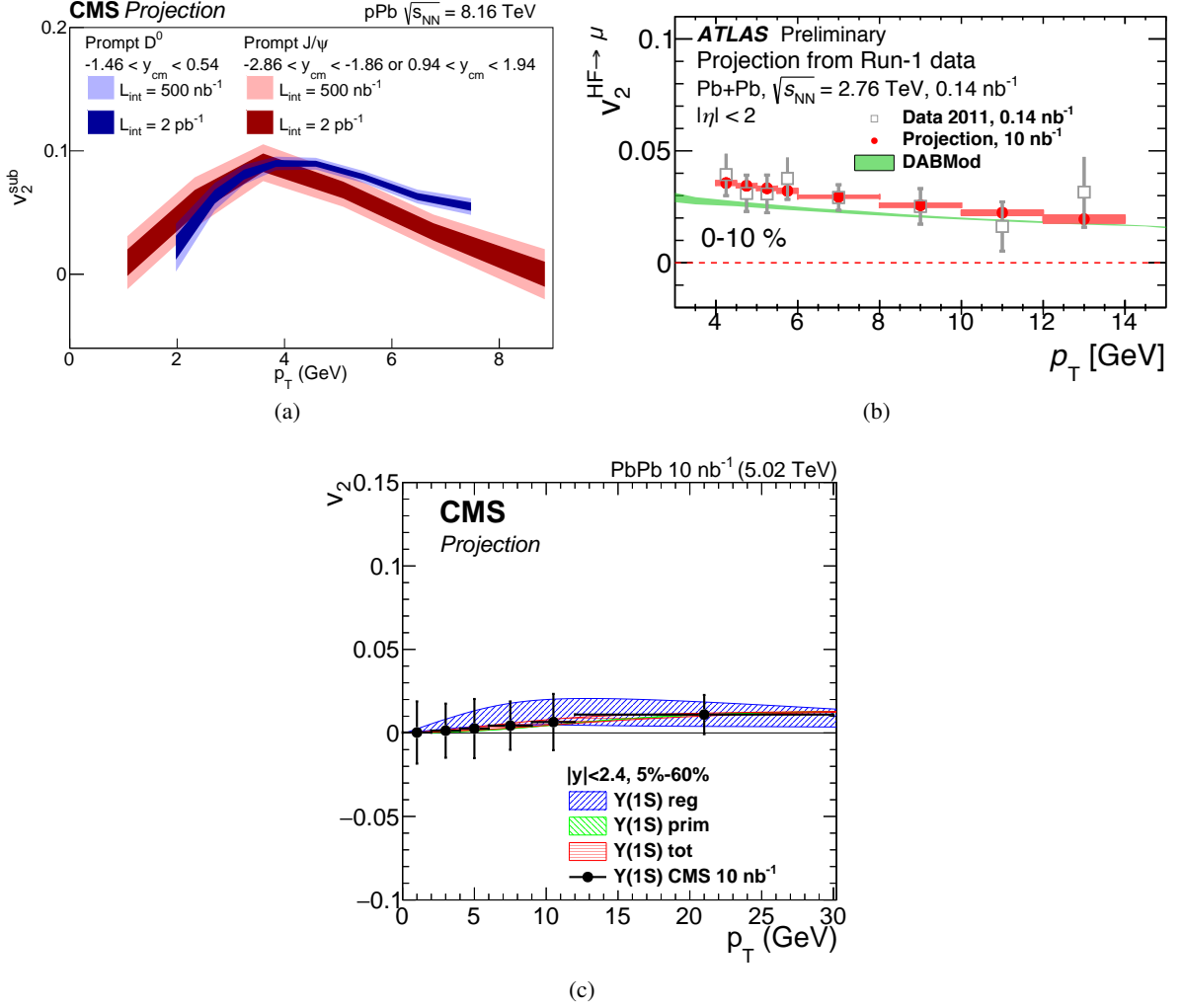
Figure 41: Elliptic flow projections as a function of p_T of: (a) prompt D and J/ψ mesons in CMS in high-multiplicity p-Pb collisions at $\sqrt{s_{NN}}$ = 8.16 TeV [194], (b) HF decay muons in ATLAS in Pb-Pb collisions at $\sqrt{s_{NN}}$ = 2.76 TeV [195] and (c) $\Upsilon(1S)$ mesons in CMS in Pb-Pb collisions at $\sqrt{s_{NN}}$ = 5.02 TeV [193].

9.1.3 Particle collectivity in small and large systems

With the large minimum bias samples of pp, pPb and PbPb datasets of HL-LHC, it will be possible to reach an unprecedented experimental precision that will help us to understand the collectivity of small and large systems. The pivotal upgrades of trackers in CMS and ATLAS will enable the measurement of charged particles in the wide pseudo-rapidity range ($|\eta| < 4$). In small systems, a significant statistical improvement is expected for the elaborate flow variables. In particular, the symmetric cumulant observables,

SC(m, n) which are the correlations between Fourier coefficients based on 4-particle correlations will be clearly assessed [196]. Since those are very sensitive to the initial state and its fluctuation, the precision measurement of them will constrain the current interpretation of the ridge phenomenon in small systems [197–200], as well as catching hold of non-flow effects in early stages [194]. In addition, we expect a crucial improvement in our understanding for the system size of collisions by meauring the Hanbury Brown and Twiss (HBT) radii in small systems [195]. With azimuthally sensitive femtoscopy, the spatial ellipticity of the medium at freeze-out can be measured. In particular, the HL-LHC p-Pb data will allow us to unambiguously investigate the normalized second-order Fourier component of the transverse HBT radius as a function of the magnitude of flow. In Pb-Pb collisions, an interesting observable which can be highly enriched by HL-LHC data is the flow decorrelation [201]. The extended η acceptance in Run 4 will lead to significant improvement in characterizing the rapidity dependence of the factorization breaking. A significant improvement of the forward-backward multiplicity correlation and multi-particle cumulants will bring a better understanding of the fluctuations of medium in early stages [195].

9.1.4 Nuclear parton distribution functions

The structure of nucleons and nuclei are both key to understanding heavy-ion collisions as well as fundamental features of the nucleus. In particular, knowledge of particle production at small x of the nucleus and the possible effects, or even presence, of a Color Glass Condensate [202] regime are poorly constrained. Measurements made during the LHC Run 1 and Run 2 in Pb-Pb and especially p-Pb collisions, have favored the inclusion of nuclear modification to the parton distribution functions (PDF) extracted for free protons. The p-Pb collision system is an excellent tool to study and constrain these nuclear parton distribution functions (nPDF) since the asymmetric system allows one to select low x regions of the nucleus by looking at forward, i.e. proton-going direction, rapidity and vice-versa.

To this end ATLAS and CMS both intend to measure W and Z boson production, especially differentially in rapidity (or lepton pseudo-rapidity in the W boson case) from p-Pb collisions to constrain the quark nPDF [203, 204]. Complementing these measurements, CMS has projected the measurement of dijet pseudorapidity which is sensitive to the gluon nPDF [203]. The measurement of differential $t\bar{t}$ cross sections in p-Pb collisions is a novel and potentially precise probe of the nuclear gluon density. Figure 42 shows the mass distributions of the top quark and relevant backgrounds projected for p-Pb collisions for three different selections on the number of b-tagged jets [203]. Additional experimental leverage of the event-by-event sensitivity to Q^2 and nuclear x may be obtained by EW boson (W and Z) plus jet events, as projected by ATLAS [204].

9.1.5 Ultra-peripheral collisions

In addition to the fully hadronic collisions that are the main focus of the heavy-ion program at the LHC, the large EM fields generated by ultra-relativistic charged ions, which may be thought of as Weizsäcker-Williams photons, may also interact with the nucleus (photo-nuclear) or with each other (photon-photon). These UPCs, characterized by an impact parameter greater than twice the nuclear radius, have become an important part of the heavy-ion program allowing unique avenues of study for both EM and nuclear interactions. Both CMS and ATLAS have a suite of planned measurements, and it is worth noting that the ZDCs - key detectors for the identification of UPC - are being upgraded for better triggering capabilities, segmentation, and radiation hardness in both experiments.
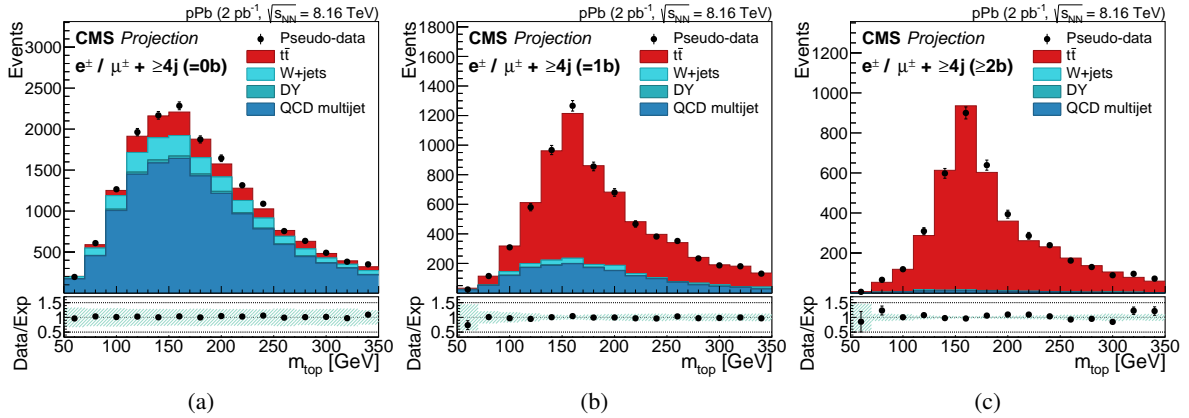
Figure 42: Distributions of m_{top} in the (a) 0, (b) 1, and (c) 2 b-tagged jet categories. The sum of the predictions for the $t\bar{t}$ signal and background is compared to pseudo-data (sampled randomly from the total of the predictions in each category). The bottom panels show the ratio between the pseudo-data and the sum of the predictions. The shaded band represents the relative uncertainty due to the limited event count in the simulated samples and the estimate of the normalization of the QCD multijet background [203].

Photo-nuclear collisions are an effective tool for the study of the nuclear structure, and several photo-nuclear collision observables may be used to constrain the nPDF (similar to the p-Pb studies discussed in Section 9.1.4). It is expected that the cross section for coherent photoproduction of vector mesons is proportional to the gluon density, and in particular the HL-LHC will allow CMS to extend these measurements to the $\Upsilon(1S)$ meson [203]. The ATLAS measurement of di-jets from photonuclear Pb-Pb collisions is expected to be statistically significant down to nuclear $x \approx 10^{-4}$ with the full integrated luminosity of the HL-LHC [3].

Besides photo-nuclear interactions, photon-photon interactions are also of great interest. The ATLAS measurement of exclusive dimuons from $\gamma\gamma \to \mu^+\mu^-$ will reach a precision that can be used to calibrate the photon flux and reduce the uncertainty on the nuclear charge distribution [205]. The rare light-by-light (LbyL) scattering process, measured by both ATLAS and CMS, is to this point statistics starved and will greatly benefit from the increased luminosity as well as improvements in triggering capabilities [205]. Of particular note is the search for BSM axion-like particles, which may be detectable via $\gamma\gamma \to a \to \gamma\gamma$, and where LbyL interactions from Pb-Pb measured by both ATLAS and CMS already set the most stringent limits for axion masses between $\sim 5 - 100$ GeV and will improve with the new data as shown in Figure 43.

9.2 New results

9.2.1 Measurement of the $\gamma\gamma \to \tau^+\tau^-$ process with CMS at the HL-LHC [208]

Ultra-peripheral heavy ion collisions, where there is no hadronic interaction between the nuclei, provide a very clean environment to study various $\gamma\gamma$-induced processes. These reactions also give rise to the production of τ lepton pairs. With this projection study, we highlight the importance of measuring the $\gamma\gamma \to \tau^+\tau^-$ process using UPC at HL-LHC. We focus on the final state involving one muon and three charged particles, and hence taking full advantage of the clean photon fusion $\gamma\gamma \to \tau^+\tau^-$ events to
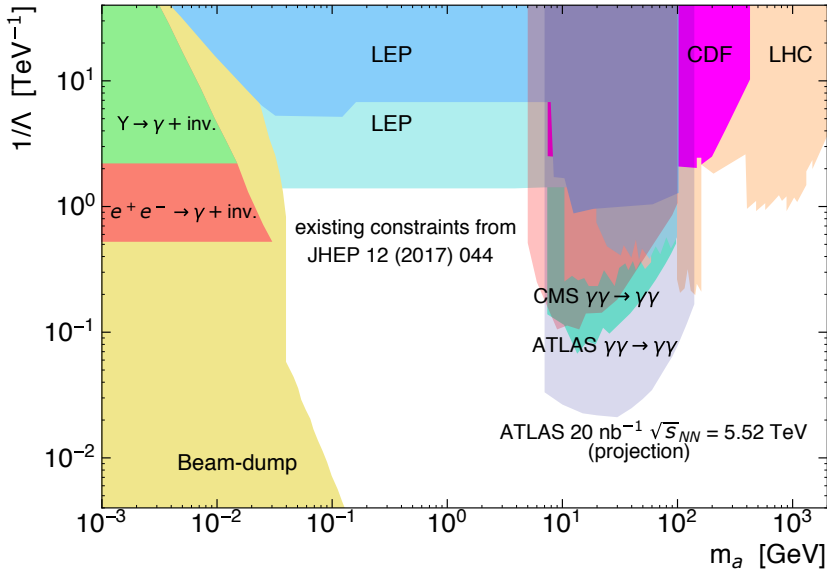
Figure 43: Compilation of exclusion limits obtained by different experiments [3, 206]. In light grey, the ATLAS $\gamma\gamma \to \gamma\gamma$ from 20 nb^{-1} limit at $\sqrt{s_{NN}}$ = 5.52 TeV is presented. The ATLAS $\gamma\gamma \to \gamma\gamma$ represents the exclusion limit derived from the LbyL cross section measured in Pb-Pb collisions by ATLAS [205], while the CMS $\gamma\gamma \to \gamma\gamma$ limit comes from the recent analysis described in Ref. [207].

reconstruct leptonic and hadronic τ lepton decays, respectively. The $\gamma\gamma \to \tau^+\tau^-$ process is sensitive to physics beyond the standard model since it paves the way for improved constraints on the anomalous magnetic moment of the τ lepton, currently known with poor precision from past lepton-lepton collider [209].

The projection is based on analysis described in Ref. [208] assuming the following uncertainties at the HL-LHC.

Over 10^6 (2.5×10^3) $\gamma\gamma \to \tau^+\tau^-$ UPC events are expected inclusively (in the fiducial phase space region) for the expected 13 nb^{-1} Pb-Pb dataset, hence the statistical uncertainty is expected to affect the $\sigma^{PbPb}_{\gamma\gamma\to\tau^+\tau^-}$ measurement by $\lesssim 2\%$.

The leptonic background ($\gamma\gamma \to \ell^+\ell^-$; $\ell \in [e, \mu]$) is suppressed by track impact parameters by exploiting the displaced τ lepton decays. The hadronic background ($\gamma\gamma \to q\bar{q}$) will be estimated using data-driven techniques, and we expect its impact to be nondominant ($\lesssim 1\%$), which is supported by the current LHC measurement [208]. Lepton and tracking reconstruction can be better controlled using clean and abundant $\gamma\gamma \to \ell^+\ell^-$, J/$\psi$, Υ and D$^0 \to$ Kppp, Kp events at the HL-LHC, respectively, therefore we consider the respective uncertainties at the HL-LHC performance of $\lesssim 2\%$ for both. The luminosity uncertainty can be controlled at a level of $\lesssim 1.5\%$ [210]. Theoretical systematic uncertainties are expected to be dominated by modeling of the photon flux, nuclear form factors, and nucleon dissociation as shown in Figure 44.

We therefore foresee $\lesssim 4$ (<2) % systematic (statistical) uncertainty in the HL-LHC measurement, representing approximately a factor of four improvement relative to the current measurement at LHC [208]. By including more decay channels and with improved analysis techniques (e.g., shape analysis of a kinematical ratio $\sigma^{PbPb}_{\gamma\gamma\to\tau^+\tau^-}/\sigma^{PbPb}_{\gamma\gamma\to\ell^+\ell^-}$) the precision in the anomalous magnetic moment of the τ lepton is expected to surpass the existing measurements.
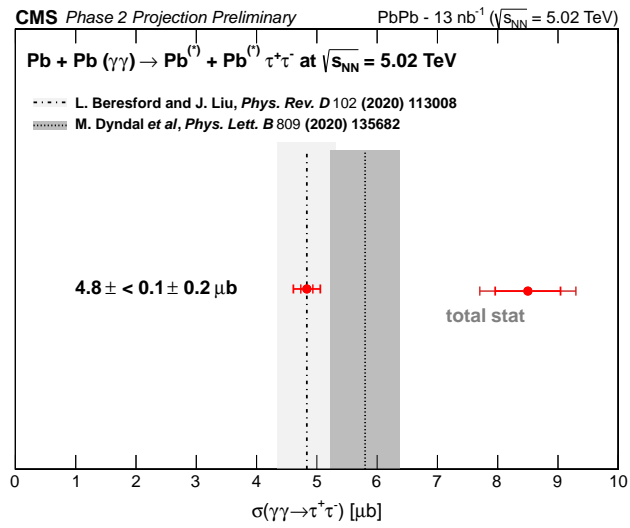
Figure 44: The $\gamma\gamma \to \tau^+\tau^-$ cross section, as expected to be measured in a fiducial phase space region in CMS assuming 13 nb^{-1} of Pb-Pb integrated luminosity at the HL-LHC at $\sqrt{s_{NN}}$ = 5.02 TeV and total uncertainty of 4%, is compared to the current theoretical predictions [211, 212].

10 EF08: BSM: Model specific explorations

10.1 Yellow Report summary

The ATLAS and CMS Collaborations studied the expected sensitivity to several BSM models as documented in Ref. [3]. This section provides a high-level summary of these studies on searches for R-parity conserving SUSY processes, leptoquark (LQ) production, and two-Higgs-doublet plus additional pseudoscalar (2HDMa) models, while new searches are presented in dedicated sections. Expected limits are evaluated at 95% CL, and discovery potential is quoted at 5σ expected sensitivity.

SUSY remains one of the more plausible theories for BSM physics as it answers many of the open questions in the SM. Searches carried out with the LHC Run 1 and Run 2 datasets have placed stringent constraints on SUSY particles, in particular for squarks and gluinos in scenarios with large mass differences between the relevant states. With the increased center-of-mass energy and, more importantly, the factor of ten larger dataset, the HL-LHC will enable the ATLAS and CMS experiments to probe challenging and unexplored regions of SUSY phase-space. For example, processes with small cross-sections (*e.g.* EWK production) and scenarios with small mass differences between the sparticles will greatly benefit from the larger dataset. Additionally, the upgraded detectors will offer new capabilities. This includes improved reconstruction of high momentum particles thanks to the tracker and calorimeter upgrades, improved resolution of missing transverse momentum allowing for lower trigger thresholds, and precision measurement of the particles' arrival time provided by the new MIP Timing Detector in CMS.

10.1.1 Searches for wino-like electroweakinos

In many realizations of SUSY, electroweak gauginos (EWKinos) can have masses of the order of a few hundred GeV and thus be within the reach of the HL-LHC. Once pair-produced, heavy EWKinos can decay into the lightest neutralino, typically assumed to be stable, by emitting gauge and Higgs bosons. As a part of the expected comprehensive search program at the HL-LHC, the ATLAS and CMS Collaborations investigated the prospects of several searches optimized for different EWKino compositions (wino-, bino-, or higgsino-like). Unless specified, the branching fraction in the mode of interest is assumed to be 100%.

Sensitivity projections for wino-like $\tilde{\chi}_1^\pm \tilde{\chi}_2^0$ production with decays into either a WZ or Wh pair were developed in Ref. [213], where h is the SM Higgs boson. In the case with a Z boson in the $\tilde{\chi}_2^0$ decay chain, a three-lepton final state is used. Signal-like events without b-tagged jets, large m_T, and large E_T^{miss} are selected. With 5% experimental and 10% theory uncertainties, chargino and neutralino masses up to 1150 GeV could be excluded (Figure 45(a)), compared to ~650 GeV from similar Run 2 analyses [218, 219]. The discovery potential extends to 920 GeV. Sensitivity to even higher mass EWKinos is achievable by exploring fully hadronic final-states as demonstrated in Run 2 searches [220, 221] and in the recent HL-LHC study described in Section 10.2.1.

The second search for wino-like $\tilde{\chi}_1^\pm \tilde{\chi}_2^0$ production, with $h \to bb$ in the decay, considers events with exactly one lepton and two b-tagged jets, with up to one additional non-b-tagged jet [213]. A loose pre-selection, including $E_T^{\text{miss}} > 200$ GeV and an m_{bb} consistent with the Higgs boson, is applied before training three BDTs: one each for small, medium, and large mass splittings. A 7% theory uncertainty on the main top-quark backgrounds and experimental jet uncertainties of 6% are assumed. Chargino $\tilde{\chi}_1^\pm$ and neutralino $\tilde{\chi}_2^0$ masses up to 1280 GeV could be excluded, compared to 740 GeV in the corresponding Run 2 analysis [222]. The discovery potential reaches 1080 GeV. Using dedicated MVA discriminants to identify
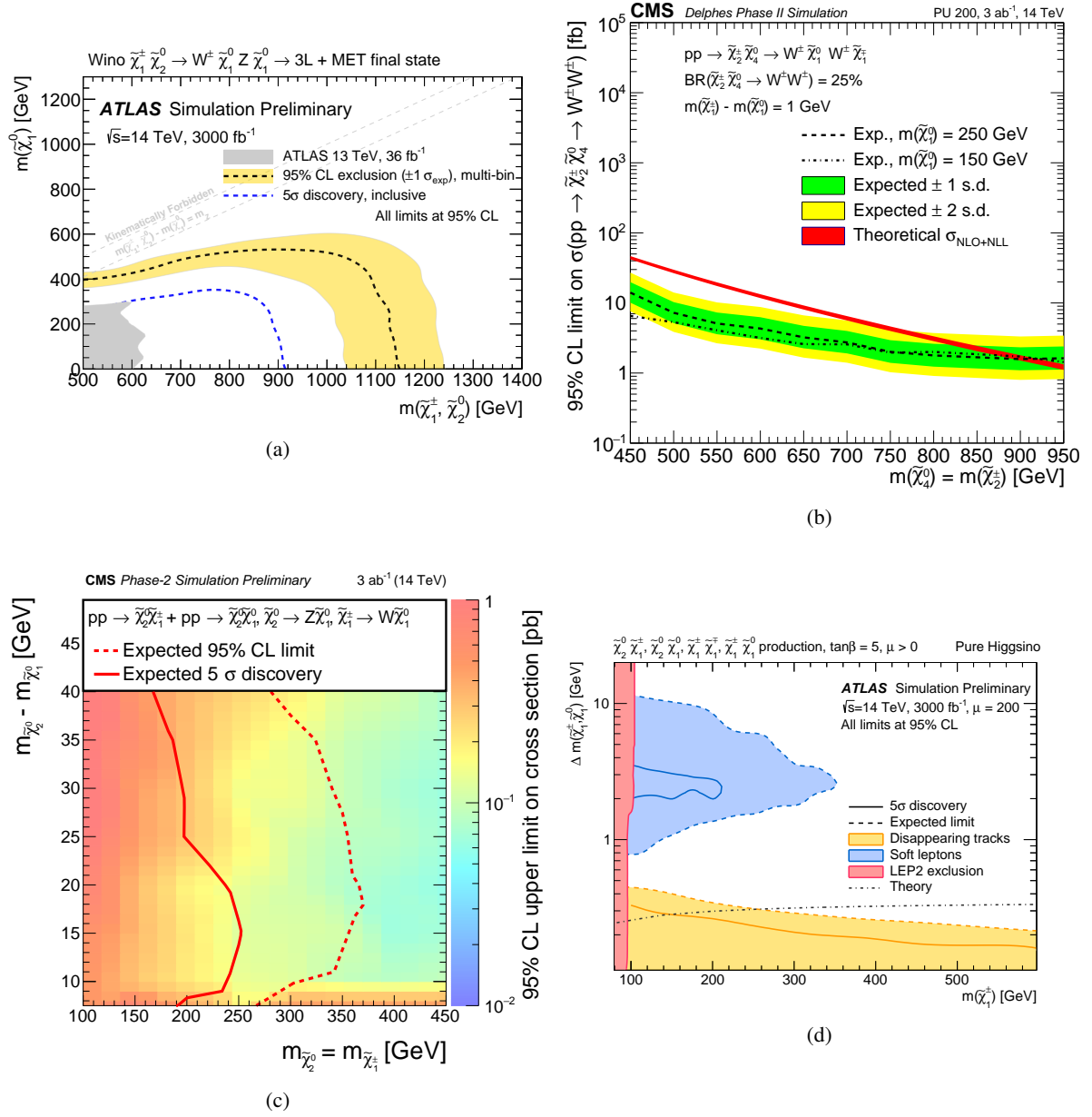
Figure 45: Projected limits and discovery potential at the HL-LHC for various SUSY processes: (a) wino-like $\tilde{\chi}_1^\pm \tilde{\chi}_2^0$ production (WZ decay mode) [213]; (b) wino-like $\tilde{\chi}_2^\pm \tilde{\chi}_4^0$ production ($W^\pm W^\pm$ decay mode) [3]; (c) higgsino-like $\tilde{\chi}\tilde{\chi}$ production, $m_{\tilde{\chi}_1^\pm} = m_{\tilde{\chi}_2^0}$ [214]; and (d) higgsino-like $\tilde{\chi}\tilde{\chi}$ production, $m_{\tilde{\chi}_1^\pm} = 0.5 \times [m_{\tilde{\chi}_1^0} + m_{\tilde{\chi}_2^0}]$ [215];

(a)

(b)

(c)
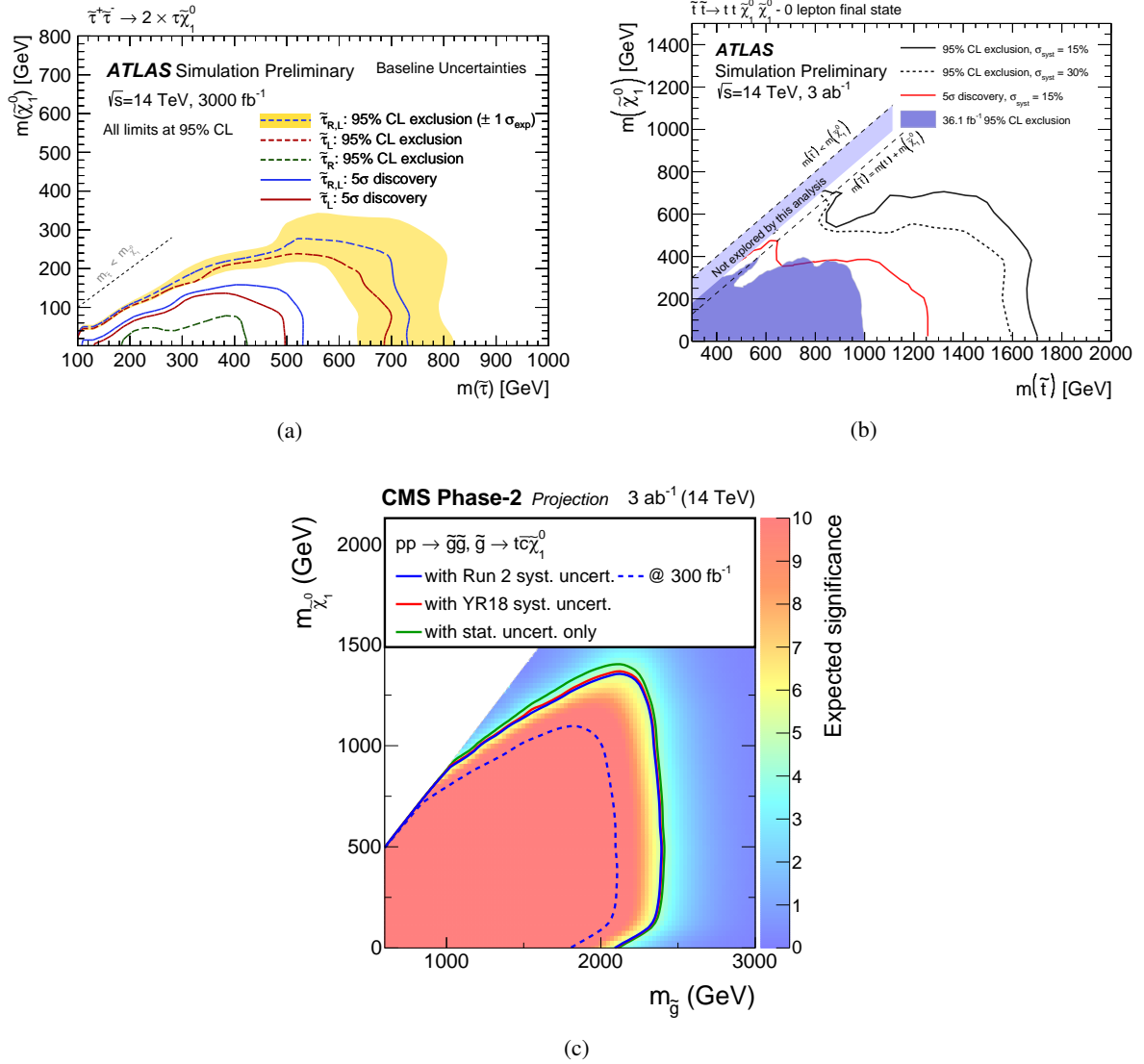
Figure 46: Projected limits and discovery potential at the HL-LHC for various SUSY processes: (a) $\tilde{\tau}_{L,R}\tilde{\tau}_{L,R}$ (fully hadronic mode) [213]; (b) $\tilde{t}_1\tilde{t}_1$ (fully hadronic mode) [216]; and (c) gluino-mediated production of $\tilde{t}_1\tilde{t}_1$ ($\tilde{t} \to c\tilde{\chi}_1^0$ mode) [217]

Higgs bosons at large transverse momentum, as done in a Run 2 search [223], could further improve the reach at large masses. As in the *WZ* channel, Run 2 searches with fully hadronic final-states [220, 221] out-perform those with leptons at high EWKino masses and large mass splittings, yielding sensitivities to masses as high as 1050 GeV. A new targeted search at the HL-LHC is presented in Section 10.2.1.

The wino-like $\tilde{\chi}_1^+ \tilde{\chi}_1^-$ pair-production cross-section is smaller than that of $\tilde{\chi}_1^\pm \tilde{\chi}_2^0$, but it is not negligible. Prospects for searching for $\tilde{\chi}_1^+ \tilde{\chi}_1^-$ pairs decaying into $W^\pm$ and $\tilde{\chi}_1^0$ were studied in Ref. [213]. A two-lepton and $E_T^{miss} > 110$ GeV final state with no *b*-tagged jet is used. With 5% experimental and 5% modeling uncertainties on the SM background, this search could exclude $\tilde{\chi}_1^\pm$ masses up to 840 GeV, compared to roughly 400 GeV from the Run 2 analysis [224]. Discovery potential reaches up to $m_{\tilde{\chi}_1^\pm} = 600$ GeV. While not dominating the sensitivity of the experiments to wino-like EWKinos, the search for chargino pairs does increase the overall sensitivity. In addition, the inclusion of fully hadronic channels could further boost the yield as shown in Refs. [220, 221], where chargino masses in the range 300–750 GeV are probed with Run 2 data.

Lastly, the analysis in Ref. [3] targets the pair production of high mass wino-like $\tilde{\chi}_2^\pm \tilde{\chi}_4^0$ decaying into highly compressed higgsino states, thus assumed to be undetectable, and two same-charge *W* bosons. The existence of these complex spectra with almost-mass-degenerate higgsino-like EWKinos at low mass and heavier wino-like sparticles is highly motivated by naturalness arguments. The analysis uses events with two high transverse-momentum leptons with the same electric charge. A sample of events with high transverse missing-momentum and moderate hadronic activities is expected to provide the best sensitivity. Wino-like mass-degenerate $\tilde{\chi}_2^\pm$s and $\tilde{\chi}_4^0$s could be excluded up to masses of 900 GeV (Figure 45(b)) for two assumptions on the value of $\tilde{\chi}_1^0$ mass: 150 GeV (representative of the region of parameter space outside the reach of the Run 2 search for direct production of higgsinos) and 250 GeV (close to the sensitivity reach of the same search when extrapolated to the HL-LHC).

10.1.2 Searches for compressed mass spectrum

Searches for the direct production of higgsino states are documented in Refs. [214, 215]. The first search is based on events with two same-flavor low-transverse-momentum (5–30 GeV) leptons with opposite electric charge accompanied by one high-momentum jet and missing transverse momentum. The invariant mass of the dilepton system, the missing transverse momentum and the momentum of the sub-leading lepton are found to provide the best signal-to-background discrimination in events with no jets identified as originating from a *b*-quark. With experimental systematic uncertainties up to 2.5% (30%) on the prompt (non-prompt) background yields and 10% on the signal acceptance, mass-degenerate $\tilde{\chi}_1^\pm$ and $\tilde{\chi}_2^0$ particles with masses up to 250 GeV can be discovered for a mass difference of 15 GeV relative to the lightest neutralino (Figure 45(c)). For these scenarios, $\tilde{\chi}_1^\pm$ and $\tilde{\chi}_2^0$ with masses up to 360 GeV can be excluded. The second, similar search is tailored to smaller mass splittings (few GeV) and only considers events with muons, down to $p_T > 3$ GeV [215]. It could exclude $\tilde{\chi}_2^0$ masses up to 350 GeV and to mass splittings between 2–25 GeV for $m_{\tilde{\chi}_2^0} = 100$ GeV (Figure 45(d)). The discovery potential extends slightly above $m_{\tilde{\chi}_2^0} = 200$ GeV for mass splittings near 5 GeV. It is important to highlight that the Run 2 analyses in Refs. [225, 226] already exclude masses up to 205 GeV for mass splittings of 7.5 GeV and mass splittings as small as 2.4 GeV for $\tilde{\chi}_1^\pm$ masses at the edge of LEP exclusions. This originates from the use of additional channels and the deployment of more advanced techniques than those used for the HL-LHC projections. Therefore, the HL-LHC projections quoted above should be considered conservative.

A third search, designed to probe for both pure-higgsino and pure-winos EWKinos in scenarios with highly compressed spectra (mass differences in the MeV range), is performed in events with disappearing tracks (short tracklets), large E_T^{miss} with an ISR jet, and no leptons [215]. Backgrounds depend on the detector layout and material and are scaled from Run 2 based on simulation of the upgraded inner detector and its layout. Exclusion sensitivity in $m_{\tilde{\chi}_1^\pm}$ reaches up to 600 GeV for the higgsino scenario with a mass splitting of 0.2 GeV, or up to mass splittings of 0.4 GeV at $m_{\tilde{\chi}_1^\pm}$ = 100 GeV (Figure 45(d)). A recent Run 2 search [227] is already able to exclude masses up to 500 GeV or mass splittings up to 0.37 GeV respectively by improving the track-quality requirements compared to the previous search that this projection is based on.

10.1.3 Searches for staus

Prospects for searches of stau pair-production (either the $\tilde{\tau}_L$, $\tilde{\tau}_R$, or both) in final states with two hadronic taus were assessed [213]. Events with exactly two hadronic taus and $E_T^{miss} > 200$ GeV are selected; events with electrons, muons, b-tagged jets, or high-p_T jets are vetoed. Assuming 20% experimental uncertainties and improved modeling uncertainties, exclusion limits could reach stau masses of 430/730 GeV ($\tilde{\tau}_R$/combined $\tilde{\tau}_R + \tilde{\tau}_L$) (Figure 46(a)) compared to the 120–390 GeV region for the combined scenario with Run 2 data [228]. The discovery potential spans 110–530 (500) GeV for the combined $\tilde{\tau}_R + \tilde{\tau}_L$ ($\tilde{\tau}_L$) scenario (no sensitivity for $\tilde{\tau}_R$). A similar study [229] shows that adding the $\ell\tau_h$ decay mode extends the exclusion bounds by about 60–80 GeV.

10.1.4 Searches for stops

Relatively light stops and gluinos are also a part of natural SUSY models. The large dataset of the HL-LHC will allow for searches for stops well above 1 TeV in mass, as well as to improve sensitivity in the region where small mass splittings between the sparticles makes it difficult to discern the signal from SM processes. The expected sensitivity to stop-pair production with all-hadronic final states was evaluated in Refs. [216, 217]. In the first search, only the regions with mass differences near the top-quark mass and above were considered. The large mass difference regime is targeted by requiring high momentum jets, large E_T^{miss}, and the presence of b-tagged jets. Stop masses up to 1.7 (1.6) TeV could be excluded under the assumption of a 15 (30)% uncertainty on the background (Figure 46(b)). For mass differences near the top-quark mass, an ISR jet is required and the recursive-jigsaw reconstruction technique is employed, and exclusion sensitivity extends to $m_{\tilde{t}}$ = 850 GeV. The discovery potential extends up to $m_{\tilde{t}}$ = 1.25 and 0.65 TeV for these two mass splitting scenarios respectively. The Run 2 analysis excludes stop masses up to 1.25 TeV for large mass splittings and in the range 300–630 GeV for mass splittings near the top-quark mass [230].

The second search [217] also targets scenarios where the mass difference between the stop and the neutralino is small and the $\tilde{t}$ is kinematically unable to decay to an on-shell top quark. The stop is assumed to decay into either $bff\tilde{\chi}_1^0$ (where f is any fermion) or $c\tilde{\chi}_1^0$. Since the search for direct stop pair production would face major experimental challenges in these scenarios, this analysis looks instead for gluino pair production where each gluino decays into a stop and a high momentum top quark, used as key signature to discriminate the signal from the background. The analysis is performed as a projection of a Run 2 search for new physics in hadronic final states with boosted W bosons or top-quarks, identified using the jet mass, the n-subjettiness variables and subjet b-tagging. Signal regions are defined based on the number of W boson and top-quark candidates, the number of jets, and the value of the razor kinematic variables M_R and R^2. The projection results in Figure 46(c) show that HL-LHC would achieve sensitivity for exclusion (discovery) up to gluino

masses of 2.6 TeV (2.4 TeV) in the considered scenarios. Recent studies in Run 2 data [231] demonstrate that using algorithms based on deep neural networks to identify hadronically decaying top-quarks and *W* bosons can significantly extend the sensitivity of the search with respect to the analysis the projection is based on [232].

10.1.5 Searches for scalar leptoquarks

Third-generation scalar LQs have recently received considerable interest from the theory community, as the existence of LQs with large couplings ($\lambda \sim m_{LQ}$, measured in TeV) can explain the anomalies in the B sector reported by the BaBar, Belle, and LHCb Collaborations [233–241]. A search for single and pair-produced third-generation scalar LQs, followed by the LQ's decay into a τ lepton and a *b*-quark, is performed in events with two hadronically decaying τs and one or two jets, respectively [242]. A binned maximum likelihood fit to the distribution of the scalar sum of the transverse momenta is used to extract the signal. Exclusion sensitivity (discovery potential) to the single LQ production extends to LQ masses as high as 1130 GeV (800 GeV) assuming a Yukawa coupling of one for the LQ-*b*-τ vertex. This represents an improvement of approximately 400 GeV in exclusion sensitivity and 200 GeV in discovery potential with respect to the projection for the assumed Run 3 luminosity of 300 fb^{-1}. In the 300 (3000) fb^{-1} scenario, the corresponding limits for pair production are 1249 GeV (1518 GeV) while the discovery potential reaches up to a mass of 1200 (1500) GeV. A second search [243] instead addresses the pair-production of scalar LQs decaying into top-quarks and μs or τs. In the case of mixed decays between these two channels, the discovery potential (exclusion sensitivity) for leptoquark masses ranges from 1200 to 1700 GeV (1400 to 1900 GeV) depending on the value of the branching fraction as shown in Figure 47(a).

(a)

(b)

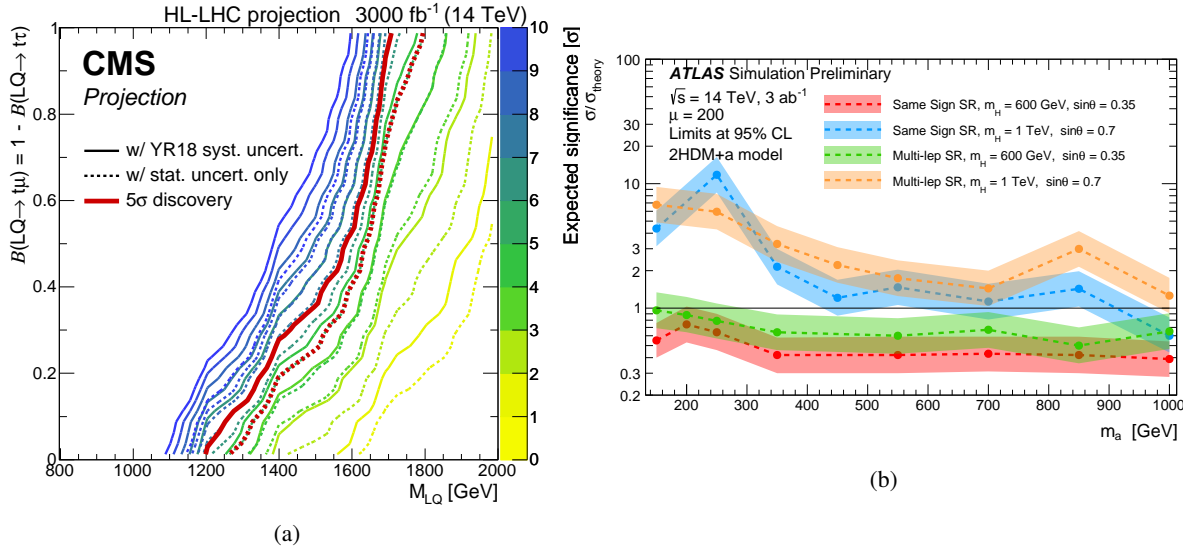Figure 47: (a) Expected discovery significance for LQ pair-production as a function of the LQ mass and the branching fraction. Color-coded lines represent lines of a constant expected significance and the thicker red-line constant cross-section limits. The red lines indicate the discovery potential [243]. (b) Projected exclusion limits on the cross-section normalized to the 2HDM*a* model versus pseudoscalar mass [244].

10.1.6 Search for a 2HDM*a* model with four top quarks

Prospects for a class of 2HDM*a* simplified models, where the additional pseudoscalar *a* couples to dark matter, were evaluated [244]. These models are a relatively simple way to investigate spin-0 mediator-based DM models. Four benchmark models with different light CP-odd and heavy CP-even boson (H) masses, as well as with different mixing angles between the two CP-odd weak states were considered. The study targets models decaying into four top-quarks. The search targets a final state with two same-charge leptons or three-or-more leptons, as well as at least three *b*-tagged jets. The one lepton and all-hadronic final states are also powerful, but not included in this study. A background uncertainty of 20% is used. The sensitivity to the four scenarios varies with the mass and mixing angles, shown in Figure 47(b). For example, for $\sin\theta < 0.35$ all $m_a \leq 1$ TeV are expected to be excluded for $m_H = 600$ GeV. While mixing angles, $\sin\theta > 0.95$, are expected to be excluded for $m_a = 350$ GeV and $m_H = 1$ TeV.

10.2 New results

10.2.1 Hadronic electroweak supersymmetry search with CMS at the HL-LHC [221]

This section presents the projection from a Run 2 CMS search with 137 fb^{-1} of data for electroweak production of supersymmetric particles [221] to the full expected luminosity of the HL-LHC with 3000 fb^{-1}. The search is performed by selecting events with at least two large-area jets (AK8) jets with $p_T > 200$ GeV and $p_T^{\mathrm{miss}} > 200$ GeV.

The AK8 jets are tagged as hadronic W, Z, or Higgs boson candidates. Events are classified into signal categories consistent with a given diboson pair plus p_T^{miss} where the combinations W^+W^-, $W^{\pm}H$, Z^0H, or $W^{\pm}Z^0$ are considered. The search regions are further binned in p_T^{miss} to improve sensitivity to electroweak supersymmetric particle pair production.

The HL-LHC projection described here uses the Run 2 approach for the prediction of SM backgrounds. The major backgrounds are $t\bar{t}$, W plus jets, Z plus jets, and diboson production. The signal binning is kept consistent with the Run 2 search. The signal and background yields are scaled up by the ratio of luminosity in the Run 2 search to the 3000 fb^{-1} expected at the HL-LHC, as well as the ratio of production cross-sections at proton-proton collisions of $\sqrt{s} = 13$ TeV to 14 TeV, as expected at the HL-LHC. Within the YR18 systematic uncertainties, the W- and Higgs-boson tagging uncertainties are reduced by a factor of 2 compared to the Run 2 search based on better available precision in data control samples for data to Monte Carlo comparisons. The search sensitivity is limited by the statistical precision available in search region data for both Run 2 and the HL-LHC projection.

The projection is interpreted in two models of supersymmetry, both with a bino-like lightest supersymmetric particle (LSP): one with a higgsino-like next-to-LSP (NLSP) and one with a wino-like NLSP. The higgsino-like NLSP scenario considers one charged and two neutral higgsinos, $\widetilde{\chi}_1^{\pm}$, $\widetilde{\chi}_2^0$, and $\widetilde{\chi}_3^0$, respectively, that are produced in pairs. The bino-like LSP is $\widetilde{\chi}_1^0$. The following decays are assumed with 100% branching ratios: $\widetilde{\chi}_1^{\pm} \rightarrow W^{\pm}\widetilde{\chi}_1^0$, $\widetilde{\chi}_2^0 \rightarrow Z\widetilde{\chi}_1^0$, and $\widetilde{\chi}_3^0 \rightarrow H\widetilde{\chi}_1^0$. Higgsino pair production thus results in a combination of the following signals: $W^{\pm}W^{\mp}$, $W^{\pm}H$, $W^{\pm}Z$, and ZH, which are combined to give the 95% CL expected upper limit as shown in Figure 48(a). The wino-like scenario includes one charged and one neutral wino, $\widetilde{\chi}_1^{\pm}$ and $\widetilde{\chi}_2^0$. The $\widetilde{\chi}_1^{\pm}$ decays into $W^{\pm}\widetilde{\chi}_1^0$ while the $\widetilde{\chi}_2^0$ is allowed to decay into either $Z\widetilde{\chi}_1^0$ or $H\widetilde{\chi}_1^0$. Results for Z and H decays are shown in Figures 48(b) and 48(c), respectively. The HL-LHC projection results

are compared to the Run 2 results, where gains in sensitivity of around 500 GeV are expected, pushing higgsino (wino) sensitivty as high as 1390 (1590) GeV.

(a)

(b)

(c)
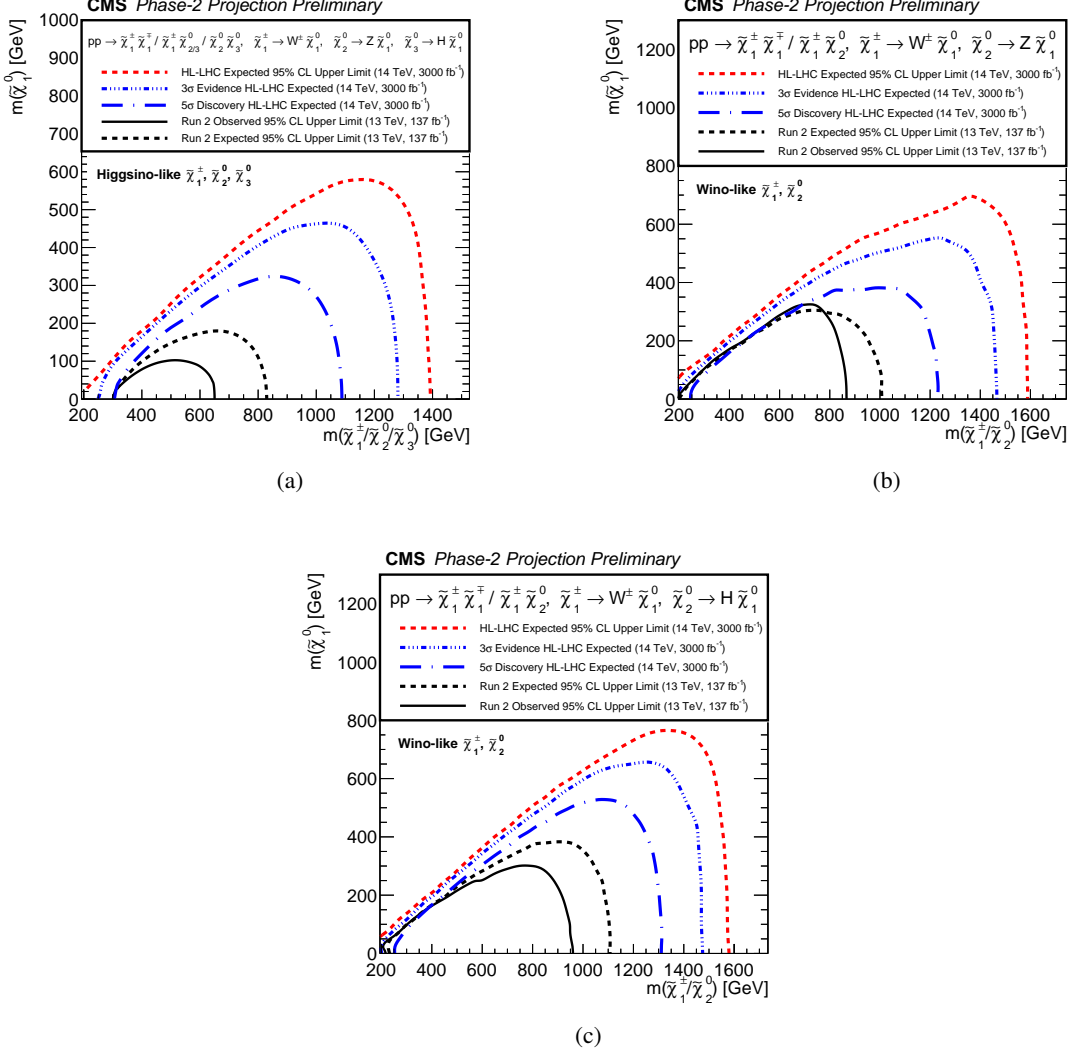
Figure 48: Projected 95% CL exclusion for 3000 fb^{-1} (red) for (a) mass-degenerate higgsino-like $\widetilde{\chi}_1^\pm \widetilde{\chi}_2^0$, $\widetilde{\chi}_1^\pm \widetilde{\chi}_3^0$, $\widetilde{\chi}_1^\pm \widetilde{\chi}_1^\mp$, and $\widetilde{\chi}_2^0 \widetilde{\chi}_3^0$ production, and wino-like $\widetilde{\chi}_1^\pm \widetilde{\chi}_1^\mp$ and $\widetilde{\chi}_1^\pm \widetilde{\chi}_2^0$ production assuming (b) $\mathcal{B}(\widetilde{\chi}_2^0 \to Z\widetilde{\chi}_1^0) = 1$ or (c) $\mathcal{B}(\widetilde{\chi}_2^0 \to H\widetilde{\chi}_1^0) = 1$ as functions of the NLSP and LSP masses. Projections are compared to results from the LHC Run 2 with 137 fb^{-1} (black). Projected 5σ and 3σ expected significance curves (blue) are also included. [221]

10.2.2 Search for top squarks in final states with two top quarks and several light-flavor jets with CMS at the HL-LHC [245]

This section presents the projection of a CMS Run 2 search for top squark pair production under R-parity violating (RPV) and stealth models of supersymmetry [245]. In the RPV model considered here, $\tilde{\chi}_1^0$ is the LSP, and it decays into three light-flavor quarks via an off-shell squark as a result of a trilinear Yukawa coupling between quarks and squarks. The benchmark stealth model for this search (SY$\overline{\text{Y}}$) assumes a

minimal stealth sector with only one scalar particle S with even R-parity and its nearly mass-degenerate superpartner S̃ (both of which are singlets under all SM interactions), and a portal mediated by loop interactions involving a new vector-like messenger field (Y), the gluon (g), $\tilde{\chi}_1^0$, S, and S̃. Each top squark decays to a gluon, top quark, and S̃. Each S̃ then decays to a very light gravitino (carrying away very little E_T^{miss}) and S, which decays to jets via S → gg.

Thus, in both scenarios, the final state is $t\bar{t}$ + jets with minimal additional E_T^{miss}. As this final state looks very similar to pair production of top quarks with additional jets in the standard model, the $t\bar{t}$ + jets process is the dominant, irreducible background process for the analysis. The main topology feature that does differentiate the signal and background is the high jet multiplicity. The analysis selects events that contain exactly one isolated lepton, at least seven jets, and at least one b-tagged jet.

The difficulty in discerning signal from background via any single object- or event-level variable further motivates how the backgrounds are to be estimated. To discriminate signal from background, the analysis uses a binary classifier neural network, trained using jet four-vectors and event shape information as input features, and including a gradient reversal layer to ensure that the neural network output score S_{NN} remains largely independent of the jet multiplicity. Events are grouped into four categories or S_{NN} bins. The $S_{\text{NN},1}$ category contains the most background-like events while $S_{\text{NN},4}$ would be the most enriched with signal events. In each of these bins, the N_{jets} spectrum is the focus and the S_{NN} bins are defined such that the shape of the $t\bar{t}$ + jets N_{jets} spectrum is the same in each of the four categories, removing any residual differences present after the gradient reversal approach.

A simultaneous fit of the N_{jets} spectrum in the four S_{NN} bins is used to estimate the background component from $t\bar{t}$ + jets. The background dominated region $S_{\text{NN},1}$ acts as a quasi-control region and constrains the overall fit. The QCD multijet background is estimated from a dedicated control region, while other minor backgrounds are estimated directly from simulation. A presence of signal would alter the N_{jets} shape differently in each of the four S_{NN} bins, which could not be absorbed by the fit. Systematic uncertainties in the $t\bar{t}$ modeling may have a similar effect and are a limiting factor for the search sensitivity.

For the HL-LHC projection, the same analysis strategy is used. A background-only fit to the N_{jets} distributions using 2016 data is scaled up, bin-by-bin, by the ratio of the 3000 fb^{-1} expected at the HL-LHC to the 2016 luminosity. The production cross sections are maintained at the values for 13 TeV pp collisions, as the increase in energy to 14 TeV is not expected to have a significant impact, given the relatively low top squark masses ($\lesssim$ 1.4 TeV) considered.

Monte Carlo statistical uncertainties are eliminated from the fit for the projection. Modeling uncertainties associated with renormalization and factorization scales, the underlying event, and the modeling of H_T, jet mass, and jet p_T are all halved. Experimental uncertainties related to JER and JEC are reduced based on the HL-LHC expectations. Uncertainties with negligible impacts either remain unchanged from Run 2 or are removed entirely.

For the HL-LHC, in the RPV and stealth SUSY models, projected 95% CL exclusion upper limits on the top squark pair production cross section are shown in Figure 49. With the improvements for the HL-LHC, the cross-section sensitivity is projected to improve by a factor of ~3–7 across the range of top squark masses considered. The limit on the top squark mass is projected to reach approximately 870 GeV (1190 GeV) in the RPV (stealth) SUSY scenario. This limit can be compared to that observed in Run 2 with 137 fb^{-1}, which excludes top squark masses above 670 GeV (870 GeV) at the 95% CL for RPV (stealth) SUSY models.
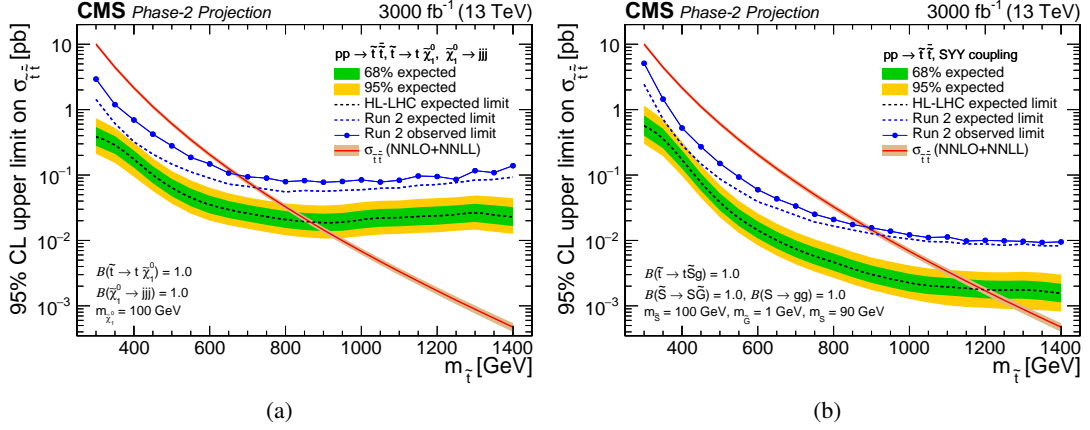
Figure 49: Projected 95% CL upper limit on the top squark pair production cross section as a function of the top squark mass for the (a) RPV and (b) stealth SUSY models for 3000 fb^{-1}. Observed limits with the Run 2 dataset of 137 fb^{-1} are also overlaid. Assumed particle masses and branching fractions are included on the plot. The expected cross section computed at NNLO+NNLL accuracy is shown in the red curve.

10.2.3 Search for leptophobic Z' resonances decaying to charginos in the dilepton plus missing transverse energy final state with CMS at the HL-LHC [246]

Searches for high mass resonances have been performed by ATLAS and CMS since the beginning of LHC data taking, however these searches mainly focus on direct resonance decays to SM particles. Yet, well-motivated theoretical mechanisms also suggest scenarios where resonances decay to BSM particles. One example is the leptophobic Z' bosons appearing within the context of the U(1)' MSSM (UMSSM) scenario, which is derived by embedding supersymmetry in the unified gauge group E_6. The leptophobic Z' can decay into a chargino pair, where each chargino decays into a leptonically decaying W boson and a neutralino, leading to a clean opposite charge dilepton plus missing transverse momentum final state. A dedicated analysis is designed to explore the sensitivity of HL-LHC and the Phase-2 CMS detector to Z' decays to charginos in this final state in the e^+e^-, $\mu^+\mu^-$ and $e^\pm\mu^\mp$ plus missing transverse momentum channels [246].

The study is based on signal and background events generated at a center-of-mass energy of $\sqrt{s} = 14$ TeV. Leptophobic Z' exclusively decaying as $Z' \to \tilde{\chi}_1^+\tilde{\chi}_1^- \to W^+\tilde{\chi}_1^0 W^-\tilde{\chi}_1^0 \to \ell^+\nu\tilde{\chi}_1^0\ell^-\nu\tilde{\chi}_1^0$ is considered as the signal process and events are generated for varying masses $m(Z')$ and $m(\tilde{\chi}_1^\pm)$ with the constraint $m(\tilde{\chi}_1^\pm) = 2m(\tilde{\chi}_1^0)$. A theoretical framework with a narrow Z' width is considered, where the width is calculated to be approximately 1.5% of the Z' mass, depending on the signal point. Backgrounds include the dileptonic decays of $t\bar{t}$+jets (80.22 pb), Drell-Yan+jets with $m_{\ell\ell} > 100$ GeV (246.5 pb), $WZ(\to 3\ell+\nu)$+0jets (3.125 pb), $WZ(\to 3\ell+\nu)$ + 1jet (0.955 pb), $VV \to 2l + 2\nu$ and $V = W, Z$ (13.23 pb). The Phase-2 CMS detector response is simulated using the DELPHES fast detector simulation framework.

A preliminary selection is applied enhancing the features of signal and eliminating most of the reducible backgrounds. Events are required to have an opposite charge lepton pair with leading (trailing) lepton transverse momenta > 80 GeV (40 GeV), missing transverse momentum $p_T^{\text{miss}} \geq 80$ GeV, dilepton invariant mass > 110 GeV, and zero jets identified as originating from b-quarks. A deep neural network (DNN) is constructed for signal extraction, as individual variables are not sufficient to effectively discriminate

signals from the backgrounds. The DNN allows to boost the signal sensitivity without loss of signal events by additional selection. Inputs to the DNN consist of the kinematic features $p_T(\ell_{lead})$, $p_T(\ell_{trail})$, $M(\ell\ell)$, p_T^{miss}, $|\vec{p}_T(\ell\ell) + \vec{p}_T^{miss}|$, $|\vec{p}_T(\ell\ell) + \vec{p}_T^{miss}| - p_T(\ell\ell)$, transverse mass $M_T(\vec{\ell\ell}, \vec{p}_T^{miss})$ and the stransverse mass M_{T2}, along with the topological features $\Delta\phi(\ell, \ell)$, $\Delta\phi(\vec{p}_T^{miss}, \vec{p}_T(\ell\ell))$, $\Delta\phi(\vec{p}_T^{miss}, \vec{p}_T(\ell))$, $\Delta R(\ell, \ell)$ and $\Delta R(\vec{p}_T(\ell\ell), \vec{p}_T^{miss})$. The DNN is constructed using a supervised learning algorithm. It is trained in the e^+e^-, $\mu^+\mu^-$ and $e^\pm\mu^\mp$ channels separately and individually for each signal mass point in order to optimize the performance for each mass point.

The expected upper limits at 95% CL on the $pp \to Z'$ production cross section computed with the CLs method for the YR18 systematic uncertainties scenario are shown versus Z' and chargino masses in Figure 50. Branching ratio for the $Z' \to \tilde{\chi}_1^+ \tilde{\chi}_1^- \to W^+ \tilde{\chi}_1^0 W^- \tilde{\chi}_1^0$ decay is considered to be 1. With the combination of e^+e^-, $\mu^+\mu^-$ and $e^\pm\mu^\mp$ channels, the analysis will be able to exclude Z' masses up to 4.5 TeV for the narrow Z' width scenario for an integrated luminosity of 3000 fb^{-1}.
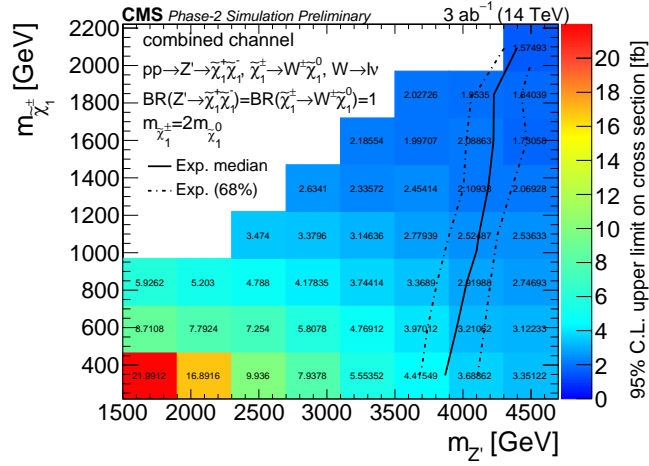

Figure 50: The expected upper limits at 95% CL on the $pp \to Z'$ production cross section computed with the CLs method for the combination of e^+e^-, $\mu^+\mu^-$ and $e^\pm\mu^\mp$ channels for a narrow width Z' scenario, with Z' width approximately 1.5% of the Z' mass. Branching ratio for the $Z' \to \tilde{\chi}_1^+ \tilde{\chi}_1^-$ decay is considered to be 1 and neutralino masses are taken to be half the chargino masses. [246]

10.2.4 Seesaw model searches using multilepton final states with CMS at the HL-LHC [247]

The discovery of neutrino flavor oscillations in experiments by Ray Davis in the late 1960s and subsequent studies indicated that neutrinos have non-zero masses much smaller than those of the charged leptons. SM predicts massless neutrinos and does not offer an explanation for the origin of those small masses. The experimental results and the SM predictions can be reconciled by addition of new terms to the SM Lagrangian. One of the best known proposals is the seesaw mechanism, in which a small Majorana mass can be generated for each of the known neutrinos by introducing massive states with Yukawa couplings to leptons and to the Higgs field. Seesaw mechanism can be realized in three scenarios, called Type-I, Type-II and Type-III which introduce heavy states of mass M, that involve, respectively, weak-isospin singlets, scalar triplets, and fermion triplets.

Since Run 1 of the LHC, numerous studies have been performed both by ATLAS and CMS to search for the various BSM particles predicted by the three types of seesaw models in different decay channels. This study

explores the projected sensitivity of the HL-LHC and the Phase-2 CMS detector to Type-I and Type-II seesaw models in final states with at least three leptons, which can be achieved by both scenarios [247]. The $n_\ell \geq 3$ final state also allows to avoid most of the SM backgrounds with large cross-sections such as those arising from W plus jets, Drell-Yan and top quark pair production processes.

The study is performed using signal and background Monte Carlo events generated at a center-of-mass energy of $\sqrt{s} =$ 14 TeV. Signal events are produced for the following BSM particles, productions and decays predicted by the two scenarios, for different values of BSM particle masses:

- Type-I: $pp \rightarrow N\ell^\pm$ and $p\gamma \rightarrow N\ell^\pm j$ with $N \rightarrow \nu Z$ and $N \rightarrow \ell^\pm W^\mp$;

- Type-II: $pp \rightarrow \Delta^{\pm\pm}\Delta^{\mp\mp}$ and $pp \rightarrow \Delta^{\pm\pm}\Delta^{\mp}$ with $\Delta^{\pm\pm} \rightarrow \ell^\pm \ell^\pm$ and $\Delta^\pm \rightarrow \ell^\pm \nu$;

Background processes considered are $t\bar{t}$, WZ, WW, ZZ, $t\bar{t}Z$, $t\bar{t}W$, WWW, WWZ, WZZ and ZZZ. The Phase-2 CMS detector response is simulated using the DELPHES fast detector simulation framework.

Events are required to have at least three tightly identified and isolated leptons (electrons or muons) with $p_T > 30$ GeV and $|\eta| < 2.1$. The signal processes consist of multiple leptons with large boosts originating from high mass resonances. This feature is exploited by requiring high values of L_T, the scalar p_T sum of all charged leptons. Moreover, dilepton invariant masses are calculated from each possible dilepton combination in an event, and the minimum and maximum invariant mass values $\min(m_{\ell\ell})$ and $\max(m_{\ell\ell})$ are obtained. The minimum invariant mass is required to be $\min(m_{\ell\ell}) > 120$ GeV. Signal regions are defined for 3 high L_T bins of 300-400, 400-600 and 600-14000 GeV; and 3 high $\max(m_{\ell\ell})$ bins of 120-300, 300-500 and 500-14000 GeV. Events in each L_T-$\max(m_{\ell\ell})$ bin are further categorized into 11 lepton flavor configurations $3e0\mu$, opposite charge $2e1\mu$, same charge $2e1\mu$, opposite charge $1e2\mu$, same charge $1e2\mu$, $0e3\mu$, $4e0\mu$, $3e1\mu$, $2e2\mu$, $1e3\mu$ and $0e4\mu$, which subsequently lead to 99 signal regions.

Figure 51 shows the exclusion limits at 95% CL on the N and $\Delta\Delta$ production cross sections as functions of N and Δ masses at an integrated luminosity of 3000 fb^{-1}.
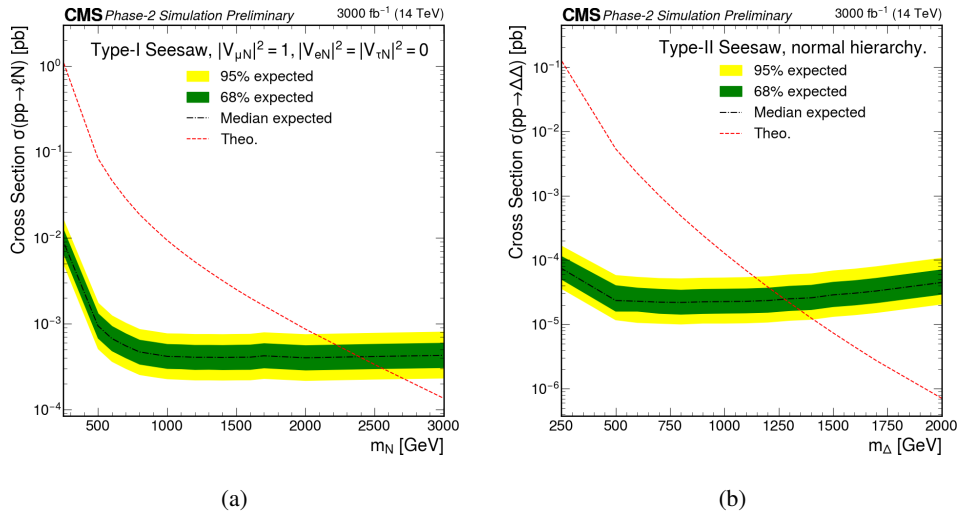

(a)

(b)

Figure 51: Exclusion limits at 95% CL on the N and $\Delta\Delta$ production cross sections as functions of m_N, and m_Δ for (a) the Type-I scenario where N only mixes with a muon with $\left|V_{lN}\right|^2 = 1.0$ and (b) the Type-II scenario with nominal neutrino mass hierarchy. [247]

11 EF09: BSM: More general explorations

11.1 Yellow Report summary

This section showcases a few examples from [3] with references to the detailed studies. For the majority of CMS analyses, signals and background were simulated with present tools (generators, PDF sets) and the detector response refers to the envisaged Phase-2 detector and HL-LHC conditions including PU. Systematic uncertainties are included based on the present understanding. The ATLAS studies are based on generator-level information with parameterized estimates applied to the final state particles to simulate the response of the upgraded ATLAS detector under Phase-2 PU conditions.

11.1.1 Compositeness

Compositeness models, which assume new substructures of particles considered as "fundamental" in the SM, can predict the existence of excited leptons (ℓ^*) and quarks (q^*) or heavy Majorana neutrinos (N). Model parameters are the compositeness scale Λ and the mass of the excited particle such as M_{ℓ^*}, M_{q^*} or $M(N_\ell)$. The CMS searches for compositeness in these channels at the HL-LHC are summarized below.

Discovery limits for excited electrons (e^*) and muons (μ^*) have been investigated [248]. The excited lepton, produced in conjunction with its SM lepton partner, emits a high-energy photon while transitioning into its SM state resulting in a final state of $\ell\ell\gamma$. Both leptons (with leading and subleading p_T) and the photon are reconstructed, but which of the leptons derives from the decay cannot be identified. In fact their p_T ranking changes as a function of the excited lepton mass (m_{ℓ^*}). Thus two masses are reconstructed by pairing the (sub)leading lepton with the photon, a minimal ($m_{\ell\gamma}^{min}$) and a maximal mass ($m_{\ell\gamma}^{max}$). Plotting both masses against each other, the signal is concentrated in two bands of an inverted L shape in this plane while the background is scattered in an uncorrelated way at low masses (see example of the electron channel in Figure 52). The analysis optimized for HL-LHC conditions indicates that the discovery potential 3σ evidence (5σ discovery) is possible for both excited electrons and muons with masses up to 5.5 (5.1) TeV. If no significant discrepancies are seen, excited leptons with masses below 5.8 TeV could be excluded at 95% CL, compared to 3.9 TeV for the excited muon and 3.8 TeV for the excited electron mass at present [249].

Heavy composite Majorana neutrinos are new particles which would result from compositeness as well. From the various production and decay channels, the final state with two same-flavor leptons and at least one large-radius jet was studied [250]. The heavy Majorana neutrino, N_ℓ, is produced in conjunction with the same flavor SM lepton ($\ell = e, \mu$) and subsequently decays into a second SM lepton and a quark pair, according to $pp \rightarrow \ell N_\ell \rightarrow \ell\ell q\bar{q}'$. The analysis reconstructs the quark pair as a large-radius jet (labelled J) and both isolated leptons. The resulting invariant mass $M(\ell\ell J)$ has a good separation power to distinguish the high-mass signal from the background. Figure 53 shows the background after all selection steps along with a signal example in the muon channel for $\Lambda = M(N_\ell) = 6$ TeV. The electron channel is comparable. At the HL-LHC, CMS will be able to exclude heavy electron and muon neutrinos masses up to 7.6 TeV for a compositeness scale $\Lambda = M(N_\ell)$. Exclusion will be possible for masses up to 8 TeV and Λ up to 40 TeV (see Figure 53) compared to the present mass limits of 4.6 and 4.7 TeV from the electron and muon channels, respectively [251].

(a)

(b)
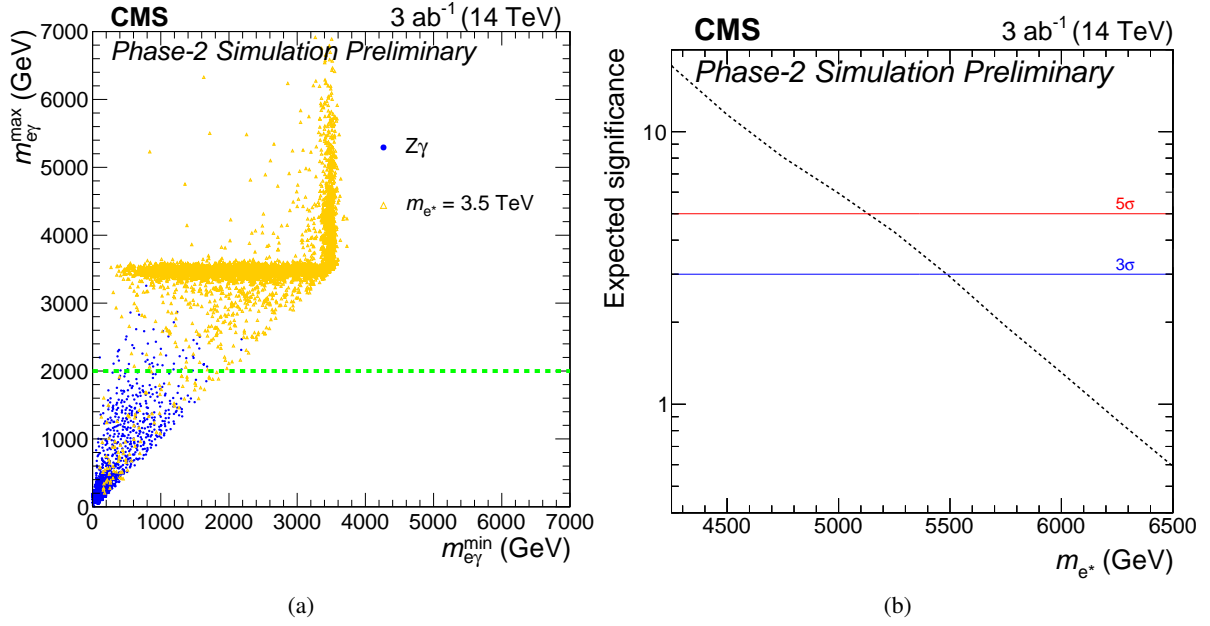
Figure 52: Searches for compositeness. (a) Excited leptons are searched for in a two dimensional plane defined by the two invariant masses $m_{e\gamma}^{min}$ and $m_{e\gamma}^{max}$. (b) CMS discovery reach for excited electrons at the HL-LHC as a function of the excited electron mass m_{e^*}. [248]

(a)

(b)
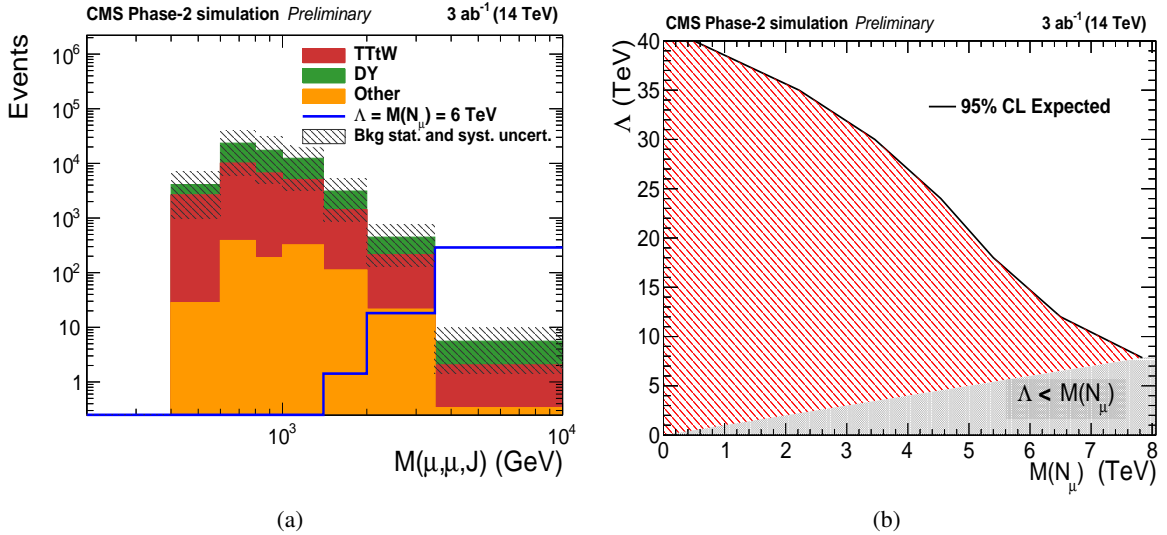
Figure 53: Searches for compositeness. (a) Distribution of the discriminating variable $M(\mu\mu J)$ in the search for heavy Majorana neutrinos, considering for signal example $\Lambda = M(N_\ell) = 6$ TeV. (b) Expected lower limits on the compositeness scale Λ as a function of the mass of the heavy composite Majorana neutrino in $\mu\mu q\bar{q}$ channel. [250]

(a)   (b)

Figure 54: (a) Transverse mass distributions for events satisfying all selection criteria in the $W'_{SSM} \rightarrow e\nu$ search. Expected signal (mass 6.5 TeV) is compared to the stacked sum of the main expected backgrounds. (b) ATLAS exclusion (red) and discovery reach (blue) for the search for Z'_{SSM} and Z'_{χ} bosons as a function of the center-of-mass energy. Dilepton results are combination of electron and muon channel results [252].
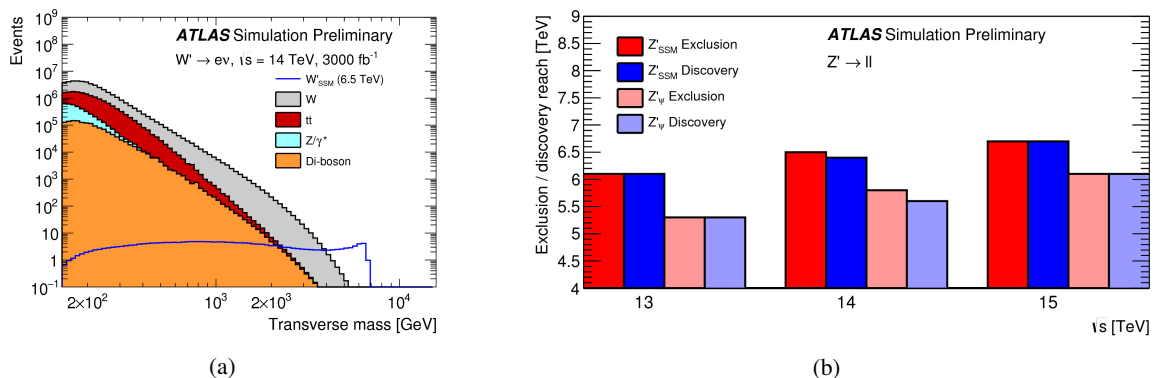
11.1.2 New gauge bosons and resonances

New gauge bosons are predicted in several extensions to the SM. The predicted discovery potential of the new heavy W' and Z' bosons in 3000 fb^{-1} of simulated $\sqrt{s}$=14 TeV proton–proton collision data have been investigated.

W' bosons are searched for by ATLAS in final states with a bottom and a top quark or with a lepton plus missing transverse energy [252]. Assuming a right-handed W' boson, W' masses up to 4.9 TeV can be excluded with the first search, while the latter search excludes W' bosons predicted in the Sequential Standard Model (SSM) for masses up to 7.9 TeV (see Figure 54(a)). The ATLAS Run 2 searches for W' bosons in the $W' \rightarrow t\bar{b} \rightarrow l\nu b\bar{b}$ final state excluded, at the 95% confidence limit (CL), right-handed W' bosons (W'_R, with a coupling to the SM particles equal to the SM weak coupling constant, masses up to 3.15 TeV using 36 fb^{-1} of data [253].

Searches for Z' bosons at the HL-LHC are performed in several decay channels for a range of center-of-mass energies and luminosities. ATLAS has performed sensitivity studies for Z' bosons decaying to two top quarks and to two lepton (electron and muon) final states. The latter channel produces the best limits, excluding masses below 6.5 TeV for Sequential Standard Model Z' bosons in the combined dimuon and dielectron channel [252]. Exclusion and discovery limits are also predicted for different center-of-mass energies of $\sqrt{s}$ =13, 14 and 15 TeV [252]. These are summarised in Figure 54(b). As for $Z' \rightarrow t\bar{t}$ final states, masses below 4 TeV are expected to be excluded in the Topcolour-assisted Technicolour model considered. This can be compared to the Run 2 search for $Z' \rightarrow t\bar{t}$ using 36.1 fb^{-1} of data, which allowed the exclusion at 95% CL of the Z' bosons,using a width of 1% for the Topcolour-assisted Technicolour model boson, upper limits on the production cross-sections vary from 25 pb to 0.02 pb for masses from 0.4 TeV to 5 TeV[254].

In CMS, a study was performed in the challenging tau plus missing transverse momentum final state [255]. Among many interpretations, a key case is a W' within the context of the SSM. Scenarios with SM-like and also weaker couplings $g_{W'}/g_W \neq 1$ are studied. For the τ lepton, the analysis uses the dominant hadronic decays ($\sim$60%), which are reconstructed as jets with a τ identification algorithm. The discriminating variable for the search is the transverse mass (m_T) calculated from the transverse momentum of the hadronic τ and the missing transverse momentum due to neutrinos. Unlike the light lepton W' search channels,
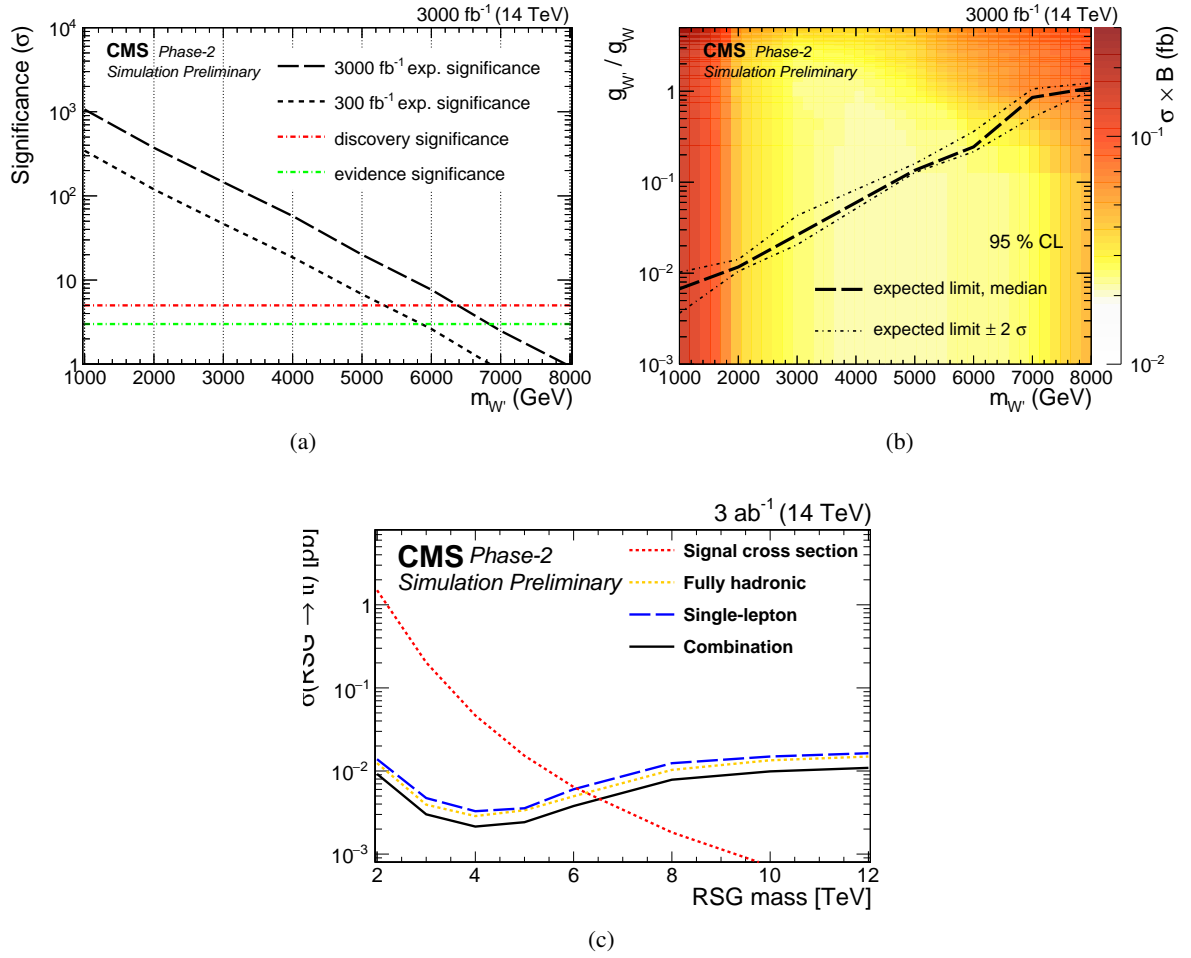
Figure 55: (a) Discovery significance for a SSM W' boson decaying to $\tau + p_T^{\text{miss}}$. (b) Expected limit on the coupling ratio $g_{W'}/g_W$ as a function of the W' boson mass decaying to $\tau + p_T^{\text{miss}}$ with the 2D cross-section limit represented by the color code. [255] (c) Expected cross-section limits for a Randall-Sundrum gluon decaying to $t\bar{t}$ with contributions from the various final states. [257]

the signal shape does not exhibit a Jacobian peak due to the presence of two neutrinos in the final state but it is expected to concentrate at high m_T where the SM background is low. Using the hadronically decaying τ lepton, the W' mass reach for a potential discovery increases to 6.9 TeV for a 3σ evidence and 6.4 TeV for a 5σ observation, as shown in Figure 55. The present Run 2 SSM W' mass exclusion limit reach is 4.6 TeV [256]. The sensitivity to smaller values for the couplings extends significantly, as shown in Figure 55.

Another interesting channel to search for new heavy resonances, such as Randall-Sundrum (RS) gluons, is the $t\bar{t}$ final state [257]. Reconstructing the event topology of a $t\bar{t}$ state requires special techniques. The fully hadronic top quark decays, where the decay products are merged into a single jet, are analysed using jet substructure variables and top quark identification algorithms. Events are classified according to the number of b-tagged jets (0, 1 or 2). In the lepton+jets final state the single lepton (e, μ) provides a handle to extract the signal. A strong discrimination can be achieved by reconstructing the mass of the $t\bar{t}$ system using the W boson mass constraint and the z-component of the neutrino system. To improve the sensitivity,

the events are categorized according to their lepton flavor and the number of t-tagged (0 or 1) large-radius jets. At the end, all channels are combined to determine the HL-LHC sensitivity, gaining about a factor two with respect to a single channel. A comparison of the contributions from each final state to the combination is shown in Figure 55. Discovery with 5σ significance reaches a heavy resonance mass up to 5.7 TeV. The production of an RS gluon with a mass up to 6.6 TeV is excluded at 95% CL at the HL-LHC, improving the present limit of 4.5 TeV [258].

11.1.3 Long-lived particles and displaced signatures

Long-lived particles (LLP) arise in several new physics models which answer open questions in particle physics relating to dark matter, neutrino mass, matter-antimatter asymmetry and naturalness. Many of these theoretical models predict the existence of new neutral particles that can be long-lived, which may be produced in the proton-proton collisions of the LHC and decay back into SM particles far from the interaction point resulting in displaced signatures.

Long-lived particles decaying within the tracking volume to multiple outgoing charged particles can be searched for using a signature of a displaced vertex and missing transverse momentum, in the upgraded ATLAS detector for the HL-LHC. The replacement of the existing tracking detector with a full-silicon inner tracker (ITk) significantly changes the search sensitivity, which is estimated using extrapolations of the reconstruction capabilities for displaced tracks and displaced vertices from a combination of the performance of the current detector and a simulation of the proposed upgraded detector.

The signature of a displaced vertex and missing transverse momentum, resulting from an LLP, is studied to determine limits on gluino R-hadron pair production [259]. For long-lived gluinos that decay to SM quarks and a 100 GeV stable neutralino, ATLAS has the sensitivity to discover R-hadrons with lifetimes from 0.1 to 10 ns with masses up to 2.8 TeV, as shown in Figure 56(a) [259]. In the absence of long-lived gluino production, the 95% CL upper limit on gluino masses will reach 3.4 TeV. These limits exceed those achieved in the Run 2 search using 32.8 fb^{-1} of data, which excluded, at 95% CL, the production of long-lived gluinos with masses up to 2.37 TeV and lifetimes ranging from the order of 10^{-2} to 10 ns, in a simplified model inspired by Split Supersymmetry [260].

Displaced jets of particles are predicted in several BSM models. For example some dark matter models predict dark photons which decay to leave give displaced, collimated jets of muons [261]. These particles can also be long-lived with decay lengths comparable to, or even larger than, the dimensions of the LHC experiments. The triggering and track reconstruction capabilities of the ATLAS muon spectrometer have been exploited to search for neutral long-lived particles decaying to pairs of muons in Run 2 and set exclusion limits on their mass and lifetime. ATLAS has investigated this signature in the context of a Hidden Sector model and determined the sensitivity prospects for HL-LHC [261]. Two new muon trigger algorithms are studied to improve the selection efficiency of displaced muon pairs. The resulting cross-section times branching fraction of $H \rightarrow 2\gamma_d + X$, at 95% CL upper limit, as a function of the dark photon (γ_d) lifetime, considering 45% dark photon branching fraction to muons is summarized in Figure 56(b). The exclusion contour plot in the plane defined by the γ_d mass and the kinetic mixing parameter, ϵ, is shown in Figure 56(c), for the scenario assuming a Higgs boson decay branching fraction to the hidden sector of 1%. The contour achievable in Run 3 with 300 fb^{-1}, shown in red, is compared to that accessible with 3000 fb^{-1} at the HL-LHC including the multi-muon scan trigger improvement, drawn in orange. The 95% CL exclusion limit on the dark photon average $c\tau$, where τ is the lifetime, is expected to improve, extending the lower bound down to 0.97 mm and the upper bound up to 597 mm,
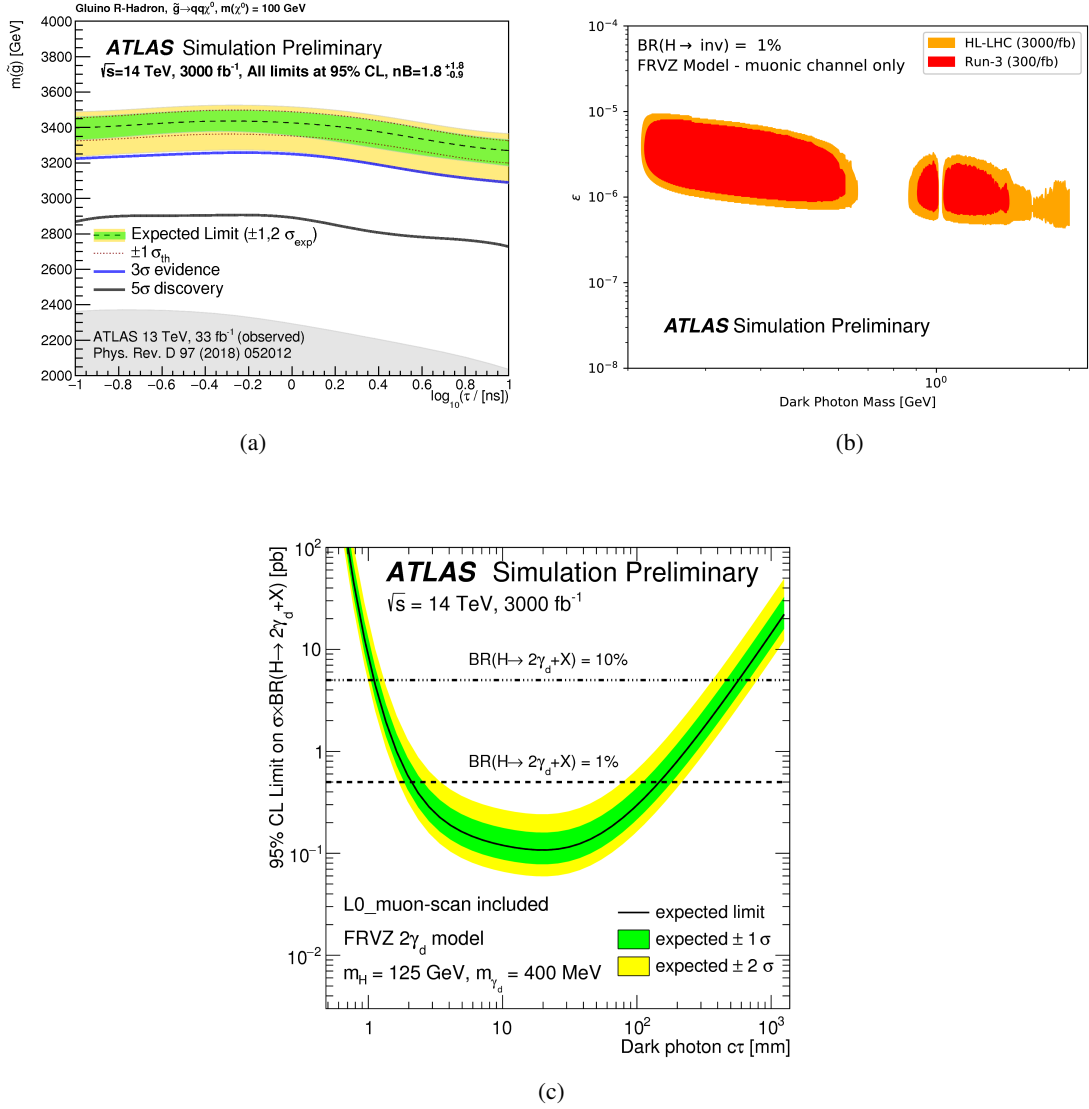
(a)

(b)

(c)

Figure 56: (a) Discovery reach and upper limit on the mass of gluino R-hadrons as a function of the gluino lifetime, for a background of $1.8^{+1.8}_{-0.9}$ events. [259] (b) Exclusion contour plot in the plane defined by the dark photon (γ_d) mass and the kinetic mixing parameter ϵ. (c) 95% CL upper limit on the cross-section times branching fraction of $H \rightarrow 2\gamma_d + X$ as a function of the γ_d lifetime, considering 45% dark photon branching ratio to muons. [261]

assuming a branching ratio of the Higgs boson decay to the Hidden sector of 10%. Moreover, the search at the HL-LHC is expected to probe $\mathrm{BR}\left(H \rightarrow 2\gamma_d + X\right)$ down to ~1%, where the Run 2 analysis lacks of sensitivity [261]. ATLAS has performed Run 2 searches for displaced decays of dark photons to muon pairs using Run 2 data [262].

Heavy stable charged particles (HSCP) are expected to move slower than the speed of light ($\beta = 1$) and hence could be identified based on their longer time-of-flight (TOF) from the center of CMS to the outer muon system. The RPC part of the CMS muon system will improve its time resolution substantially, from the current 25 ns to 1 ns in Phase-2. This can be exploited in model-independent HSCP searches based on

an improved reconstruction efficiency as a function of η and β [15]. For $\eta < 1.5$, an efficiency of about 90% can be reached for values of $\beta > 0.25$. For comparison, in Run 2, the trigger is highly efficient between 0.6 $< \beta < 1$, but only about 20% efficient for $\beta < 0.5$.

11.2 New results

11.2.1 Sensitivity projections for a search for new phenomena at high dilepton mass with CMS at the HL-LHC [263]

A search for new physics in high-mass dielectron and dimuon final states with the full Run 2 dataset at $\sqrt{s}$ = 13 TeV, including for the first time a test of lepton flavor universality (LFU) in these final states, has been reported by CMS [264]. Expected lower mass limits and the discovery sensitivity for narrow resonances, as well as the sensitivity to LFU violation in the dimuon-to-dielectron cross-section ratio $R_{\mu^+\mu^-/e^+e^-}$, for the Run 2 + 3 and HL-LHC datasets are derived based on these results. Background and signal yields are scaled to the expected luminosities, taking into account changes in $\sqrt{s}$ and detector acceptance. A detailed description of the extrapolation techniques and the results can be found in Ref. [263].

Minimal lepton p_{T} requirements (35 GeV for electrons, 53 GeV for muons) are assumed to be unchanged from Run 2, whereas the maximum lepton pseudorapidity is extended from $|\eta| < 2.4$ (2.5) to $|\eta| < 2.8$ (3.0) for muons (electrons) with the upgraded Phase-2 detector. Events with two electrons with $|\eta| > 1.56$, rejected in Run 2 due to high background levels from jets misidentified as electrons in this region, are included in the extrapolated results for the HL-LHC dataset, but not the Run 3 dataset. The impact of the change in acceptance on background and signal yields is evaluated, respectively, using Z' and Drell–Yan (DY) events. Lepton trigger, reconstruction, and selection efficiencies, as well as the detector resolution, are assumed to be constant from Run 2 to Run 3 and the Phase-2 detector for the leptons selected in this search.

To account for the different $\sqrt{s}$ values, signal cross-sections for the Z'_{SSM} and Z'_{ψ} benchmark models and the dominant DY background are calculated at $\sqrt{s}$ = 13, 13.6, and 14 TeV at LO. The cross-sections of subdominant backgrounds are scaled in the same way as the DY backgrounds.

Using these extrapolations, expected limits on Z' resonant production are derived as a function of the resonance mass (m) for narrow spin-1 resonances, which are shown in Figure 57(a) for the HL-LHC scenario. The lower mass limits for both Z'_{SSM} and Z'_{ψ} are expected to increase by about 300 GeV for the Run 2 + 3 dataset and 1.7 TeV with the full HL-LHC dataset, with respect to Run 2. As the impact of systematic uncertainties on these results was found to be negligible, the uncertainties from Run 2 are used without modifications.

The resulting product of the signal cross-section and branching fraction for a $5\,\sigma$ local significance ranges from 9.0×10^{-5} pb at $m = 1$ TeV to 1.8×10^{-6} pb at $m = 7$ TeV. The largest mass that would lead to a 5σ discovery at the HL-LHC is 6.27 TeV for the Z'_{SSM} model and 5.72 TeV for the Z'_{ψ} model.

To test LFU at high dilepton masses, the cross-section ratio $R_{\mu^+\mu^-/e^+e^-}$ for the DY process is measured using a profile-likelihood method, where the likelihood describes the shapes of the mass distributions above a mass value $m^{\mathrm{threshold}}$ and includes corrections for the different acceptance and efficiency in the dimuon and dielectron final states. The expected uncertainty on measurement as a function of $m^{\mathrm{threshold}}$ is shown in Figure 57(b). For dilepton masses above 1 TeV, the expected uncertainty improves by a factor of 2 (5) with

respect to Run 2 results for the Run 2 + 3 (HL-LHC) dataset. Reducing the systematic uncertainties for the HL-LHC dataset has a negligible effect on the uncertainty on $R_{\mu^+\mu^-/e^+e^-}$.
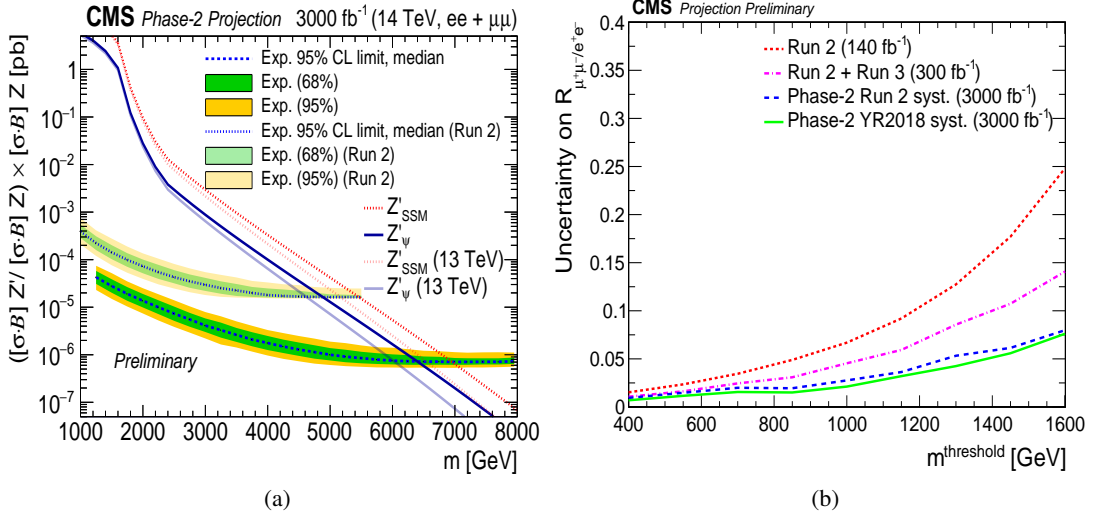
Figure 57: (a) Expected exclusion limits at 95% CL as a function of resonance mass m for narrow spin-1 resonances with the full HL-LHC dataset, compared to Run 2 (shaded). Signal cross-sections for the Z'_{SSM} and Z'_{ψ} benchmark models are also shown. (b) Uncertainty on the measurement of the dimuon-to-dielectron cross-section ratio $R_{\mu^+\mu^-/e^+e^-}$ as a function of the lower mass threshold $m^{\text{threshold}}$ for the Run 2, Run 2+3, and HL-LHC datasets. [263]

12 EF10: BSM: Dark matter at colliders

12.1 Yellow Report summary

The existence of dark matter (DM) is implied from astrophysical observations. In spite of the abundance of DM, its origin and nature remain unknown. This mystery is the subject of an active experimental program planned for the HL-LHC, extending the current existing limits on mass and coupling parameters. In addition to traditional searches, there is an increasing interest in new physics models which predict long-lived particles (LLPs).

DM particles are not expected to interact with the detector, but can be inferred by a large amount of missing transverse momentum (p_T^{miss}). The specific search strategy depends on the type of particle or system accompanying the unseen DM. Both the ATLAS and CMS Collaborations have performed searches for DM particles produced in association with jets, photons, W or Z and Higgs bosons, significantly constraining the allowed parameter space for generic classes of models predicting DM candidates [265]. The sensitivities for ATLAS and CMS to detect DM in association with a Z boson [266], monophoton [267], monojet [268] and monotop [265] at the HL-LHC are described below. In addition to these searches, the prospective sensitivity for long-lived dark photons which decay into displaced muons has been studied by the CMS Collaboration [100].

12.1.1 Search for DM produced in association with a Z boson

CMS has performed a study which considers a scenario with a vector mediator Z' decaying into a pair Dirac fermion DM candidates χ, recoiling against a leptonically decaying Z boson. In addition to the masses of vector mediator and DM candidate, m_{med} and m_{DM}, the model has two free coupling parameters; g_q, the universal mediator-quark coupling, and g_{DM}, the mediator-DM coupling. In addition to the simplified model, one with a second higgs doublet and a pseudoscalar (a+2HDM) is considered. This is a gauge-invariant and renormalizable model that contains two neutral and charged scalars, h, H and $H\pm$, and two pseudoscalars (a,A) where the a and A bosons mix, allowing $h \to aZ$ decays. The a boson subsequently decays to DM particles producing a $Z + p_T^{miss}$ signature. While this signature is similar to the simplified models, there is a Jacobian peak present in both the p_T^{miss} and the p_T^Z distributions, caused by the resonant $h \to aZ$ decay.

The signal consists of events that have a well-reconstructed Z boson with large amounts of missing transverse momentum. Except for the effects of initial state radiation, the invisible particles and the Z boson are expected to be produced back-to-back in the laboratory frame. As such, the signal selection focuses on extracting events with a balanced topology. Three control regions are used to predict the SM backgrounds: the opposite-flavor lepton region, used to estimate non-resonant backgrounds; the low-p_T^{miss}, used to estimate the contribution from the Drell-Yan process; and the 3-lepton/4-lepton regions used to estimate the diboson processes which are the largest backgrounds. The signal extraction is performed using a maximum-likelihood fit to the p_T^{miss} spectrum simultaneously in the signal and control regions.

To compensate for differences between Run 2 and HL-LHC conditions, additional rescaling procedures are applied. Scaling takes into consideration the change in center-of-mass energy from $\sqrt{s} = 13$ TeV to 14 TeV, the increased pile-up which may result in degradation of the p_T^{miss} resolution by a factor of 1.5-2, conservatively taken as a factor of 2, and the increased integrated luminosity. To account for the latter the normalization of simulation samples is scaled to integrated luminosities of between 300 fb^{-1} and 3000 fb^{-1}.
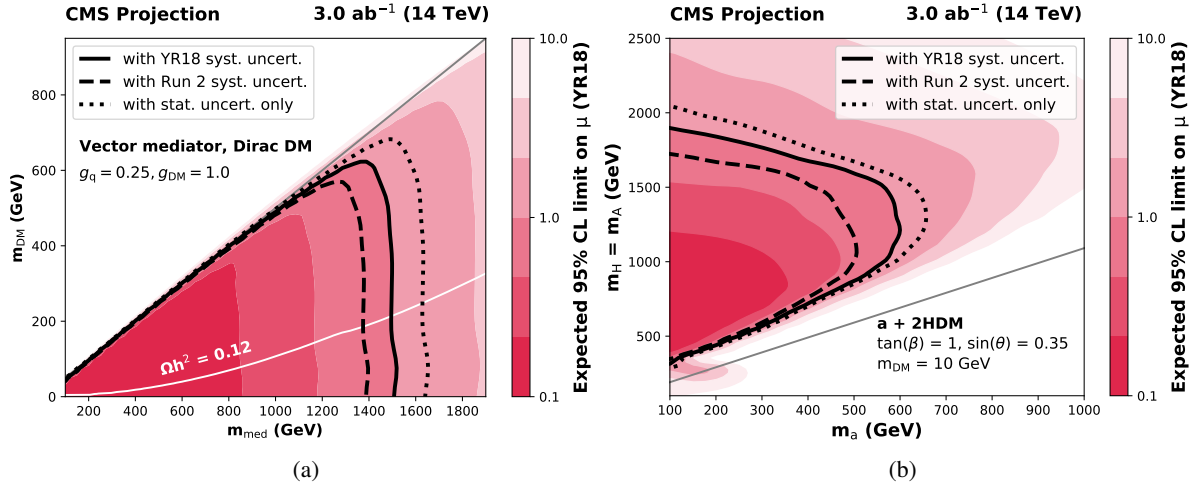
Figure 58: Expected 95% CL exclusion limits on the signal strength for (a) vector-mediated DM production in the plane of mediator and DM masses and (b) the a+2HDM scenario as a function of the mass of the main DM mediator, a, and the masses of the H and A bosons $m_h = m_A$ [266]. Results are presented for different systematic scenarios. Scenario labeled as "Run 2" corresponds to Ref [269].

Signal significances and exclusion limits are calculated with the asymptotic approximation of the *CLs* method and are shown in Figure 58. Figure 59 shows the expected discovery significance and exclusion sensitivity for the vector-mediated DM scenario as a function of integrated luminosity [266].

12.1.2 VBF+E_T^{miss} and mono-photon final states

Simplified models, inspired by SUSY and the Minimal Dark Matter models, predict extensions of the SM by the addition of an electroweak fermionic triplet with null hyper charge. In this scenario, the lightest mass state of the triplet constitutes a weakly interacting massive particle DM candidate. ATLAS has performed searches for DM in the mono-photon and Vector Boson Fusion (VBF)+E_T^{miss} final states and projected Run 2 analyses strategies [267] to HL-LHC conditions. Complementary collider searches, such as mono-jet searches and disappearing track signatures, as well as direct DM searches, would also set stringent constraints on this model.

The main background to the (VBF)+E_T^{miss} search is from Z+jets events, where the Z decays to neutrinos. The pseudorapidity distribution of the two leading jets, $\Delta\eta(j_1, j_2)$, in events with at least two jets each with $p_T > 50$ GeV, is used as a discriminating variable. The expected upper limit on the production cross-section of neutralino (χ) in the VBF+E_T^{miss} final state is presented in Figure 60(a) for an integrated luminosity of 3000 fb^{-1}. In this channel it will be possible to test the lower masses of this model to ~110 GeV.

Mono-photons have a distinct signature in the detector, resulting from an undetectable DM candidate recoiling against the observable photon. Searches typically require the photons to have high E_T. The search is described in detail in Ref [267]. The expected upper limits at 95% CL on the production cross-section of χ as a function of χ_0 mass in a mono-photon final state corresponding to an integrated luminosity of 3000 fb^{-1} are presented in Figure 60(b), where the red line shows the theoretical cross-section. Masses of χ_0 below 310 GeV will be excluded at 95% CL assuming the same systematic uncertainties adopted in the

(a)

(b)
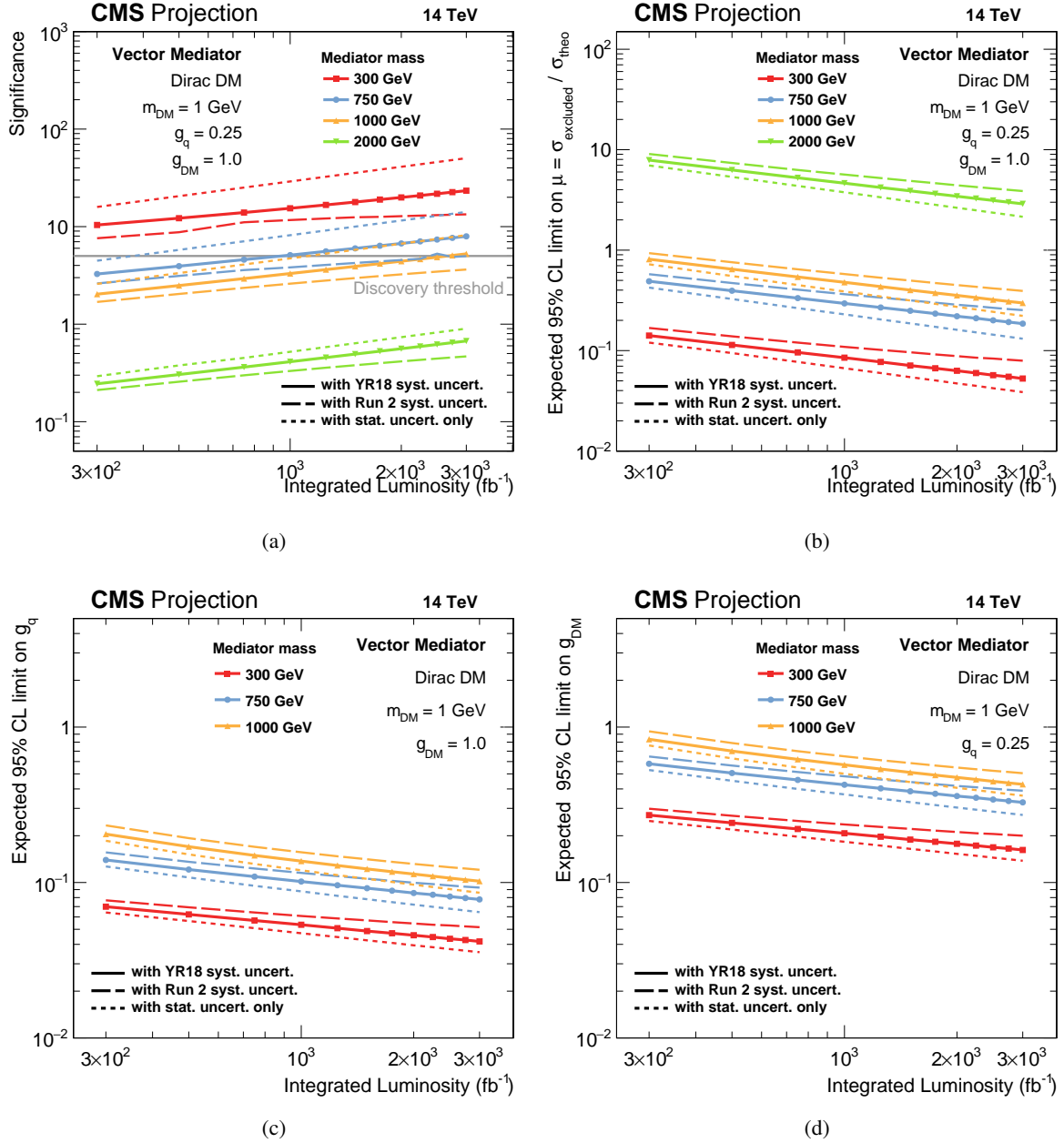

(c)

(d)

Figure 59: (a) Expected discovery significance, (b) signal strength exclusion limits, (c) exclusion sensitivity for the couplings g_q and (d) g_{DM} are shown for the vector-mediated DM scenario as a function of integrated luminosity [266]. Different mediator masses are shown for different systematic uncertainty scenarios, with the "Run 2" scenario corresponding to Ref [269].
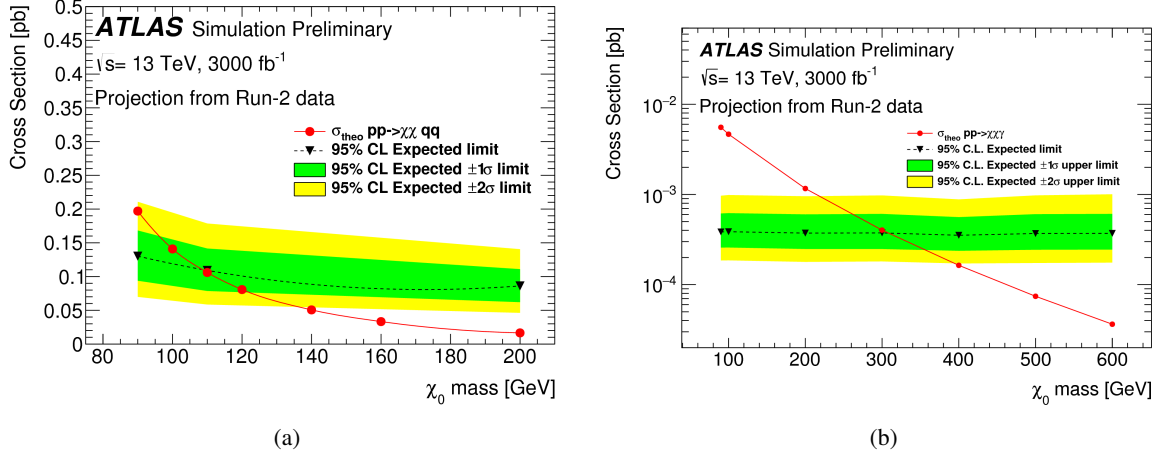
Figure 60: Expected upper limit on the production cross-section as a function of χ_0 mass in (a) the VBF+E_T^{miss} and (b) the mono-photon final state for 3000 fb^{-1}. The red line shows the theoretical cross-section. [267]

Run 2 analysis, which is higher than achievable in the VBF+E_T^{miss} channel search. The latter search is more challenging due to rejection of PU jets, identification of the primary vertex, and the resolution of low p_T jets. For both analyses, a slight improvement with respect to Run 2 in the signal significance is expected, due to the increase of the center-of-mass energy to $\sqrt{s}$=14 TeV at the HL-LHC.

12.1.3 Monojet search for WIMPS

ATLAS has performed a search for weakly-interacting massive particles (WIMPs) in the monojet signature [268]. The A simplified model, in which WIMPs are pair-produced from the s-channel exchange of an axial vector Z_A mediator, is used as a benchmark to test the sensitivity of the analysis to DM. In this model, the Z_A mediator couples to neutralino (χ) (g_χ) and to gluons (g_q). The resulting final state has at least one jet and large missing transverse momentum. The prospective sensitivities were evaluated by extrapolating the ATLAS results obtained using 36 fb^{-1} of pp collisions at a center-of-mass energy of $\sqrt{s}$=13 TeV during Run 2 to integrated luminosities of 300 fb^{-1} and 3000 fb^{-1} at $\sqrt{s}$=14 TeV. The impact of different systematic uncertainty scenarios (standard, reduced by factors 2 and 4) on the sensitivity of the search was investigated. The resulting mass limits for the axial-vector simplified model with couplings g_χ = 1 and g_q = 0.25, for 3000 fb^{-1} are shown in Figure 61(a).

12.1.4 Single-top quark in association with invisible particles

The single top ("mono-top") signature is predicted in certain DM models. The ATLAS experiment has studied the expected sensitivity of a search for events with one top quark and large missing transverse momentum at the HL-LHC [265]. The search targets the non-resonant production of an exotic state decaying into a pair of invisible DM particle candidates in association with a right-handed top quark. This analysis considers only topologies where the W boson from the top quark decays into a lepton and a neutrino. These final-state events are expected to have a reasonably small background contribution from SM processes. The distributions of transverse mass of the lepton-E_T^{miss} system for the signal, of mediator mass of 2.5 and 4.0 TeV, and the stacked background predicted distributions (which includes $t\bar{t}$, single-top,

W+jets and other (i.e. Z+jets, dibosons, $t\bar{t}\,W/Z$ and tZq)) are shown in Figure 61(b). All samples are normalised using their corresponding theoretical production cross-sections. A BDT-based analysis and a cut-based analysis are performed. The BDT is trained to discriminate the monotop signal from the dominant $t\bar{t}$ background. The predicted event yields in both the pre-selection region and the signal regions of the BDT- and cut-based analyses were compared. In both analyses the dominant background is the $t\bar{t}$ production. In the BDT-based analysis, the $t\bar{t}$ background represents the 65 % of the total background, in contrast to 90 % in the cut-based analysis. The BDT analysis has about two orders of magnitude larger signal-to-background ratios than the cut-based analysis. Assuming an integrated luminosity of 3000 fb^{-1}, the expected exclusion limit (discovery reach) at 95% CL on the mass of the exotic state is 4.6 TeV (4.0 TeV) using a multivariate analysis based on a BDT.

### 12.1.5 Heavy quarks produced in association with dark matter

Prospects of searches for weakly interacting DM (ϕ/a $\to \chi\bar{\chi}$) produced in association with heavy flavor quarks (b or t) at the HL–LHC have been studied by the ATLAS experiment [270]. The search is performed assuming 3000 fb^{-1} of pp collisions collected by the ATLAS detector at a center-of-mass energy of $\sqrt{s}$ =14 TeV. Two experimental signatures are investigated, characterized by missing transverse momentum and either a pair of bottom quarks or two opposite-charge leptons (electrons or muons) resulting from the decay of a top quark pair or a top quark and a W-boson. The results are interpreted within the framework of Simplified Model, which couples the dark and SM sectors via the exchange of color-neutral spin-0 mediators, assuming unitary couplings and a DM mass of 1 GeV.

The reach achievable for DM detection in events with bottom quarks is extended by a factor of 3.0–8.7 compared to the previous search conducted with 36.1 fb^{-1} of data at $\sqrt{s}$=13 TeV. For the DM+ $b\bar{b}$ channel, cross-sections ~ 45-100 times the theoretically predicted for g = 1.0 and masses m(ϕ/a) < 100 GeV are excluded with the anticipated HL-LHC dataset. This corresponds to a factor of 3.0–3.5 (3.0–4.3) improvement with respect to the previous reach achievable for the scalar (pseudoscalar) mediator model. For m(ϕ/a) > 100 GeV, the extended coverage in pseudorapidity enabled by the upgrade to the ATLAS Inner Tracker allows for better exploitation of anti-correlations in jet and b-jet spin-sensitive variables like $\cos\theta_{bb}$. This results in a larger gain in the exclusion potential for the high-mass region, equivalent to a factor of 5.8-8.7 (3.0-5.0) increase with respect to the $\sqrt{s}$ =13 TeV limit for scalar (pseudoscalar) masses in the range 100-500 GeV.

For events with top quarks in the final state, the expected sensitivity to scalar mediator production improves by a factor of 5, and pseudoscalar mediator masses can be excluded up to masses of 385 GeV. Figure 61(c) presents a comparison between ATLAS and direct-detection experiments, of the 90% CL limits on the spin-independent DM-nucleon cross-section as a function of DM mass, in the context of the color-neutral simplified model with scalar mediator.

12.1.6 Search sensitivity for dark photons decaying to displaced muons

CMS has explored a class of supersymmetric models which contain an additional $U_D(1)$ symmetry which gives rise to a massive long-lived boson called a dark photon (γ_D) [100]. This dark photon, with mass m_{γ_D}, can have kinetic mixing with the SM photon and couples to SM charged particles similarly to the SM photon. The strength of the kinetic mixing is ϵ and the lifetime of the dark photon is proportional to $1/\epsilon^2$, which leads to long dark photon lifetimes for smaller values of ϵ. In the MSSM model studied, the dark
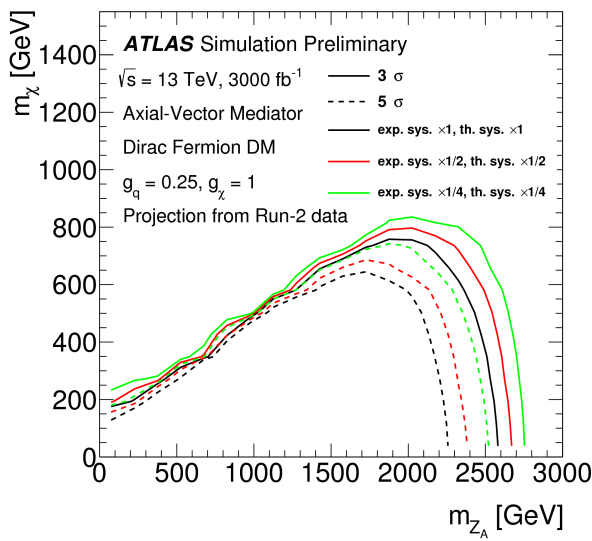
(a)
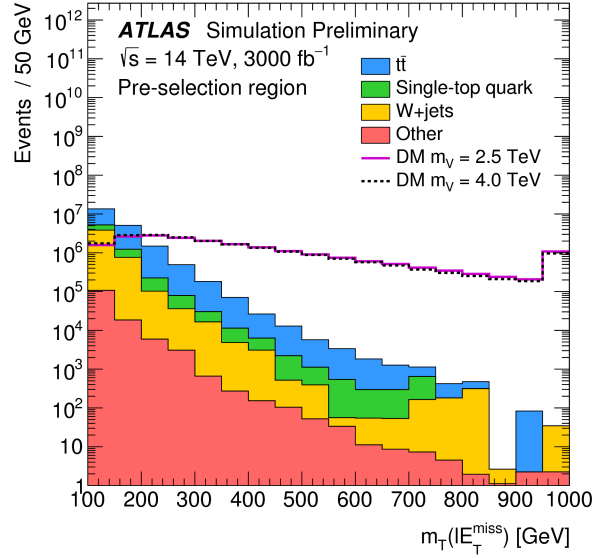
(b)
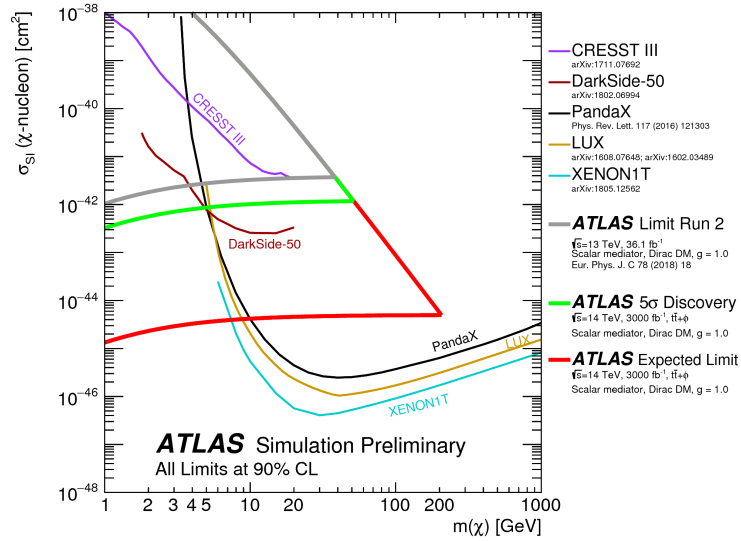
(c)

Figure 61: (a) Mono-jet search: Expected 3σ (solid) and 5σ (dashed) discovery contours on the (m_χ, m_{Z_A}) mass plane for the model described in the text. Three systematic uncertainty scenarios are shown [268]. (b) Mono-top search: Distributions of transverse mass of the lepton-E_T^{miss} system for the signal of mediator mass 2.5 GeV (solid line) and 4.0 TeV (dashed), and stacked predicted background predictions [265]. (c) Heavy quarks: Comparison of the 90% CL limits on the spin-independent DM-nucleon cross-section as a function of DM mass, between these results and the direct-detection experiments, for color-neutral simplified model with scalar mediator. The green contour indicates the 5σ discovery potential at HL–LHC. The lower horizontal line of the DM–nucleon scattering cross-section for the red (green) contour corresponds to value of the cross-section for m(ϕ)=430 GeV (m(ϕ)=105 GeV). The grey contour indicates the exclusion derived from the observed limits for 36.1 fb^{-1} at $\sqrt{s}$ =13 TeV [270].
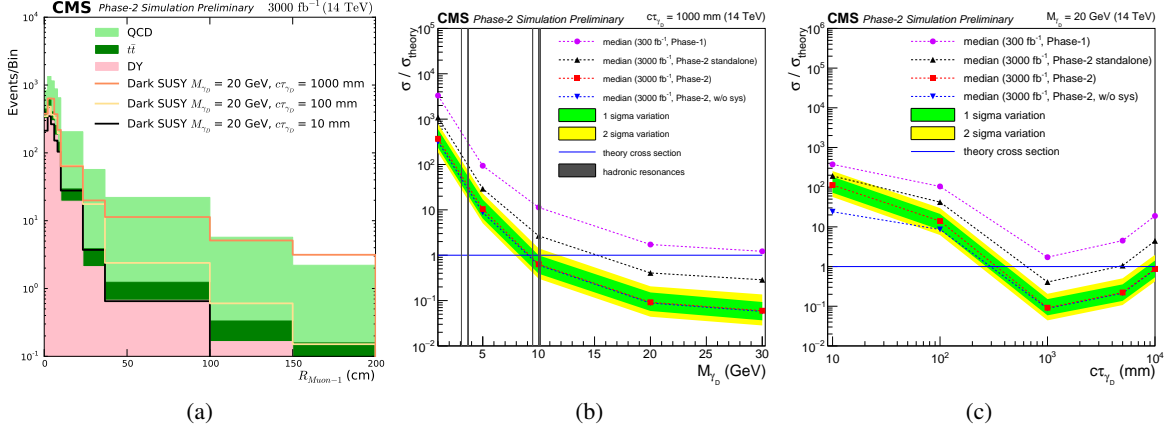
Figure 62: (a) The R_{muon} distribution for the highest p_T muon, named R_{muon-1}. (b) The 95% CL upper limits on the production cross-section σ/σ_{theory} are shown for several dark photon masses with a fixed decay length $c\tau = 1000$ mm and (c) for a fixed dark photon mass of $m_{\gamma_D} = 20$ GeV as a function of the dark photon decay length. [100]

photons can be produced in the decays of the SM higgs boson, where the higgs boson decays into a pair of MSSM-like lightest neutralinos (n_1), which each subsequently decays into a dark sector neutralino (n_D) and the dark photon. The dark photon then decays resulting in displaced muons.

This search relies on the displaced standalone algorithm (DSA), a dedicated muon reconstruction algorithm, designed to identify highly displaced muons [15]. This algorithm uses a Kalman-filter technique without imposing the primary vertex constraint and can identify displaced muons that may leave hits only in the muon system. The offline selection requires two DSA muons that are separated and have opposite charge. Additionally, events are required to have large amounts of missing transverse momentum to account for the dark neutralinos. The distance from the primary vertex to the point of closest approach of the extrapolated displaced muon track, indicated by the vector R_{muon}, is used to search for the signal as shown in Figure 62(a). The dominant background for this search comes from QCD multijet events where displaced muons are produced in the decay of mesons inside heavy quark jets.

The results are interpreted for three scenarios: the Phase-2 scenario using the DSA algorithm; Phase-2 scenario using the traditional standalone muon reconstruction; and the Phase-1 scenario based on the Run 2 data taking. Phase-2 searches are sensitive to higher dark photon masses and lower values of ϵ, which corresponds to longer lifetimes. The use of the dedicated displaced muon reconstruction algorithm drives the difference in the exclusion ranges between Run 2 (Figure 63(a)) and Phase-2. Upper limits at 95% confidence level (CL) are calculated and Figures 62(b) and (c) show the limits on the production cross-section ratio (σ/σ_{theory}). Figure 63(b) shows the exclusion and discovery sensitivity in the $\epsilon - m_{\gamma_D}$ parameter plane.
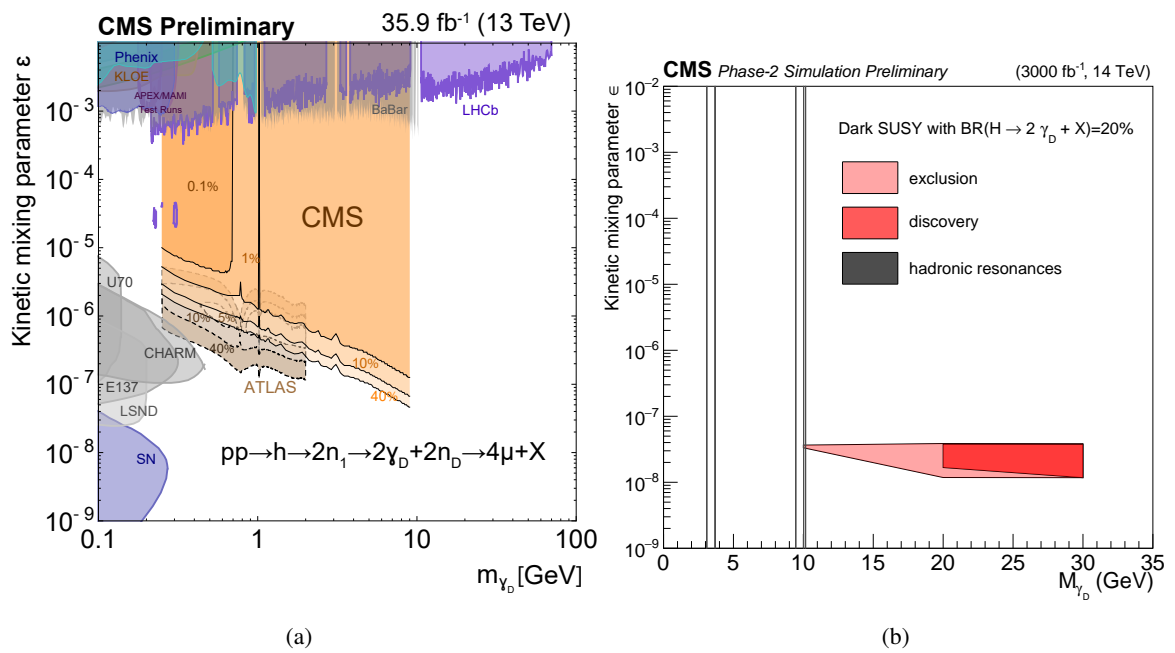
Figure 63: Parameter scan in the $\epsilon - m_{\gamma_D}$ plane for (a) the Run 2 results [271] and (b) Phase-2 with 3000 fb^{-1}. The grey lines indicate the regions of narrow hadronic resonances where the analysis does not claim any sensitivity. [100]

13 Summary

This document summarizes the most up-to-date studies from the ATLAS and CMS Collaborations concerning their physics program for the HL-LHC. Some studies are summarized from the CERN Yellow Report on the Physics at the HL-LHC, and Perspectives for the HE-LHC, but new recent results are also presented. This program spans a very wide range of physics topics, within the Standard Model and beyond, where the sensitivities of measurements or searches are expected to reach unprecedented levels. While the figures of merit have been obtained based on the current best knowledge of the upgraded ATLAS and CMS detectors, these estimates are expected to be further refined by the start of the HL-LHC data-taking, following developments in the object reconstruction performance and analysis methods. Among the final HL-LHC legacy ATLAS and CMS results, some are expected to remain the most sensitive in the world for a long period of time after the end of the HL-LHC data-taking. In that context, the ATLAS and CMS Collaborations recognize the importance of the Snowmass process to the high-energy physics community in the US and beyond. Continued strong US participation is in particular critical to the success of the HL-LHC physics program, as the Phase-2 detector upgrades, the HL-LHC data-taking operations and the physics analyses based on the HL-LHC dataset will not be able to proceed without the support of the US community.

References

[1] ATLAS Collaboration, *The ATLAS Experiment at the CERN Large Hadron Collider*, JINST **3** (2008) S08003 (cit. on p. 5).

[2] CMS Collaboration, *The CMS experiment at the CERN LHC*, JINST **3** (2008) S08004 (cit. on p. 5).

[3] A. Dainese et al., *Report on the Physics at the HL-LHC, and Perspectives for the HE-LHC*, CERN Yellow Report CERN-2019-007, 2019, URL: https://cds.cern.ch/record/2703572 (cit. on pp. 5, 7–9, 14, 15, 23, 28, 32–35, 37, 61, 65, 66, 68, 69, 71, 80).

[4] ATLAS Collaboration, *ATLAS Inner Tracker Strip Detector: Technical Design Report*, ATLAS-TDR-025; CERN-LHCC-2017-005, 2017, URL: https://cds.cern.ch/record/2257755 (cit. on pp. 6, 48).

[5] ATLAS Collaboration, *ATLAS Muon Spectrometer Phase-II Upgrade: Technical Design Report*, ATLAS-TDR-026; CERN-LHCC-2017-017, 2017, URL: https://cds.cern.ch/record/2285580 (cit. on p. 6).

[6] ATLAS Collaboration, *ATLAS LAr Calorimeter Phase-II Upgrade: Technical Design Report*, ATLAS-TDR-027; CERN-LHCC-2017-018, 2017, URL: https://cds.cern.ch/record/2285582 (cit. on p. 6).

[7] ATLAS Collaboration, *ATLAS Tile Calorimeter Phase-II Upgrade: Technical Design Report*, ATLAS-TDR-028; CERN-LHCC-2017-019, 2017, URL: https://cds.cern.ch/record/2285583 (cit. on p. 6).

[8] ATLAS Collaboration, *ATLAS TDAQ Phase-II Upgrade: Technical Design Report*, ATLAS-TDR-029; CERN-LHCC-2017-020, 2017, URL: https://cds.cern.ch/record/2285584 (cit. on p. 6).

[9]   ATLAS Collaboration, *ATLAS Inner Tracker Pixel Detector: Technical Design Report*,
        ATLAS-TDR-030; CERN-LHCC-2017-021, 2017,
        URL: https://cds.cern.ch/record/2285585 (cit. on pp. 6, 48).

[10]   ATLAS Collaboration,
        A High-Granularity Timing Detector for the ATLAS Phase-II Upgrade: Technical Design Report,
        ATLAS-TDR-031; CERN-LHCC-2020-007, 2020,
        URL: https://cds.cern.ch/record/2719855 (cit. on p. 6).

[11]   CMS Collaboration, *Technical Proposal for the Phase-II Upgrade of the CMS Detector*,
        CMS Technical Design Report CERN-LHCC-2015-010, LHCC-P-008, CMS-TDR-15-02, 2015,
        URL: https://cds.cern.ch/record/2020886 (cit. on p. 6).

[12]   CMS Collaboration, *The Phase-2 Upgrade of the CMS Tracker*,
        CMS Technical Design Report CERN-LHCC-2017-009, CMS-TDR-014, 2017,
        URL: https://cds.cern.ch/record/2272264 (cit. on pp. 6, 13).

[13]   CMS Collaboration,
        The Phase-2 Upgrade of the CMS Barrel Calorimeters Technical Design Report,
        CMS Technical Design Report CERN-LHCC-2017-011, CMS-TDR-015, 2017,
        URL: https://cds.cern.ch/record/2283187 (cit. on p. 6).

[14]   CMS Collaboration, *The Phase-2 Upgrade of the CMS Endcap Calorimeter*,
        CMS Technical Design Report CERN-LHCC-2017-023, CMS-TDR-019, 2017,
        URL: https://cds.cern.ch/record/2293646 (cit. on p. 6).

[15]   CMS Collaboration, *The Phase-2 Upgrade of the CMS Muon Detectors*,
        CMS Technical Design Report CERN-LHCC-2017-012, CMS-TDR-016, 2017,
        URL: https://cds.cern.ch/record/2283189 (cit. on pp. 6, 11, 86, 94).

[16]   CMS Collaboration, *The Phase-2 Upgrade of the CMS Level-1 Trigger*,
        CMS Technical Design Report CERN-LHCC-2020-004, CMS-TDR-021, 2020,
        URL: https://cds.cern.ch/record/2714892 (cit. on pp. 6, 33).

[17]   CMS Collaboration, *A MIP Timing Detector for the CMS Phase-2 Upgrade*, tech. rep.,
        CERN, 2019, URL: https://cds.cern.ch/record/2667167 (cit. on pp. 6, 61).

[18]   ATLAS Collaboration, *ATLAS HL-LHC Computing Conceptual Design Report*, tech. rep.,
        CERN, 2020, URL: https://cds.cern.ch/record/2729668 (cit. on p. 6).

[19]   European Strategy Group, *2020 Update of the European Strategy for Particle Physics (Brochure)*,
        tech. rep. CERN-ESU-015, 2020, URL: http://cds.cern.ch/record/2721370 (cit. on p. 6).

[20]   J. Albrecht et al., *A Roadmap for HEP Software and Computing R&D for the 2020s*,
        Comput. Softw. Big Sci. **3** (2019) 7, arXiv: 1712.06982 [physics.comp-ph] (cit. on p. 6).

[21]   CMS Collaboration,
        Expected performance of the physics objects with the upgraded CMS detector at the HL-LHC,
        CERN Note CERN-CMS-NOTE-2018-006, 2018,
        URL: https://cds.cern.ch/record/2650976 (cit. on p. 6).

[22]   ATLAS Collaboration, *Expected performance of the ATLAS detector at the High-Luminosity LHC*,
        ATL-PHYS-PUB-2019-005, 2019, URL: https://cds.cern.ch/record/2655304
        (cit. on p. 6).

[23] ATLAS Collaboration,
Expected performance of the ATLAS detector under different High-Luminosity LHC conditions,
ATL-PHYS-PUB-2021-023, 2021, URL: https://cds.cern.ch/record/2765851
(cit. on p. 6).

[24] ATLAS Collaboration, *Expected tracking and related performance with the updated ATLAS Inner Tracker layout at the High-Luminosity LHC*, ATL-PHYS-PUB-2021-024, 2021,
URL: https://cds.cern.ch/record/2776651 (cit. on pp. 6, 28).

[25] J. de Favereau et al.,
DELPHES 3, A modular framework for fast simulation of a generic collider experiment,
JHEP **02** (2014) 057, arXiv: 1307.6346 [hep-ex] (cit. on pp. 6, 32).

[26] ATLAS Collaboration, *Observation of a new particle in the search for the Standard Model Higgs boson with the ATLAS detector at the LHC*, Phys. Lett. B **716** (2012) 1,
arXiv: 1207.7214 [hep-ex] (cit. on p. 7).

[27] CMS Collaboration,
Observation of a new boson at a mass of 125 GeV with the CMS experiment at the LHC,
Phys. Lett. B **716** (2012) 30, arXiv: 1207.7235 [hep-ex] (cit. on p. 7).

[28] CMS Collaboration,
Observation of a new boson with mass near 125 GeV in pp collisions at $\sqrt{s}$ = 7 and 8 TeV,
JHEP **06** (2013) 081, arXiv: 1303.4571 [hep-ex] (cit. on p. 7).

[29] CMS Collaboration, *A measurement of the Higgs boson mass in the diphoton decay channel*,
Phys. Lett. B **805** (2020) 135425, arXiv: 2002.06398 [hep-ex] (cit. on pp. 7, 10, 12).

[30] ATLAS Collaboration, *Measurement of the Higgs boson mass in the $H \rightarrow ZZ^* \rightarrow 4\ell$ and $H \rightarrow \gamma\gamma$ channels with $\sqrt{s}$ = 13 TeV pp collisions using the ATLAS detector*,
Phys. Lett. B **784** (2018) 345, arXiv: 1806.00242 [hep-ex] (cit. on p. 7).

[31] CMS Collaboration, *Evidence for Higgs boson decay to a pair of muons*, JHEP **01** (2021) 148,
arXiv: 2009.04363 [hep-ex] (cit. on pp. 7, 13).

[32] ATLAS Collaboration,
A search for the dimuon decay of the Standard Model Higgs boson with the ATLAS detector,
Phys. Lett. B **812** (2021) 135980, arXiv: 2007.07830 [hep-ex] (cit. on p. 7).

[33] ATLAS Collaboration, *A search for the $Z\gamma$ decay mode of the Higgs boson in pp collisions at $\sqrt{s}$ = 13 TeV with the ATLAS detector*, Phys. Lett. B **809** (2020) 135754,
arXiv: 2005.05382 [hep-ex] (cit. on p. 7).

[34] CMS Collaboration,
Search for the Higgs boson decay to $Z\gamma$ in proton-proton collisions at $\sqrt{s}$ = 13 TeV,
CMS Physics Analysis Summary, CERN, 2021,
URL: https://cds.cern.ch/record/2784454 (cit. on p. 7).

[35] ATLAS Collaboration, *Projections for measurements of Higgs boson cross sections, branching ratios, coupling parameters and mass with the ATLAS detector at the HL-LHC*,
ATL-PHYS-PUB-2018-054, 2018, URL: https://cds.cern.ch/record/2652762
(cit. on p. 8).

[36] CMS Collaboration,
Sensitivity projections for Higgs boson properties measurements at the HL-LHC,
CMS Physics Analysis Summary CMS-PAS-FTR-18-011, 2018,
URL: http://cds.cern.ch/record/2647699 (cit. on pp. 8–10).

[37] S. Heinemeyer et al., *Handbook of LHC Higgs Cross Sections: 3. Higgs Properties: Report of the LHC Higgs Cross Section Working Group*, CERN Yellow Reports: Monographs,
Working Group web page: https://twiki.cern.ch/twiki/bin/view/LHCPhysics/CrossSections, 2013,
URL: https://cds.cern.ch/record/1559921 (cit. on p. 8).

[38] ATLAS Collaboration,
Search for exclusive Higgs and Z boson decays to $\phi\gamma$ and $\rho\gamma$ with the ATLAS detector,
JHEP **07** (2018) 127, arXiv: 1712.02758 [hep-ex] (cit. on p. 8).

[39] ATLAS Collaboration, *Searches for exclusive Higgs and Z boson decays into $J/\psi\gamma$, $\psi(2S)\gamma$, and $\Upsilon(nS)\gamma$ at $\sqrt{s} = 13$ TeV with the ATLAS detector*, Phys. Lett. B **786** (2018) 134,
arXiv: 1807.00802 [hep-ex] (cit. on p. 8).

[40] CMS Collaboration, *Search for Higgs boson decays into Z and J/ψ and for Higgs and Z boson decays into J/ψ or Υ pairs at CMS*, CMS Physics Analysis Summary, CERN, 2022,
URL: https://cds.cern.ch/record/2799200 (cit. on pp. 8, 16).

[41] ATLAS Collaboration,
Prospects for differential cross-section measurements of Higgs boson production measured in decays to ZZ and $\gamma\gamma$ with the ATLAS Experiment at the High-Luminosity LHC,
ATL-PHYS-PUB-2018-040, 2018, URL: https://cds.cern.ch/record/2649879
(cit. on p. 9).

[42] CMS Collaboration, *Constraints on the Higgs boson self-coupling from ttH+tH, H to gamma gamma differential measurements at the HL-LHC*,
CMS Physics Analysis Summary CMS-PAS-FTR-18-020, 2018,
URL: http://cds.cern.ch/record/2647986 (cit. on pp. 9, 24).

[43] ATLAS Collaboration, *Estimate of the m_H shift due to interference between signal and background processes in the $H \to \gamma\gamma$ channel, for the $\sqrt{s} = 8$ TeV dataset recorded by ATLAS*,
ATL-PHYS-PUB-2016-009, 2016, URL: https://cds.cern.ch/record/2146386
(cit. on p. 10).

[44] CMS Collaboration,
First evidence for off-shell production of the Higgs boson and measurement of its width, (2022),
arXiv: 2202.06923 [hep-ex] (cit. on p. 10).

[45] ATLAS Collaboration, *Constraints on off-shell Higgs boson production and the Higgs boson total width in $ZZ \to 4\ell$ and $ZZ \to 2\ell2\nu$ final states with the ATLAS detector*,
Phys. Lett. B **786** (2018) 223, arXiv: 1808.01191 [hep-ex] (cit. on p. 10).

[46] ATLAS Collaboration, *Off-shell Higgs boson couplings measurement using $H \to ZZ \to 4\ell$ events at High Luminosity LHC*, ATL-PHYS-PUB-2015-024, 2015,
URL: https://cds.cern.ch/record/2037715 (cit. on p. 10).

[47] CMS Collaboration,
Limits on the Higgs boson lifetime and width from its decay to four charged leptons,
Phys. Rev. D **92** (2015) 072010, arXiv: 1507.06656 [hep-ex] (cit. on p. 10).

[48] CMS Collaboration, *Constraints on the spin-parity and anomalous HVV couplings of the Higgs boson in proton collisions at 7 and 8 TeV*, Phys. Rev. D **92** (2015) 012004, arXiv: `1411.3441 [hep-ex]` (cit. on p. 10).

[49] ATLAS Collaboration, *Probing the CP nature of the Higgs boson coupling to τ leptons at HL-LHC*, ATL-PHYS-PUB-2019-008, 2019, URL: `https://cds.cern.ch/record/2665667` (cit. on p. 10).

[50] CMS Collaboration, *Projection of the Higgs boson mass and on-shell width measurements in $H \to ZZ \to 4\ell$ decay channel at the HL-LHC*, CMS Physics Analysis Summary CMS-PAS-FTR-21-007, 2022, URL: `https://cds.cern.ch/record/2804004` (cit. on p. 10).

[51] CMS Collaboration, *Measurements of properties of the Higgs boson decaying into the four-lepton final state in pp collisions at $\sqrt{s}$ = 13 TeV*, JHEP **11** (2017) 047, arXiv: `1706.09936 [hep-ex]` (cit. on p. 10).

[52] CMS Collaboration, *Measurements of production cross sections of the Higgs boson in the four-lepton final state in proton–proton collisions at $\sqrt{s}$ = 13 TeV*, (2021), arXiv: `2103.04956 [hep-ex]` (cit. on p. 10).

[53] CMS Collaboration, *A projection of the precision of the Higgs boson mass measurement in the diphoton decay channel at the High Luminosity LHC*, CMS Physics Analysis Summary CMS-PAS-FTR-21-008, 2022, URL: `https://cds.cern.ch/record/2804042` (cit. on pp. 12, 13).

[54] CMS Collaboration, *Analysis of the CP structure of the Yukawa coupling between the Higgs boson and τ leptons in proton-proton collisions at $\sqrt{s}$ = 13 TeV*, (2021), Submitted to *JHEP*, arXiv: `2110.04836 [hep-ex]` (cit. on pp. 12, 14).

[55] CMS Collaboration, *Prospects for the precise measurement of the Higgs boson properties in the $H \to \mu\mu$ decay channel at the HL-LHC*, CMS Physics Analysis Summary CMS-PAS-FTR-21-006, 2022, URL: `https://cds.cern.ch/record/2804002` (cit. on pp. 13, 15).

[56] CMS Collaboration, *Projected Performance of an Upgraded CMS Detector at the LHC and HL-LHC: Contribution to the Snowmass Process*, 2013, arXiv: `1307.7135 [hep-ex]` (cit. on pp. 14, 15).

[57] *Direct search for the standard model Higgs boson decaying to a charm quark-antiquark pair*, CMS Physics Analysis Summary, CERN, 2022, URL: `https://cds.cern.ch/record/2802742` (cit. on pp. 14, 17).

[58] H. Qu and L. Gouskos, *ParticleNet: Jet Tagging via Particle Clouds*, Phys. Rev. D **101** (2020) 056019, arXiv: `1902.08570 [hep-ph]` (cit. on p. 15).

[59] CMS Collaboration, *Identification of highly Lorentz-boosted heavy particles using graph neural networks and new mass decorrelation techniques*, CMS Detector Performance Note CMS-DP-2020-002, 2020, URL: `https://cds.cern.ch/record/2707946` (cit. on pp. 15, 34).

[60] CMS Collaboration, *Search for rare Higgs boson decays with mesons at the HL-LHC*, CMS Physics Analysis Summary CMS-PAS-FTR-21-009, 2022, URL: `https://cds.cern.ch/record/2803919` (cit. on pp. 16, 18).

[61] CMS Collaboration, *Prospects for the measurement of $t\bar{t}H$ production in the opposite-sign dilepton channel at $\sqrt{s}$ = 14 TeV at the High-Luminosity LHC*, CMS Physics Analysis Summary CMS-PAS-FTR-21-002, 2022, URL: https://cds.cern.ch/record/2804006 (cit. on pp. 18, 19).

[62] CMS Collaboration, *Measurement of $t\bar{t}H$ production in the $H \rightarrow b\bar{b}$ decay channel in 41.5 fb^{-1} of proton-proton collision data at $\sqrt{s}$ = 13 TeV*, CMS Physics Analysis Summary CMS-PAS-HIG-18-030, 2019, URL: https://cds.cern.ch/record/2675023 (cit. on p. 19).

[63] ATLAS Collaboration, *Extrapolation of ATLAS sensitivity to $H \rightarrow b\bar{b}$ and $H \rightarrow c\bar{c}$ decays in VH production at the HL-LHC*, ATL-PHYS-PUB-2021-039, 2021, URL: https://cds.cern.ch/record/2788490 (cit. on pp. 19, 20).

[64] ATLAS Collaboration, *Measurements of WH and ZH production in the $H \rightarrow b\bar{b}$ decay channel in pp collisions at 13 TeV with the ATLAS detector*, Eur. Phys. J. C **81** (2021) 178, arXiv: 2007.02873 [hep-ex] (cit. on p. 19).

[65] N. Berger et al., *Simplified Template Cross Sections - Stage 1.1*, (2019), arXiv: 1906.02754 [hep-ph] (cit. on p. 19).

[66] ATLAS Collaboration, *Direct constraint on the Higgs-charm coupling from a search for Higgs boson decays into charm quarks with the ATLAS detector*, (2022), arXiv: 2201.11428 [hep-ex] (cit. on pp. 19, 20).

[67] ATLAS Collaboration, *Projection of $H \rightarrow \tau\tau$ cross-section measurement results to the HL-LHC*, ATL-PHYS-PUB-2022-003, 2022, URL: http://cds.cern.ch/record/2801396 (cit. on pp. 20, 22).

[68] ATLAS Collaboration, *Measurements of Higgs boson production cross-sections in the $H \rightarrow \tau^{+}\tau^{-}$ decay channel in pp collisions at $\sqrt{s}$ = 13 TeV with the ATLAS detector*, (2022), arXiv: 2201.08269 [hep-ex] (cit. on p. 20).

[69] CMS Collaboration, *Prospects for HH measurements at the HL-LHC*, CMS Physics Analysis Summary CMS-PAS-FTR-18-019, 2018, URL: http://cds.cern.ch/record/2652549 (cit. on p. 23).

[70] ATLAS Collaboration, *Measurement prospects of the pair production and self-coupling of the Higgs boson with the ATLAS experiment at the HL-LHC*, ATL-PHYS-PUB-2018-053, 2018, URL: https://cds.cern.ch/record/2652727 (cit. on pp. 23, 28, 30, 31).

[71] ATLAS Collaboration, *Constraint of the Higgs boson self-coupling from Higgs boson differential production and decay measurements*, ATL-PHYS-PUB-2019-009, 2019, URL: https://cds.cern.ch/record/2667570 (cit. on p. 24).

[72] CMS Collaboration, *Search for nonresonant Higgs boson pair production in final states with two bottom quarks and two photons in proton–proton collisions at $\sqrt{s}$ = 13 TeV*, JHEP **03** (2021) 257, arXiv: 2011.12373 [hep-ex] (cit. on p. 24).

[73] CMS Collaboration, *Combined Higgs boson production and decay measurements with up to 137 fb-1 of proton-proton collision data at sqrts = 13 TeV*, tech. rep., CERN, 2020, URL: https://cds.cern.ch/record/2706103 (cit. on p. 24).

[74] CMS Collaboration, *Prospects for non-resonant Higgs boson pair production measurement in bbγγ final states in proton-proton collisions at $\sqrt{s}$ = 14 TeV at the High-Luminosity LHC*, CMS Physics Analysis Summary CMS-PAS-FTR-21-004, 2022, URL: https://cds.cern.ch/record/2803918 (cit. on p. 24).

[75] CMS Collaboration, *Prospects for HH measurements in the WWγγ and ττγγ final states in proton-proton collisions at $\sqrt{s}$ = 14 TeV at the High Luminosity-LHC*, CMS Physics Analysis Summary CMS-PAS-FTR-21-003, 2022, URL: https://cds.cern.ch/record/2804003 (cit. on p. 25).

[76] CMS Collaboration, *Search for the nonresonant tt̄HH production in the semileptonic decay of the top pair and the Higgs pair decay into b quarks at the HL-LHC*, CMS Physics Analysis Summary CMS-PAS-FTR-21-010, 2022, URL: https://cds.cern.ch/record/2804085 (cit. on pp. 26, 27).

[77] ATLAS Collaboration, *Expected b-tagging Performance with the upgraded ATLAS Inner Tracker Detector at the High-Luminosity LHC*, ATL-PHYS-PUB-2020-005, 2020, URL: https://cds.cern.ch/record/2713377 (cit. on pp. 28, 31).

[78] ATLAS Collaboration, *Projected sensitivity of Higgs boson pair production in the bbττ final state using proton-proton collisions at HL-LHC with the ATLAS detector*, ATL-PHYS-PUB-2021-044, 2021, URL: https://cds.cern.ch/record/2798448 (cit. on pp. 28, 29).

[79] ATLAS Collaboration, *Measurement prospects of Higgs boson pair production in the bb̄γγ final state with the ATLAS experiment at the HL-LHC*, ATL-PHYS-PUB-2022-001, 2022, URL: https://cds.cern.ch/record/2799146 (cit. on pp. 28–30).

[80] ATLAS Collaboration, *Projected sensitivity of Higgs boson pair production combining the bb̄γγ and bb̄τ⁺τ⁻ final states with the ATLAS detector at the HL-LHC*, ATL-PHYS-PUB-2022-005, 2022, URL: http://cdsweb.cern.ch/record/2802127 (cit. on pp. 28, 30, 31).

[81] ATLAS Collaboration, *Search for resonant and non-resonant Higgs boson pair production in the bb̄τ⁺τ⁻ decay channel using 13 TeV pp collision data from the ATLAS detector*, ATLAS-CONF-2021-030, 2021, URL: https://cds.cern.ch/record/2777236 (cit. on p. 28).

[82] ATLAS Collaboration, *Search for Higgs boson pair production in the two bottom quarks plus two photons final state in pp collisions at $\sqrt{s}$ = 13 TeV with the ATLAS detector*, (2021), arXiv: 2112.11876 [hep-ex] (cit. on pp. 28, 29).

[83] ATLAS Collaboration, *ATLAS b-jet identification performance and efficiency measurement with tt̄ events in pp collisions at $\sqrt{s}$ = 13 TeV*, Eur. Phys. J. C **79** (2019) 970, arXiv: 1907.05120 [hep-ex] (cit. on p. 28).

[84] ATLAS Collaboration, *Identification of hadronic tau lepton decays using neural networks in the ATLAS experiment*, ATL-PHYS-PUB-2019-033, 2019, URL: https://cds.cern.ch/record/2688062 (cit. on p. 28).

[85] ATLAS Collaboration, *Jet reconstruction and performance using particle flow with the ATLAS Detector*, Eur. Phys. J. C **77** (2017) 466, arXiv: 1703.10485 [hep-ex] (cit. on p. 28).

[86] ATLAS Collaboration, *Search for Higgs boson pair production in the γγbb̄ final state with 13 TeV pp collision data collected by the ATLAS experiment*, JHEP **11** (2018) 040, arXiv: 1807.04873 [hep-ex] (cit. on p. 29).

[87] ATLAS Collaboration,
Combination of searches for non-resonant and resonant Higgs boson pair production in the $b\bar{b}\gamma\gamma$, $b\bar{b}\tau^+\tau^-$ and $b\bar{b}b\bar{b}$ decay channels using pp collisions at $\sqrt{s}$ = 13 TeV with the ATLAS detector,
ATLAS-CONF-2021-052, 2021, URL: https://cds.cern.ch/record/2786865 (cit. on p. 30).

[88] A. Djouadi, A. Falkowski, Y. Mambrini and J. Quevillon,
Direct detection of Higgs–portal dark matter at the LHC,
The European Physical Journal C **73** (2013) 2455, arXiv: hep-ph/1205.3169 (cit. on p. 32).

[89] E. Gabrielli, M. Heikinheimo, B. Mele and M. Raidal,
Dark photons and resonant monophoton signatures in Higgs boson decays at the LHC,
Phys. Rev. D **90** (2014) 055032, arXiv: 1405.5196 [hep-ph] (cit. on p. 32).

[90] CMS Collaboration, *Projection of searches for exotic Higgs boson decays to light pseudoscalars for the High-Luminosity LHC*, CMS Physics Analysis Summary CMS-PAS-FTR-18-035, 2019,
URL: http://cds.cern.ch/record/2655340 (cit. on pp. 32, 33).

[91] ATLAS Collaboration, *Search for invisible Higgs-boson decays in events with vector-boson fusion signatures using 139 fb^{-1} of proton-proton data recorded by the ATLAS experiment*, (2022),
arXiv: 2202.07953 [hep-ex] (cit. on p. 32).

[92] ATLAS Collaboration,
Combination of searches for invisible Higgs boson decays with the ATLAS experiment,
ATLAS-CONF-2020-052, 2020, URL: https://cds.cern.ch/record/2743055 (cit. on p. 32).

[93] CMS Collaboration, *Search for invisible decays of a Higgs boson produced via vector boson fusion with 138 fb^{-1} of proton-proton collisions at $\sqrt{s}$ = 13 TeV*, CMS Physics Analysis Summary,
CERN, 2021, URL: https://cds.cern.ch/record/2784571 (cit. on p. 32).

[94] CMS Collaboration, *Search for dark matter produced in association with a leptonically decaying Z boson in proton–proton collisions at $\sqrt{s}$ = 13 TeV*, Eur. Phys. J. C **81** (2021) 13,
arXiv: 2008.04735 [hep-ex] (cit. on p. 32).

[95] ATLAS Collaboration, *Search for associated production of a Z boson with an invisibly decaying Higgs boson or dark matter candidates at $\sqrt{s}$ = 13 TeV with the ATLAS detector*, (2021),
arXiv: 2111.08372 [hep-ex] (cit. on p. 32).

[96] ATLAS Collaboration,
Primary Vertex Selection in VBF Higgs to Invisibles at mu 200 with the ATLAS Experiment,
tech. rep. IDTR-2019-004, 2019,
URL: https://atlas.web.cern.ch/Atlas/GROUPS/PHYSICS/PLOTS/IDTR-2019-004/
(cit. on p. 32).

[97] CMS Collaboration, *Search for invisible decays of a Higgs boson produced through vector boson fusion at the High-Luminosity LHC*, CMS Physics Analysis Summary CMS-PAS-FTR-18-016,
2018, URL: http://cds.cern.ch/record/2647700 (cit. on p. 32).

[98] CMS Collaboration, *Search for invisible decays of a Higgs boson produced through vector boson fusion in proton–proton collisions at $\sqrt{s}$ = 13 TeV*, Phys. Lett. B **793** (2019) 520,
arXiv: 1809.05937 [hep-ex] (cit. on p. 32).

[99] ATLAS Collaboration, *Projections for measurements of Higgs boson cross sections, branching ratios and coupling parameters with the ATLAS detector at a HL-LHC*,
ATL-PHYS-PUB-2013-014, 2013, URL: https://cds.cern.ch/record/1611186
(cit. on p. 33).

[100] CMS Collaboration, *Search sensitivity for dark photons decaying to displaced muons with CMS at the high-luminosity LHC*, CMS Physics Analysis Summary CMS-PAS-FTR-18-002, 2018, URL: http://cds.cern.ch/record/2644533 (cit. on pp. 33, 88, 92, 94, 95).

[101] CMS Collaboration, *First Level Track Jet Trigger for Displaced Jets at High Luminosity LHC*, CMS Physics Analysis Summary CMS-PAS-FTR-18-018, 2018, URL: http://cds.cern.ch/record/2647987 (cit. on p. 33).

[102] CMS Collaboration, *A deep neural network to search for new long-lived particles decaying to jets*, Mach. Learn. Sci. Tech. **1** (2020) 035012, arXiv: 1912.12238 [hep-ex] (cit. on p. 33).

[103] G. C. Branco et al., *Theory and phenomenology of two-Higgs-doublet models*, Phys. Rept. **516** (2012) 1, arXiv: 1106.0034 [hep-ph] (cit. on p. 33).

[104] CMS Collaboration, *Projection of the Run 2 MSSM H $\to \tau\tau$ limits for the High-Luminosity LHC*, CMS Physics Analysis Summary CMS-PAS-FTR-18-017, 2018, URL: http://cds.cern.ch/record/2650912 (cit. on p. 33).

[105] ATLAS Collaboration, *Prospects for the search for additional Higgs bosons in the ditau final state with the ATLAS detector at HL-LHC*, ATL-PHYS-PUB-2018-050, 2018, URL: https://cds.cern.ch/record/2652284 (cit. on p. 33).

[106] CMS Collaboration, *Search for a new scalar resonance decaying to a pair of Z bosons in proton–proton collisions at $\sqrt{s} = 13\,TeV$*, JHEP **06** (2018) 127, arXiv: 1804.01939 [hep-ex] (cit. on p. 33).

[107] CMS Collaboration, *Search for a new scalar resonance decaying to a pair of Z bosons at the High-Luminosity LHC*, CMS Physics Analysis Summary CMS-PAS-FTR-18-040, 2019, URL: http://cds.cern.ch/record/2658263 (cit. on p. 33).

[108] CMS Collaboration, *Search for vector boson fusion production of a massive resonance decaying to a pair of Higgs bosons in the four b quark final state at the HL-LHC using the CMS Phase 2 detector*, CMS Physics Analysis Summary CMS-PAS-FTR-18-003, 2018, URL: http://cds.cern.ch/record/2628598 (cit. on p. 34).

[109] ATLAS Collaboration, *Identification of Boosted Higgs Bosons Decaying Into $b\bar{b}$ With Neural Networks and Variable Radius Subjets in ATLAS*, ATL-PHYS-PUB-2020-019, 2020, URL: https://cds.cern.ch/record/2724739 (cit. on p. 34).

[110] CMS Collaboration, *Mass regression of highly-boosted jets using graph neural networks*, CMS Detector Performance Summary CMS-DP-2021-017, 2021, URL: http://cds.cern.ch/record/2777006 (cit. on p. 34).

[111] CMS Collaboration, *Search for high mass resonances decaying into W^+W^- in the dileptonic final state with $138\,fb^{-1}$ of proton-proton collisions at $\sqrt{s} = 13\,TeV$*, CMS Physics Analysis Summary CMS-PAS-HIG-20-016, 2022, URL: https://cds.cern.ch/record/2803723 (cit. on pp. 35, 36).

[112] CMS Collaboration, *ECFA 2016: Prospects for selected standard model measurements with the CMS experiment at the High-Luminosity LHC*, CMS Physics Analysis Summary CMS-PAS-FTR-16-006, 2017, URL: https://cds.cern.ch/record/2262606 (cit. on p. 37).

[113] ATLAS Collaboration, *Prospects for measurement of the top quark mass using $t\bar{t}$ events with $J/\psi \to \mu^+\mu^-$ decays with the upgraded ATLAS detector at the High Luminosity LHC*, ATL-PHYS-PUB-2018-042, 2018, URL: https://cds.cern.ch/record/2649882 (cit. on p. 37).

[114] CMS Collaboration, *Projection of measurements of differential ttbar production cross sections in the e/u+jets channels in pp collisions at the HL-LHC*, CMS Physics Analysis Summary CMS-PAS-FTR-18-015, 2018, URL: http://cds.cern.ch/record/2651195 (cit. on pp. 37, 38).

[115] CMS Collaboration, *Projections of sensitivities for tttt production at HL-LHC and HE-LHC*, CMS Physics Analysis Summary CMS-PAS-FTR-18-031, 2019, URL: http://cds.cern.ch/record/2650211 (cit. on p. 38).

[116] ATLAS Collaboration, *Prospects for the measurement of $t\bar{t}\gamma$ with the upgraded ATLAS detector at the High-Luminosity LHC*, ATL-PHYS-PUB-2018-049, 2018, URL: https://cds.cern.ch/record/2652168 (cit. on pp. 38, 39).

[117] ATLAS Collaboration, *Measurements of inclusive and differential fiducial cross-sections of $t\bar{t}\gamma$ production in leptonic final states at $\sqrt{s}$ = 13 TeV in ATLAS*, Eur. Phys. J. C **79** (2019) 382, arXiv: 1812.01697 [hep-ex] (cit. on p. 38).

[118] CMS Collaboration, *Prospects for the search for gluon-mediated FCNC in top quark production with the CMS Phase-2 detector at the HL-LHC*, CMS Physics Analysis Summary CMS-PAS-FTR-18-004, 2018, URL: http://cds.cern.ch/record/2638815 (cit. on pp. 39, 40).

[119] ATLAS Collaboration, *Sensitivity of searches for the flavour-changing neutral current decay $t \to qZ$ using the upgraded ATLAS experiment at the High Luminosity LHC*, ATL-PHYS-PUB-2019-001, 2019, URL: https://cds.cern.ch/record/2653389 (cit. on p. 39).

[120] ATLAS Collaboration, *Search for flavour-changing neutral current top-quark decays $t \to qZ$ in proton–proton collisions at $\sqrt{s}$ = 13 TeV with the ATLAS detector*, JHEP **07** (2018) 176, arXiv: 1803.09923 [hep-ex] (cit. on p. 39).

[121] CMS Collaboration, *Anomalous couplings in the tt+Z final state at the HL-LHC*, CMS Physics Analysis Summary CMS-PAS-FTR-18-036, 2018, URL: http://cds.cern.ch/record/2652018 (cit. on pp. 39, 40).

[122] ATLAS Collaboration, *Extrapolation of ATLAS sensitivity to the measurement of the Standard Model four top quark cross section at the HL-LHC*, ATL-PHYS-PUB-2022-004, 2022, URL: http://cds.cern.ch/record/2801400 (cit. on pp. 40, 41).

[123] ATLAS Collaboration, *Evidence for $t\bar{t}t\bar{t}$ production in the multilepton final state in proton–proton collisions at $\sqrt{s}$ = 13 TeV with the ATLAS detector*, Eur. Phys. J. C **80** (2020) 1085, arXiv: 2007.14858 [hep-ex] (cit. on p. 40).

[124] R. Frederix, D. Pagani and M. Zaro, *Large NLO corrections in $t\bar{t}W^\pm$ and $t\bar{t}t\bar{t}$ hadroproduction from supposedly subleading EW contributions*, JHEP **02** (2018) 031, arXiv: 1711.02116 [hep-ph] (cit. on p. 41).

[125] S. Descotes-Genon, L. Hofer, J. Matias and J. Virto, *Global analysis of $b \to s\ell\ell$ anomalies*, JHEP **06** (2016) 092, arXiv: 1510.04239 [hep-ph] (cit. on p. 42).

[126] J. Matias, F. Mescia, M. Ramon and J. Virto,
Complete Anatomy of $\bar{B}_d-> \bar{K}^{*0}(-> K\pi)l^+l^-$ and its angular distribution, JHEP **04** (2012) 104,
arXiv: 1202.4266 [hep-ph] (cit. on p. 42).

[127] ATLAS Collaboration, *Prospects for the $\mathcal{B}(B^0_{(s)} \to \mu^+\mu^-)$ measurements with the ATLAS
detector in the Run 2 and HL-LHC data campaigns*, ATL-PHYS-PUB-2018-005, 2018,
URL: https://cds.cern.ch/record/2317211 (cit. on pp. 43, 44).

[128] CMS Collaboration,
Measurement of rare $B \to \mu^+\mu^-$ decays with the Phase-2 upgraded CMS detector at the HL-LHC,
CMS Physics Analysis Summary CMS-PAS-FTR-18-013, CERN, 2018,
URL: https://cds.cern.ch/record/2650545 (cit. on pp. 43, 45).

[129] ATLAS Collaboration, *Study of the rare decays of B^0_s and B^0 into muon pairs from data collected
during the LHC Run 1 with the ATLAS detector*, Eur. Phys. J. C **76** (2016) 513,
arXiv: 1604.04263 [hep-ex] (cit. on p. 43).

[130] CMS Collaboration, *Measurement of the $B^0_s \to \mu^+\mu^-$ Branching Fraction and Search for
$B^0 \to \mu^+\mu^-$ with the CMS Experiment*, Phys. Rev. Lett. **111** (2013) 101804,
arXiv: 1307.5025 [hep-ex] (cit. on p. 43).

[131] C. Bobeth et al., *$B_{s,d} \to l^+l^-$ in the Standard Model with Reduced Theoretical Uncertainty*,
Phys. Rev. Lett. **112** (2014) 101801,
URL: https://link.aps.org/doi/10.1103/PhysRevLett.112.101801 (cit. on p. 44).

[132] CMS Collaboration,
Study of the expected sensitivity to the P'_5 parameter in the $B^0 \to K^{*0}\mu^+\mu^-$ decay at the HL-LHC,
CMS Physics Analysis Summary CMS-PAS-FTR-18-033, 2018,
URL: http://cds.cern.ch/record/2651298 (cit. on pp. 43, 46).

[133] ATLAS Collaboration,
$B^0_d \to K^{*0}\mu\mu$ angular analysis prospects with the upgraded ATLAS detector at the HL-LHC,
ATL-PHYS-PUB-2019-003, 2019, URL: https://cds.cern.ch/record/2654519
(cit. on pp. 43, 46).

[134] S. Descotes-Genon, L. Hofer, J. Matias and J. Virto,
On the impact of power corrections in the prediction of $B \to K^*\mu^+\mu^-$ observables,
JHEP **12** (2014) 125, arXiv: 1407.8526 [hep-ph] (cit. on pp. 43, 46).

[135] LHCb Collaboration, *Measurements of the S-wave fraction in $B^0 \to K^+\pi^-\mu^+\mu^-$ decays and the
$B^0 \to K^*(892)^0\mu^+\mu^-$ differential branching fraction*,
JHEP **11** (2016) 047, [Erratum: JHEP04,142(2017)], arXiv: 1606.04731 [hep-ex]
(cit. on p. 44).

[136] ATLAS Collaboration, *Studies of radial distortions of the ATLAS Inner Detector*,
ATL-PHYS-PUB-2018-003, 2018, URL: https://cds.cern.ch/record/2309785
(cit. on p. 44).

[137] M. Ciuchini et al., *$B \to K^*\ell^+\ell^-$ decays at large recoil in the Standard Model: a theoretical
reappraisal*, JHEP **06** (2016) 116, arXiv: 1512.07157 [hep-ph] (cit. on p. 46).

[138] S. Jäger and J. Martin Camalich, *On $B \to V\ell\ell$ at small dilepton invariant mass, power
corrections, and new physics*, JHEP **05** (2013) 043, arXiv: 1212.2263 [hep-ph] (cit. on p. 46).

[139] ATLAS Collaboration, *CP-violation measurement prospects in the $B_s^0 \to J/\psi\phi$ channel with the upgraded ATLAS detector at the HL-LHC*, ATL-PHYS-PUB-2018-041, 2018, URL: https://cds.cern.ch/record/2649881 (cit. on pp. 45–47).

[140] CMS Collaboration, *CP-violation studies at the HL-LHC with CMS using B_s^0 decays to J/$\psi\phi$(1020)*, CMS Physics Analysis Summary CMS-PAS-FTR-18-041, 2018, URL: http://cds.cern.ch/record/2650772 (cit. on pp. 45–47).

[141] ATLAS Collaboration, *Measurement of the CP-violating phase ϕ_s and the B_s^0 meson decay width difference with $B_s^0 \to J/\psi\phi$ decays in ATLAS*, JHEP **08** (2016) 147, arXiv: 1601.03297 [hep-ex] (cit. on p. 45).

[142] CMS Collaboration, *Measurement of the CP-violating weak phase ϕ_s and the decay width difference $\Delta\Gamma_s$ using the $B_s^0 \to J/\psi\phi$(1020) decay channel in pp collisions at $\sqrt{s} = 8\,TeV$*, Phys. Lett. B **757** (2016) 97, arXiv: 1507.07527 [hep-ex] (cit. on p. 45).

[143] M. Tanabashi et al., *Review of Particle Physics (RPP)*, Phys. Rev. **D98** (2018) 030001 (cit. on p. 47).

[144] Y. Amhis et al., *Averages of b-hadron, c-hadron, and τ-lepton properties as of summer 2016*, Eur. Phys. J. **C77** (2017) 895, updated results and plots available at https://hflav.web.cern.ch, arXiv: 1612.07233 [hep-ex] (cit. on p. 47).

[145] The ALEPH, DELPHI, L3, OPAL and SLD Collaborations, the LEP Electroweak Working Group, the SLD electroweak, heavy flavour groups, *Precision electroweak measurements on the Z resonance*, Phys. Rept. **427** (2006) 257, arXiv: hep-ex/0509008 [hep-ex] (cit. on p. 48).

[146] CMS Collaboration, *Measurement of the weak mixing angle with the Drell-Yan process in proton–proton collisions at the LHC*, Phys. Rev. D **84** (2011) 112002, arXiv: 1110.2682 [hep-ex] (cit. on p. 48).

[147] ATLAS Collaboration, *Measurement of the forward-backward asymmetry of electron and muon pair-production in pp collisions at $\sqrt{s} = 7\,TeV$ with the ATLAS detector*, JHEP **09** (2015) 049, arXiv: 1503.03709 [hep-ex] (cit. on p. 48).

[148] LHCb Collaboration, *Measurement of the forward-backward asymmetry in $Z/\gamma^* \to \mu^+\mu^-$ decays and determination of the effective weak mixing angle*, JHEP **11** (2015) 190, arXiv: 1509.07645 [hep-ex] (cit. on p. 48).

[149] CDF Collaboration, *Indirect measurement of $\sin^2\theta_W$ (or M_W) using $\mu^+\mu^-$ pairs from γ^*/Z bosons produced in $p\bar{p}$ collisions at a center-of-momentum energy of 1.96 TeV*, Phys. Rev. D **89** (2014) 072005, arXiv: 1402.2239 [hep-ex] (cit. on p. 48).

[150] CDF Collaboration, *Measurement of $\sin^2\theta_{eff}^{lept}$ using e^+e^- pairs from γ^*/Z bosons produced in $p\bar{p}$ collisions at a center-of-momentum energy of 1.96 TeV*, Phys. Rev. D **93** (2016) 112016, arXiv: 1605.02719 [hep-ex] (cit. on p. 48).

[151] D0 Collaboration, *Measurement of the effective weak mixing angle in $p\bar{p} \to Z/\gamma^* \to e^+e^-$ events*, Phys. Rev. Lett. **115** (2015) 041801, arXiv: 1408.5016 [hep-ex] (cit. on p. 48).

[152] ATLAS Collaboration, *Prospect for a measurement of the Weak Mixing Angle in $pp \to Z/\gamma^* \to e^+e^-$ events with the ATLAS detector at the High Luminosity Large Hadron Collider*, ATL-PHYS-PUB-2018-037, 2018, URL: https://cds.cern.ch/record/2649330 (cit. on pp. 48, 49).

[153]   CMS Collaboration, *A proposal for the measurement of the weak mixing angle at the HL-LHC*, CMS Physics Analysis Summary CMS-PAS-FTR-17-001, 2017, URL: http://cds.cern.ch/record/2294888 (cit. on pp. 48, 49).

[154]   ATLAS Collaboration, *Measurement of the effective leptonic weak mixing angle using electron and muon pairs from Z-boson decay in the ATLAS experiment at $\sqrt{s}$ = 8 TeV*, ATLAS-CONF-2018-037, 2018, URL: https://cds.cern.ch/record/2630340 (cit. on p. 48).

[155]   ATLAS Collaboration, *Observation of Electroweak Production of a Same-Sign W Boson Pair in Association with Two Jets in pp Collisions at $\sqrt{s}$ = 13 TeV with the ATLAS Detector*, Phys. Rev. Lett. **123** (2019) 161801, arXiv: 1906.03203 [hep-ex] (cit. on pp. 48, 50).

[156]   CMS Collaboration, *Measurements of production cross sections of polarized same-sign W boson pairs in association with two jets in proton–proton collisions at $\sqrt{s}$ = 13 TeV*, Phys. Lett. B **812** (2021) 136018, arXiv: 2009.09429 [hep-ex] (cit. on pp. 48, 50, 53).

[157]   ATLAS Collaboration, *Observation of electroweak $W^{\pm}Z$ boson pair production in association with two jets in pp collisions at $\sqrt{s}$ = 13 TeV with the ATLAS detector*, Phys. Lett. B **793** (2019) 469, arXiv: 1812.09740 [hep-ex] (cit. on pp. 48, 50).

[158]   CMS Collaboration, *Measurements of production cross sections of WZ and same-sign WW boson pairs in association with two jets in proton–proton collisions at $\sqrt{s}$ = 13 TeV*, Phys. Lett. B **809** (2020) 135710, arXiv: 2005.01173 [hep-ex] (cit. on pp. 48, 50, 53).

[159]   ATLAS Collaboration, *Observation of electroweak production of two jets and a Z-boson pair with the ATLAS detector at the LHC*, (2020), arXiv: 2004.10612 [hep-ex] (cit. on p. 48).

[160]   CMS Collaboration, *Evidence for electroweak production of four charged leptons and two jets in proton–proton collisions at $\sqrt{s}$ = 13 TeV*, Phys. Lett. B **812** (2021) 135992, arXiv: 2008.07013 [hep-ex] (cit. on p. 48).

[161]   ATLAS Collaboration, *Evidence for electroweak production of two jets in association with a $Z\gamma$ pair in pp collisions at $\sqrt{s}$ = 13 TeV with the ATLAS detector*, Phys. Lett. B **803** (2020) 135341, arXiv: 1910.09503 [hep-ex] (cit. on p. 48).

[162]   ATLAS Collaboration, *Prospects for the measurement of the $W^{\pm}W^{\pm}$ scattering cross section and extraction of the longitudinal scattering component in pp collisions at the High-Luminosity LHC with the ATLAS Experiment*, ATL-PHYS-PUB-2018-052, 2018, URL: https://cds.cern.ch/record/2652447 (cit. on pp. 50, 51).

[163]   CMS Collaboration, *Study of $W^{\pm}W^{\pm}$ production via vector boson scattering at the HL-LHC with the upgraded CMS detector*, CMS Physics Analysis Summary CMS-PAS-FTR-18-005, 2018, URL: http://cds.cern.ch/record/2646870 (cit. on pp. 50, 51).

[164]   ATLAS Collaboration, *Prospective study of vector boson scattering in WZ fully leptonic final state at HL-LHC*, ATL-PHYS-PUB-2018-023, 2018, URL: https://cds.cern.ch/record/2645271 (cit. on p. 50).

[165]   CMS Collaboration, *Prospects for the measurement of electroweak and polarized WZ to 3lv production cross sections at the High-Luminosity LHC*, CMS Physics Analysis Summary CMS-PAS-FTR-18-038, 2018, URL: http://cds.cern.ch/record/2650774 (cit. on p. 50).

[166] CMS Collaboration, *Vector Boson Scattering prospective studies in the ZZ fully leptonic decay channel for the High-Luminosity and High-Energy LHC upgrades*, CMS Physics Analysis Summary CMS-PAS-FTR-18-014, 2018, URL: http://cds.cern.ch/record/2650915 (cit. on p. 50).

[167] ATLAS Collaboration, *Prospect study of electroweak production of a Z boson pair plus two jets at the HL-LHC*, ATL-PHYS-PUB-2018-029, 2018, URL: https://cds.cern.ch/record/2647219 (cit. on p. 50).

[168] ATLAS Collaboration, *HL-LHC prospects for diboson resonance searches and electroweak vector boson scattering in the $WW/WZ \to \ell\nu qq$ final state*, ATL-PHYS-PUB-2018-022, 2018, URL: https://cds.cern.ch/record/2645269 (cit. on pp. 50, 51).

[169] ATLAS Collaboration, *Search for the electroweak diboson production in association with a high-mass dijet system in pp collisions at $\sqrt{s} = 13\,TeV$ with the ATLAS detector*, Phys. Rev. D **100** (2019) 032007, arXiv: 1905.07714 [hep-ex] (cit. on p. 50).

[170] ATLAS Collaboration, *Probing lepton flavour violation via neutrinoless $\tau \to 3\mu$ decays with the ATLAS detector*, Eur. Phys. J. C **76** (2016) 232, arXiv: 1601.03567 [hep-ex] (cit. on p. 52).

[171] ATLAS Collaboration, *Prospects for lepton flavour violation measurements in $\tau \to 3\mu$ decays with the ATLAS detector at the HL-LHC*, ATL-PHYS-PUB-2018-032, 2018, URL: https://cds.cern.ch/record/2647956 (cit. on p. 52).

[172] ATLAS Collaboration, *Prospects for the measurement of the W-boson mass at the HL- and HE-LHC*, ATL-PHYS-PUB-2018-026, 2018, URL: https://cds.cern.ch/record/2645431 (cit. on pp. 52, 53).

[173] CMS Collaboration, *Prospects for the measurement of vector boson scattering production in leptonic $W^{\pm}W^{\pm}$ and WZ diboson events at $\sqrt{s} = 14$ TeV at the High-Luminosity LHC*, CMS Physics Analysis Summary, CERN, 2021, URL: http://cds.cern.ch/record/2776773 (cit. on pp. 53, 54).

[174] ATLAS Collaboration, *Prospects for jet and photon physics at the HL-LHC and HE-LHC*, ATL-PHYS-PUB-2018-051, 2018, URL: https://cds.cern.ch/record/2652285 (cit. on pp. 55–57).

[175] CMS Collaboration, *High-p_T jet measurements at the HL-LHC*, CMS Physics Analysis Summary CMS-PAS-FTR-18-032, 2018, URL: http://cds.cern.ch/record/2651219 (cit. on pp. 55, 57, 58).

[176] R. Abdul Khalek, S. Bailey, J. Gao, L. Harland-Lang and J. Rojo, *Towards Ultimate Parton Distributions at the High-Luminosity LHC*, Eur. Phys. J. C **78** (2018) 962, arXiv: 1810.03639 [hep-ph] (cit. on pp. 55, 57).

[177] ATLAS Collaboration, *Measurement of the inclusive and dijet cross-sections of b-jets in pp collisions at $\sqrt{s} = 7\,TeV$ with the ATLAS detector*, Eur. Phys. J. C **71** (2011) 1846, arXiv: 1109.6833 [hep-ex] (cit. on p. 57).

[178] ATLAS Collaboration,
Measurement of the $b\bar{b}$ dijet cross section in pp collisions at $\sqrt{s}$ = 7 TeV with the ATLAS detector,
Eur. Phys. J. C **76** (2016) 670, arXiv: 1607.08430 [hep-ex] (cit. on p. 57).

[179] CMS Collaboration,
Studies of inclusive four-jet production with two b-tagged jets in proton–proton collisions at 7 TeV,
Phys. Rev. D **94** (2016) 112005, arXiv: 1609.03489 [hep-ex] (cit. on p. 57).

[180] CMS Collaboration, *Inclusive b-jet production in pp collisions at $\sqrt{s}$ = 7 TeV*,
JHEP **04** (2012) 084, arXiv: 1202.4617 [hep-ex] (cit. on p. 57).

[181] ATLAS Collaboration, *ATLAS Forward Proton Phase-I Upgrade: Technical Design Report*,
ATLAS-TDR-024; CERN-LHCC-2015-009, 2015,
URL: https://cds.cern.ch/record/2017378 (cit. on p. 59).

[182] CMS-TOTEM Collaboration, *CMS-TOTEM Precision Proton Spectrometer*, tech. rep., 2014,
URL: https://cds.cern.ch/record/1753795 (cit. on p. 59).

[183] ATLAS Collaboration,
Sensitivity to exclusive WW production in photon scattering at the High Luminosity LHC,
ATL-PHYS-PUB-2021-026, 2021, URL: https://cds.cern.ch/record/2776764
(cit. on pp. 59, 60).

[184] ATLAS Collaboration, *Observation of photon-induced W^+W^- production in pp collisions at $\sqrt{s}$ = 13 TeV using the ATLAS detector*, Phys. Lett. B **816** (2021) 136190,
arXiv: 2010.04019 [hep-ex] (cit. on p. 59).

[185] E. Chapon, C. Royon and O. Kepka, *Anomalous quartic W W gamma gamma, Z Z gamma gamma, and trilinear WW gamma couplings in two-photon processes at high luminosity at the LHC*,
Phys. Rev. D **81** (2010) 074003, arXiv: 0912.5161 [hep-ph] (cit. on p. 59).

[186] ATLAS Collaboration, *A Radiation-Hard Zero Degree Calorimeter for ATLAS in the HL-LHC era*,
CERN-LHCC-2021-018, LHCC-P-019, 2021, URL: https://cds.cern.ch/record/2781150
(cit. on p. 61).

[187] Y. Bashan et al., *A Run 4 Zero Degree Calorimeter for CMS*, tech. rep.,
This is a joint project with the ATLAS heavy ion group: CERN, 2021,
URL: https://cds.cern.ch/record/2791533 (cit. on p. 61).

[188] CMS Collaboration,
Performance of jet quenching measurements in pp and PbPb collisions with CMS at the HL-LHC,
CMS Physics Analysis Summary CMS-PAS-FTR-18-025, 2018,
URL: http://cds.cern.ch/record/2651892 (cit. on pp. 61, 62).

[189] ATLAS Collaboration, *Projections for ATLAS Measurements of Jet Modifications in Pb+Pb Collisions in LHC Runs 3 and 4*, ATL-PHYS-PUB-2018-019, 2018,
URL: https://cds.cern.ch/record/2644406 (cit. on pp. 61, 62).

[190] B. Z. Kopeliovich, I. K. Potashnikova, I. Schmidt and M. Siddikov,
Survival of charmonia in a hot environment, Phys. Rev. C **91** (2015) 024911,
arXiv: 1409.5147 [hep-ph] (cit. on p. 62).

[191] S. Aronson, E. Borras, B. Odegard, R. Sharma and I. Vitev,
Collisional and thermal dissociation of J/ψ and Υ states at the LHC,
Phys. Lett. B **778** (2018) 384, arXiv: 1709.02372 [hep-ph] (cit. on p. 62).

[192] X. Du, R. Rapp and M. He,
Color Screening and Regeneration of Bottomonia in High-Energy Heavy-Ion Collisions,
Phys. Rev. C **96** (2017) 054901, arXiv: `1706.08670 [hep-ph]` (cit. on p. 62).

[193] CMS Collaboration, *Open heavy flavor and quarkonia in heavy ion collisions at HL-LHC*,
CMS Physics Analysis Summary CMS-PAS-FTR-18-024, 2018,
URL: `http://cds.cern.ch/record/2650897` (cit. on pp. 62, 63).

[194] CMS Collaboration, *Predictions on the precision achievable for small system flow observables in the context of HL-LHC*, CMS Physics Analysis Summary CMS-PAS-FTR-18-026, 2018,
URL: `http://cds.cern.ch/record/2650773` (cit. on pp. 62–64).

[195] ATLAS Collaboration, *Projections for ATLAS Measurements of Bulk Properties of Pb+Pb, p+Pb, and pp Collisions in LHC Runs 3 and 4*, ATL-PHYS-PUB-2018-020, 2018,
URL: `https://cds.cern.ch/record/2644407` (cit. on pp. 62–64).

[196] ALICE Collaboration,
Correlated event-by-event fluctuations of flow harmonics in Pb-Pb collisions at $\sqrt{s_{NN}}$ = 2.76 TeV,
Phys. Rev. Lett. **117** (2016) 182301, arXiv: `1604.07663 [nucl-ex]` (cit. on p. 64).

[197] CMS Collaboration,
Observation of long-range, near-side angular correlations in proton–proton collisions at the LHC,
JHEP **09** (2010) 091, arXiv: `1009.4122 [hep-ex]` (cit. on p. 64).

[198] CMS Collaboration,
Observation of long-range, near-side angular correlations in pPb collisions at the LHC,
Phys. Lett. B **718** (2013) 795, arXiv: `1210.5482 [hep-ex]` (cit. on p. 64).

[199] ALICE Collaboration, *Long-range angular correlations on the near and away side in p-Pb collisions at $\sqrt{s_{NN}}$ = 5.02 TeV*, Phys. Lett. B **719** (2013) 29, arXiv: `1212.2001 [nucl-ex]`
(cit. on p. 64).

[200] ATLAS Collaboration, *Observation of Associated Near-Side and Away-Side Long-Range Correlations in $\sqrt{s_{NN}}$ = 5.02 TeV Proton–Lead Collisions with the ATLAS Detector*,
Phys. Rev. Lett. **110** (2013) 182302, arXiv: `1212.5198 [hep-ex]` (cit. on p. 64).

[201] F. G. Gardim, F. Grassi, M. Luzum and J.-Y. Ollitrault,
Breaking of factorization of two-particle correlations in hydrodynamics,
Phys. Rev. C **87** (2013) 031901, arXiv: `1211.0989 [nucl-th]` (cit. on p. 64).

[202] F. Gelis, E. Iancu, J. Jalilian-Marian and R. Venugopalan, *The Color Glass Condensate*,
Ann. Rev. Nucl. Part. Sci. **60** (2010) 463, arXiv: `1002.0333 [hep-ph]` (cit. on p. 64).

[203] CMS Collaboration, *Constraining nuclear parton distributions with heavy ion collisions at the HL-LHC with the CMS experiment*, CMS Physics Analysis Summary CMS-PAS-FTR-18-027,
2018, URL: `http://cds.cern.ch/record/2652030` (cit. on pp. 64, 65).

[204] ATLAS Collaboration, *Expected ATLAS Measurement Capabilities of Observables Sensitive to Nuclear Parton Distributions*, ATL-PHYS-PUB-2018-039, 2018,
URL: `https://cds.cern.ch/record/2649445` (cit. on p. 64).

[205] ATLAS Collaboration, *Prospects for Measurements of Photon-Induced Processes in Ultra-Peripheral Collisions of Heavy Ions with the ATLAS Detector in the LHC Runs 3 and 4*,
ATL-PHYS-PUB-2018-018, 2018, URL: `https://cds.cern.ch/record/2641655`
(cit. on pp. 65, 66).

[206] M. Bauer, M. Neubert and A. Thamm, *Collider Probes of Axion-Like Particles*,
JHEP **12** (2017) 044, arXiv: 1708.00443 [hep-ph] (cit. on p. 66).

[207] CMS Collaboration, *Evidence for light-by-light scattering and searches for axion-like particles in ultraperipheral PbPb collisions at $\sqrt{s_{NN}}$ = 5.02 TeV*, Phys. Lett. B **797** (2019) 134826,
arXiv: 1810.04602 [hep-ex] (cit. on p. 66).

[208] CMS Collaboration,
Observation of tau lepton pair production in ultraperipheral nucleus-nucleus collisions,
CMS Physics Analysis Summary CMS-PAS-HIN-21-009, 2022,
URL: http://cds.cern.ch/record/2803742 (cit. on pp. 65, 66).

[209] DELPHI Collaboration, *Study of τ-pair production in photon-photon collisions at LEP and limits on the anomalous electromagnetic moments of the τ lepton*, Eur. Phys. J. C **35** (2004) 159,
arXiv: hep-ex/0406010 (cit. on p. 66).

[210] CMS Collaboration,
The Phase-2 Upgrade of the CMS Beam Radiation Instrumentation and Luminosity Detectors,
tech. rep., CERN, 2021, URL: https://cds.cern.ch/record/2759074 (cit. on p. 66).

[211] L. Beresford and J. Liu, *New physics and tau g − 2 using LHC heavy ion collisions*,
Phys. Rev. D **102** (2020) 113008, arXiv: 1908.05180 [hep-ph] (cit. on p. 67).

[212] M. Dyndal, M. Klusek-Gawenda, M. Schott and A. Szczurek, *Anomalous electromagnetic moments of τ lepton in $\gamma\gamma \to \tau^+\tau^-$ reaction in Pb+Pb collisions at the LHC*,
Phys. Lett. B **809** (2020) 135682, arXiv: 2002.05503 [hep-ph] (cit. on p. 67).

[213] ATLAS Collaboration, *Prospects for searches for staus, charginos and neutralinos at the high luminosity LHC with the ATLAS Detector*, ATL-PHYS-PUB-2018-048, 2018,
URL: https://cds.cern.ch/record/2651927 (cit. on pp. 68–72).

[214] CMS Collaboration, *Searches for light higgsino-like charginos and neutralinos at the HL-LHC with the Phase-2 CMS detector*, CMS Physics Analysis Summary CMS-PAS-FTR-18-001, 2018,
URL: http://cds.cern.ch/record/2648538 (cit. on pp. 69, 71).

[215] ATLAS Collaboration,
ATLAS sensitivity to winos and higgsinos with a highly compressed mass spectrum at the HL-LHC,
ATL-PHYS-PUB-2018-031, 2018, URL: https://cds.cern.ch/record/2647294
(cit. on pp. 69, 71, 72).

[216] ATLAS Collaboration, *ATLAS sensitivity to top squark pair production at the HL-LHC*,
ATL-PHYS-PUB-2018-021, 2018, URL: https://cds.cern.ch/record/2644831
(cit. on pp. 70, 72).

[217] CMS Collaboration, *HL-LHC searches for new physics in hadronic final states with boosted W bosons or top quarks using razor variables*,
CMS Physics Analysis Summary CMS-PAS-FTR-18-037, 2019,
URL: http://cds.cern.ch/record/2658262 (cit. on pp. 70, 72).

[218] ATLAS Collaboration, *Search for chargino–neutralino pair production in final states with three leptons and missing transverse momentum in $\sqrt{s}$ = 13 TeV pp collisions with the ATLAS detector*,
(2021), arXiv: 2106.01676 [hep-ex] (cit. on p. 68).

[219] CMS Collaboration, *Search for electroweak production of charginos and neutralinos in proton-proton collisions at $\sqrt{s}$ = 13 TeV*, (2021), arXiv: 2106.14246 [hep-ex] (cit. on p. 68).

[220] ATLAS Collaboration,
Search for charginos and neutralinos in final states with two boosted hadronically decaying bosons and missing transverse momentum in pp collisions at $\sqrt{s} = 13$ TeV with the ATLAS detector,
Phys. Rev. D **104** (2021) 112010, arXiv: 2108.07586 [hep-ex] (cit. on pp. 68, 71).

[221] CMS Collaboration, *Search for electroweak production of supersymmetric particles in final states containing hadronic decays of WW, WZ, or WH and missing transverse momentum*,
CMS Physics Analysis Summary CMS-PAS-SUS-21-002, 2021,
URL: https://cds.cern.ch/record/2779116 (cit. on pp. 68, 71, 74, 75).

[222] ATLAS Collaboration, *Search for direct production of electroweakinos in final states with one lepton, missing transverse momentum and a Higgs boson decaying into two b-jets in pp collisions at $\sqrt{s} = 13$ TeV with the ATLAS detector*, Eur. Phys. J. C **80** (2020) 691,
arXiv: 1909.09226 [hep-ex] (cit. on p. 68).

[223] CMS Collaboration, *Search for chargino-neutralino production in events with Higgs and W bosons using 137 fb^{-1} of proton-proton collisions at $\sqrt{s} = 13$ TeV*, JHEP **10** (2021) 045,
arXiv: 2107.12553 [hep-ex] (cit. on p. 71).

[224] ATLAS Collaboration,
Search for electroweak production of charginos and sleptons decaying into final states with two leptons and missing transverse momentum in $\sqrt{s} = 13$ TeV pp collisions using the ATLAS detector,
Eur. Phys. J. C **80** (2020) 123, arXiv: 1908.08215 [hep-ex] (cit. on p. 71).

[225] ATLAS Collaboration, *Searches for electroweak production of supersymmetric particles with compressed mass spectra in $\sqrt{s} = 13$ TeV pp collisions with the ATLAS detector*,
Phys. Rev. D **101** (2020) 052005, arXiv: 1911.12606 [hep-ex] (cit. on p. 71).

[226] CMS Collaboration, *Search for supersymmetry in final states with two or three soft leptons and missing transverse momentum in proton-proton collisions at $\sqrt{s} = 13$ TeV*, (2021),
arXiv: 2111.06296 [hep-ex] (cit. on p. 71).

[227] ATLAS Collaboration, *Search for long-lived charginos based on a disappearing-track signature using 136 fb^{-1} of pp collisions at $\sqrt{s} = 13$ TeV with the ATLAS detector*, (2022),
arXiv: 2201.02472 [hep-ex] (cit. on p. 72).

[228] ATLAS Collaboration, *Search for direct stau production in events with two hadronic τ-leptons in $\sqrt{s} = 13$ TeV pp collisions with the ATLAS detector*, Phys. Rev. D **101** (2020) 032009,
arXiv: 1911.06660 [hep-ex] (cit. on p. 72).

[229] CMS Collaboration, *Search for supersymmetry with direct stau production at the HL-LHC with the CMS Phase-2 detector*, CMS Physics Analysis Summary CMS-PAS-FTR-18-010, 2019,
URL: http://cds.cern.ch/record/2647985 (cit. on p. 72).

[230] ATLAS Collaboration, *Search for a scalar partner of the top quark in the all-hadronic $t\bar{t}$ plus missing transverse momentum final state at $\sqrt{s} = 13$ TeV with the ATLAS detector*,
Eur. Phys. J. C **80** (2020) 737, arXiv: 2004.14060 [hep-ex] (cit. on p. 72).

[231] CMS Collaboration, *Search for top squark production in fully-hadronic final states in proton–proton collisions at $\sqrt{s} = 13$ TeV*, (2021), arXiv: 2103.01290 [hep-ex] (cit. on p. 73).

[232] CMS Collaboration, *Inclusive search for supersymmetry in pp collisions at $\sqrt{s} = 13$ TeV using razor variables and boosted object identification in zero and one lepton final states*,
JHEP **03** (2019) 031, arXiv: 1812.06302 [hep-ex] (cit. on p. 73).

[233] BaBar Collaboration,
Measurement of an Excess of $\bar{B} \to D^{(*)}\tau^-\bar{\nu}_\tau$ Decays and Implications for Charged Higgs Bosons,
Phys. Rev. D **88** (2013) 072012, arXiv: 1303.0571 [hep-ex] (cit. on p. 73).

[234] Belle Collaboration, *Measurement of the branching ratio of $\bar{B} \to D^{(*)}\tau^-\bar{\nu}_\tau$ relative to $\bar{B} \to D^{(*)}\ell^-\bar{\nu}_\ell$ decays with hadronic tagging at Belle*, Phys. Rev. D **92** (2015) 072014,
arXiv: 1507.03233 [hep-ex] (cit. on p. 73).

[235] LHCb Collaboration,
Measurement of the ratio of branching fractions $\mathcal{B}(\bar{B}^0 \to D^{*+}\tau^-\bar{\nu}_\tau)/\mathcal{B}(\bar{B}^0 \to D^{*+}\mu^-\bar{\nu}_\mu)$,
Phys. Rev. Lett. **115** (2015) 111803, [Erratum: Phys.Rev.Lett. 115, 159901 (2015)],
arXiv: 1506.08614 [hep-ex] (cit. on p. 73).

[236] Belle Collaboration,
Measurement of the τ lepton polarization and $R(D^*)$ in the decay $\bar{B} \to D^*\tau^-\bar{\nu}_\tau$,
Phys. Rev. Lett. **118** (2017) 211801, arXiv: 1612.00529 [hep-ex] (cit. on p. 73).

[237] LHCb Collaboration,
Measurement of the ratio of branching fractions $\mathcal{B}(B_c^+ \to J/\psi\tau^+\nu_\tau)/\mathcal{B}(B_c^+ \to J/\psi\mu^+\nu_\mu)$,
Phys. Rev. Lett. **120** (2018) 121801, arXiv: 1711.05623 [hep-ex] (cit. on p. 73).

[238] LHCb Collaboration,
Angular analysis of the $B^0 \to K^{*0}\mu^+\mu^-$ decay using 3 fb^{-1} of integrated luminosity,
JHEP **02** (2016) 104, arXiv: 1512.04442 [hep-ex] (cit. on p. 73).

[239] Belle Collaboration, *Lepton-Flavor-Dependent Angular Analysis of $B \to K^*\ell^+\ell^-$*,
Phys. Rev. Lett. **118** (2017) 111801, arXiv: 1612.05014 [hep-ex] (cit. on p. 73).

[240] LHCb Collaboration, *Test of lepton universality with $B^0 \to K^{*0}\ell^+\ell^-$ decays*, JHEP **08** (2017) 055,
arXiv: 1705.05802 [hep-ex] (cit. on p. 73).

[241] LHCb Collaboration, *Test of lepton universality in beauty-quark decays*, (2021),
arXiv: 2103.11769 [hep-ex] (cit. on p. 73).

[242] CMS Collaboration, *Prospects for exclusion or discovery of a third generation leptoquark decaying into a τ lepton and a b quark with the upgraded CMS detector at the HL-LHC*,
CMS Physics Analysis Summary CMS-PAS-FTR-18-028, 2018,
URL: http://cds.cern.ch/record/2652363 (cit. on p. 73).

[243] CMS Collaboration, *Projection of searches for pair production of scalar leptoquarks decaying to a top quark and a charged lepton at the HL-LHC*,
CMS Physics Analysis Summary CMS-PAS-FTR-18-008, 2018,
URL: http://cds.cern.ch/record/2645611 (cit. on p. 73).

[244] ATLAS Collaboration,
ATLAS sensitivity to Two-Higgs-Doublet models with an additional pseudoscalar exploiting four top quark signatures with 3ab^{-1} of $\sqrt{s}$ = 14 TeV proton–proton collisions,
ATL-PHYS-PUB-2018-027, 2018, URL: https://cds.cern.ch/record/2645845
(cit. on pp. 73, 74).

[245] CMS Collaboration, *Search for top squarks in final states with two top quarks and several light-flavor jets in proton–proton collisions at $\sqrt{s}$ = 13 TeV*, Phys. Rev. D **104** (2021) 032006,
arXiv: 2102.06976 [hep-ex] (cit. on p. 75).

[246] CMS Collaboration, *Search for leptophobic Z' resonances decaying to charginos in the dilepton plus missing transverse momentum final state at the HL-LHC*, CMS Physics Analysis Summary CMS-PAS-FTR-21-011, 2022, URL: https://cds.cern.ch/record/2804043 (cit. on pp. 77, 78).

[247] CMS Collaboration, *Seesaw Model Searches Using Multilepton Final States at the HL-LHC*, CMS Physics Analysis Summary CMS-PAS-FTR-22-003, 2022, URL: https://cds.cern.ch/record/2804044 (cit. on pp. 78, 79).

[248] CMS Collaboration, *Search for excited leptons in llgamma final states in proton-proton collisions at the HL-LHC*, CMS Physics Analysis Summary CMS-PAS-FTR-18-029, 2019, URL: http://cds.cern.ch/record/2652017 (cit. on pp. 80, 81).

[249] CMS Collaboration, *Search for excited leptons in $\ell\ell\gamma$ final states in proton–proton collisions at $\sqrt{s} = 13\,TeV$*, JHEP **04** (2019) 015, arXiv: 1811.03052 [hep-ex] (cit. on p. 80).

[250] CMS Collaboration, *Search for heavy composite Majorana neutrinos at the High-Luminosity and the High-Energy LHC*, CMS Physics Analysis Summary CMS-PAS-FTR-18-006, 2018, URL: http://cds.cern.ch/record/2650355 (cit. on pp. 80, 81).

[251] CMS Collaboration, *Search for a heavy composite Majorana neutrino in the final state with two leptons and two quarks at $\sqrt{s} = 13\,TeV$*, Phys. Lett. B **775** (2017) 315, arXiv: 1706.08578 [hep-ex] (cit. on p. 80).

[252] ATLAS Collaboration, *Prospects for searches for heavy Z′ and W′ bosons in fermionic final states with the ATLAS experiment at the HL-LHC*, ATL-PHYS-PUB-2018-044, 2018, URL: https://cds.cern.ch/record/2650549 (cit. on p. 82).

[253] ATLAS Collaboration, *Search for vector-boson resonances decaying to a top quark and bottom quark in the lepton plus jets final state in pp collisions at $\sqrt{s} = 13\,TeV$ with the ATLAS detector*, Phys. Lett. B **788** (2019) 347, arXiv: 1807.10473 [hep-ex] (cit. on p. 82).

[254] ATLAS Collaboration, *Search for heavy particles decaying into top-quark pairs using lepton-plus-jets events in proton–proton collisions at $\sqrt{s} = 13\,TeV$ with the ATLAS detector*, Eur. Phys. J. C **78** (2018) 565, arXiv: 1804.10823 [hep-ex] (cit. on p. 82).

[255] CMS Collaboration, *Sensitivity study for a heavy gauge boson W' in the decay channel with a tau lepton and a neutrino at the High-Luminosity LHC*, CMS Physics Analysis Summary CMS-PAS-FTR-18-030, 2019, URL: http://cds.cern.ch/record/2655312 (cit. on pp. 82, 83).

[256] CMS Collaboration, *Search for a W′ boson decaying to a τ lepton and a neutrino in proton–proton collisions at $\sqrt{s} = 13\,TeV$*, Phys. Lett. B **792** (2019) 107, arXiv: 1807.11421 [hep-ex] (cit. on p. 83).

[257] CMS Collaboration, *Search for ttbar resonances at the HL-LHC and HE-LHC with the Phase-2 CMS detector*, CMS Physics Analysis Summary CMS-PAS-FTR-18-009, 2018, URL: http://cds.cern.ch/record/2649032 (cit. on p. 83).

[258] CMS Collaboration, *Search for resonant $t\bar{t}$ production in proton–proton collisions at $\sqrt{s} = 13\,TeV$*, JHEP **04** (2019) 031, arXiv: 1810.05905 [hep-ex] (cit. on p. 84).

[259] ATLAS Collaboration, *Sensitivity of the ATLAS experiment to long-lived particles with a displaced vertex and E_T^{miss} signature at the HL-LHC*, ATL-PHYS-PUB-2018-033, 2018, URL: https://cds.cern.ch/record/2647992 (cit. on pp. 84, 85).

[260] ATLAS Collaboration, *Search for long-lived, massive particles in events with displaced vertices and missing transverse momentum in $\sqrt{s} = 13$ TeV pp collisions with the ATLAS detector*, Phys. Rev. D **97** (2018) 052012, arXiv: 1710.04901 [hep-ex] (cit. on p. 84).

[261] ATLAS Collaboration, *Search prospects for dark-photons decaying to displaced collimated jets of muons at HL-LHC*, ATL-PHYS-PUB-2019-002, 2019, URL: https://cds.cern.ch/record/2654518 (cit. on pp. 84, 85).

[262] ATLAS Collaboration, *Search for long-lived particles in final states with displaced dimuon vertices in pp collisions at $\sqrt{s} = 13$ TeV with the ATLAS detector*, Phys. Rev. D **99** (2019) 012001, arXiv: 1808.03057 [hep-ex] (cit. on p. 85).

[263] CMS Collaboration, *Sensitivity projections for a search for new phenomena at high dilepton mass for the LHC Run 3 and the HL-LHC*, CMS Physics Analysis Summary CMS-PAS-FTR-21-005, 2022, URL: https://cds.cern.ch/record/2804005 (cit. on pp. 86, 87).

[264] CMS Collaboration, *Search for resonant and nonresonant new phenomena in high-mass dilepton final states at $\sqrt{s} = (13$ TeV*, (2021), arXiv: 2103.02708 [hep-ex] (cit. on p. 86).

[265] ATLAS Collaboration, *Prospects for a search of invisible particles produced in association with single-top quarks with the ATLAS detector at the HL-LHC*, ATL-PHYS-PUB-2018-024, 2018, URL: https://cds.cern.ch/record/2645274 (cit. on pp. 88, 91, 93).

[266] CMS Collaboration, *Projection of the Mono-Z search for dark matter to the HL-LHC*, CMS Physics Analysis Summary CMS-PAS-FTR-18-007, 2018, URL: http://cds.cern.ch/record/2644529 (cit. on pp. 88–90).

[267] ATLAS Collaboration, *Prospects for Dark Matter searches in mono-photon and VBF+E_T^{miss} final states in ATLAS*, ATL-PHYS-PUB-2018-038, 2018, URL: https://cds.cern.ch/record/2649443 (cit. on pp. 88, 89, 91).

[268] ATLAS Collaboration, *Extrapolation of E_T^{miss} + jet search results to an integrated luminosity of 300 fb^{-1}*, ATL-PHYS-PUB-2018-043, 2018, URL: https://cds.cern.ch/record/2650050 (cit. on pp. 88, 91, 93).

[269] CMS Collaboration, *Search for new physics in events with a leptonically decaying Z boson and a large transverse momentum imbalance in proton–proton collisions at $\sqrt{s} = 13$ TeV*, Eur. Phys. J. C **78** (2018) 291, arXiv: 1711.00431 [hep-ex] (cit. on pp. 89, 90).

[270] ATLAS Collaboration, *ATLAS sensitivity to dark matter produced in association with heavy quarks at the HL-LHC*, ATL-PHYS-PUB-2018-036, 2018, URL: https://cds.cern.ch/record/2649243 (cit. on pp. 92, 93).

[271] CMS Collaboration, *A search for pair production of new light bosons decaying into muons in proton–proton collisions at 13 TeV*, Phys. Lett. B **796** (2019) 131, arXiv: 1812.00380 [hep-ex] (cit. on p. 95).